Universidade do Porto
Faculdade de Engenharia
FEUP

Diana Cristina Silva de Azevedo

Separation/Reaction in Simulated Moving Bed

Application to the Production of Industrial Sugars

Porto, 2001

FEUP

Separation/Reaction in Simulated Moving Bed

Application to the Production of Industrial Sugars

A dissertation presented to the
FACULDADE DE ENGENHARIA DA UNIVERSIDADE DO PORTO
for the degree of Doctor in Chemical Engineering

by

Diana Cristina Silva de Azevedo

SUPERVISION
Dr. Alírio Egídio Rodrigues
Full Professor

July 2001

Laboratory of Separation and Reaction Engineering
Department of Chemical Engineering
School of Engineering
University of Porto
Porto, Portugal

Constituição do Júri

Presidente

Doutor Sebastião Cabral Feyo de Azevedo
Professor Catedrático
Faculdade de Engenharia da Universidade do Porto

Vogais

Doutor Michel Bailly - Argüente
Investigador do *Laboratoire des Sciences du Génie Chimique* (CNRS)
E.N.S.I.C.-I.N.P.L. (França)

Doutor Roger-Marc Nicoud - Argüente
Presidente da Sociedade NOVASEP, SAS (França)

Doutor Luís Manuel dos Santos Pais
Professor Auxiliar
Instituto Politécnico de Bragança

Doutora Madalena Maria Gomes Queirós Dias
Professora Associada
Faculdade de Engenharia da Universidade do Porto

Doutor José Miguel Loureiro
Professor Associado
Faculdade de Engenharia da Universidade do Porto

Doutor Alírio Egídio Rodrigues - Orientador
Professor Catedrático
Faculdade de Engenharia da Universidade do Porto

ERRATA

• On the Portuguese version of the thesis abstract ("Resumo")	Read ***"abordagens"*** instead of *"abordagem"* on the fifth line of the second paragraph ("As duas abordagem fornecem...").
	Read ***"sacarose"*** instead of *"sucrose"*.
• Page 22, third line of first paragraph	Read ***"per unit volume of particle"*** instead of *"per kg of particles"*.
• Page 23, figure 2.6 (b), equations (2.4) and (2.5). Page 24, equation (2.6). Page 25, equation (2.12).	Disregard the term $(1-\varepsilon_p)$.
• Page 48, last line of third paragraph	Read ***"sections"*** instead of *"section"*.
• Page 56, equation (3.30)	Read ***"-1"*** instead of *"0"*.
• Page 78, figure 3.10	Read ***"l/kg"*** instead of *"m^3/kg"* on the right vertical axis.
• Page 118	Fifth line. Read ***"The curves represent simulated results obtained for the product concentrations averaged over each period."*** instead of *"The curves do not represent...experimental points."*.
	Eighth line. Disregard the sentence *"The calculations at steady state...plot."*.
• Page 128, fourth line	Read ***"SMB"*** instead of *"SMBR"*.
• Page 134, last line	Disregard the word *"principle"*.

Acknowledgements

Firstly, and above all, I wish to thank God and my parents for having given me existence and for having filled it with a sense of morality, responsibility, affection and respect for mankind.

I am also deeply indebted to my husband, Epitácio, and my daughter, Gabriela, without whom this work could not possibly have come to a successful term. I thankfully acknowledge Epitácio's unconditional love and support and for having temporarily, but gladly, changed the route of his professional life in the benefit of our common family project.

To my supervisor, Prof. Alírio Rodrigues, for his constant encouragement and support in all aspects of life, for the fruitful discussion he continuously nurtured throughout the entire period of thesis construction and for always challenging me to reach higher goals within research.

To the CAPES foundation, from the Ministry for Education of Brazil, for sponsoring my PhD grant (no. 1140/96-5) in Portugal. To FCT, from the Ministry for Science and Technology of Portugal, for providing financial aid to this research project (PCTI/P/EQU/32470/99).

To Prof. Célio Loureiro Cavalcante Jr. and Prof. Antônio Eurico Belo Torres, my colleagues from the Department of Chemical Engineering at the Universidade Federal do Ceará, where I academically belong, for having instilled me their obstinate enthusiasm towards this enterprise.

I wish to thank all my relatives and friends involved in the shipping of cashew apple juice to Portugal. I especially acknowledge the efforts of Dr. Men de Sá, from the Research Institute of Tropical Agriculture (CNPAT), Empresa Brasileira de Agropecuária (EMBRAPA, Brazil).

To all my workmates from LSRE, for their enlivening friendship and availability to help me in all issues. I especially thank Dr. Luís Pais and Dr. Mariana Santos for their valuable aid in the set-up of experiments and Eng. Celina Leão for the advice on numerical methods. I also wish to express my sincere gratitude to Miss Susana Cruz, together with all of the staff from LSRE, the Department of Chemical Engineering and FEUP, for their competence and readiness to assist me whenever requested to.

I am most grateful to Brother José de Lima and to the five *Couples of Our Lady* from Matosinhos: Adriana and Leonel; Manuela and António; Odete and José Reis; Mimosa and José Remelgado; Celeste and José Augusto. Joined to us by common Christian beliefs, they have played the role of our closest relatives in nearly every aspect: from our monthly shared meals to the deepest spiritual moments.

I could not forget to mention my "Euro-South-American family", who has made the weekends and holidays feel like home, even across the Atlantic. Thank you very much, my dearest Joyce, Alneu, Carol, Luís, Simone, Carlos and Geninha.

Last, but not least, I wish to acknowledge Portugal for the other lessons I learned: its culture, its food, its people and our common language... This is a treasure I will take back to Brazil and cherish forever.

To Epitácio, Gabriela
and Beatriz

Do poeta de cá:

«Para ser grande,
Sê inteiro.
Nada teu exagera ou exclui.
Sê todo em cada coisa.
Põe quanto és no mínimo que fazes.
Assim, em cada lago, a lua toda brilha,
Porque alta vive.»

***Fernando Pessoa** (1932)*

Do poeta de lá:

«Eu venho das dunas brancas
Aonde eu queria ficar...
Deitando os olhos cansados
Por onde a vista alcançar.
Meu céu é pleno de paz,
Sem chaminés ou fumaça.
No peito, enganos mil.
Na terra é pleno Abril.
Eu sou a mão que aperreia,
Eu tenho o sol e a areia,
Sou da América,
Sul da América, South America.
Eu sou a nata do lixo,
Eu sou do luxo da aldeia,
Eu sou do Ceará.»

***Ednardo**, compositor cearense,*
Extraído da canção "Terral" (1973)

Resumo

O presente trabalho discorre sobre aspectos teóricos e experimentais do processo cromatográfico contínuo do leito móvel simulado (*Simulated Moving Bed*, SMB), utilizado quer como separador quer como reactor. A principal aplicação prática abordada diz respeito à obtenção de açúcares industriais, quais sejam: glucose, frutose e sucrose. Em linhas gerais, a cromatografia por SMB permite a injecção e separação (com ou sem reacção química) de misturas binárias de forma contínua. Quando ocorre reacção química e separação simultânea dos productos, tem-se um reactor em leito móvel simulado (*Simulated Moving Bed Reactor*, SMBR). Em ambos os casos, ocorre a simulação de um contacto contracorrente entre a fase líquida e a fase sólida (adsorvente e/ou catalisador), o que maximiza a força motriz de transferência de massa e/ou permite o deslocamento do equilíbrio químico da reacção, favorecendo uma maior conversão.

No que diz respeito à modelização da separação de misturas de açúcares por SMB, foram utilizadas duas abordagens: a de um leito móvel verdadeiro (*True Moving Bed*, TMB) e a de um leito móvel simulado real (SMB). Na primeira abordagem, foi proposta uma descrição mais sofisticada da transferência de massa no interior das partículas adsorventes. Na segunda abordagem, utilizou-se a clássica aproximação LDF. As duas abordagem fornecem resultados idênticos estabelecidas as devidas relações de equivalência. Foi também apresentada uma metodologia de previsão das condições de operação de um SMB através da análise dos "volumes de separação". Esta análise permitiu prever a influência das razões de velocidade fluido-sólido também nas secções de regeneração 1 e 4, aspecto usualmente negligenciado por outros autores.

No tocante ao reactor em leito móvel simulado, também foram apresentados modelos detalhados baseados nas duas estratégias já referidas. Um algoritmo de projecto para dimensionar unidades SMBR foi proposto aplicado ao caso da inversão da sucrose e separação dos produtos frutose e glucose. Os resultados do algoritmo foram posteriormente utilizados em uma etapa de optimização em que a função objectivo escolhida foi a razão sucrose/enzima, isto é, a produtividade do catalisador. Os pontos óptimos de operação em termos das razões de velocidade nas secções 2 e 3 exibiram um comportamento interessante e diverso daquele esperado, dentro do escopo da teoria de equilíbrio, para um separador SMB dos produtos da reacção.

Dados experimentais para o SMB como separador (misturas glucose-fructose) e como reactor (inversão da sucrose) foram obtidos em uma unidade piloto Licosep 12-26 (Novasep, França), disponível no LSRE. Foram utilizadas doze colunas empacotadas com a resina catiónica DOWEX Monosphere 99/Ca (Sigma) de diâmetro igual a 320 μm. Os dados experimentais obtidos para a separação de misturas glucose-frutose e para a inversão da sucrose foram bem ajustados pelos respectivos modelos propostos. Os dados experimentais obtidos em SMBR confirmaram a ocorrência de imobilização da enzima pelo adsorvente, o que pode propiciar uma economia na quantidade de enzima alimentada.

Finalmente, apresentam-se resultados experimentais para a obtenção de frutose e glucose a partir da parte aquosa do sumo de caju (Anacardium occidentale, L.), um vegetal abundante e sub-utilizado no Nordeste do Brasil. A análise desta matéria-prima por HPLC revelou a presença de uma quantidade aproximadamente equimolecular de frutose e glucose. Foram realizadas separações bem sucedidas em SMB destes açúcares a partir de uma alimentação consistindo do sumo filtrado. O desempenho do SMB em estado estacionário, bem como os perfis de concentração dos açúcares, foram bem previstos pelos modelos já apresentados.

Abstract

The present work comprises theoretical and experimental aspects of the continuous chromatographic process of simulated moving bed (SMB), used either as an adsorber or as a chemical reactor. The main practical application concerns the production of industrial sugars, such as glucose, fructose and sucrose. Generally speaking, SMB chromatography allows continuous injection and separation (with or without reaction) of binary mixtures. When a chemical reaction and simultaneous separation occur, the equipment is named a simulated moving bed reactor (SMBR). In both cases, a countercurrent contact between fluid and solid (adsorbent and/or catalyst) phases is simulated, which maximises the driving force for mass transfer and/or promotes a shift in chemical reaction equilibrium favouring higher conversions.

In regards to the modeling of the separation of sugar mixtures by SMB, two approaches were followed: that of a true moving bed (TMB) and that of an actual simulated moving bed (SMB). In the first approach, we have proposed a more sophisticated description of intraparticle mass transfer. In the SMB approach, the classical LDF approximation was used. Both approaches provide identical results, as long as the proper relations of equivalence are applied. A methodology of prediction of adequate SMB operating conditions was presented by means of the analysis of "Separation Volume". This analysis makes it possible to address the effects of fluid-solid velocity ratios in regeneration sections 1 and 4, which is an often overlooked aspect by most authors.

As for the simulated moving bed reactor, detailed process models were described based on the strategies previously mentioned. A design algorithm was proposed in order to size SMBR units for the case of sucrose inversion and separation of products fructose and glucose. The algorithm results were used for optimization purposes by defining the sucrose/enzyme ratio (catalyst productivity) as the objective function. The optimal operating points, in terms of the velocity ratios in sections 2 and 3, followed an interesting behaviour, which was quite different from that expected for a non-reactive SMB in the frame of the equilibrium theory.

Experimental data for the SMB as a separator (fructose-glucose mixtures) and as a reactor-separator (inversion of sucrose) were obtained in a pilot unit Licosep 12-26 (Novasep, France), available at LSRE. Twelve columns were packed with cationic resin DOWEX Monosphere 99/Ca (Sigma) with a particle size of 320 μm. Experimental data obtained for both systems were reasonably well predicted by the respective process models. SMBR data confirmed the occurrence of enzyme immobilisation by the adsorbent, which may enhance savings in the amount of enzyme required by the reactor.

Finally, experimental results are shown for the separation of fructose and glucose from cashew (Anacardium occidentale, L.) apple juice, an abundant and sub-utilised crop in Northeastern Brazil. HPLC analysis revealed the presence of fructose and glucose in nearly equal amounts. Successful separation of fructose and glucose was achieved by SMB using filtered cashew apple juice as feed. SMB performance at steady state, as well as stationary concentration profiles of both sugars, were well simulated by the described process models.

Résumé

Le présent travail comprend les aspects théoriques et expérimentaux du procédé chromatographique continu de lit mobile simulé (*Simulated Moving Bed*, SMB), utilisé comme un séparateur ou comme un réacteur chimique. L'application pratique principale concerne la production de sucres industriels: glucose, fructose et saccharose. En général, la chromatographie SMB permet l'injection continue et la séparation (avec ou sans réaction) de mélanges binaires. Quand une réaction chimique et une séparation simultanée ont lieu, l'équipement est un réacteur de lit mobile simulé (*Simulated Moving Bed Reactor*, SMBR). Dans les deux cas, un contact contrecourant entre les phases liquide et solide (adsorbant et-ou le catalyseur) est simulé, qui maximise la force directrice pour le transfert de matière et déplace l'équilibre de réaction chimique favorisant des conversions plus hautes.

En ce qui concerne la modélisation de la séparation de mélanges de sucres par SMB, deux approches ont été suivies: Celui d'un lit mobile vrai (*True Moving Bed*, TMB) et celui d'un lit mobile simulé réel (SMB). Dans approche TMB, nous avons proposé une description plus sophistiquée de transfert de matière dans les particules. Dans l'approche de SMB, l'approximation LDF classique a été utilisée. Les deux approches fournissent des résultats identiques, tant que les relations appropriées d'équivalence sont appliquées. Une méthodologie de prédiction de conditions de fonctionnement adéquates pour SMB a été présentée au moyen de l'analyse de "Volume de Séparation". Cette analyse permet d'adresser les effets des rapport de vitesse liquides-solides dans les sections 1 et 4 de régénération, souvent ignorés par la plupart des auteurs.

Quant au réacteur de lit mobile simulé, modèles détaillés ont été décrits basés sur les stratégies précédemment mentionnées. On a proposé un algorithme de conception pour dimensioner des unités SMBR appliquée a l'inversion du saccharose et la séparation de produits: fructose et glucose. Les résultats d'algorithme ont été utilisés pour l'optimisation en définissant la proportion de saccharose/enzyme (la productivité de catalyseur) comme la fonction objective. Les points optimaux d'exploitation, en termes des rapports de vitesse dans les sections 2 et 3, ont suivi un comportement intéressant, qui différait du comportement de SMB non-réactif dans le cadre de la théorie d'équilibre.

Des données expérimentales pour le SMB comme un séparateur (des mélanges de glucose de fructose) et comme un séparateur-réacteur (l'inversion de saccharose) ont été obtenues dans une unité pilote Licosep 12-26 (Novasep, la France), disponible à LSRE. Douze colonnes ont été remplies avec la résine cationique DOWEX Monosphere 99/Ca (Sigma) avec une taille de particule de 320 μm. Des données expérimentales obtenues pour les deux systèmes ont été raisonnablement bien prévues par les modèles de procédé respectifs. Des données de SMBR ont confirmé l'occurrence d'enzyme imobilisé par l'adsorbant, qui peut augmenter des économies de l'enzyme exigée par le réacteur.

Finalement, on montre des résultats expérimentaux pour la séparation de fructose et glucose de le jus de la pomme de cajou (Anacardium occidentale, L.), une récolte abondante et sous-utilisée au Brésil Nord-est. L'analyse HPLC a révélé la présence de fructose et le glucose dans des quantités presque égales. La séparation couronnée de succès de fructose et glucose a été réalisée par SMB avec l'utilisation du jus de pomme de cajou filtré comme l'alimentation. La performance de SMB aussi bien que les profils de concentration des deux sucres a l'état stationnaire ont été bien simulé par les modèles de procédé décrits.

Resumen

El presente trabajo muestra los aspectos teóricos y experimentales del proceso cromatográfico continuo de lecho móvil simulado (*Simulated Moving Bed*, SMB), utilizado tanto como separador o como reactor. La principal aplicación práctica abordada está en la obtención de azúcares industriales, como: glucosa, fructosa y sacarosa. En líneas generales, la cromatografía por SMB permite la inyección y separación (con y sin reacción química) de mezclas binarias de forma continua. Cuando la reacción química y separación de los productos acontece simultáneamente, se tiene un reactor en lecho móvil simulado (*Simulated Moving Bed Reactor*, SMBR). Para ambos casos, se realiza la simulación de un contacto en contracorriente entre la fase líquida y la fase sólida (adsorbente y/o catalizador), lo que maximiza la fuerza motriz de la transferencia de masa y/o permite el desplazamiento del equilibrio químico de la reacción, permitiendo una mayor conversión.

Respecto al modelo de la separación de mezclas de azúcar por SMB, fueron usados dos métodos: el del lecho móvil verdadero (*True Moving Bed*, TMB) y el de un lecho móvil simulado real (SMB). Para el primer caso, se propuso una descripción más sofisticada de la transferencia de masa en el interior de las partículas adsorbentes. En el segundo caso, se utilizó la aproximación clásica de LDF. Los dos métodos proporcionan resultados idénticos después de establecidas las debidas relaciones de equivalencia. También fue presentada una metodología para la determinación de las condiciones de operación de un SMB a través del análisis de lo "volúmen de separación". Este análisis permitió prever también la influencia de la proporción de velocidad fluido-sólido en las secciones de regeneración 1 y 4, aspecto usualmente menospreciado por otros autores.

En cuanto al reactor en lecho móvil simulado, fueron presentados modelos detallados basados en las dos estrategias antes mencionadas. Un algoritmo para el diseño de unidades SMBR fue propuesto para ser aplicado en el caso de la inversión de sacarosa y separación de los productos fructosa y glucosa. Los resultados del algoritmo fueron utilizados posteriormente en una etapa de optimización en que la función objetivo seleccionada fue la proporción sacarosa/enzima, es decir, la productividad del catalizador. Los puntos óptimos de operación en función de las proporciones de velocidad en las secciones 2 y 3 mostraron un comportamiento interesante y diferente de aquel esperado según el análisis de un separador SMB no-reactivo para los productos de reacción en el marco de la teoría de equilibrio.

Los datos experimentales para el SMB como separador (mezclas glucosa-fructosa) y como separador-reactor (inversión de sacarosa) se obtuvieron de una unidad piloto Licosep 12-26 (Novasep, Francia), disponible en el LSRE. Se utilizaron doce columnas empacadas con la resina catiónica DOWEX Monosphere 99/Ca (Sigma) de 320 μm de diámetro. Los datos experimentales obtenidos para la separación de mezclas glucosa-fructosa y para la inversión de la sacarosa fueron predichos con precisión con los respectivos modelos propuestos. Los datos experimentales obtenidos con el SMBR confirmaron la ocurrencia de la inmovilización de la enzima por el adsorbente, lo que puede propiciar una economía en la cantidad de enzima alimentada.

Finalmente, se presentan resultados experimentales para la obtención de fructosa y glucosa a partir de la parte acuosa del jugo de caju (Anacardium occidentale, L.), un vegetal abundante y subutilizado en el Nordeste de Brasil. El análisis de esta materia prima por HPLC reveló una presencia de una cantidad aproximadamente equimolecular de fructosa y glucosa. Fueron realizadas separaciónes exitosas en SMB de estos azúcares a partir de una alimentación constituida por jugo filtrado. El desempeño del SMB en estado estacionario, así como los perfiles de concentración de los azúcares fueron bien previstos por los modelos antes mencionados.

Table of Contents

List of Figures

Chapter 2

Chapter 3

Chapter 4

Chapter 5

Chapter 6

Chapter 7

List of Tables

Chapter 2

Chapter 3

Chapter 4

Chapter 5

Chapter 6

Chapter 7

List of Symbols

Symbol	Description	Units (SI)
A	cross section area of a SMB column	m^2
b	parameter of Langmuir-type adsorption isotherms	m^3/kg
Bi_m	mass Biot number	
C	bulk fluid phase concentration	kg/m^3
$< C_m >$	mean concentration in a bidisperse particle (pores+microparticles)	kg/m^3
C_p	concentration in the fluid phase in the pores of an adsorbent particle	kg/m^3
$< C_p >$	pore fluid phase concentration averaged over the particle volume	kg/m^3
C_S	fluid phase concentration at the surface of an adsorbent particle	kg/m^3
D_{ax}	axial dispersion coefficient	m^2/s
D_c	column diameter	m
D_h	homogeneous diffusion coefficient	m^2/s
d_p	diameter of adsorbent particle	m
D_{p_e}	Effective pore diffusion coefficient	m^2/s
$E(t)$	residence time distribution	s^{-1}
k	mass transfer/reaction rate constant	s^{-1}
K	adsorption constant as defined in the bi-LDF approximation	
K'	adsorption constant as defined in the LDF approximation	
k_f	film mass transfer coefficient	m^2/s
k_r	rate constant of the inversion reaction kinetics	s^{-1}
K_{enz}	adsorption constant of enzyme invertase onto adsorbent resin	
K_{mm}	Michaelis-Menten constant	kg/m^3
L_c	column length	m
L_j	section length	m

m	Ratio between fluid and solid volumetric flowrates in a TMB section	
Pe	Peclet number	
$< q >$	adsorbed phase concentration averaged over a homogeneous solid	kg/ m^3
$<< q >>$	adsorbed phase concentration averaged over a bidisperse particle	kg/ m^3
q^*	adsorbed phase concentration in equilibrium with fluid phase	kg/ m^3
Q	volumetric flowrate in a SMB	m^3/s
Q'	volumetric flowrate in a TMB	m^3/s
q_h	Adsorbed phase concentration in a homogeneous solid	kg/ m^3
R_j	Reaction rate law for species j	kg/ m^3/s^{-1}
R_p	particle radius	m
r_p	microparticle (crystal) radius	m
t	time	s
t^*	switching time or rotation period	s
T	temperature	K
t_{st}	stoichiometric time	s
U_F	interstitial fluid velocity in a SMB	m/s
U_F'	interstitial fluid velocity in a TMB	m/s
U_s	interstitial solid velocity in a TMB	m/s
V_c	column volume	m^3
x	Dimensionless space co-ordinate in TMB-based model	
X	percentile reaction conversion (%)	

Greek letters

α	number of mass transfer or reaction rate units	
β	safety margin applied on TMB/SMB flowrate ratios	
γ	ratio between fluid and solid interstitial velocities in a TMB	
δ	index to define diffusion regime (equation 2.10)	
ΔP	pressure drop across a SMB column	Pa
ε	bed porosity	
ε_p	adsorbent particle porosity	
η	dimensionless feed flowrate	
θ	dimensionless time co-ordinate in TMB-based model	
λ	parameter in Langmuir-type adsorption isotherms	
μ	fluid absolute viscosity	kg/m s

ν	ratio between solid and fluid volumes in a column	
ρ	specific mass	kg/m^3
σ	stoichiometric reaction parameter	
τ	dimensionless time co-ordinate in SMB-based model	
υ	superficial fluid velocity in a SMB column	m/s
χ	space co-ordinate in SMB-based model	
Ψ	Ratio between liquid and (pseudo)solid velocity in SMB column	
Ω	scale factor	

Indexes

1,..,4	index to indicate TMB/SMB sections
C	citric acid
des	desired
enz	enzyme
E	eluent
eq	condition at thermodynamic equilibrium (superscript)
F	feed
Fr	fructose
Gl	glucose
h	referring to a homogeneous solid
i	chemical species
in	at the inlet of a column (superscript)
j	TMB section
k	SMB column
M	malic acid
o	referring to initial condition
p	referring to the pores of a bidisperse adsorbent
r	reaction
R	raffinate
rec	recycle
S	sucrose
sp	specified
X	extract
μ	referring to the microparticles of a bidisperse adsorbent

Abbreviations

Bi-LDF	Bi-Linear Driving Force
HETP	Height Equivalent to a Theoretical Plate
HFCS	High Fructose Corn Syrup
HPLC	High Performance Liquid Chromatography
LDF	Linear Driving Force
PR	productivity
PU	purity
QBAL	sum of inlet (eluent+feed) or outlet (extract+raffinate) SMB streams
RC	recovery
SC	solvent consumption
SMB	Simulated Moving Bed
SMBR	Simulated Moving bed Reactor
TMB	True moving Bed
TMBR	True Moving Bed Reactor
UOP	Universal Oil Products

1. Introduction

1.1 Relevance and Motivation

Chromatographic separation processes have been increasingly more popular for the last decades. Implementation of such processes in a continuous mode has been feasible by means of the technology of the simulated moving bed (SMB). This technology consists of an ingenious way of simulating the countercurrent motion of a solid adsorbent relative to a fluid phase. The steps of adsorption and desorption, either by elution or displacement, occur simultaneously within the same piece of equipment. Some of the main advantages of this technology as compared to conventional chromatography are enhanced productivity and less product dilution, even with low-efficiency columns. First patented by UOP (Universal Oil Products) in the early 60's for large bulk scale separations (petrochemical and sugar industry), SMB technology has also proved to be superior in preparative and semi-preparative applications such as fine chemical and enantiomer separations. Due to its operational complexity, the modeling, simulation, design, optimization and control of these processes are continuously challenging tasks, which have been addressed by an increasing number of publications.

In recent years, the possibility of combining reaction and adsorptive separation in the same piece of equipment has *caught the eye* of the scientific community, especially in the

field of Biotechnology. In the case of reversible reactions, the continuous withdrawal of products may shift reaction equilibrium, so as to allow higher yields as compared to conventional reactors.

Among the numerous applications of SMB and SMBR processes, those involving the production of sugars represent a significant share. While the technology involving the SMB separation of pure fructose/glucose mixtures is well established, the potential feedstocks from which to obtain such sugars contain a quite wide range of other components. The effects of these components on the overall separation efficiency should be investigated for each individual case and scarce literature has addressed this matter. Furthermore, the use of new feedstocks as a source of fructose and glucose may lead to a better use of currently less valuable or under-estimated agroproducts, which may contribute to a raise in employment and industrial activity in under-developed areas.

In regards to simultaneous separation and reaction in a simulated moving bed, attention has been focused on the modeling and simulation of such processes and ways of immobilizing the catalyst within the chromatographic stationary phase. Little has been published on the design and optimization of SMBR units, which are issues that we have addressed in this work.

1.2 Objectives and Outline

The general objective of this thesis is to study SMB and SMBR processes under those aspects of modeling, simulation, design and operation in view of the application of such technology to produce sugars of industrial importance. In regard to these aspects, some innovative points that were pursued in this work and should be highlighted are:

- A more detailed description of intraparticle mass transfer, which stands for a crucial non-ideality source in adsorptive processes onto ion-exchange resins;
- The introduction of the concept of "Separation Volume" as a tool to predict operating conditions which allow a desired separation for a given SMB equipment;
- A design and optimization algorithm proposed for both SMB and SMBR equipment, which uses a complete detailed process model in order to achieve a desired overall performance;

Experimental data for both SMB and SMBR has been focused on the production of industrial sugars, such as fructose, glucose and sucrose. Another unique subject dealt with in this work is the technical feasibility of obtaining fructose and glucose from the cashew (Anacardium occidentale, L.) apple juice. The cashew crop is one of the most important ones in Northeastern Brazil in terms of cultivated area. Its major economic destiny is the industrial extraction and pre-cooking of the nut, 90% of the juicy penduncle being wasted. Therefore, this work also aims to draw attention to a possibly attractive economic route for this presently under-estimated natural resource.

The thesis comprises eight chapters dealing with different aspects of SMB and SMBR processes. For chapters 2 throughout 7, there are separate sections for introduction, conclusions and references. A literature review section is also included, where pertinent.

In Chapter 2, the principles of chromatographic separation in a simulated moving bed are described. The state of the art of glucose/fructose separation by SMB is discussed, followed by a review on the current modeling strategies employed by various authors and their degree of refinement. Then, we introduce the concept of a bi-linear driving force approximation to describe diffusion in bidisperse adsorbents. Finally, the models to be used in this work for the prediction of SMB performance are presented under the strategies of a true moving bed (TMB) and a real simulated moving bed (SMB).

Chapter 3 starts by discussing the various approaches that have been reported in the literature in order to find the best set of operating conditions for SMB equipment. The analysis of "Separation Volume" is introduced and simulation examples illustrate the use of the proposed technique. A design and optimization algorithm was adapted to the case of glucose-fructose separation in order to find adequate equipment dimensions and operating conditions. Design results are shown in terms of a "path" of optimal fluid/solid velocity ratios as a function of the required equipment throughput.

In chapter 4, experimental results for the separation of fructose-glucose mixtures in a SMB pilot unit are shown. In section 4.2, we describe the experimental procedure and results obtained in the determination of fundamental SMB model parameters. Section 4.3 shows results of SMB experiments performed in a pilot unit, which illustrate some of the findings from the Separation Volume Analysis, described in the previous chapter.

The investigation that was conducted on the separation of fructose from cashew apple (Anacardium occidentale, L.) juice is detailed in Chapter 5. A literature review on the potential uses of the crop and recent advances on agronomic research is included. The aqueous phase of the juice was analysed to assess its sugar content and was used as feed in a SMB for fructose purification. These experimental results are shown and the effect of other juice components on the SMB performance is illustrated. The Chapter ends by applying the methodology described in Chapter 3 in order to propose adequate equipment dimensions and operating conditions for the obtention of fructose from cashew apple juice by SMB chromatography.

Chapter 6 summarizes the principles of simulated moving bed reactors and reviews published work about this issue. The process model formulations are applied to the inversion of sucrose and separation of the products fructose and glucose under the approaches of a true moving bed reactor (TMBR) and a simulated moving bed one (SMBR). Experimental data is shown under different conditions of enzyme strength and reactor performance is compared to that of another continuous chromatographic reactor reported in the literature for the same reaction/separation.

In Chapter 7, we present the strategy used to design a simulated moving bed reactor and determine the optimal construction parameters and operating conditions, which maximize enzyme productivity (objective function). Simulated results are shown and conclusions are drawn on the influence of such aspects as column subdivision, safety margin applied on the regeneration zones and minimum required product purities.

Finally, the general conclusions drawn from this work and the suggestions for future work are presented in Chapter 8.

2. Principles of Glucose/Fructose Separation in a Simulated Moving Bed (SMB) Adsorber

2.1 Introduction

In a conventional elution chromatographic separation, a small amount of the mixture to be fractionated is injected into a packed column, which is submitted to a continuous flow of eluent (solvent or mobile phase). Each of the species present in the mixture may interact with the packing, or stationary phase, in a different way. The least strongly interacting species will move through the column at a speed close to that of the eluent, or mobile phase. Accordingly, the more retained species will be retarded and reach the exit of the column later than the less retained one. This way, each concentration of the species present in the mixture will have a characteristic velocity within the column depending on its interaction with the stationary and, eventually, with the mobile phase. By collecting fractions at the exit of the column at different elution times, one is able to obtain virtually pure species. When the column is completely free of any of the species of the injected mixture, a new production cycle may start. This mode of operation is illustrated in Figure 2.1.

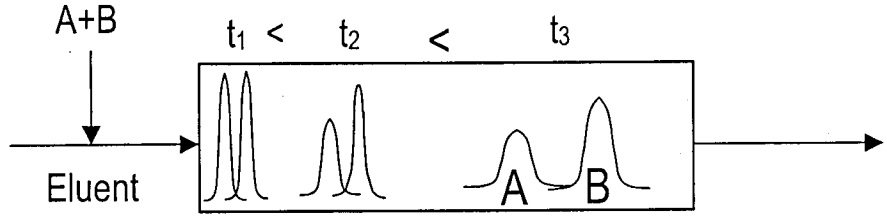

Figure 2.1 Batch Elution Chromatographic Separation

The process described above is inherently discontinuous. Other disadvantages are poor use of the adsorbent and high product dilution. Furthermore, in order to obtain better peak resolutions, columns with a high number of theoretical plates should be used, which implies either too long columns or too high pressure drops. Let us examine a situation where the stationary phase moves in the opposite direction as the mobile phase and the mixture A+B is fed somewhere around the middle of the column. If solid and fluid flowrates are carefully chosen, the band profiles of A and B will move in opposite directions, as shown in Figure 2.2 (a). By placing withdrawal nodes in positions where each of the species is pure enough (see dashed arrows), it is possible to obtain the illustrated stationary profile. Both adsorbent and eluent may be more efficiently used if they are recycled back to the system after they leave it, provided they are free of A and B. Some fresh eluent must be added so that a steady-state profile may be reached within the system. This new continuous arrangement of a chromatographic separation is shown in Figure 2.2 (b), which depicts a closed circuit of moving bed with fixed inlet and outlet points (nodes) known as a *True Moving Bed* (TMB). Between every two nodes, there are sections that must each play a certain role, so that the unit can be used for continuous production and elution. Both a mixture of species A and B and "fresh" eluent are continuously fed into the system. Likewise, two product streams are continuously withdrawn. The product stream that collects the most retained species (A) is named as *extract* and should be withdrawn after the eluent and before the feed nodes. The product stream that collects the least retained species (B) is named as *raffinate* and should be withdrawn after the feed and before the eluent node. Both extract and raffinate are much more concentrated than the fractions obtained from a batch chromatographic separation. In order to achieve separation, solid and fluid flowrates must be carefully chosen, so that each of the four TMB sections performs the following tasks.

Section 1. The function of this section is to elute/desorb A from the adsorbent. The eluent recycled from section 4 should ideally be fully regenerated and join fresh eluent so as

to promote a driving force for the desorption of A. The solid coming from section 2 should also not contain any B so as to avoid extract contamination

Section 2. The primary function of this section is to remove B from the adsorbent so that the solid moving to section 1 contains only A. The fluid phase, coming from section 1, contains no B, but only A. On the other hand, the solid coming into this section, close to the feed point, has adsorbed both A and B. As the two phases contact countercurrently, B is gradually displaced from the adsorbent and replaced by A.

Section 3. The primary function of this section is to adsorb A from the liquid. The solid coming from section 4 carries only B. As the liquid flows, A is transferred from the fluid phase to the solid phase and B is conveyed to the raffinate port.

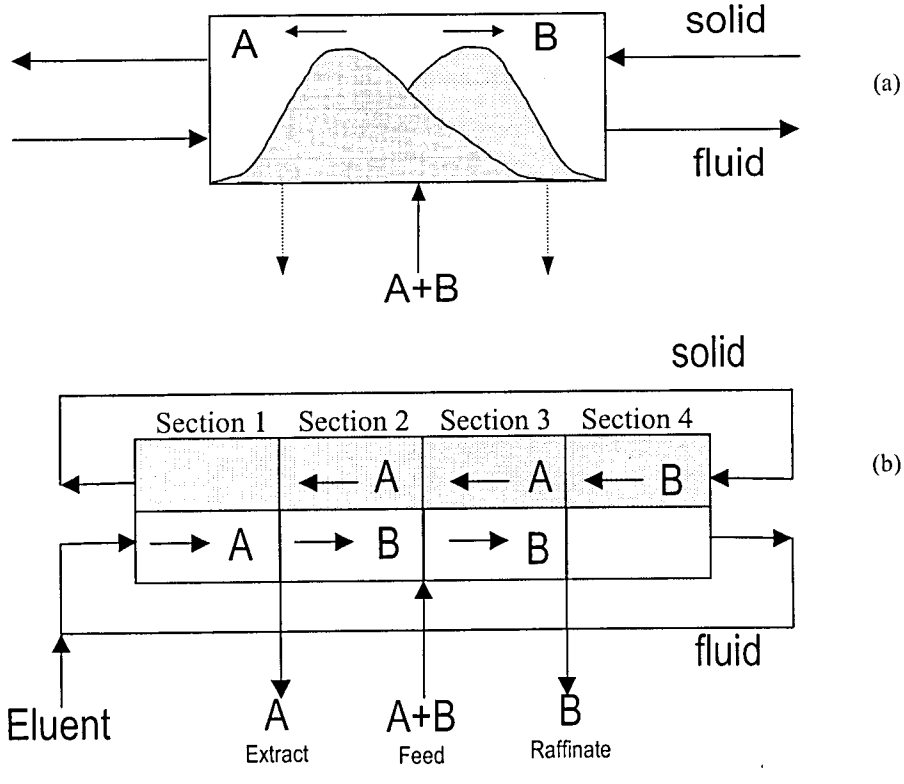

Figure 2.2 *Chromatographic separation of a mixture of components A and B in a (a) single countercurrent bed and in a (b) True Moving Bed (TMB)*

Section 4. The purpose of this section is to clean the eluent by adsorbing component B and preventing it from passing to section 1.

The first industrial process to implement the configuration of a TMB was the Hypersorption (Berg, 1946) process developed by Union Oil Company for the recovery of propane and heavier components from natural gas. However, this process proved to be less economical than cryogenic distillation and is no longer in operation. Moreover, it is rather difficult to promote a homogeneous motion of solids and overcome such problems as mechanical erosion and back-mixing. Due to these drawbacks, continuous countercurrent processes have been mostly accomplished by using a flow scheme that simulates the continuous countercurrent flow of adsorbent without actually moving it. This is achieved by holding the adsorbent bed stationary while periodically moving the points of introduction and withdrawal of liquid. This technology became known as the *Simulated Moving Bed* (SMB). The first patent was issued by UOP and licensed as the SORBEX process (Broughton and Gerhold, 1961) for a number of large scale separations in the petrochemical and sugar industries. The key feature of this process lied on a rotary valve, which implemented the port switching scheme. Figure 2.3 shows a schematic drawing of the SORBEX process with its rotary valve. With the recent expiration of former SMB patents, many companies have developed smaller multi-bed pilot SMB units (Humphey, 1995), which promote the port switching scheme by synchronizing the actuation of on/off valves and pumps.

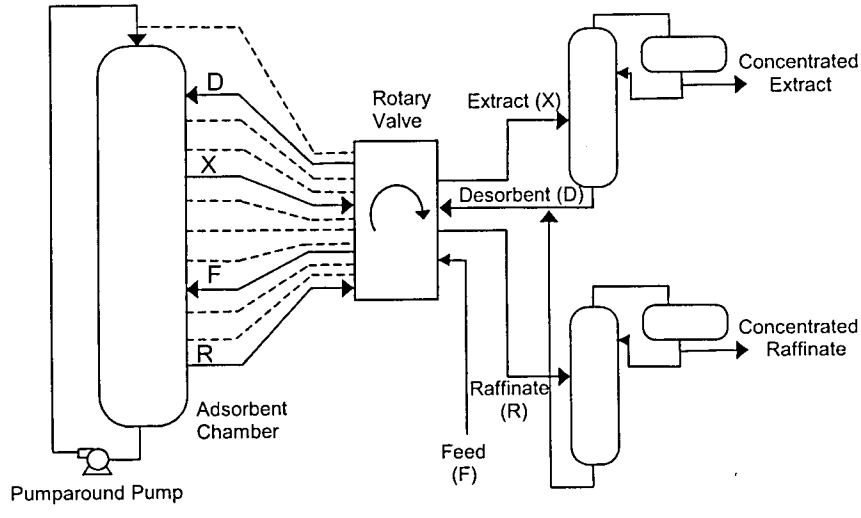

Figure 2.3 Representation of the rotary valve of a SORBEX process

Figure 2.4 shows the representation of this type of simulated moving bed. The dashed arrows represent the position of feed and draw-off streams at time "t". The solid lines represent their position at time "t+t*", where t* is the switching time or rotation period.

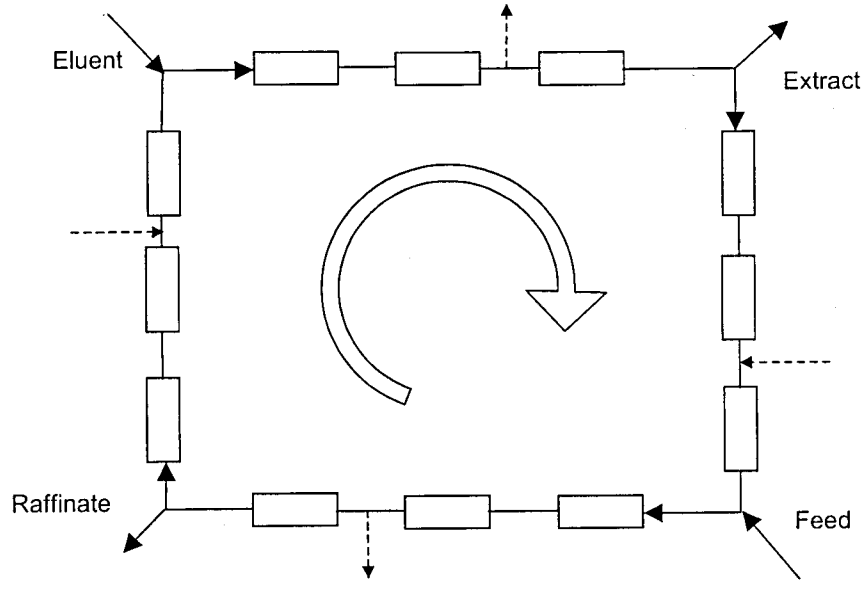

Figure 2.4 Representation of a Simulated Moving Bed (SMB). Dashed lines stand for the position of streams in the last period before the present one (continuous lines).

There are equivalence relations between the fluid flowrate and switching time in a SMB and the flowrates of a TMB. These equivalence relations are summarized in Table 2.1.

Table 2.1 Equivalence relations between a SMB and a TMB

	SMB[a]	TMB
Solid phase:		
velocity	0	$U_s=L_c/t^*$
flowrate	0	$Q_s=U_s(1-\varepsilon)A$
Liquid phase:		
velocity	U_{Fk}	$U'_{Fj}=U_{Fk}-U_s$ [a]
flowrate	Q_k	$Q'_j=Q_k-\varepsilon V_c/t^*$ [a]

[a] Equivalence for a SMB column k belonging to a section j

Source: (Leão *et al*, 1997)

The simulated moving bed technology has represented such a breakthrough in the field of Separation Engineering that over 200 patents have been issued in the U.S.A. and Europe since 1970, as found in Delphion web site for intellectual property (http://www.delphion.com). The spectrum of applications of SMB processes range from large bulk scale separations in the petrochemical and sugar industries (Johnson and Kabza, 1993) to

recent enantio- (Pais *et al*, 2000; Swarup *et al*, 1998) and bioseparations (Gottschlich and Kasche, 1997; Wu *et al*, 1998).

For the past 25 years, SMB processes have been applied on a massive scale in the carbohydrate industry, from the former SAREX process (DeRosset *et al*, 1976) to the recent isolation of betaine from sugar industry molasses (Giacobello *et al*, 2000). The SAREX process is the SORBEX version to separate fructose-glucose solutions, resulting from the enzymatic conversion of cornstarch, in order to produce "high" fructose corn syrup (HFCS). Since fructose index of sweetness is about twice as much as that of glucose, the separation of fructose from this mixture and recycling of glucose for enzymatic isomerization is of great commercial importance. Figures from the *Corn Refiners Association* (1993) showed that, in the early 90's, around 14% of all corn produced in the U.S.A. was used in the production of corn sweeteners, which in turn accounted for nearly 53% of the market of nutritive sweeteners. The first patent issued by UOP for glucose-fructose separation (Neuzil and Priegnitz, 1980) used zeolite Y, as the adsorbent, ion-exchanged with cations of metals K, Cs, Mg, Co, Sr, Ba+K and Ba+Sr. The adsorbent selectivity for fructose ranged from 1.4 to 6.2. Subsequent patents introduced the use of ion-exchange resins (Fickel, 1982) and X zeolite exchanged for potassium (Neuzil and Priegnitz, 1984). In the latter, selectivity was greater than one for glucose, rather than fructose.

Another important application of the SMB technology in the carbohydrate field is the separation of fine sugars and aminoacids from such feedstocks as molasses and biomass hydrolizates. Molasses is a by-product from the production process of sucrose, which may be obtained either from beet or sugarcane. It is the final liquor, from which additional sucrose cannot be economically crystallized, although it consists of 40-50% sucrose by weight. It accounts for nearly 15% of all sucrose present in the starting material and, since it is sold for animal feed or fermentation feedstock, it represents a loss of potential income. This material is rich not only in sucrose but in non-sugar salts, betaine (in the case of beet sugar molasses) and other saccharides of commercial interest. Companies such as Amalgamated Sugar Co. (U.S.A.), Nitten (Japan) and Organo (Japan) currently make use of the principles of SMB technology to separate sugars from non-sugars (Rearick *et al*, 1997) and isolate fine chemicals like raffinose (Sayama *et al*, 1992), and betaine (Kikuzo *et al*, 2000), respectively. Table 2.2 summarizes some relevant patents issued in the last 20 years, which illustrate the wide-spread use of SMB technology in the field of carbohydrate separations.

In this chapter, we focus on the glucose-fructose separation by SMB, as a well-known case study, to apply new modeling and design concepts. Section 2.2 brings a detailed review on published work related to this matter. In section 2.3, we introduce the mathematical models used in this work to describe the performance of SMB units and present some simulation results.

Table 2.2 Main applications of the SMB technology in carbohydrate separation

Application	***Company/Reference***	***Date Issued***	***Patent No.***
Fructose-Glucose Separation (latest improvement in SAREX process)	UOP, Inc. – USA (LeRoy, 1983)	11 Oct, 1983	US4409033
Separation of Psicose from a mixture of Monosaccharides	UOP, Inc. – USA (Chin-Hsing, 1989)	14 Nov, 1989	US4880920
Separation of glucose, maltose and oligosaccharides from starch hydrolizate	Organo Corp. - Japan (Takayuki *et al*, 1995)	21 Feb, 1995	US5391299
Separation of a water-soluble polydextrose from a glucose-based reacting mixture	Shin Dong Bang Corp. – Korea (Cheon *et al*, 1998)	03 Nov, 1998	US5831082
Separation of L-Arabinose from Sugar Beet Pulp	Cultor Corp. – Finland (Antila *et al*, 1998)	04 Mar, 1999	WO99/10542
Demineralization of a beet-sugar solution	Organo Corp. – Japan (Kikuzo *et al*, 1999)	12 Aug, 1999	WO9940228
Recovery of betaine from sugar-beet molasses with a continuous SMB	Organo Corp. – Japan (Kikuzo *et al*, 2000)	08 Aug, 2000	US6099654
Recovery of betaine from sugar-beet molasses with a sequential SMB	Dänisco Finland Oy – Finland (Heikkila *et al*, 2000)	25 Jul, 2000	US6093326

2.2 Literature Review (State of the Art)

Fructose-glucose mixtures (1:1) are commonly named as "*invert sugar*". They are most often obtained from the catalytic inversion of sucrose, either by action of acids or enzymes, according to Figure 2.5.

Sucrose is found in almost all plants, but it occurs at concentrations high enough for economic recovery only in sugarcane (*Saccharum officinarum*) and sugar beets (*Beta vulgaris*). The former is a giant grass growing in tropical and subtropical areas; the latter is a root crop growing in temperate zones. In the past few decades, world sugar prices have fluctuated widely (Schiweck and Clarke, 2001). Consequently in nations that relied heavily on sugar imports such as Japan and the USA, there has been a strong desire for an economic alternative means of producing synthetic liquid syrups. These syrups are mainly obtained from the hydrolysis of starchy material such as corn, rice and potatoes. As fructose is much sweeter than glucose, methods have been developed to isomerize the resulting dextrose syrup and obtain corn syrups containing sufficient fructose to increase its sweetness. These are commonly known as high fructose corn syrups (HFCS), the concentration of fructose ranging from 42%wt to nearly 95% of total dissolved solids.

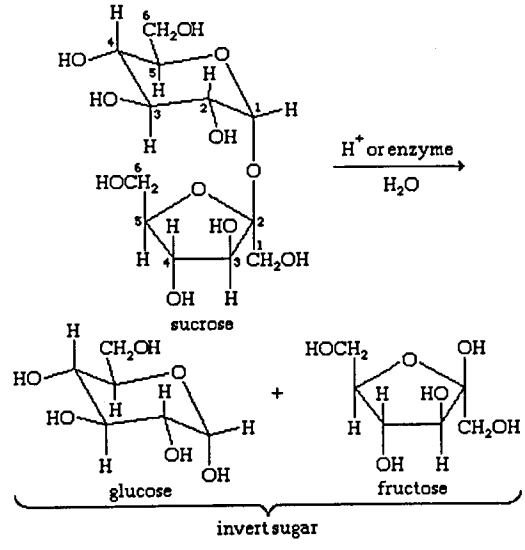

Figure 2.5 Reaction of inversion of sucrose

Since the first patent issued by UOP (Neuzil and Priegnitz, 1980), the SMB technology has been widely used for fructose-glucose separations. UOP SAREX employs CaY synthetic zeolite as the adsorbent, whereas the majority of other companies (Mitsubishi, IWT and Amalgamated) use cation-exchange resins in the Ca^{2+} form. Ho *et al* (1987) compared the kinetics and equilibria of sorption of both fructose and glucose in Ca^{2+} ion-exchanged resins and zeolite adsorbents. They found out that the ion-exchange resins have higher adsorption capacity than CaY zeolites. On the other hand, zeolitic adsorbents exhibit a much faster intraparticle diffusion than resins, given the same particle diameter. CaX zeolite was found to have no selectivity whatsoever towards one isomer relative to the other one. Ching and Ruthven (1988) then tried to exchange zeolite X for potassium and sodium in order to investigate their selectivity for one of the sugars. Zeolite KX was found to have a good capacity for both sugars with a markedly high selectivity towards glucose.

Fundamental equilibrium and kinetic data for this system are usually determined by frontal and pulse analysis, which are well-known procedures in liquid chromatography. The response of a packed column to changes in sugar inlet concentration (either a step or a pulse) is recorded. Convenient manipulation of these data allows the determination of equilibrium isotherms and pertinent dispersion and kinetic parameters. Experimental data following this procedure for glucose-fructose mixtures on resins were published by a number of authors (Altenhöner *et al*, 1997; Lee and Lee, 1992; Matijasevic *et al*, 1997; Viard and Lameloise, 1992). Ching *et al* (1990) improved this technique for multicomponent sugar mixtures in order to include interaction terms in the isotherm equations. Equilibrium isotherms for fructose and glucose onto ion-exchange resins are known to be linear over a wide concentration range (up to 100 g/l). However, since SMB operation is usually carried out under overloaded conditions, which may be as high as 400 g/l, some authors have investigated the possibility of non-linearities in this concentration range. Saska *et al* (1992) have proposed a non-linear expression for the distribution coefficient of the type $K = a + bC_F + cC_G$, where C_i is the bulk liquid concentration of sugar i and a,b,c are constants. Simulations of SMB performance taking this new formulation into account were able to predict experimental results much more accurately than those assuming linear equilibrium isotherms. Other authors (Ching *et al*, 1987; Mallmann *et al*, 1998) have further investigated non-linearities in sorption equilibria and have successfully used them in the simulation of SMB adsorbers at high sugar concentrations. Table 2.3 summarizes relevant published data concerning the adsorption isotherms of pure fructose, glucose and their mixtures onto various types of adsorbents.

Table 2.3 Summary of equilibrium adsorption data published for glucose-fructose mixtures on various kinds of adsorbents

Author	Adsorbent	Type of Equilibrium Isotherm
Altenhöner *et al* (1997)	Ca^{2+} ion-exchange resin Imac HP 1320	Linear isotherm for pure sugars in the range of 0 to 40% wt with K_{FR}=0.56 and K_{GL}=0.34 In the presence of another sugar, non-linear isotherm of type, $K_i = \frac{a}{1 + bC_{GL}^{0.8} + cC_{FR}}$
Ching and Ruthven (1988)	Zeolites NaX and KX	No selectivity for NaX. Adsorption isotherms on KX are linear with selectivity for glucose of 10.
Ching *et al* (1987)	Zeolite CaY and duolite resin at 50, 55 and 60°C	For CaY, $K_{GL} = 0.365$ and $K_{FR} = 0.675 - 0.004C_{FR} - 0.0005C_{GL}$ For duolite, $K_{GL} = 0.36 + 0.0015C_{FR} + 0.001C_{GL}$ and $K_{FR} = 0.465 + 0.005C_{FR} + 0.0015C_{GL}$
Hashimoto *et al* (1983)	Ca^{2+} ion-exchanged zeolite Y at 50°C	Linear isotherms in the range of 0-50% wt with K_{FR}=0.686 and K_{GL}=0.586
Ho *et al* (1987)	Ca^{2+} ion-exchange resin and zeolite CaY at 29-60°C	Linear isotherms in the range of 0-30% wt. Selectivity for fructose in the following intervals: 1.41-1.83 for the resin ($0.41 < K_{FR} < 0.66$, resp.) and 1.14-2.02 for the zeolite ($0.58 < K_{FR} < 0.78$, resp.)
Lee and Lee (1992)	Cation-exchange resin Dowex 50W 12X at 50°C	Linear equilibrium with K_{FR}=0.310 and K_{GL}=0.123
Mallmann *et al* (1998)	Cation-exchange resin US-Filter SM-49 at 65°C	Non-linear equilibria measured in the range of 0 up to 50% wt. Isotherms of type $q_i = \frac{a_i C_i}{1 - b_{FR}C_{FR} - b_{GL}C_{GL}}$
Saska *et al* (1992)	Resin Dowex Monosphere 99 Ca	Non-linear isotherms of type $K_{GL} = 0.245 + 0.0051C_{GL} + 0.003C_{FR}$ $K_{FR} = 0.47 + 0.007\,C_{GL} + 0.0049\,C_{FR}$
Viard and Lameloise (1992)	Ca^{2+} ion-exchange resin of types duolite and dowex	Linear isotherm for pure sugars in the range of 0 to 40% wt with K_{FR}=0.46/0.64 and K_{GL}=0.34/0.42 at 60°C and K_{FR}=0.59/0.72 and K_{GL}=0.36/0.42at 30°C for duolite/dowex.

Ching and Ruthven (1985a,b,c,d) have devoted a great deal of attention to the separation of fructose and glucose using a SMB. They analysed the performance of a three-

section SMB having a pre-feed, post-feed and purge sections. The equivalent moving bed representation was used to model the process under the approach of stages in equilibrium. The problem was addressed for the steady state (Ching and Ruthven, 1985a) and transient response (Ching and Ruthven, 1985b). Following this series of papers, the performance of a Sorbex-like system, having four distinct zones, was analysed experimentally (Ching and Ruthven, 1985c). McCabe-Thiele diagrams were used to make proper choice of operating conditions. The four-section SMB proved to yield a less diluted extract than the three-section equipment. The possibility of increasing extract concentration was also examined by applying a temperature profile to the system (Ching and Ruthven, 1986; Ching *et al*, 1986). By maintaining a temperature difference of 30-35°C across the bed, an extract product having a fructose concentration 10% higher than in the feed may be obtained.

Other authors have been working on the topic of glucose-fructose separation focusing on such aspects as modeling strategies, choice of best operating conditions and equipment optimization. Hashimoto and co-workers (1983) were one of the first authors to compare models for a real SMB and a TMB using a detailed model with external diffusion film-dependent mass transfer. Lameloise and Viard (1993) used the analytical solution of an equilibrium-dispersive model for linear isotherms applied to a TMB section. Mallman *et al* (1998) have also published a work in which a detailed model is proposed for the TMB equivalent and solved it by the theory of *Standing Wave Analysis*, as introduced by Ma and Wang (1997). An optimization procedure for fructose-glucose separation in SMB was recently introduced by Beste *et al* (2000). Both a TMB and SMB detailed models were included in the package, whose objective was to find, for a given SMB equipment, the best conditions to yield a desired performance in terms of criteria as purity, yield, productivity and dilution.

Besides those aspects of design and optimization of a SMB, which are to be treated in a following chapter, it is worth commenting on the recent innovations proposed for SMB process implementation. The main objective of these new configurations is either performance improvement or enabling the obtention of more than two products. Ching *et al* (1992) proposed two flow schemes for three-section SMB's and compared their performance with that of a four-section SMB. Mixtures of fructose, raffinose and dextran were used. They have concluded that, for cases of low separation factor, the four-section scheme generates significant savings in terms of eluent consumption and raffinate concentration. The equivalent TMB could be safely applied to the four-section SMB, but significant discrepancies arose for the three-section scheme. Sayama *et al* (1992) have introduced modifications in the way a

four-section SMB operates, so that a feed step with all columns placed in series is introduced before a second step (without feed) where the equipment works as a standard SMB. This way it is possible to recover three fractions from sugar beet molasses, one of which is the valuable sugar raffinose. The separation of three fractions from a mixture has also been reported by Hashimoto *et al* (1993) using a SMB in which columns packed with one kind of resin were arranged so as to alternate with columns packed with another kind of resin. Chiang (1998) has proposed different arrangements of two SMB's, the second one being fed by either the raffinate or the extract stream leaving the first one. The implementation of as many as nine sections in a SMB has been studied by Wooley and co-workers (1998), in order to recover four different fractions from a biomass hydrolizate. Lee (2000) claims the use of a two-section SMB for fructose-glucose separation. Experimental results show a more pure and concentrated extract and a less pure and more concentrated raffinate for this mode as compared to a three-section SMB. One of the latest breakthroughs in terms of SMB operation was the VARICOL process (Ludemann-Hombourger *et al*, 2000), which employs a shift in inlet and outlet nodes at different times so that the length of each section varies within a cycle. The productivity of such system was shown to be 18.5% greater than that of a conventional SMB. Although SMB systems may be implemented in such a variety of ways, our analysis in the following sections will be limited to the conventional four-section SMB operating in the "Sorbex" mode.

2.3 Modeling of a SMB Adsorber

The modeling of a simulated moving bed adsorber usually follows either one of two basic approaches, which represent the separator as:

- A true moving bed (TMB). Countercurrent motion of solid is actually taken into account and convenient equivalence relations are used to relate the results with a SMB adsorber;
- A simulated moving bed (SMB). Each bed is analysed individually and the periodic change in boundary conditions is taken into account.

The TMB approach has the advantage of reducing the analysis to the examination of the countercurrent sections. Concentration profiles build up around the feed node within the equipment and a single band profile is obtained at steady state. On the other hand, the SMB approach examines each bed or subsection individually. At each switching time, the boundary conditions in all columns must be updated and the steady state is not strictly reached. Instead,

an axial motion of the band profiles occur in a steady periodic fashion repeated at every period. On the bottom line, solving the model using the two approaches would be equally time consuming for a SMB with one column per section. Nevertheless, TMB analysis has also the advantage of allowing the direct calculation of the steady state performance, by simply setting the time-dependent terms in the model equations equal to zero and solving it. SMB analysis has to calculate the transient response in order to reach the steady-state solution, which may take as long as 20 cycles.

Another issue involved in the correct choice of a modeling approach is whether the TMB analysis represents accurately the performance of real equipment. Liapis and Rippin (1979) reported a comparison of a TMB and a corresponding SMB unit and concluded that, by increasing the degree of subdivision of a SMB, its performance approaches that of a TMB. Pais *et al* (1998) showed that the TMB approach may safely be used to predict the performance of SMB operation for a minimum subdivision of 2 columns per section. However, small deviations do appear between strategies especially when assessing the transient concentration profiles and if the number of columns is small (e.g. one column per section). Since the steady-state performance is what matters for design and optimization purposes, TMB may provide accurate and fast-calculating results. Other authors published similar conclusions (Lim and Ching, 1996; Lu and Ching, 1997). The eventual discrepancies observed between experimental results obtained at steady state and simulations from the TMB approach usually occur in sections 2 and 3. They have been mainly attributed to the omission of the equipment dead zones in the model and to the over-simplified description of intraparticle mass transfer brought about by the linear driving force (LDF) approximation.

2.3.1 Degrees of Complexity in SMB Modeling

Whatever modeling approach is taken, the degree of complexity of the model may vary significantly. Table 2.4 illustrates the main advantages and disadvantages of each model as a function of the modeling approach and the degree of complexity. The simplest situation is that in which each section or column is treated as a stage in equilibrium, all dispersion and mass transfer effects being neglected. The solution of such model depends only on the equilibrium isotherm, for which reason it is commonly referred to as the "Equilibrium Model". Using the TMB approach, this model provides straightforward analytical solutions for the TMB approach in the case of linear (Ching and Ruthven, 1985c), stoichiometric Langmuir (Storti *et al*, 1993), non-stoichiometric Langmuir (Mazzotti *et al*, 1996) and

Extended Langmuir isotherms (Mazzotti *et al*, 1997). Zhong and Guiochon (1996) applied the equilibrium model for a linear system examining the SMB approach. They proposed an analytical solution for the steady state concentration profiles and for the concentration histories of extract and raffinate during transient response. Although equilibrium models are always an over-simplified picture of the adsorptive process, they provide a useful check for numerical solutions of more sophisticated models. Furthermore, they have been a valuable tool in the initial screening of ideal operating conditions. They are currently used in nearly all optimization procedures that have been reported in the literature, as shall be discussed in Chapter 3.

A step further into the sophistication of SMB/TMB models is the consideration of a column/section as a series of stages in equilibrium, e. g., each stage being considered as an ideal mixing cell. Usual liquid chromatography techniques and correlations like the van Deemter (van Deemter *et al*, 1956) or Rodrigues (Rodrigues *et al*, 1991) equation may help find the number of stages or plates a column/section has. This model is often referred to as the "staged" or "plate" model. A number of authors (Ching and Ruthven, 1985d; Ernst and Hsu, 1992; Hidajat *et al*, 1986) have used this type of model to predict the performance of SMB adsorbers. Although its validity is strictly related to systems with linear isotherms, it has also been used for non-linear systems (Ching *et al*, 1988) by setting the distribution coefficients as concentration dependent in order to account for non-linearity. Due to its simplicity and fast numerical solution, the plate model has recently been used within a design algorithm (Biressi *et al*, 2000) proposed for SMB separation of non-linear equilibrium systems.

Detailed models may be defined as those which provide an accurate description of the various transport phenomena going on within a SMB column and/or TMB section. They may be as simple as the equilibrium-dispersive models, which encapsulate all non-linearities from the equilibrium model within a single lumped parameter of axial dispersion. This has been the model of choice of Yun and co-workers (1997a,b), which was applied to a SMB approach and solved numerically. Ching and Ruthven (1985a) used the equilibrium-dispersive model for a TMB approach and proposed analytical solutions for linear systems. The inclusion of a separate term in the model equations to account for mass transfer between solid and fluid was probably first proposed by Storti et al (1988), which compared simulation results using both TMB and SMB approaches for xylene separation. Despite the relative complexity and computational effort involved in their solution, detailed models have been increasingly reported (Lim and Ching, 1996; Pais et al, 1997; Strube et al, 1997). Not only available

Table 2.4 The pros ↑ and cons ↓ of different modeling approaches as a function of the degree of complexity of SMB models

Modeling Approach / Degree of Complexity	SMB MODELING		REFERENCE
	TMB APPROACH	SMB APPROACH	
Equilibrium model	↑ Readily available analytical solutions for most adsorption isotherms; ↓ Fails to predict experimental band profiles and process performance when mass transfer effects are significant;	↑ Readily available analytical solution for linear isotherms; ↓ Steady state may not be assessed directly; ↓ Non-linear systems require implicit or numerical solution;	Ching and Ruthven, 1985a; Storti *et al*, 1993; Mazzotti *et al*, 1996; Mazzotti *et al*, 1997; Zhong and Guiochon, 1996.
Stages-in-equilibrium model	↑ Fast numerical solutions, suitable for design and optimization applications; ↓ Unable to predict band broadening due to mass transfer and dispersion effects; ↓ Strictly applied to linear systems;	↑ Fast numerical solutions, suitable for control and on-line applications; ↓ Unable to predict band broadening due to mass transfer and dispersion effects; ↓ Strictly applied to linear systems; ↓ Steady state may not be assessed directly;	Ching and Ruthven, 1985d; Ernst and Hsu, 1992; Hidajat *et al*, 1986; Ching *et al*, 1988.
Equilibrium-dispersive models	↑ Fast numerical solutions, suitable for design and optimization applications; ↑ At steady state and for linear isotherms, an analytical solution may be obtained; ↓ Mass transfer effects leading to product cross contamination are overlooked;	↑ Fast numerical solutions, suitable for on-line and control applications; ↓ Steady state may not be assessed directly; ↓ Mass transfer effects leading to product cross contamination are overlooked;	Yun *et al*, 1997a; Yun *et al*, 1997b; Ching and Ruthven, 1985a; (Lameloise and Viard, 1993).
Rate model	↑ Able to predict process performance more accurately; ↓ Steady state may be directly assessed with relatively low computational effort ↓ Subject to instability and mass balance errors introduced by the numerical method of solution of PDE's	↑ Able to predict process performance and profile evolution history more accurately; ↓ Employs high computational effort ↓ Subject to instability and mass balance errors introduced by the numerical method of solution of PDE's	Storti *et al*, 1988; Lim and Ching, 1996; Pais *et al*, 1997; Strube *et al*, 1997.

computational resources have become more powerful, but also the demands set by consumers on product purity and process yield and productivity have become stricter. Therefore, it is very likely that detailed models continue to be the choice not only for process simulation, but also for design, optimization and even control purposes.

We have used both TMB and SMB strategies in this work. For each strategy, a detailed model was used, with the following assumptions taken into account:

- Isothermal operation;
- Dead volumes within the equipment were neglected;
- Axially dispersed fluid flow;
- Plug solid flow (in the case of the TMB approach);
- External diffusion in the film surrounding adsorbent particle was considered;
- Intraparticle mass transfer was described by either a LDF (linear driving force) or a bi-LDF approximations;
- Linear isotherms were considered for fructose and glucose.

2.3.2 Description of intraparticle mass transfer: the biLDF versus LDF Approximations

Most adsorbents of industrial use have a bidisperse structure composed of microparticles (crystals, for zeolites or a polymer-based matrix, for resins) held together by means of a convenient binder. This agglomeration process to form commercial pellets generates an intricate network of pores. In general, these pores may be classified as micropores, those originated from the crystal/matrix porosity, and macropores, those originated by the agglomeration process. Several mechanisms of diffusion[1] take place inside the adsorbent particles depending on the relative sorbate/pore size and the surrounding sorbate partial pressure. In the modeling of adsorption processes, an accurate description of mass transfer rates inside these adsorbent particles is often required. Accounting for all the mechanisms actually present in a given adsorption process requires extraordinary effort to solve the resulting equations. The simplest way to describe intraparticle mass transfer rates is to consider the particle as a homogeneous solid in which the sorbate diffuses according to

Fick's First Law. If a parabolic concentration profile is assumed, the integration of the diffusion equation leads to the same expression as the linear driving force (LDF) approximation, formerly proposed by Glueckauf (1955).

Some authors have attempted to account for both mass transfer resistances present in composite adsorbents. Ruckenstein (1971) analysed the competing effects of macropore and microparticle diffusion for an isolated resin particle subject to a step change in concentration at its surface (within the Henry's Law equilibrium range). Analytical solutions were shown for different macro/micro diffusional resistances and comparison with experimental data showed good agreement with the proposed model. Ma and Lee (1976) extended this solution to the more complicated boundary condition of an adsorbent particle immersed in a well-mixed solution of finite volume. The analytical solution was obtained from inversion of the Laplace transforms and could be reduced to the previous case studied by Ruckenstein. Haynes and Sarma (1973) investigated the chromatographic response of a bed packed with a bidisperse adsorbent. The proposed mathematical model was not solved but rather analysed in terms of the moments response. The relative contribution of macro- and micropore systems in the overall diffusion process was analysed by examining the second moment or the variance of the peaks in a chromatogram. Cen and Yang (1986) proposed a strategy close to a double LDF approximation to model breakthrough curves in fixed beds for gas systems. Linear equilibrium was assumed, pore accumulation and film diffusion were neglected. Analytical solutions were presented and showed good agreement with experimental data. Villermaux (1987) also proposed a simple model based on the so-called "Chemical Engineering Approach" in order to represent intraparticle diffusion in multiporosity adsorbents in linear chromatography. Macropore, micropore and external mass transfer resistances are all grouped in a single mass transfer time constant.

In this section, a bi-linear driving force approximation is proposed to describe intraparticle mass transfer rates in bidisperse adsorbents. Equivalence with the simple LDF formulation is demonstrated.

2.3.2.1 The Linear Driving Force Approximation

Let us consider an isolated homogeneous particle subject to a step change in concentration of an adsorbable species in the fluid phase. The rate of adsorption, in spherical co-ordinates, can be expressed as follows:

$$\frac{\partial q_h}{\partial t} = D_h \frac{1}{r^2}\frac{\partial}{\partial r}\left(r^2 \frac{\partial q_h}{\partial r}\right) \tag{2.1}$$

where D_h is the particle homogeneous diffusion coefficient, r is the radial co-ordinate and q_h is the adsorbed phase concentration in the homogeneous solid expressed in moles adsorbed per kg of particles. Averaging equation (2.1) over the particle radius r_p and using the linear driving force approximation, one gets:

$$\frac{d < q_h >}{d t} = k_h\left(q^*_{sh} - < q_h >\right) \tag{2.2}$$

where $< q_h >$ is the mean solid concentration averaged over the particle volume, k_h is the homogeneous diffusion rate constant ($= 15 D_h / r_p^2$) and q^*_{sh} is the concentration at the surface of the particle in equilibrium with the external phase concentration. This is the well-known linear driving force approximation, which has been proved by Glueckauf (1955) to provide an excellent description of mass transfer rates in linear chromatography.

2.3.2.2 The Bi-linear Driving Force Approximation

Let us now suppose that the particle we have just considered is a microparticle and there are thousands of other particles similar to it agglomerated so as to form a pellet. This representation is pictured in Figure 2.6.

Each microparticle has its own mean concentration $< q_h >$, which depends on the concentration at the surface. For the sake of clarity, this concentration will be expressed as $< q >$ from this point on. If there is a concentration profile throughout the pellet, each microparticle may have a different $< q >$ from one another. An average calculated from the mean concentration $< q >$ of the microparticles present in a pellet can be calculated from equation (2.2) by averaging it over the pellet volume.

$$\frac{d << q >>}{d t} = k_\mu\left(< q_s > - << q >>\right) \tag{2.3}$$

The rate constant k_h was replaced by k_μ ($= 15 D_c / r_p^2$) to denote that it is the *microparticle* (crystal) diffusion rate constant. The variables $<< q >>$ and $< q_s >$ represent

the mean microparticle concentration and the microparticle surface concentration, both averaged over the pellet volume, respectively.

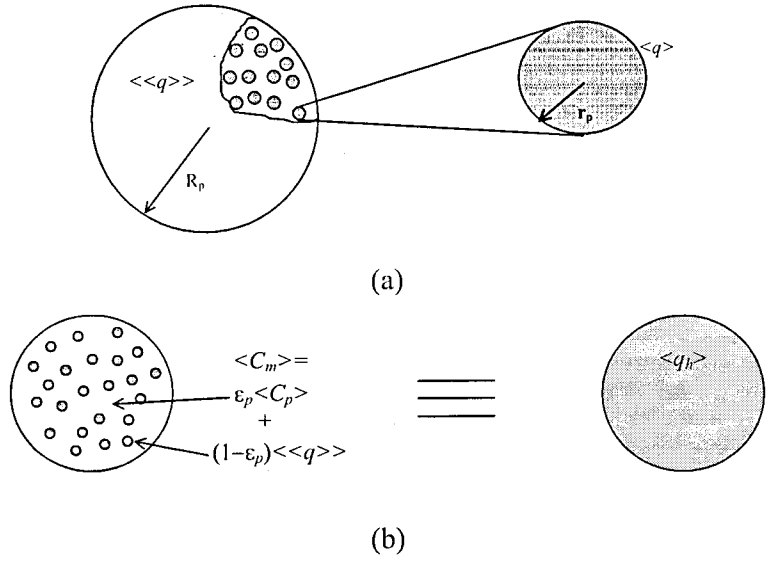

Figure 2.6 *Representation of a bidisperse pellet of radius R_p containing microparticles with radius r_p (a) and the equivalence between a homogeneous and a bidisperse solid (b).*

Let us now write a mass balance over a volume element of a pellet, such as the one shown in Figure 2.6, subject to a concentration C_S at the pellet surface. Taking C_p as the pore concentration, we have:

$$\varepsilon_p \frac{\partial C_p}{\partial t} + (1-\varepsilon_p)\frac{\partial < q >}{\partial t} = D_{pe}\frac{1}{R^2}\frac{\partial}{\partial R}\left(R^2 \frac{\partial C_p}{\partial R}\right) \qquad (2.4)$$

Averaging equation (2.4) over the pellet volume (radius=R_p) and using the LDF approximation:

$$\varepsilon_p \frac{d < C_p >}{dt} + (1-\varepsilon_p)\frac{d << q >>}{dt} = k_p\left(C_S - < C_p >\right) \qquad (2.5)$$

where C_S is the concentration at the surface of the pellet, $<< q >>$ and $< C_p >$ are the mean microparticle concentration and pore concentration, respectively, averaged over the pellet volume, ε_p is the pellet void fraction and k_p $(=15D_{p_e}/R_p^2)$ is the macropore diffusion rate constant. The left-hand term on equation (2.5) is actually an overall particle concentration which takes into account not only the solute present in the pores but also that present in the

microparticles (taken as a homogeneous solid). This concentration, expressed as $< C_m >$ and defined in equation (2.6), will be used to establish the equivalence between the LDF approximation, as described before for a homogeneous solid, and the bi-LDF approximation, as described in this work for bidisperse solids, i.e.,

$$< C_m >= \varepsilon_p < C_p > + (1 - \varepsilon_p) << q >> \tag{2.6}$$

Equations (2.3) and (2.5) are the basis of the bi-linear driving force approximation which leads to the calculation of mean concentrations in the pores and microparticles independently on pellet and microparticle radial co-ordinates. Numerical solution of such systems is perfectly feasible and does not demand an extraordinary computational effort. In order to solve equations (2.3) and (2.5), the isotherm equilibrium relation must be provided. For a linear equilibrium system, such as fructose and glucose, the bi-LDF equations are equations (2.5) and the following:

$$\frac{d << q >>}{d t} = k_\mu \left(K < C_p > - << q >> \right) \tag{2.7}$$

since the equilibrium adsorption isotherm is $q_s = KC_p$ and, therefore, $< q_s >= K < C_p >$.

Solving equation (2.7) for $< C_p >$ and substituting its value in equation (2.5), the bi-LDF equations are reduced to the following:

$$\frac{\varepsilon_p}{k_p k_\mu} \frac{d^2 << q >>}{d t^2} + \left(\frac{\varepsilon_p + K}{k_p} + \frac{1}{k_\mu} \right) \frac{d << q >>}{d t} + << q >> = KC_S \tag{2.8}$$

Rewriting equation (2.8) in terms of a corrected k_p^* $(= k_p / \varepsilon_p)$, a dimensionless equilibrium constant K^* $(= K / \varepsilon_p)$ and q_S $(= K \times C_S)$:

$$\frac{1}{k_p^* k_\mu} \frac{d^2 << q >>}{d t^2} + \left(\frac{1 + K^*}{k_p^*} + \frac{1}{k_\mu} \right) \frac{d << q >>}{d t} + << q >> = q_S \tag{2.9}$$

Convenient manipulation of equation (2.9) allows the study of the limiting cases, that is, those where diffusion is controlled either by the macropores or by the microparticles (or micropores).

Macropore Controlled Diffusion - If macropore diffusion is the limiting step in an adsorption process, $k_\mu >> 1$ and equation (2.9) is reduced to:

$$\frac{d << q >>}{dt} = \frac{k_p *}{1 + K *}(q_S - << q >>) \tag{2.10}$$

Microparticle (or micropore) Controlled Diffusion - On the other hand, if microparticle diffusional resistance is much stronger than macropore resistance, $k_p >> 1$ and equation (2.9) is reduced to:

$$\frac{d << q >>}{dt} = k_\mu (q_S - << q >>) \tag{2.11}$$

In both cases, an equivalent form of the simple LDF approximation is obtained. Nevertheless, the term $<< q >>$ present in the bi-LDF equations is different from the term $< q_h >$ present in the simple LDF approximation (see equation 2.2). From the LDF approximation perspective, for homogeneous particles, adsorption equilibrium occurs on the pellet surface, whereas for the bi-LDF approach, adsorption equilibrium occurs on the surface of the microparticles. In fact, for model equivalence purposes, we should compare $< C_m >$, as defined for the bi-LDF approximation in equation (2.6), and $< q_h >$, as defined for the LDF approximation in equation (2.2). This can be more clearly seen in Figure 2.6(b), where an homogeneous particle and a bidisperse particle having the same diameter are shown. For them to have the same adsorption capacity, $< C_m >$ must be the same as $< q_h >$ when equilibrium is reached. Therefore:

$$< C_m >= \varepsilon_p < C_p > + (1 - \varepsilon_p) << q >> = < q_h > \tag{2.12}$$

In equilibrium, the following is true:

$$< C_p >= C_S \tag{2.13}$$

$$<< q >> = < q >= K < C_p >= K C_S \tag{2.14}$$

$$< q_h >= K_h C_S \tag{2.15}$$

so that

$$K_h = K + \varepsilon_p \tag{2.16}$$

where K_h is the equilibrium constant as measured for a homogeneous particle (simple LDF model) and K is the corrected equilibrium constant considering a bidisperse adsorbent.

With equilibrium constants corrected, the equivalence between the simple LDF approximation and the bi-LDF approximation needs to be established with respect to the kinetics of mass transfer. This is more clearly visualized in the Laplace domain. The Laplace transforms of equations (2.3) and (2.5) may be grouped into a single equation in terms of the overall particle concentration $< \overline{C}_m >$ as follows:

$$\frac{< \overline{C}_m >}{\overline{C}_s} = \frac{\frac{\varepsilon_p}{k_\mu} s + \varepsilon_p + K}{\frac{\varepsilon_p}{k_p k_\mu} s^2 + \left(\frac{1}{k_\mu} + \frac{\varepsilon_p + K}{k_p} \right) s + 1} \tag{2.17}$$

where the dashes over the variables $< C_m >$ and C_s denote their Laplace transforms. The transfer function for the LDF approximation as described in equation (2.2) is:

$$\frac{< \overline{q}_h >}{\overline{C}_S} = \frac{K_h}{\left(1/k_h \right) s + 1} \tag{2.18}$$

with $q^*_{s_h} = K_h C_s$. The dashes above $< q_h >$ and C_s indicate their Laplace transforms. It is clear that the simple LDF model leads to a first order system whereas the bi-LDF model is a more complex system. If the same input $C_s(t)$ is applied to both systems, they will only respond the same way either if $k_\mu \to \infty$ or for low "s" values. In these situations, equation (2.17) is reduced to a first-order system.

When $k_\mu \to \infty$, mass transfer inside the particle is governed by diffusion in the macropores and the equivalence between the two models is verified as follows:

$$k_h = \frac{k_p}{K + \varepsilon_p} \tag{2.19}$$

On the other hand, when diffusion in the microparticles is the limiting step in intraparticle mass transfer, that is $k_p \to \infty$, equation (2.17) is not reduced to a first order system, since the s-dependent term, $(\varepsilon_p / k_\mu)s$, remains in the numerator of the transfer

function. Equivalence between the two models is not always possible. The remaining equation may behave as a first order system, but only for small "s" values. The steady-state gain is then $K_h = K + \varepsilon_p$ and the time constant is $\tau = \frac{K}{(\varepsilon_p + K)k_\mu} \equiv \frac{1}{k_h}$. For the sake of comparison between model, the equivalence relations summarized in Table 2.5 will be used in this work.

Table 2.5 Equivalence relations between LDF and bi-LDF approximations

	Bi-LDF Approximation	LDF Approximation
Macropore Diffusion Control	k_p, k_μ	$k_h = \frac{k_p}{K + \varepsilon_p}$
Microparticle Diffusion Control		$k_h = \frac{k_\mu (K + \varepsilon_p)}{K}$
Mixed Diffusion Control		$k_h = \left(\frac{K + \varepsilon_p}{k_p} + \frac{K}{(K + \varepsilon_p)k_\mu} \right)^{-1}$
Adsorption Capacity	K	$K' = K + \varepsilon_p$

According to Ruthven (1984), the value of a constant δ, which depends on the macropore and micropore diffusional time constants, indicates the governing diffusion resistance for linear systems.

$$\delta = \frac{k_\mu (1 + K^*)}{k_p^*} = \frac{k_\mu (K + \varepsilon_p)}{k_p} \qquad (2.20)$$

If $\delta < 0.1$, mass transfer is governed by micropore-controlled diffusion

If $\delta > 10$, mass transfer is governed by macropore-controlled diffusion

We have used this approximation in recently published work (Azevedo and Rodrigues, 1999). A model was proposed for a fixed bed and a true moving bed including the bi-LDF concept. Figure 2.7 shows simulated breakthrough curves obtained for a 50-cm long fixed bed (i.d. = 2.6 cm). The step concentration was 30 g/l of each sugar. The solid lines were obtained by using the bi-LDF approximation whereas a single LDF expression was used to simulate the dashed lines. Perfect equivalence may be observed for the three kinetic regimes illustrated.

Details of the fixed bed model may be found elsewhere (Azevedo and Rodrigues, 1999). The bi-LDF approximation was also used in the modeling of the steady state of a TMB and the obtained concentration profiles were compared with simulations using the single LDF expression. Details of the former model may be found in sub-section 2.3.3.1. The input parameters for the simulation are summarized in Table 2.6, in the form of conditions for an

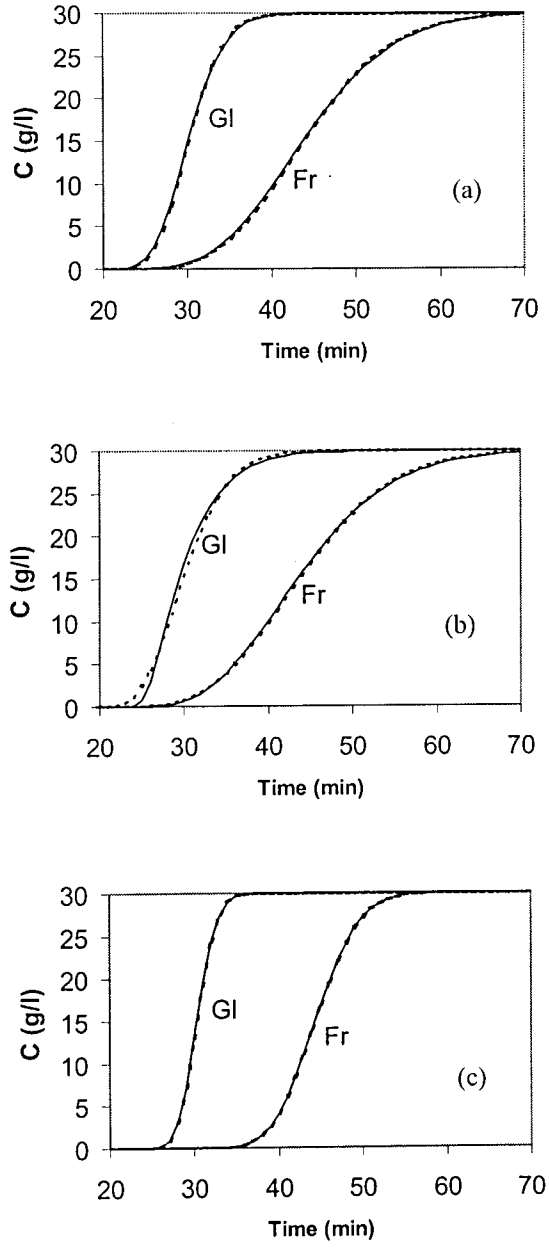

Figure 2.7 *Breakthrough curves for fructose (Fr) and glucose (Gl) mixtures under different kinetic regimes: (a) macropore, (b) microparticle and (c) intermediate diffusion control.*

equivalent SMB. Figure 2.8 shows the steady state concentration profiles of glucose and fructose, as obtained from simulations using both bi-LDF (solid lines) and LDF (dashed lines)

Table 2.6 Input parameters used in TMB simulations.

Operating conditions of equivalent SMB		**Columns**
T=20°C	Feed concentration = 30 g/l each	D_b = 2.6 cm
t* = 3.3 min		L_b = 11.5 cm
Q_{Rec}=8.55 ml/min	Q_X=16.339 ml/min	Configuration: 3-3-3-3
Q_E=20 ml/min	Q_{FEED}=0.740 ml/min	Zone length = 34.5 cm

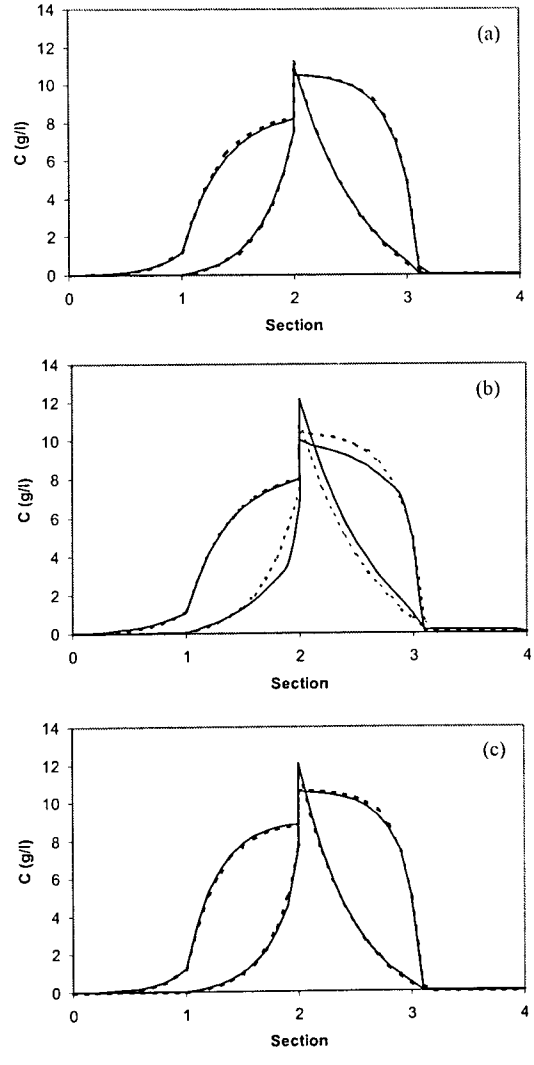

Figure 2.8 TMB Concentration profiles for fructose (Fr) and glucose (Gl) mixtures under different kinetic regimes: (a) macropore, (b) microparticle and (c) intermediate diffusion control.

approximations. Different situations of diffusion control are depicted. For each situation, the equivalent rate constant, k_h, was calculated using the equations from Table 2.5. Perfect equivalence occurs for the macropore and mixed diffusion control. However, for microparticle diffusion control, which is the case in most ion-exchange resins, discrepancies appear in sections 2 and 3. Even though both approximations have been proved to be equivalent representations, the use of a more "complex model" has the advantage of offering a more realistic picture of the actual structure of solid adsorbents. Hence, it may allow assessing the effects of changes in pellet and microparticle sizes as well as temperature on the SMB performance and design. In this work, the bi-LDF approximation was used for TMB-based models and the LDF approximation was used for SMB-based models.

2.3.3 TMB and SMB Models

As stated before in the beginning of this section, the TMB modeling strategy requires much less computational effort to be solved and steady state may be calculated directly. Its steady state form was used in the design and optimization packages to be described in Chapter 3. In this work, the TMB model employed the bi-LDF approximation to describe mass transfer within the adsorbent.

The SMB modeling strategy is more precise than the previous one since it depicts the actual physical equipment operation. It allows the visualization of the axial movement of concentration profiles and the variations in extract and raffinate concentrations within a period. However, it demands considerably higher computational effort than the TMB strategy, especially when a large number of columns are involved. Hence, in this work, the model equations for the SMB strategy used the simple LDF approximation.

2.3.3.1 Model Equations using a TMB Strategy

The following partial differential equations are proposed to represent the dimensionless mass balance of species i in an infinitesimal volume element of section j of a true countercurrent bed.

- Mass balance in the bulk fluid phase between adsorbent particles:

$$\frac{\partial C_{i,j}}{\partial \theta} = \frac{\gamma_j}{Pe_j}\frac{\partial^2 C_{i,j}}{\partial x^2} - \gamma_j \frac{\partial C_{i,j}}{\partial x} - \frac{(1-\varepsilon)}{\varepsilon}\left[\frac{Bi_{mj}}{5+Bi_{mj}}\alpha_{pj}\left(C_{i,j} - < C_p >_{i,j}\right)\right] \quad (2.21)$$

- Mass balance in pore fluid phase (inside adsorbent particles):

$$\frac{\partial < C_p >_{i,j}}{\partial \theta} = \frac{\partial < C_p >_{i,j}}{\partial x} + \frac{Bi_{mj}}{5+Bi_{mj}}\frac{\alpha_{pj}}{\varepsilon_p}\left(C_{i,j} - < C_p >_{i,j}\right) - \frac{\alpha_{\mu j}}{\varepsilon_p}\left[K_i < C_p >_{i,j} - << q >>_{i,j}\right] \quad (2.22)$$

- Mass balance in intraparticle "solid" phase (microparticles):

$$\frac{\partial << q >>_{i,j}}{\partial \theta} = \frac{\partial << q >>_{i,j}}{\partial x} + \alpha_{\mu_j}\left[K_i < C_p >_{i,j} - << q >>_{i,j}\right] \quad (2.23)$$

- Boundary conditions for section j:

$$C^{in}_{i,j}(0,\theta) = C_{i,j}(0,\theta) - \frac{1}{Pe_j}\frac{\partial C_{i,j}}{\partial x}(0,\theta) \quad (2.24)$$

$$\frac{\partial C_{i,j}}{\partial x}(1,\theta) = 0 \quad (2.25)$$

$$< C_p >_{i,j}(1,\theta) = < C_p >_{i,j+1}(0,\theta) \quad (2.26)$$

$$<< q >>_{i,j}(1,\theta) = << q >>_{i,j+1}(0,\theta) \quad (2.27)$$

- Initial conditions:

$$C_{i,j}(x,0) = C^o_{i,j}(x) \quad (5.28)$$

$$< C_p >_{i,j}(x,0) = < C_p >^o_{i,j}(x) \quad (5.29)$$

$$<< q >>_{i,j}(x,0) = << q >>^o_{i,j}(x) \quad (2.30)$$

The dimensionless variables are $x = z / L_j$ and $\theta = t \times \left(U_S / L_j\right)$, where L_j is the length of section j and U_S is the solid velocity. The dimensionless numbers present in the model equations are:

$$\gamma_j = \frac{U'_{Fj}}{U_S}$$ Fluid/solid interstitial velocity ratio (2.31)

$$Pe_j = U'_{F_j} L_j / \mathrm{D_{ax_j}}$$ Peclet number (2.32)

$$\alpha_{pj} = \frac{k_p L_j}{U_S}$$ Number of macropore mass transfer units (2.33)

$$\alpha_{\mu j} = \frac{k_\mu L_j}{U_S}$$ Number of microparticle mass transfer units (2.34)

$$Bi_{mj} = \frac{k_{fj} R_p}{D_{pe}}$$ Mass Biot number (2.35)

$C_{i,j}^{in}$, present in the boundary condition at the section inlet, can be found from global mass balances in the feed and draw-off nodes, as follows:

Eluent node: $$C_{i,1}^{in} = \frac{Q'_4}{Q'_4 + Q_E} C_{i,4}(1)$$ (2.36)

Extract node: $$C_{i,2}^{in} = C_{i,1}(1)$$ (2.37)

Feed node: $$C_{i,3}^{in} = \frac{Q'_2}{Q'_3} C_{i,2}(1) + \frac{Q_F}{Q'_3} C_{i,F}$$ (2.38)

Raffinate node: $$C_{i,4}^{in} = C_{i,3}(1)$$ (2.39)

2.3.3.2 Model Equations using a SMB Strategy

The following partial differential equations are proposed to represent the dimensionless mass balance of species i in an infinitesimal volume element of column k of a simulated moving bed. Axially dispersed flow is assumed for the fluid phase and diffusion through the external film is also considered. However, intraparticle mass transfer is

represented by a single LDF approximation, so that the required computational time is not too high and mass balance errors may be minimized.

- Global mass balance:

$$\frac{\partial C_{i,k}}{\partial \tau} + \nu \frac{\partial < q >_{i,k}}{\partial \tau} = \frac{\psi_k}{Pe_k} \frac{\partial^2 C_{i,k}}{\partial \chi^2} - \psi_k \frac{\partial C_{i,k}}{\partial \chi} \tag{2.40}$$

- Mass balance in homogeneous solid-phase:

$$\frac{\partial < q >_{i,k}}{\partial \tau} = \alpha_i \frac{Bi_{m_k}}{5 + Bi_{m_k}} \left(q^*_{i,k} - < q >_{i,k} \right) \tag{2.41}$$

- Equilibrium isotherm equation:

$$q^*_{i,k} = K_i C_{i,k} \tag{2.42}$$

- Boundary conditions:

$$C^{in}_{i,k} = C_{i,k}(0,\tau) - \frac{1}{Pe_k} \frac{\partial C_{i,k}}{\partial \chi} \tag{2.43}$$

$$\frac{\partial C_{i,k}}{\partial \chi}(1,\tau) = 0 \tag{2.44}$$

- Initial conditions:

$$C_{i,k}(\chi,0) = C^o_{i,k}(\chi) \tag{2.45}$$

$$< q >_{i,k} (\chi,0) = < q >^o_{i,k} (\chi) \tag{2.46}$$

The dimensionless variables are $\chi = z / L_c$ and $\tau = t / t^*$, where L_c is the length of a column and t^* is the switching time. The parameters Pe, Bi_m are defined as in equations (2.32) and (2.35), respectively, using the column length, L_c, instead of the section length. The other dimensionless numbers present in equations (2.40) and (2.41) are:

$$\psi_k = U_{F_k} t^* / L_c \tag{2.47}$$

$$\alpha_i = k_{h_i} t^* \tag{2.48}$$

where, for model equivalence between the simple LDF and the bi-LDF approximations,

$$k_h = \left(\frac{K + \varepsilon_p}{k_p} + \frac{K}{k_\mu (K + \varepsilon_p)} \right)^{-1} \tag{2.49}$$

and

$$K' = K + \varepsilon_p \tag{2.50}$$

If extra-column effects are neglected, the concentration at the inlet of each column k is usually the concentration leaving the previous column, that is:

$$C_{i,k}^{in} = C_{i,k-1}(1,\tau) \tag{2.51}$$

If k is the column before which either eluent or feed is introduced,

$$C_{i,k}^{in} = \frac{Q_4 C_{i,k-1}(1,\tau)}{Q_1} \qquad \text{for the eluent node} \tag{2.52}$$

$$C_{i,k}^{in} = \frac{Q_F C_{i,F} + Q_2 C_{i,k-1}(1,\tau)}{Q_3} \qquad \text{for the feed node} \tag{2.53}$$

Equations (2.51), (2.52) and (2.53) are true for all k, except when $k = 1$; then $k - 1 = NC$, where NC is the total number of columns. For a 12-column SMB, the total number of differential equations to be solved is (2 equations)*(2 components)*(12 columns) = 48. They were integrated simultaneously until the switching time was reached. The inlet (feed and eluent) and outlet (extract and raffinate) streams are shifted one bed ahead and the relative position of each bed is updated in terms of flowrate and relative position to the inlet and outlet ports.

2.3.3.3 Numerical Solution of Model Equations

The two systems of partial differential equations obtained using the TMB and SMB strategies were solved by the public-domain subroutine PDECOL (Madsen and Sincovec, 1979). It implements finite element collocation methods, with B-splines as basis functions, for the spatial discretization. The PDE system is then reduced to an initial-value ODE system, which is solved with a time integrator derived from GEARIB (Hindmarsh, 1976). For the

TMB strategy, each section was divided in 30 elements with 2 collocation points. Other run parameters were typically a time step of 10^{-6} and an error tolerance of 10^{-9}. The steady state took 10-15 cycles to be reached, which corresponded to run times of 150 to 180 min in a PC with Pentium-II 300 MHz processor. To solve the PDE system obtained from the SMB strategy, stricter parameters were used to minimize mass balance errors. The error tolerance was the same, but the time step was reduced to 10^{-9}. Each bed was also divided in 30 elements having 2 collocation points each. Since simulations were usually performed for a total of 12 columns, much higher computational effort was required, despite the lower number of equations. Run times were typically 600-800 min in the same processor.

The TMB strategy was heavily used in this work as part of design and optimization algorithms, to be described in Chapter 3. The steady state version of the model equations was obtained by setting the time-dependent terms ($\partial / \partial\theta$) as zero. The resulting system of ODE's was solved numerically using the subroutine COLNEW (Bader and Ascher, 1987). This package solves a general class of mixed-order systems of boundary value ordinary differential equations and is a modification of the COLSYS package developed by Ascher *et al* (1979; 1981). It incorporates a new basis representation replacing b-splines, and improvements for the linear and nonlinear algebraic equation solvers. The sections were taken to have 30 elements each and the error tolerance was set as 10^{-10}. On the same processor, the routine took about 10 seconds to solve the ODE system.

Pais (1999) summarized the procedure that a user of both packages must follow when trying to solve PDE and ODE systems. For both solvers described above, execution proceeded until steady state or cyclic steady state was reached. By then, the following conditions were met:

- Global mass balances were checked, that is, the amount of both fructose and glucose entering the unit in a cycle time must be same as the amount that leaves it in the same time interval;

- No variation in product concentration (within a certain error tolerance) was calculated in either two successive cycles (for the PDE systems) or two successive iterations (for the ODE system)

2.3.3.4 Simulation Results using TMB- and SMB-Based Models

The simulation of the separation of a fructose-glucose mixture by SMB was performed using the two models described previously. The operating conditions and column dimensions were those shown in Table 2.7. They were chosen according to an algorithm to be described in Chapter 3. The model parameters, also condensed on the Table, were mostly determined experimentally and the proper materials and methods employed are described in Chapter 4.

By using the TMB-based model, one obtains a single concentration profile when the steady state is reached. The concentration of products remains unchanged with time. These are shown in Figure 2.9, as thick solid lines. For the sake of clarity, the plots in (a) refer to fructose and the plots in (b) refer to glucose. On the other hand, for the SMB-based model, the cyclic steady state is actually a periodically transient state. The concentration profiles move in the direction of fluid flow within the time elapsed in a period, that is, between every two port switches. This is clearly understood in Figure 2.9. For each sugar, there are thin lines, which stand for the position of the concentration profiles at different time fractions within a period.

Table 2.7 Operating conditions and model parameters used as input for simulations performed for TMB- and SMB-based models. Data refer to real SMB equipment

Model parameters	**Operating conditions**	**Columns**
Pe=500/column	T=50°C	D_c = 2.6 cm
Bi_m=30	Feed concent. = 40 g/l each	L_c = 29 cm
k_p = 2.5 min^{-1}	t*= 3.3 min	Configuration: 3-3-3-3
k_μ = 1.5 min^{-1}	Q_{rec}=24 ml/min	
K_{FR} = 0.43 K_{GL} = 0.17	Q_E=14.27 ml/min	
ν=1.5 ε_p=0.1	Q_X=10.36 ml/min	
	Q_F=3.36 ml/min	

Hence, product concentrations vary along a cycle in a periodic fashion. The reaching of a pseudo-steady is signalled when the mean concentrations averaged over a period become constant and equal to those averaged over a cycle.

Figure 2.10 presents plots of the extract and raffinate concentration histories for a SMB initially filled with eluent only. This simulation was run under the same conditions stated in Table 2.7, but with eluent and extract flowrates reduced to 11.47 and 7.56 ml/min,

respectively. The cyclic variation of concentrations acquires a constant pattern after approximately 300 minutes or 8 cycles. The monotonic lines in each plot represent the average concentrations calculated over each period.

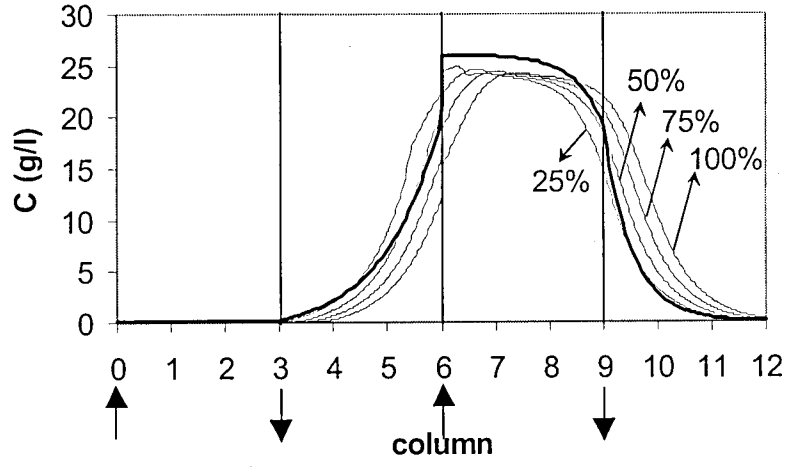

(a)

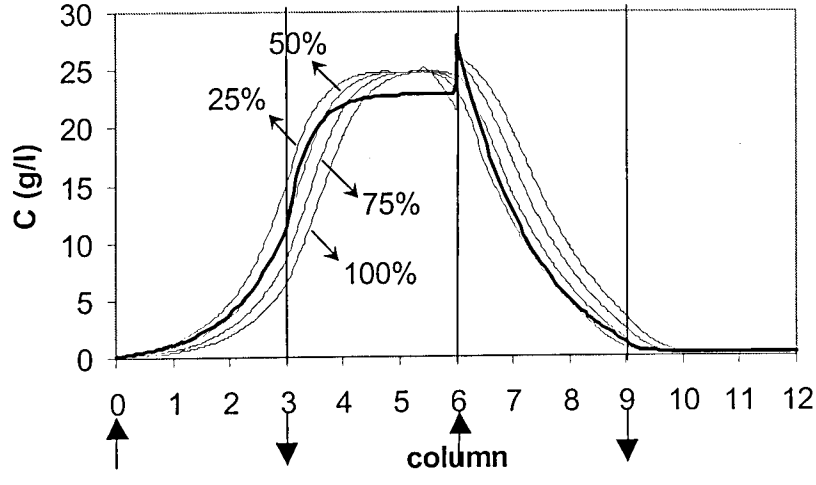

(b)

Figure 2.9 *Concentration profiles for glucose (a) and fructose (b) from simulations using the TMB-based (thick lines) and SMB-based (thin lines) strategies*

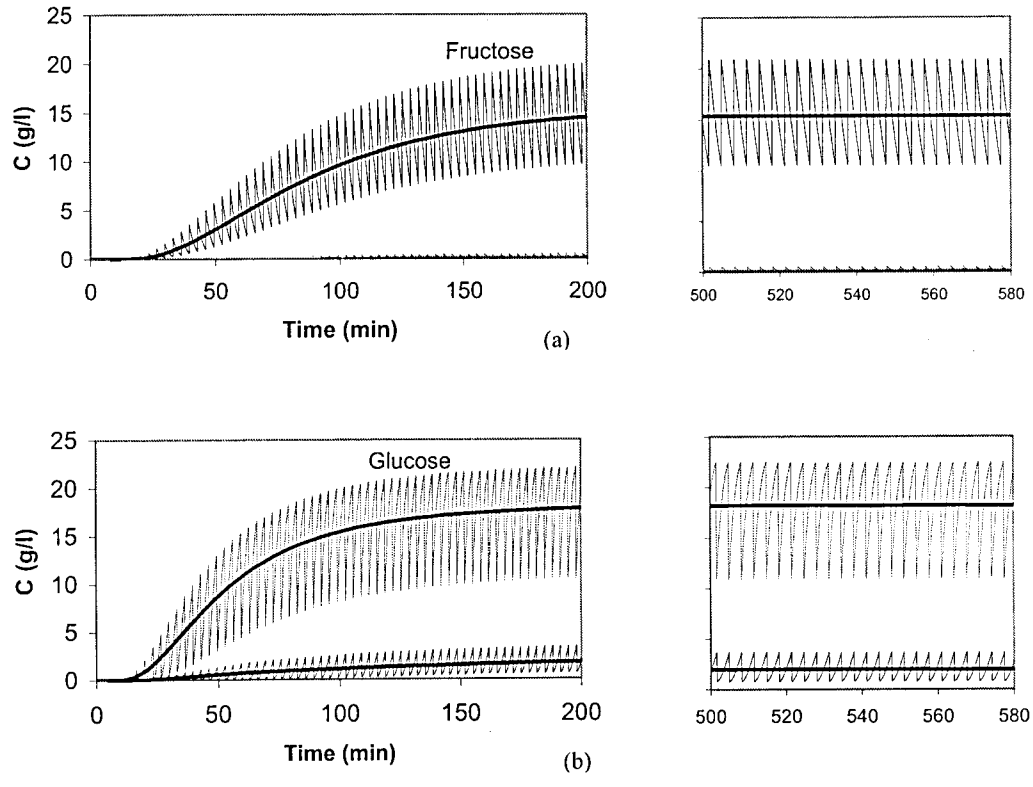

Figure 2.10 Extract (a) and Raffinate (b) histories obtained by simulation using a SMB-based strategy. The thick lines join the points that stand for concentrations averaged over each period.

In all models described so far, local equilibrium between the adsorbent surface and fluid phase was assumed to be reached instantaneously. For many systems (proteins, certain stationary phases with steric hindrances), this hypothesis is unrealistic and adsorption actually follows a given kinetics before equilibrium is attained. Appendix A presents a model for a simulated moving bed which incorporates the description of the kinetics of adsorption and simulates its effects on the process performance.

2.4 Conclusions

In this Chapter, a review of the principles of the simulated moving bed technology was presented together with applications in the separation of glucose-fructose mixtures. Current modeling trends to predict the transient and stationary behaviour of a simulated moving bed were also addressed. The detailed process models, to be used in this work, were

described under the strategies of a TMB and a SMB. Simulation results indicate that both model formulations are consistent. The SMB-based model allows the observation of product histories and the periodic character of the process pseudo-steady state. As $t \to \infty$, about the same performance is obtained as compared to that calculated from a TMB-based model. The model following the TMB strategy proved to be as accurate as the dynamic SMB-based model and able to predict steady state performance much faster, despite its more complex formulation. Therefore, it should be preferably used in future chapters for design and optimization purposes.

A description of mass transfer within bidisperse adsorbents was introduced as the bi-linear driving force (bi-LDF) approximation. Simulation results including this concept were shown for breakthrough curves in a fixed bed and for the steady state profiles of a true moving bed. They were compared with results obtained for the same situations, in which a single LDF approximation was employed. By using pertinent equivalence relationships, derived for linear systems, model equivalence was clearly evidenced. For the cases in question, the bi-LDF approximation did not dramatically increase computational effort required to solve model equations. Moreover, the discrimination of mass transfer mechanisms at the level of pores and microparticles makes it possible to address the effect of particle size and temperature on the overall process performance. Appendix A presents another refinement in the modeling of SMB processes. The usual hypothesis of local instantaneous equilibrium is questioned and a first-order kinetic law for adsorption is included in TMB- and SMB-based models.

2.5 References

"Nutritive Sweeteners from Corn", catalog from Corn Refiners Association, Inc., 32p. (1993).

U. Altenhöner, M. Meurer, J. Strube, H. Schmidt-Traub, "Parameter Estimation for the Simulation of Liquid Chromatography", *J. Chromatography A*, **769**, 59-69 (1997).

J. Antila, V. Ravanko, P. Walliander, "Method of Preparing L-Arabinose from Sugar Beet Pulp", WO Patent No. 99/10542 (1998).

U. Ascher, J. Christiansen, R. D. Russel, "A Collocation Solver for Mixed Order Systems of Boundary Value Problems", *Math. Comput.* **33**, 659-679 (1979).

U. Ascher, J. Christiansen, R. D. Russel, "Collocation Software for Boundary-Value ODEs", *ACM Trans. Math. Software* **7**, 209-222 (1981).

D. C. S. Azevedo, A. E. Rodrigues, "Bi-linear driving force approximation in the modeling of simulated moving bed using bidisperse adsorbents", *Ind. Eng. Chem. Res.* **38**, 3519-3529 (1999).

G. Bader, U. Ascher, "A New Basis Implementation for a Mixed Order Boundary Value ODE Solver", *SIAM J. Sci. Stat. Comput.* **8**, 483-500 (1987).

C. Berg, "Hypersorption Process for Separation of Light Gases", *Trans. Am. Inst. Chem. Eng.* **42**, 665-680 (1946).

Y. A. Beste, M. Lisso, G. Wozny, W. Arlt, "Optimization of Simulated Moving Bed Plants with Low Efficient Stationary Phases: Separation of Fructose and Glucose", *J. Chromatography A* **868**, 169-188 (2000).

G. Biressi, O. Ludemann-Hombourger, M. Mazzotti, R.-M. Nicoud, M. Morbidelli, "Design and Optimisation of a SMB Unit: Role of Deviations from Equilibrium Theory", *J. Chromatography A* **876**, 3-15 (2000).

D. B. Broughton, C. G. Gerhold, "Continuous Sorption Process Employing Fixed Bed of Sorbent and Moving Inlets and Outlets", U.S. Patent No. 2,985,589 (1961).

P. L. Cen, R. T. Yang, "Analytic Solution for Adsorber Breakthrough Curves with Bidisperse Sorbents (Zeolites)", *AIChE J.* **32**, 1635-1641 (1986).

A. S. Cheon, D. M. Hoe, J. H. Soon, "Process for Obtaining, by Separation, Highly Pure Water-Soluble Polydextrose", US Patent No. 5,831,082 (1998).

A. S. T. Chiang, "Continuous Chromatographic Process Based on SMB Technology", *AIChE J.* **44**, 1930-1932 (1998).

C. B. Ching, K. H. Chu, K. Hidajat, M. S. Uddin, "Comparative Study of Flow Schemes for a Simulated Countercurrent Adsorption Separation Process", *AIChE J.* **38**, 1744-1750 (1992).

C. B. Ching, C. Ho, K. Hidajat, D. M. Ruthven, "Experimental Study of a Simulated Counter-Current Adsorption System - V. Comparison of Resin and Zeolite Adsorbents for Fructose-Glucose Separation at High Concentration", *Chem. Eng. Sci.* **42**, 2547-2555 (1987).

C. B. Ching, C. Ho, D. M. Ruthven, "An Improved Adsorption Process for the Production of High-Fructose Syrup", *AIChE J.* **32**, 1876-1880 (1986).

C. B. Ching, C. Ho, D. M. Ruthven, "Experimental Study of a Simulated Counter-Current Adsorption System - VI. Non-Linear Systems", *Chem. Eng. Sci.* **43**, 703-711 (1988).

C. B. Ching, D. M. Ruthven, "An Experimental Study of a Simulated Counter-Current Adsorption System - I. Isothermal Steady State Operation", *Chem. Eng. Sci.* **40**, 877-885 (1985a).

C. B. Ching, D. M. Ruthven, "An Experimental Study of a Simulated Counter-Current Adsorption System - II. Transient Response", *Chem. Eng. Sci.* **40**, 887-885 (1985b).

C. B. Ching, D. M. Ruthven, "Experimental Study of a Simulated Counter-Current Adsorption System - III. Sorbex Operation", *Chem. Eng. Sci.* **40**, 1411-1417 (1985c).

C. B. Ching, D. M. Ruthven, "Separation of Glucose and Fructose by Simulated Counter-Current Adsorption", *AIChE Symp. Series - Adsorption and Ion Exchange* **81**, 1-8 (1985d).

C. B. Ching, D. M. Ruthven, "Experimental Study of a Simulated Counter-Current Adsorption System - IV. Non-Isothermal Operation", *Chem. Eng. Sci.* **41**, 3063-3071 (1986).

C. B. Ching, D. M. Ruthven, "A Liquid Phase Chromatographic Study of Sorption and Diffusion of Glucose and Fructose in NaX and KX Zeolite Crystals", *Zeolites* **8**, 68-73 (1988).

C.-B. Ching, K. H. Chu, D. M. Ruthven, "A Study of Multicomponent Adsorption Equilibria by Liquid Chromatography", *AIChE J.* **36**, 275281 (1990).

C. Chin-Hsing, "Process for Separating Ketoses from Alcaline- or Pyridine-Catalyzed Isomerization Products", US Patent No. 4,880,920 (1989).

A. J. DeRosset, R. W. Neuzil, D. J. Korous, "Liquid Column Chromatography as a Predictive Tool for Continuous Counter Adsorptive Separations", *Ind. Eng. Chem. Proc. Des. Dev.* **15**, 261-266 (1976).

U. P. Ernst, J. T. Hsu, "Theoretic Study of Backmixing in Simulated Moving-Bed Adsorption Process with Multiple Equilibrium Stages Between Ports", *Sep. Technol.* **2**, 197-207 (1992).

R. G. Fickel, "Simulated Countercurrent Sorption Process employing Ion Exchange Resins with Periodic Backflushing", US Patent No. 4,319,929 (1982).

S. Giacobello, G. Storti, G. Tola, "Design of a Simulated Moving Bed Unit for Sucrose-Betaine Separations", *J. Chromatography A* **872**, 23-35 (2000).

E. Glueckauf, "Theory of chromatography. Part 10. Formulae for Diffusion into Spheres and Their Application to Chromatography", *Trans. Faraday Soc.* **51**, 1540-1551 (1955).

N. Gottschlich, V. Kasche, "Purification of Monoclonal Antibodies by Simulated Moving-Bed Chromatography", *J. Chromatography A* **765**, 201-206 (1997).

K. Hashimoto, S. Adachi, H. Noujima, H. Maruyama, "Models for the Separation of Glucose/Fructose Mixture using a Simlated Moving-Bed Adsorber", *J. Chem. Eng. Jpn.* **16**, 400-406 (1983).

K. Hashimoto, Y. Shirai, S. Adachi, "A Simulated Moving-Bed Adsorber for the Separation of Tricomponents", *J. Chem. Eng. Jpn.* **26**, 52-56 (1993).

H. W. Haynes Jr., P. N. Sarma, "A Model for the Application of Gas Chromatography to Measurements of Diffusion in Bidisperse Structured Catalysts", *AIChE J.* **19**, 1043-1046 (1973).

H. Heikkila, G. Hyoky, J. Kuisma, "Method for the Fractionation of Molasses", US Patent No. 6,093,326 (2000).

K. Hidajat, C. B. Ching, D. M. Ruthven, "Numerical Simulation of a Semi-Continuous Counter-Current Adsorption Unit for Fructose-Glucose Separation", *The Chem. Eng. J.* **33**, B55-B61 (1986).

A. Hindmarsh, "Preliminary Documentation of GEARIB - Solution of Implicit Systems of Ordinary Differential Equations with Banded Jacobian", *Report UCID-30130,*Lawrence Livermore Laboratory, (1976).

C. Ho, C. B. Ching, D. M. Ruthven, "A Comparative Study of Zeolite and Resin Adsorbents for the Separation of Fructose-Glucose Mixtures", *Ind. Eng. Chem. Res.* **26**, 1407-1412 (1987).

J. L. Humphey, "Separation Processes: Playing a Critical Role", *Chem. Eng. Prog.* , 31-40 (1995).

J. A. Johnson, R. G. Kabza, "Sorbex: Industrial-Scale Adsorptive Separation", in *Preparative and Production Scale Chromatography* G. Ganetsos, P. E. Barker, Eds. (Marcel Dekker, New York, 1993) pp. 257-271.

K. Kikuzo, M. Takayuki, S. Kohei, T. Kouji, M. Fumihiko, "Process for Recovering Betaine", US Patent No. 6,099,654 (2000).

K. Kikuzo, M. Takayuki, T. Kouji, T. Makoto, M. Fumihiko, "Process for Demineralizing a Sugar Solution", WO Patent No. 9,940,228 (1999).

M. L. Lameloise, V. Viard, "Modelling and Simulation of a Glucose-Fructose Simulated Moving Bed Adsorber", *Trans IChemE* **71C**, 27-32 (1993).

C. P. Leão, L. S. Pais, M. Santos, A. E. Rodrigues, "Simulated moving-bed adsorptive reactor", in *Process Intensification in Practice - Applications and Opportunities* J. Semel, Ed. (BHR Group, Mechanical Engineering Publications Limited, London, 1997) pp. 143-155.

K. Lee, "Two-Section Simulated Moving-Bed Process", *Sep. Sci. & Technol.* **35**, 519-534 (2000).

K. N. Lee, W. K. Lee, "A Theoretical Model for the Separation of Glucose and Fructose Mixtures by using a Semicontinuous Chromatographic Refiner", *Sep. Sci. & Technol.* **27**, 295-311 (1992).

C. F. LeRoy, "Simulated Moving Bed Separation Process for High Viscosity Feed Streams", US Patent No. 4,409,033 (1983).

A. I. Liapis, D. W. T. Rippin, "The Simulation of Binary Adsorption in Continuous Countercurrent Operation and a Comparison with other Operating Modes", *AIChE J.* **25**, 455 (1979).

B.-G. Lim, C.-B. Ching, "Modelling Studies on the Transient and Steady State Behaviour of a Simulated Counter-Current Chromatographic System", *Sep. Technol.* **6**, 29-41 (1996).

Z. P. Lu, C. B. Ching, "Dynamics of Simulated Moving-Bed Adsorption Separation Processes", *Sep. Sci. & Technol.* **32**, 1993-2010 (1997).

O. Ludemann-Hombourger, R. M. Nicoud, M. Bailly, "The "VARICOL" Process: A New Multicolumn Continuous Chromatographic Process", *Sep. Sci. & Technol.* **35**, 1829-1862 (2000).

Y. H. Ma, T. Y. Lee, "Transient Diffusion in Solids with a Bipore Distribution", *AIChE J.* **22**, 147-152 (1976).

Z. Ma, N.-H. L. Wang, "Standing Wave Analysis of SMB Chromatography: Linear Systems", *AIChE J.* **43**, 2488-2508 (1997).

N. K. Madsen, R. F. Sincovec, "PDECOL: General Collocation Software for Partial Differential Equations", *ACM Trans. Math. Software* **5**, 326-351 (1979).

T. Mallmann, B. D. Burris, Z. Ma, N.-H. L. Wang, "Standing Wave Design of Nonlinear SMB Systems for Fructose Purification", *1998* **44**, 2628-2646 (1998).

L. Matijasevic, D. Vasic-Racki, N. Pavlovic, "Separation of Glucose/Fructose Mixtures. Analysis of Elution Profiles", *The Chem. Eng. J.* **65**, 209-212 (1997).

M. Mazzotti, G. Storti, M. Morbidelli, "Robust Design of Countercurrent Adsorption Separation: 3. Nonstoichiometric Systems", *AIChE J.* **42**, 2784-2796 (1996).

M. Mazzotti, G. Storti, M. Morbidelli, "Optimal Operation of Simulated Moving Bed Units for Nonlinear Chromatographic Separations", *J. Chromatography A* **769**, 3-24 (1997).

R. W. Neuzil, J. W. Priegnitz, "Process for Separating a Ketose from an Aldose by Selective Adsorption", US Patent No. 4,226,977 (1980).

R. W. Neuzil, J. W. Priegnitz, "Process for Separating Glucose from Fructose by Selective Adsorption", US Patent No. 4,442,285 (1984).

L. M. S. Pais, "Chiral Separation by Simulated Moving Bed Chromatography", PhD thesis, University of Porto (1999).

L. S. Pais, J. M. Loureiro, A. E. Rodrigues, "Modeling, Simulation and Operation of a Simulated Moving Bed for Continuous Chromatographic Separation of 1,1'-bi-2-naphtol Enantiomers", *J. Chromatography A* **827**, 215-233 (1997).

L. S. Pais, J. M. Loureiro, A. E. Rodrigues, "Modeling Strategies for Enantiomers Separation by SMB Chromatography", *AIChE J.* **44**, 561-569 (1998).

L. S. Pais, J. M. Loureiro, A. E. Rodrigues, "Chiral Separation by SMB Chromatography", *Sep. Pur. Technol.* **20**, 67-77 (2000).

D. E. Rearick, M. Kearney, D. Costesso, "Simulated Moving-Bed Technology in the Sweetener Industry", *Chemtech* **27**, 36-40 (1997).

A. E. Rodrigues, Z. P. Lu, J. M. Loureiro, "Residence Time Disttribution of Inert and Linearly Adsorbed Species in a Fixed-Bed containing Large-Pore Supports: Applications in Separation Engineering", *Chem. Eng. Sci.* **46**, 2765-2773 (1991).

E. Ruckenstein, A. S. Vaidyanathan, G. R. Youngquist, "Sorption by Solids with Bidisperse Pore Structures", *Chem. Eng. Sci.* **26**, 1305-1318 (1971).

D. M. Ruthven, *Principles of Adsorption and Adsorption Processes*, Wiley, New York, 464 p. (1984).

M. Saska, S. J. Clarke, M. D. Wu, K. Iqbal, "Glucose/Fructose Equilibria on Dowex Monosphere 99 Ca Resin under Overloaded Conditions", *J. Chromatography A* **590**, 147-158 (1992).

K. Sayama, T. Kamada, S. Oikawa, T. Masuda, "Production of Raffinose: A New Byproduct of the Beet Sugar Industry", *Zuckerind.* **117**, 893-898 (1992).

H. Schiweck, M. Clarke, "Sugar-Economic Aspects", *Ullmann's Encyclopedia of Industrial Chemistry*. Chapter 23, Web version, Wiley-VCH, Weinheim, 2001.

G. Storti, M. Masi, M. Morbidelli, S. Carrá, "Adsorption Separation Processes: Countercurrent and Simulated Countercurrent Operations", *Comp. Chem. Eng.* **12**, 475-482 (1988).

G. Storti, M. Mazzotti, M. Morbidelli, S. Carrá, "Robust Design of Binary Countercurrent Adsorption Separation Processes", *AIChE J.* **39**, 471-492 (1993).

J. Strube, U. Altenhöner, M. Meurer, H. Schmidt-Traub, M. Schulte, "Dynamic Simulation of Simulated Moving-Bed Chromatographic Processes for the Optimization of Chiral Separations", *J. Chromatography A* **769**, 81-92 (1997).

S. Swarup, G. Duan, C. B. Ching, "Chiral Separations by Simulated Continuous Countercurrent Chromatography", in *Fundamentals of Adsorption 6* F. Meunier, Ed. (Elsevier, Amsterdam, 1998) pp. 533-538.

M. Takayuki, K. Kuniaki, M. Isamu, "Process for Production of Starch Sugars", US Patent No. 5,391,299 (1995).

J. van Deemter, F. Zuiderweg, A. Klinkenerg, "Longitudinal Diffusion and Resistance to Mass Transfer as Causes on Nonideality in Chromatography", *Chem. Eng. Sci.* **5**, 271-289 (1956).

V. Viard, M.-L. Lameloise, "Modelling Glucose-Fructose Separation by Adsorption Chromatography on Ion Exchange Resins", *J. Food Eng.* **17**, 29-48 (1992).

J. Vilermaux, "Chemical Engineering Approach to Dynamic Modelling of Linear Chromatography: A Flexible Method for Representing Complex Phenomena from Simple Concepts", *J. Chromatography A* **406**, 11-26 (1987).

R. Wooley, Z. Ma, N.-H. L. Wang, "A Nine-Zone Simulating Moving Bed for the Recovery of Glucose and Xylose from Biomass Hydrolyzate", *Ind. Eng. Chem. Res.* **37**, 3699-3709 (1998).

D.-J. Wu, Y. Xie, Z. Ma, N.-H. L. Wang, "Design of Simulated Moving Bed Chromatography for Amino Acid Separations", *Ind. Eng. Chem. Res.* **37**, 4023-4035 (1998).

T. Yun, Z. Bensetiti, G. Zhong, G. Guiochon, "Effect of Column Efficiency on the Internal Concentration Profiles and the Performance of a Simulated Moving Bed Unit in the Case of a Linear Isotherm", *J. Chromatography A* **758**, 175-190 (1997a).

T. Yun, G. Zhong, G. Guiochon, "Simulated Moving Bed under Linear Conditions: Experimental vs. Calculated Results", *AIChE J.* **43**, 935-945 (1997b).

G. Zhong, G. Guiochon, "Analytical Solution for the Linear Ideal Model of Simulated Moving Bed Chromatography", *Chem. Eng. Sci.* **51**, 4307-4319 (1996).

3. Design of a SMB Adsorber

3.1 Introduction

Due to the relative complexity of its physical implementation, the definition of operating conditions (flowrates and switching time) of a SMB adsorber is not a straightforward task. The flowrates and switching time must be such in order to allow the strongly retained species to concentrate around the extract port and be majorily adsorbed around the raffinate port. The reverse must be true for the weakly adsorbed species: it should concentrate in the bulk liquid phase surrounding the raffinate port.

At this point, it is convenient to distinguish between the terms «design» and «optimization». By design, we denote the selection of suitable operating conditions (flowrates, switching time, etc.) or geometric parameters (column dimensions, extra-column piping, etc.), which allow a certain SMB equipment to fulfill a desired condition. For instance, we may design the operating conditions of an existing SMB plant, so that the extract and raffinate products reach a minimum purity of 95%. The result of a design procedure like this may be sets of permissible operating conditions under which the equipment may be operated. Otherwise, one may find that the plant is unable to reach the desired performance with its present physical configuration. Another possibility in design is finding the geometric parameters of a SMB adsorber yet to be constructed. This procedure is usually coupled to the

definition of allowable operating conditions and it also aims to find suitable equipment dimensions, so that a certain performance is achieved.

By optimization, it is meant the process of selecting either operating conditions or geometric parameters that minimise/maximise a given objective function(s), provided that certain constraint(s) is (are) fulfilled. For instance, in the example from the previous paragraph, let us assume that the design procedure led to a group of allowable operating conditions under which the SMB adsorber may be operated with minimum product purities of 95%. In this case, the constraint was set on product purity. To optimise the operating conditions of this unit, an objective function must be chosen, for example, the adsorbent productivity. Then, the initial sets of conditions defined by the design step will be further reduced to a narrower group of conditions, which maximise the function adsorbent productivity. Likewise, optimising the geometric parameters of a SMB plant consists in finding the adequate number of columns, column dimensions and section configuration, which cause the objective function to reach a minimum/maximum value.

This Chapter starts by reviewing recently published work concerning the issues of design and optimization of SMB adsorbers. In section 3.3, the concept of "Separation Volume" will be introduced in order to aid the design of operating conditions of existing SMB equipment applied to the separation of fructose-glucose mixtures. In section 3.4, the adaptation of a previously reported optimization algorithm is described. The proposed optimization package is used to define both optimal and robust geometric parameters and operating conditions for a SMB adsorber used to separate fructose-glucose mixtures. The effects of section subdivision, purity constraints and safety margins applied on the regeneration section are investigated on the results of the optimization algorithm.

For a better understanding of this Chapter, it is convenient to define the criteria to be used in order to measure the performance of a SMB adsorber. They are purity, recovery (also called yield), solvent consumption and adsorbent productivity. They are represented by the abbreviated forms PU_i, RC_i, SC_i and PR_i, respectively, where the subscript i may refer either to the extract ($i = X$) or to the raffinate ($i = R$) products. Each performance criteria is defined as follows:

$$PU_i\,(\%) = \frac{\text{Mass rate (kg/s) of intended sugar * obtained in product } i}{\text{Total mass rate (kg/s) of sugars obtained in product } i} \qquad (3.1)$$

$$RC_i\ (\%) = \frac{\text{Mass rate (kg/s) of intended sugar * obtained in product } i}{\text{Mass rate (kg/s) of intended sugar * introduced in the feed stream}} \quad (3.2)$$

$$SC_i\ (\text{m}^3/\text{kg}) = \frac{\text{Flowrate of solvent present in the feed and eluent streams (m}^3/\text{s)}}{\text{Mass rate (kg/s) of intended sugar * obtained in product } i} \quad (3.3)$$

$$Pr_i\ (\text{kg/m}^3/\text{hr}) = \frac{\text{Mass rate (kg/hr) of intended sugar * obtained in product } i}{\text{Volume (m}^3\text{) of stationary phase}} \quad (3.4)$$

* Fructose is the "intended sugar" in the extract and glucose, in the raffinate.

3.2 Literature Review

Since it is a fruitless effort to search for suitable SMB operating conditions by trial-and error procedures, the design of SMB adsorbers has attracted significant attention from the academic community. The simplest case may be formulated for systems with linear uncoupled adsorption isotherms. The analysis of the equivalent representation of a true moving bed under an equilibrium model leads to explicit inequality relations between solid and liquid flowrates in the four TMB sections (see Table 3.1). Nicoud (1992) as well as Ching and Ruthven (1985) changed these inequality relations into design equations by introducing a common safety margin β, as shall be described in the next section. Therefore, for linear systems, the SMB system is exclusively a flow-controlled process. That is to say, its design does not depend on the feed concentration in the frame of equilibrium theory.

Non-linear behaviour of the isotherms adds to the dependency of the flowrates the feed concentration as an influencing factor. Storti *et al* (1993) addressed the issue of SMB design for a system whose equilibria was described by the constant selectivity stoichiometric Langmuir isotherm, while mass transfer resistances and axial mixing were neglected. The authors made use of the analytic solution proposed by Rhee *et al* (1971) for a single moving bed section and derived explicit expressions for the boundaries of the complete separation region in the $m_2 \times m_3$ plane. The variables m_2 and m_3 are defined as the ratio between the net fluid flowrate and the adsorbed phase flowrate in sections 2 and 3 of a true moving bed. The role of sections 1 and 4 was found to be less important and the constraints on them were much simpler. Following this analysis provided by the equilibrium models, numerous subsequent publications have reported the derivation of explicit relations to define the region

of complete separation in the $m_2 \times m_3$ plane. Mazzotti *et al* (1996) developed an analogous work in order to define the separation region for adsorption equilibria described by a constant selectivity non-stoichiometric Langmuir model. These studies have been carried out in view of their applicability to the separation of hydrocarbons, as a key example of SMB use in the petrochemical industry. For such systems, the adsorbent regeneration is carried out by displacement of the species to be separated by a stronger adsorbing species, the desorbent. Hence, the equilibrium isotherm of the desorbent is an essential input parameter in the design of the SMB adsorber in the frame of equilibrium theory.

With the increasing number of applications of the SMB in chiral separations, more recent work has been published on the design of such systems (Mazzotti *et al*, 1997; Pais *et al*, 1998; Migliorini *et al*, 1999; Lehoucq *et al*, 2000). Most of the isotherms that describe the adsorption of optical isomers onto adsorbents with chiral resolution are of the modified or extended Langmuir type. The isotherm parameters of the individual isomers constitute relevant information for the design in the frame of the equilibrium theory. Mazzotti *et al* (1997) proposed explicit relationships to locate the boundaries of the separation region in a $m_2 \times m_3$ plane for variable selectivity modified Langmuir isotherms. The main finding provided by the equilibrium theory is certainly the explicit definition of the boundaries of separations regions in terms of the solid and fluid flowrates in SMB sections. Furthermore, it is always a useful check and source of comparison for design strategies that incorporate nonideal effects. The resulting equations reported in the literature for the most common equilibrium isotherms found in SMB elution chromatography are summarized in Table 3.1, Table 3.2 and Table 3.3.

All results presented in Table 3.1, Table 3.2 and Table 3.3 refer to flowrate conditions under which a SMB adsorber may achieve 100% purity for both extract and raffinate products, independently on column number and dimensions. In practice, the results are only applicable for columns with a sufficiently high plate number. Fortunately, for most applications, fairly inefficient columns may safely be used in a SMB operated under the conditions stated by the equilibrium theory (Charton and Nicoud, 1995). Alternatively, adsorbent particle size and column dimensions may also be tailored to overcome such effects as axial mixing and mass transfer resistances, which are sources of deviation from the results of the equilibrium theory. Nevertheless, some authors have attempted to refine the scope of the equilibrium theory, so as to include those non-ideality effects into the design of operating

conditions of SMB adsorbers. Pais *et al* (1997) shaped the regions of separation under nonideal effects by using a detailed model with intraparticle mass transfer being described with a simple LDF approximation. It was shown that the set of values of fluid/solid flowrate ratios in the $m_2 \times m_3$ is considerably reduced when mass transfer effects are present, even for a constraint of 99% on product purities. Similar results were obtained by Migliorini *et al* (1999). By using a complete detailed model, they defined the regions of separation in the $m_2 \times m_3$ plane for decreasing purity requirements (99%, 95%, ..., 60%). For SMB columns having the number of theoretical stages above a threshold value (40), the regions of separation would enlarge with decreasing purity requirements as compared to the region defined by the equilibrium theory. On the other hand, for less efficient columns, the regions of separation will virtually "shrink" in comparison with the ideal region and they may eventually not exist whether the constraint on purity is too strict or the columns have a plate number far below the limiting value. Both of these works attributed values to the flowrate ratios in sections 1 and 4 in accordance with the explicit relations defined in the equilibrium theory with a given safety margin. Azevedo and Rodrigues (1999) observed the impact of varying the values of the constraints for these sections on the resulting separation regions obtained for low-efficient columns. Instead of a 2-dimensional parameter space, a three dimensional parameter space is used to present the obtained separation regions. This concept, which became known as the "Separation Volume Analysis", will be presented in detail in section 3.3.

The theory underlying the equilibrium models is a very useful starting point when it comes to the design of SMB construction parameters. More or less sophisticated process models are used so as to assess the performance criteria on which the optimization and design steps are based. Charton and Nicoud (1995) published a pioneer work where the authors describe the steps to be followed in designing not only the flowrates but also the construction parameters such as column dimensions and adsorbent particle size. The proposed design procedure makes use of the following pieces of information: adsorption isotherms; optimal flowrate ratios as defined from the equilibrium theory; relationship giving the HETP as a function of mobile phase interstitial velocity (van Deemter); and a relationship for the calculation of pressure drop across packed beds. For a given bead diameter, optimum column length and mobile phase velocity are derived. Following a similar approach, other optimization strategies have been reported (Biressi *et al*, 2000; Ludemann-Hombourger *et al*, 2000), which basically elected the adsorbent productivity as an objective function to be maximized. With the ever-growing spectrum of applications of SMB technology in chiral

separations, the main cost associated to the process relies on the adsorbent. Thus, it is of utmost commercial interest to make the most effective use of the stationary phase, given their cost and the high added value of pure enantiomers.

Table 3.1 *Operating Conditions for the Complete Separation under the Equilibrium Theory. Linear Adsorption Isotherms.*

(Ching and Ruthven, 1985; Nicoud, 1992)

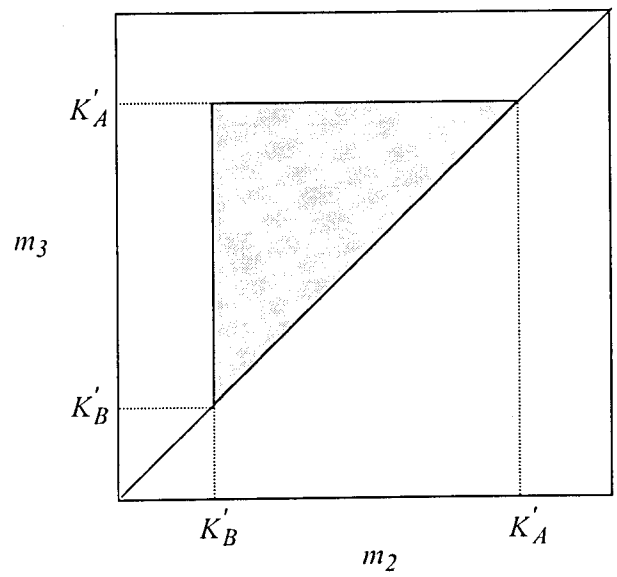

Isotherm equation: $q_i^* = K_i' C_i$ where $i = A,B$ (3.5)

$$K'_A < m_1 < \infty \quad (3.6)$$

$$K'_B < m_2 < m_3 < K'_A \quad (3.7)$$

$$0 < m_4 < K'_B \quad (3.8)$$

Table 3.2 *Operating Conditions for the Complete Separation under the Equilibrium Theory. Constant Selectivity Langmuir Adsorption Isotherm. (Mazzotti et al, 1997)*

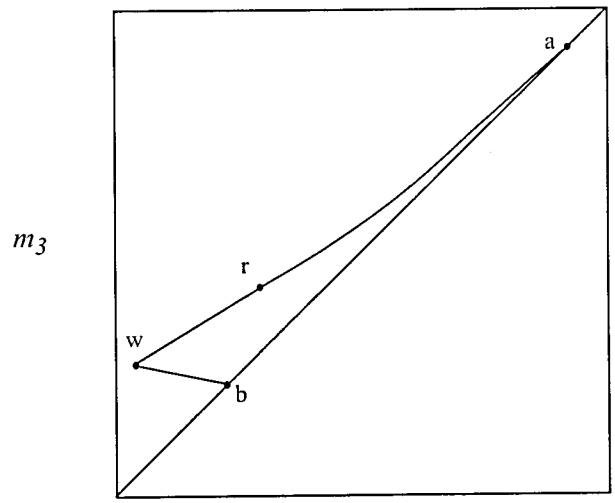

Isotherm equation: $q_i^* = \dfrac{\lambda_i C_i}{1 + b_A C_A + b_B C_B}$ where $i = A, B$ (3.9)

$$\lambda_A = m_{1,min} < m_1 < \infty \tag{3.10}$$

$$m_{2,min}(m_2, m_3) < m_2 < m_3 < m_{3,max}(m_2, m_3) \tag{3.11}$$

$$\frac{-\varepsilon_p}{1-\varepsilon_p} < m_4 < m_{4,max}(m_2, m_3)$$

$$= \frac{1}{2}\left\{\lambda_B + m_3 + b_B C_B^F (m_3 - m_2) - \sqrt{\left[\lambda_B + m_3 + b_B C_B^F (m_3 - m_2)\right]^2 - 4\lambda_B m_3}\right\} \tag{3.12}$$

Boundaries of the complete separation region in the (m_2, m_3) plane:

Straight line wr:

$$\left[\lambda_A - \omega_G\left(1 + b_A C_A^F\right)\right] m_2 + b_A C_A^F \omega_G m_3 = \omega_G(\lambda_A - \omega_G) \tag{3.13}$$

Table 1.2 (continued) Operating Conditions for the Complete Separation under the Equilibrium Theory. Constant Selectivity Langmuir Adsorption Isotherm. (Mazzotti et al, 1997)

Straight line wb:

$$\left[\lambda_A - \lambda_B\left(1 + b_A C_A^F\right)\right] m_2 + b_A C_A^F \lambda_B m_3 = \lambda_B\left(\lambda_A - \lambda_B\right) \tag{3.14}$$

Curve ra:

$$m_3 = m_2 + \frac{\left(\sqrt{\lambda_A} - \sqrt{m_2}\right)^2}{b_A C_A^F} \tag{3.15}$$

Straight line ab:

$$m_3 = m_2 \tag{3.16}$$

The coordinates of the intersection points are given by:

$$\text{Point a} \quad (\lambda_A, \lambda_A) \tag{3.17}$$

$$\text{Point b} \quad (\lambda_B, \lambda_B) \tag{3.18}$$

$$\text{Point r} \quad \left(\frac{\omega_G^2}{\lambda_A}, \frac{\omega_G\left[\omega_F\left(\lambda_A - \omega_G\right)\left(\lambda_A - \lambda_B\right) + \lambda_B \omega_G\left(\lambda_A - \omega_F\right)\right]}{\lambda_A \lambda_B\left(\lambda_A - \omega_F\right)}\right) \tag{3.19}$$

$$\text{Point w} \quad \left(\frac{\lambda_B \omega_G}{\lambda_A}, \frac{\omega_G\left[\omega_F\left(\lambda_A - \lambda_B\right) + \lambda_B\left(\lambda_B - \omega_F\right)\right]}{\lambda_B\left(\lambda_A - \omega_G\right)}\right) \tag{3.20}$$

with $\omega_G > \omega_F > 0$, which are given by the roots of the following quadratic equation:

$$\left(1 + b_A C_A^F + b_B C_B^F\right)\omega^2 - \left[\lambda_A\left(1 + b_B C_B^F\right) + \lambda_B\left(1 + b_A C_A^F\right)\right]\omega + \lambda_A \lambda_B = 0 \tag{3.21}$$

In the above equations, C_A^F and C_B^F are the feed concentrations of species A and B, respectively.

Table 3.3 *Operating Conditions for the Complete Separation under the Equilibrium Theory. Variable Selectivity Modified Langmuir Adsorption Isotherm. (Mazzotti et al, 1997)*

Isotherm Equation: $q_i^* = KC_i + \dfrac{\lambda_i C_i}{1 + b_A C_A + b_B C_B}$ where $i = A,B$ (3.22)

The complete separation region in the space spanned by the flowrate ratios m_j is obtained by shifting the one obtained in the m_j' space of a quantity equal to the value of the linear term coefficient K. Therefore:

$$m_j = m_j' + K \tag{3.23}$$

where m_j' are defined from equations (3.10) through (3.21).

3.3 The Concept of Separation Volume

In the previous section, the design problem of a TMB based on the equilibrium theory was presented for both linear and non-linear (Langmuir and extended Langmuir isotherms) systems. Constraints on the solid-fluid velocity ratios in the four TMB sections were stated by analytical expressions which implied complete separation (100% pure extract and raffinate). The basic assumption of these equilibrium-based models is that dispersion and mass transfer effects may be neglected. In practice, the non-ideality sources are accounted for by setting a safety margin β to the limiting (maximum or minimum) values of flowrate ratios defined by the equilibrium model.

In this section we shall discuss the effects of mass transfer limitations in the results given by the equilibrium theory. For the sake of simplicity, the analysis will be done for linear systems only, the non-linear systems following an analogous approach. The first concept to be questioned is that of "complete separation". Very often, 100% purity in both extract or raffinate is either unnecessary or would require an extremely large adsorbent inventory to be accomplished. Therefore, in this section, we will refer to "desired separation" instead of "complete separation", which may be as low as 90%. The detailed TMB model, as presented in Chapter 2, was used to shape areas of desired separation, as confronted with the complete

separation area defined by the equilibrium theory. The representation of the flowrate ratios which enable a given desired separation will be shown in 3-dimensional plots, instead of the classical 2-D plots. This way, the role of the four TMB/SMB sections may be more clearly understood.

For a mixture $A+B$ to be separated in a SMB or equivalent TMB, certain flow conditions for each of the species must be valid, as represented in Figure 2.2. If A is the more retained species and B, the weakly adsorbed one, these flow restrictions may be stated as follows:

$$\frac{Q_1' \times C_{A,1}}{Q_S' \times < q >_{A,1}} > 1 \tag{3.24}$$

$$\frac{Q_2' \times C_{A,2}}{Q_S' \times < q >_{A,2}} < 1 \quad \text{and} \quad \frac{Q_2' \times C_{B,2}}{Q_S' \times < q >_{B,2}} > 1 \tag{3.25}$$

$$\frac{Q_3' \times C_{A,3}}{Q_S' \times < q >_{A,3}} < 1 \quad \text{and} \quad \frac{Q_3' \times C_{B,3}}{Q_S' \times < q >_{B,3}} > 1 \tag{3.26}$$

$$\frac{Q_4' \times C_{B,4}}{Q_S' \times < q >_{B,4}} < 1 \tag{3.27}$$

with $Q_2' < Q_3'$. C and $< q >$ are the concentrations in bulk fluid phase and in the average adsorbed phase, respectively. Q_j' and Q_S' stand for the fluid flowrate in section j and solid flowrate in a TMB, respectively. For a system with linear adsorption isotherms, equivalent flow constraints as those stated by equations (3.5) through (3.8) may be written:

$$\nu K_A' < \gamma_1 < \infty \tag{3.28}$$

$$\nu K_B' < \gamma_2 < \gamma_3 < \nu K_A' \tag{3.29}$$

$$0 < \gamma_4 < \nu K_B' \tag{3.30}$$

where $\nu = (1-\varepsilon)/\varepsilon$ and $\gamma_i = \nu m_i$.

In a $\gamma_2 \times \gamma_3$ Cartesian space, this region corresponds to the triangle AWB, analogous to that shown in Table 3.1. The equilibrium model predicts that, for any values of γ_1 and γ_4 in accordance with equations (3.28) and (3.30), respectively, the region of separation in a $\gamma_2 \times \gamma_3$ plane will be constant and defined only by the solid/fluid volume ratio, ν, and the equilibrium constants. However, when mass transfer resistances are significant, the concentration in the stationary phase $< q >_{i,j}$ cannot be considered equal to the theoretical concentration in equilibrium with the bulk fluid phase $q^*_{i,j}$, as defined by the equilibrium isotherm. Therefore, the simplifications brought about in equations (3.24) through (3.27) are not valid and the separation region is expected to be different from that given by the equilibrium theory with new boundaries being dependent on mass transfer rate constants.

The dependency of flowrate constraints on mass transfer effects may be more clearly verified from a qualitative examination of a TMB simplified model. Let us consider the two sections where separation actually occurs, those are, sections 2 and 3, as shown in Figure 3.1. For the sake of simplicity, axial dispersion will be neglected and only one mass transfer resistance will be taken into consideration (simple LDF approximation to describe intraparticle mass transfer).

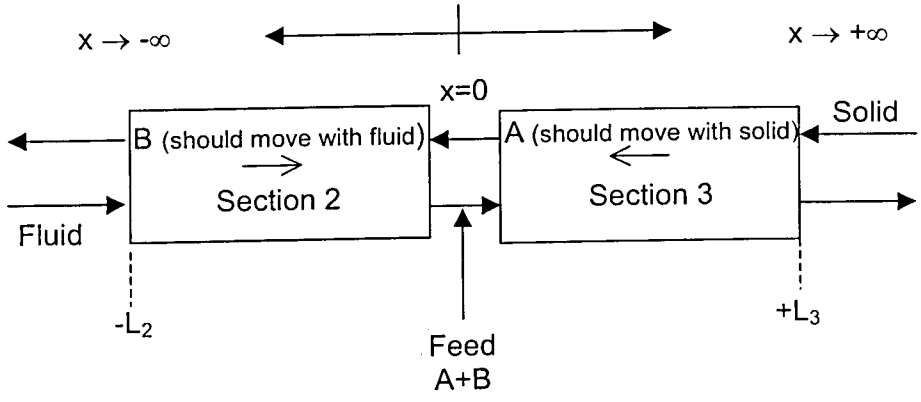

Figure 3.1 TMB sections 2 and 3 and relative motion of species A (more retained) and B (less retained)

The following equations are valid for a species *i* (linearly adsorbed) in a section *j* of a TMB at steady state:

$$\frac{dC_{i,j}}{dx} + \frac{\nu\alpha_{i,j}}{\gamma_j}\left(K'_i C_{i,j} - < q >_{i,j}\right) = 0 \qquad (3.31)$$

$$\frac{d<q>_{i,j}}{dx} + \alpha_{i,j}\left(K_i' C_{i,j} - <q>_{i,j}\right) = 0 \tag{3.32}$$

where $\alpha_{i,j} = \frac{k_{p_i} L_j}{U_S}$ and $<q>_{i,j} = \frac{\int_0^{R_p} q_{i,j}(R) R^2 dR}{\int_0^{R_p} R^2 dR}$

The analytical solution for the bulk fluid phase concentration is:

$$C_{i,j}(x) = c_1 + c_2 \exp\left(\frac{\alpha_{i,j}\left(\gamma_j - \nu K_i'\right)}{\gamma_j} x\right) \tag{3.33}$$

where c_1 and c_2 are integration constants, which may determined from the conditions at the boundaries. For section 2, for instance:

$$\text{At x=0,} \qquad C_{B,2}(0) = C_B^{SS} \tag{3.34}$$

$$\text{At x= -}\infty\text{,} \qquad C_{B,2}(-\infty) = 0 \tag{3.35}$$

For these boundary conditions, $c_1 = 0$ and $c_2 = C_B^{SS}$, so that:

$$C_{B,2}(x) = C_B^{SS} \exp\left(\frac{\alpha\left(\gamma_2 - \nu K_B'\right)}{\gamma_2} x\right) \tag{3.36}$$

For the sake of clarity, the subscripts for 'α' have been withdrawn. If $C_{B,2}(x)$ is evaluated at the boundaries, that is, at x=0 and x= -1, the following is true:

$$\Phi_{B,2} = \frac{C_{B,2}(x=0)}{C_{B,2}(x=-1)} = \exp\left(\frac{\alpha(\gamma_2 - \nu K_B')}{\gamma_2}\right) . \tag{3.37}$$

and solving for γ_2:

$$\gamma_2\big|^{min} = \frac{\alpha}{-\ln \Phi_{B,2} + \alpha} \nu K_B' = \frac{\alpha}{-\ln \Phi_{B,2} + \alpha} \gamma_2\big|_{eq}^{min} \tag{3.38}$$

An analogous analysis may be done for species A in section 3 since the equilibrium data for this component sets the upper limit of the region of separation in this section. In this case, the following boundary conditions apply:

$$\text{At x=0,} \qquad C_{A,3}(0) = C_A^{SS} \tag{3.39}$$

$$\text{At x=}\infty, \qquad C_{A,3}(\infty) = 0 \tag{3.40}$$

For these boundary conditions, $c_1 = 0$ and $c_2 = C_A^{SS}$, so that:

$$C_{A,3}(x) = C_A^{SS} \exp\left(\frac{\alpha\left(\gamma_3 - \nu K'_A\right)}{\gamma_3} x\right) \tag{3.41}$$

The profile of A in section 3 will be that of an exponential function of a negative number. If $C_{A,3}(x)$ is evaluated at the boundaries, that is, at $x = 0$ and $x = 1$, the following is true:

$$\Phi_{A,3} = \frac{C_{A,3}(x=0)}{C_{A,3}(x=1)} = exp\left(\frac{\alpha(\nu K'_A - \gamma_3)}{\gamma_3}\right) \tag{3.42}$$

and solving for γ_3:

$$\gamma_3\big|^{max} = \frac{\alpha}{ln\Phi_{A,3} + \alpha} \nu K'_A = \frac{\alpha}{ln\Phi_{A,3} + \alpha} \gamma_3\big|_{eq}^{max} \tag{3.43}$$

The equations refer to species B (weakly adsorbed component) in section 2 and species A (strongly adsorbed component) in section 3, which impose the relevant restrictions in these sections for separation to occur. To sum it up, for sections 2 and 3, in the presence of one mass transfer resistance

$$\gamma_2\big|^{min} = \frac{\alpha}{-\Theta_{B,2} + \alpha} \nu K'_B = \frac{\alpha}{-\Theta_{B,2} + \alpha} \gamma_2\big|_{eq}^{min} \tag{3.44}$$

$$\gamma_3\big|^{max} = \frac{\alpha}{\Theta_{A,3} + \alpha} \nu K'_A = \frac{\alpha}{\Theta_{A,3} + \alpha} \gamma_3\big|_{eq}^{max} \tag{3.45}$$

where $\gamma_2|_{eq}^{min}$ and $\gamma_3|_{eq}^{max}$ are the minimum and maximum bounds for γ_2 and γ_3 as given by the equilibrium model, respectively, and $\Theta_{i,j} = ln\Phi_{i,j}$. Depending on the value of $\Theta_{i,j}$, the new constraints may be greater or less than the value from the ideal model. For section 2, the fluid phase concentration of B at $x = 0$ should always be greater than at $x = -1$, so that $\Theta_{B,2} > 0$. The same is true for species A in section 3, so that the following are true:

$$\gamma_2|^{min} > \gamma_2|_{eq}^{min} \tag{3.46}$$

$$\gamma_3|^{max} < \gamma_3|_{eq}^{max} \tag{3.47}$$

When either mass transfer is too fast or the section length is infinitely long, $\alpha \rightarrow \infty$ and the flowrate constraints become those derived from the equilibrium theory.

In order to analyse the influence of mass transfer effects on the region of separation, the TMB model, as described in equations (2.21) to (2.39), was successively solved for several pairs (γ_2, γ_3) within the separation region defined by the equilibrium model. To reduce computational time, the steady-state form of the model was used by setting the time dependent terms $(\partial / \partial\theta)$ to zero and solving the remaining system of ODEs. The mass transfer effects on the flow restrictions of sections 1 and 4 were also examined. This was also done through numerical simulation in order to find a three dimensional separation ***volume*** in the parameter space $\gamma_1 \times \gamma_2 \times \gamma_3$, instead of a two-dimensional separation ***area*** in plane $\gamma_2 \times \gamma_3$. Two strategies were used to find these *separation volumes*, namely, strategy 1 and strategy 2. The objective of both strategies was to find the sets of operating points in a three-dimensional space which resulted in purities above 99% for both raffinate and extract streams. Both procedures were applied for a given fixed value of γ_4 lower than $\nu K_B'$, according to the pertinent equilibrium constraint.

For strategy 1, values of γ_1 were attributed from a minimum of $\nu K_A'$, from constraint equation (3.28), and gradually incremented according to the package user. For each value of γ_1, the steady state performance of the TMB or equivalent SMB was simulated for different values of γ_2 and γ_3 within the range of $\left[\nu K_B', \nu K_A'\right]$. Figure 3.2 shows the algorithm used for this strategy.

The column dimensions and model parameters are summarised in Table 3.4. The mixture fructose and glucose, having linear adsorption isotherms on cation exchange resin Amberlyte (d_p=320 μm), was used in the simulations. The procedure was performed for three values of γ_4 (0.155, 0.290 and 0.392), all of which obeyed the equilibrium constraint as given in equation (3.30).

Table 3.4 Model parameters and column dimensions used in the simulations to find the separation volume for a desired separation of a fructose-glucose separation (99% purity)

Model parameters	Operating conditions	Columns
$Pe = 2000$	T=20°C	$D_c = 2.6$ cm
$Bi_m = 500$	$C_i^F = 30$ g/l $i = F,G$	$L_c = 11.5$ cm
$k_p = 20$ min^{-1}	$t^* = 3.3$ min	Columns/section: 3
$k_\mu = 1.2$ min^{-1}	For equivalent TMB,	Section length =
$K_A' = K_{FR}' = 0.635$	$U_S = 3.48$ cm/min	34.5 cm
$K_B' = K_{GL}' = 0.314$	$\gamma_4 = 0.155, 0.290, 0.392$	$\nu = 1.5$
		$\varepsilon_p = 0.2$

The obtained regions of separation are shown in the plots of Figure 3.3 in a three-parameter space $(\gamma_1 \times \gamma_2 \times \gamma_3)$ for three different values of γ_4. The inclined plane represents the $\gamma_2 = \gamma_3$ plane. The minimum value shown on the γ_1 axis for all graphs corresponds to $\nu K_{FR}'$, that is, the equilibrium constraint value as given in equation (3.28). It is interesting to note that the regions of separation only occur at approximately γ_1=1.20, which is considerably greater than $\nu K_{FR}'$ (=0.95). Another evidence is that the regions of separation only have a constant size at γ_1 greater than 1.60. There is a kind of "transition region" ($1.20<\gamma_1<1.60$), in which the regions of separation have a varying size, probably dependent on the mass transfer effects. The figures also show that γ_4 does not affect significantly the size of the separation region, except in the "transition region".

For strategy 2, the same methodology as described in strategy 1 was applied, but $QBAL\,(=Q_F+Q_E=Q_R+Q_X)$ was incremented instead of γ_1. $QBAL$ stands for the total

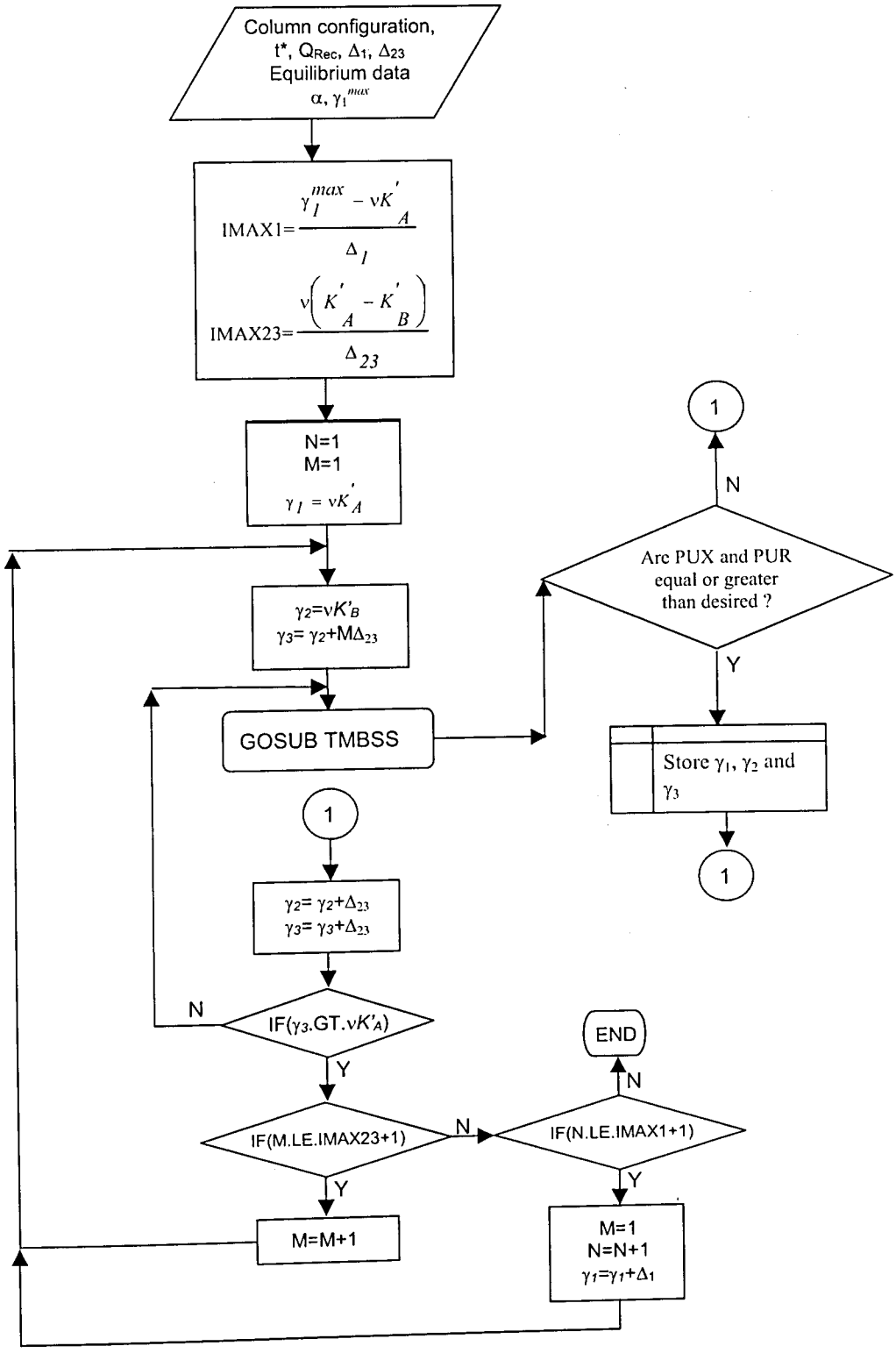

Figure 3.2 Flowsheet for strategy 1, used to find the 3-D parameter space for a desired separation of 99% for both extract and raffinate.

inlet or outlet flowrate. It is related to the velocity ratio in section 1, γ_1, by the following equation:

$$QBAL = \frac{\varepsilon V_c}{t^*}(\gamma_1 - \gamma_4 + \gamma_3 - \gamma_2) \tag{3.48}$$

where V_c is the volume of a column and t^* is the switching time of an equivalent SMB.

This strategy is actually equivalent to that described in the flowsheet shown in Figure 3.2, with $QBAL$ being incremented instead of γ_1. As there is a compromise between $QBAL$, γ_1, γ_2, γ_3 and γ_4, given by equation (3.48), both strategies 1 and 2 are expected to yield the same results. In order to compare the two strategies, the region of separation for γ_4= 0.290 was searched using the two procedures. The results would be difficult to compare in a 3-D plot since the third axis would stand for γ_1 in one graph and $QBAL$ in the other graph. In order to verify clearly the equivalence between the two strategies, some points obtained from strategy 1 were chosen so that the values of $QBAL$, calculated from equation (3.48), were equal to 11 ml/min. These selected points $(\gamma_1,\gamma_2,\gamma_3)$ were recorded. Accordingly, from the results obtained using strategy 2 for a constant value of $QBAL$=11 ml/min, points were selected so that the calculated value of γ_1 (from equation 3.48) were approximately the same as those γ_1 values recorded from strategy 1. These two sets of points were plotted in a $\gamma_2 \times \gamma_3$ plane shown in figure 9.7, together with the procedure involved in obtaining these points. It is clear that both strategies define the same separation area and either one may be used to design the operating conditions of a given SMB plant. Figure 9.8(a) shows the regions of separation found from both strategies in the same system of co-ordinates $(\gamma_1 \times \gamma_2 \times \gamma_3)$. The results obtained from strategy 1 are represented as a group of dark planes standing in a 90° angle with respect to the $\gamma_2 \times \gamma_3$ plane. For strategy 2, the results obtained for different $QBAL$ values are shown as light-coloured inclined planes. Geometrically, they are standing in a 45° angle with respect to the $\gamma_2 \times \gamma_3$ plane. Despite the more complicated representation, it is clear that both strategies convey the same information.

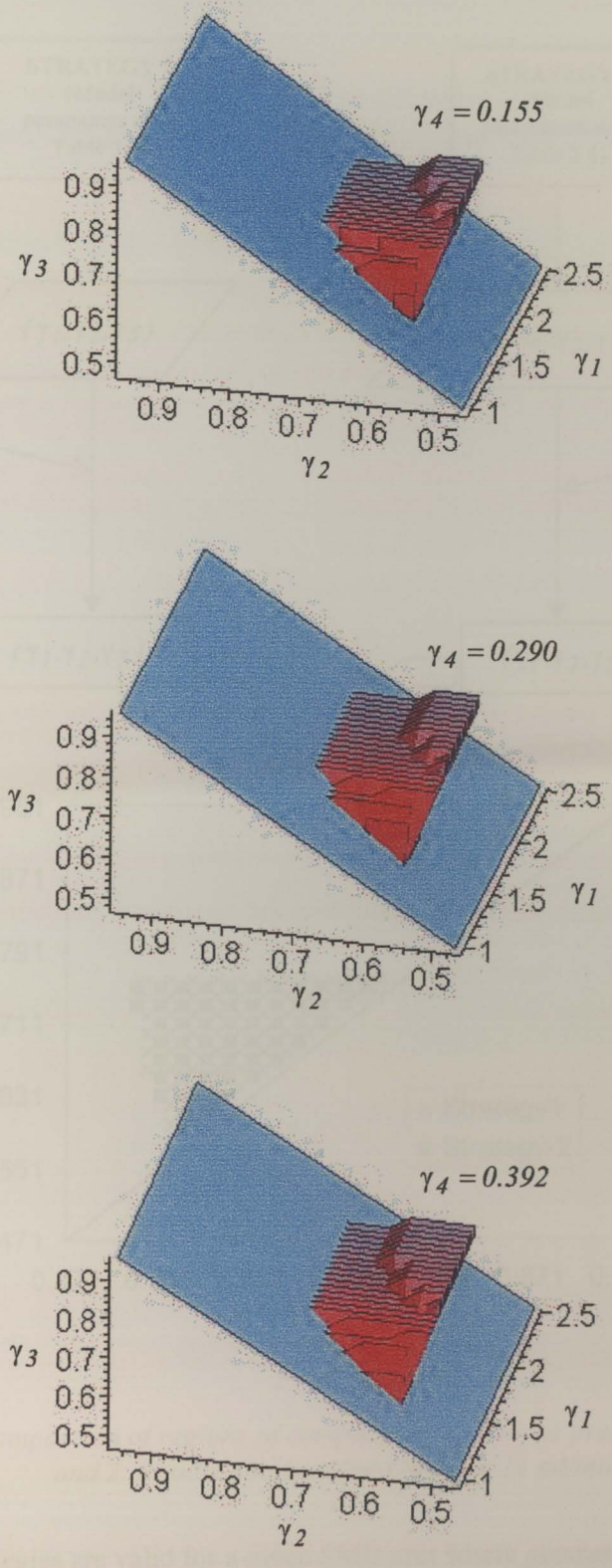

Figure 3.3 *"Separation volumes" for different values of γ_4. Simulation input parameters are those summarized in Table 3.4.*

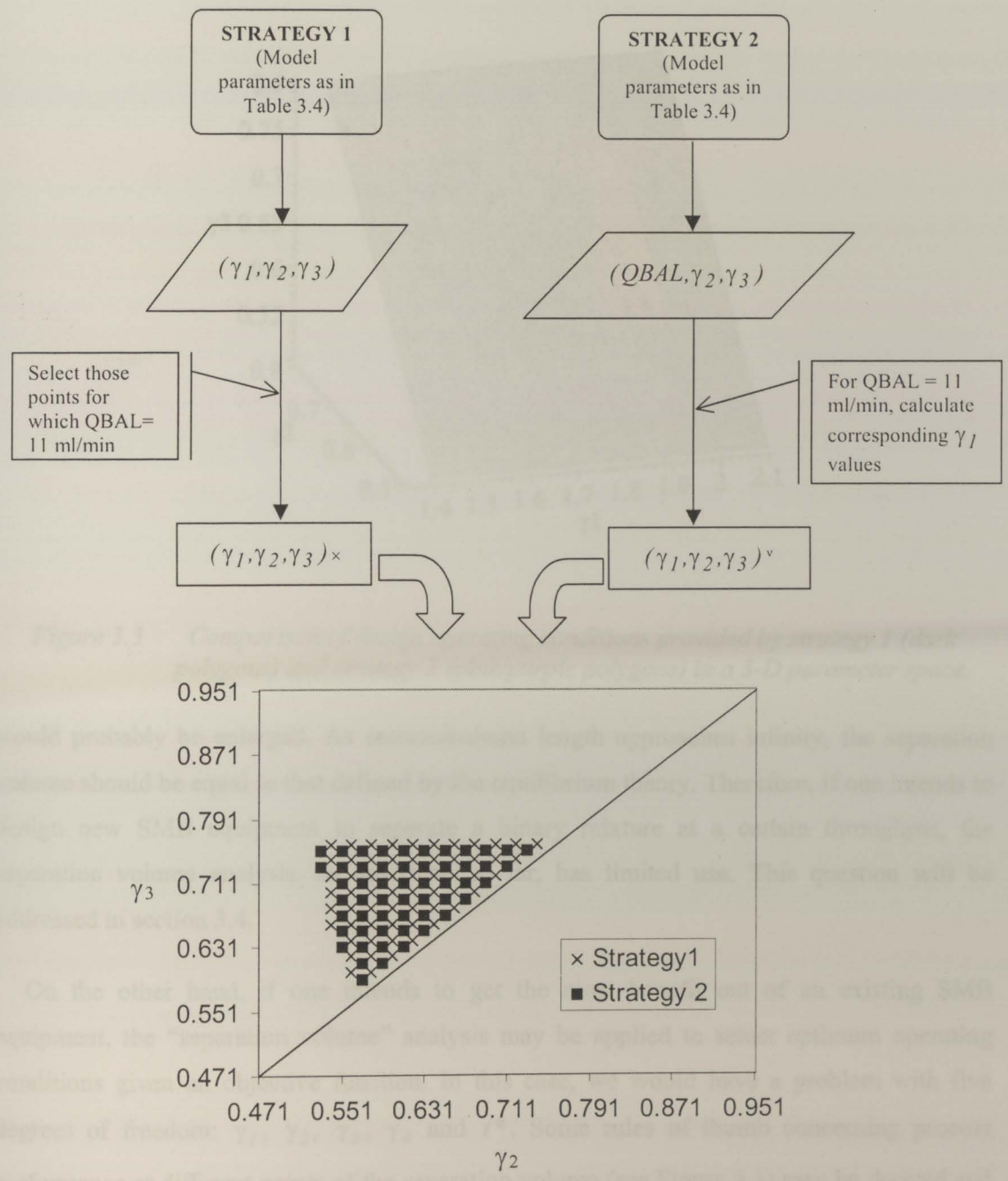

Figure 3.4 *Comparison of regions of complete separation as predicted from strategies 1 and 2. Results obtained for QBAL = 11 ml/min and γ_4=0.290.*

These strategies are valid for a given SMB unit where geometrical parameters, such as adsorbent particle size, column length and cross section, are fixed. Using the 3-D separation plots, it is possible to foresee the mass transfer effects on the performance of given equipment. In the examples illustrated, if column length were increased, separation volumes

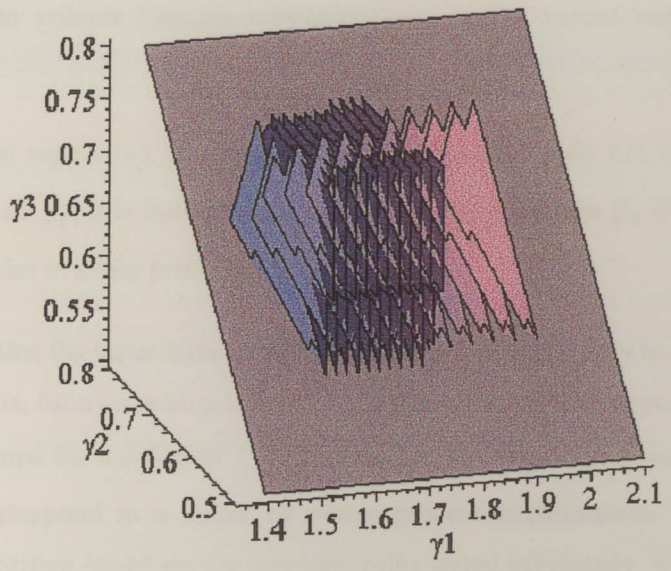

Figure 3.5 Comparison of design operating conditions provided by strategy 1 (dark polygons) and strategy 2 (pink/purple polygons) in a 3-D parameter space.

would probably be enlarged. As section/column length approaches infinity, the separation volume should be equal to that defined by the equilibrium theory. Therefore, if one intends to design new SMB equipment to separate a binary mixture at a certain throughput, the separation volume analysis, as described so far, has limited use. This question will be addressed in section 3.4.

On the other hand, if one intends to get the most benefit out of an existing SMB equipment, the "separation volume" analysis may be applied to select optimum operating conditions given an objective function. In this case, we would have a problem with five degrees of freedom: γ_1, γ_2, γ_3, γ_4 and t^*. Some rules of thumb concerning process performance at different points of the separation volume (see Figure 3.3) may be derived and stated as follows:

- Operation of the SMB close to or at the vertex of the "triangles" means achieving the highest productivities for given γ_1 and γ_4 values.

- It is most convenient to operate at the threshold value of γ_1 (where the cross sections of the separation volume become constant) since higher values imply in more diluted products.

- Although the separation volumes depicted in Figure 3.3 do not change much for the given values of γ_4, it is intuitive that the lowest safety margin β_4 ($\gamma_4 = \gamma_4^{eq}/\beta_4$) should be used in order to avoid product dilution.

Note also that the separation volumes in Figures 3.3 apply only to the conditions stated in Table 3.4, that is, for a switching time of 3.3 minutes. A different separation volume would probably be obtained for a different t^*. Furthermore, the threshold point where γ_1 becomes constant may correspond to a better or worse process performance. Therefore, we have developed an algorithm based on the heuristic rules stated previously. The main objective is to find the most adequate switching time and the minimum safety factors β_1 and β_4, which maximize productivity and minimize solvent consumption for a given equipment configuration (number and dimensions of columns fixed) provided a given constraint on product purity is satisfied.

Having set the column dimensions, distribution in sections and a switching time t*, the algorithm firstly assumes $\gamma_4 = \nu K_{GL}$ or β_4=1. Then, it searches for the vertex of the separation regions $\gamma_2 \times \gamma_3$ for each value of γ_1, starting from β_1=1. The objective is to find the maximum feed flowrate attainable at the lowest value of γ_1. This point corresponds to the threshold value of γ_1 above which the cross section of the separation volume is constant. The same procedure is repeated for decreasing values of γ_4, or by increasing β_4. Both the size and the number of increments to be implemented on γ_1 and γ_4 are set by the user of the design package. At the end, a set of data $(\gamma_1,\gamma_2,\gamma_3,\gamma_4,Q_F,<Pr>,<SC>)$ will be obtained for increasing β_4, or decreasing γ_4. The flowsheet of the design/optimization algorithm is shown in Figure 3.6. An optimal operating point is then chosen as that for which the feed flowrate is maximum at minimum β_4. As expected, this point corresponds to the minimum solvent consumption of the set.

The procedure described in the previous paragraph leads to the optimized operation of a SMB for a given switching time t*. The initial guess of t* may be made based on pressure

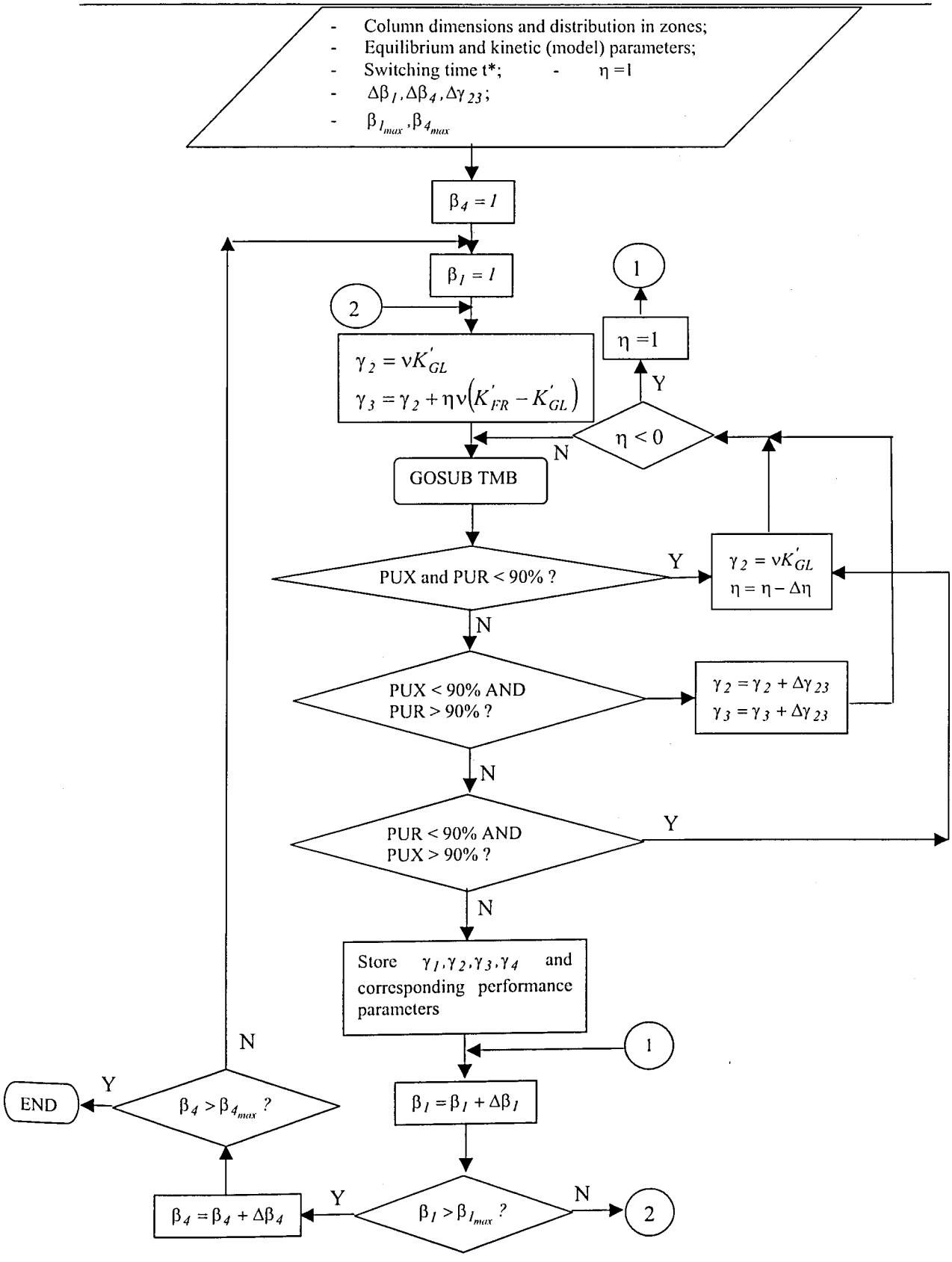

Figure 3.6 Flowsheet of the design algorithm based on the methodology of separation volume.

drop considerations or pumping limitations applied to section 1 (where flowrate is highest). Our choice was based on experimental work (see Chapter 4). For the separation system (sugars and cationic resin) and equipment (Licosep12-26, Novasep) examined in this work, mass transfer resistance is a major source of column HETP and pressure drop considerations are not applicable. The algorithm may be applied for other values of t*. The optimal operating points obtained from this algorithm for various t* may be compared in terms of productivity and solvent consumption in order to choose the most appropriate switching time for that plant.

The equipment being designed is a pilot unit Licosep 12-26 (by Novasep, France) comprising 12 columns (3 per section) with a length of 29 cm and 2.6 cm internal diameter each. The assumed section subdivision was 3-3-3-3. Table 3.5 illustrates the type of output produced by the design algorithm. For each group of constant γ_4, it may be observed that the feed flowrate increases with increasing γ_1 up to a certain point. A row is selected from each group of constant γ_4 corresponding to the point of maximum Q_F for minimum γ_1. By comparing the selected rows, one verifies that higher feed flowrates may be treated by the SMB as the safety margin on γ_4 is increased until a constant value is reached. This point is taken as the optimal operating condition for that given switching time (3.3 minutes). Note that it also coincides with the point of minimum solvent consumption.

The same type of data as that shown in Table 3.5 was obtained for different switching times t*. Tested switching times were 2.0, 2.5, 3.0, 3.2, 3.3, 3.4, 3.6, 4.0, 4.5 and 5.0 minutes. Figure 3.7 compares the different performance calculated for the optimized conditions obtained at each of these values of t*. The performance criteria are the average adsorbent productivity $<Pr_i>$ and solvent consumption $<SC_i>$. The lines in both plots are smooth curves drawn to evidence trends. In Figure 3.7(a), it may be observed that the adsorbent productivity tends to be maximum and constant for switching times lower than 3 min. On the other hand, the respective solvent consumption increases in a much steeper fashion for t^* below 3 min. This indicates that a best trade-off in performance may be achieved when the SMB is operated at $3.2 \leq t^* \leq 3.6$ min, as indicated in the plots. In plot (b), the corresponding maximum feed flowrates attained for each switching time are shown. As the switching time is reduced, a higher feed flowrate may be treated. However, for $t^* < 3$ min, the increase in feed flowrate and productivity is marginal whereas the solvent consumption peaks up. Accordingly, for $t^* > 3.6$ min, the maximum attainable throughput is significantly reduced but the solvent consumption decreases only marginally.

Table 3.5 Output of the design algorithm for t=3.3 min*

γ_1	γ_2	γ_3	γ_4	Q_F (ml/min)	$<Pr_i>$ (kg/m^3/hr)	$<SC_i>$ (l/kg)
0.795	0.445	0.635	0.405	3.546	6.913	84.74
0.845	0.425	0.695	0.405	5.039	9.828	72.97
0.895	0.425	0.715	0.405	5.412	10.624	74.16
0.945	0.425	0.735	0.405	5.786	11.363	75.56
0.995	0.425	0.735	0.405	5.786	11.418	79.62
1.045	0.425	0.755	0.405	6.159	12.087	81.07
1.095	0.425	0.755	0.405	6.159	12.111	85.08
1.145	0.425	0.755	0.405	6.159	12.125	89.14
1.195	0.425	0.755	0.405	6.159	12.135	93.23
1.245	0.425	0.755	0.405	6.159	12.141	97.34
0.795	0.425	0.635	0.386	3.919	7.708	81.16
0.845	0.405	0.695	0.386	5.412	10.598	71.42
0.895	0.405	0.715	0.386	5.786	11.401	72.59
0.945	0.405	0.735	0.386	6.159	12.144	73.70
0.995	0.405	0.735	0.386	6.159	12.203	77.75
1.045	0.405	0.755	0.386	6.532	12.875	79.19
1.095	0.405	0.755	0.386	6.532	12.900	82.95
1.145	0.405	0.755	0.386	6.532	12.917	86.75
1.195	0.405	0.755	0.386	6.532	12.928	90.58
1.245	0.405	0.755	0.386	6.532	12.935	94.44
0.795	0.405	0.635	0.368	4.292	8.407	78.92
0.845	0.405	0.695	0.368	5.412	10.681	72.53
0.895	0.385	0.715	0.368	6.159	12.063	71.75
0.945	0.385	0.735	0.368	6.532	12.812	73.07
0.995	0.385	0.755	0.368	6.905	13.506	74.55
1.045	0.385	0.755	0.368	6.905	13.548	78.05
1.095	0.385	0.755	0.368	6.905	13.575	81.61
1.145	0.385	0.755	0.368	6.905	13.583	85.28
1.195	0.385	0.755	0.368	6.905	13.595	88.92
1.245	0.385	0.755	0.368	6.905	13.604	92.58
0.795	0.405	0.635	0.352	4.292	8.442	80.51
0.845	0.385	0.695	0.352	5.786	11.290	71.83
0.895	0.385	0.715	0.352	6.159	12.100	72.86
0.945	0.385	0.735	0.352	6.532	12.856	74.08
0.995	0.385	0.755	0.352	6.905	13.552	75.50
1.045	0.385	0.755	0.352	6.905	13.594	78.98
1.095	0.385	0.755	0.352	6.905	13.612	82.58
1.145	0.385	0.755	0.352	6.905	13.631	86.17
1.195	0.385	0.755	0.352	6.905	13.643	89.79
1.245	0.385	0.755	0.352	6.905	13.652	93.43

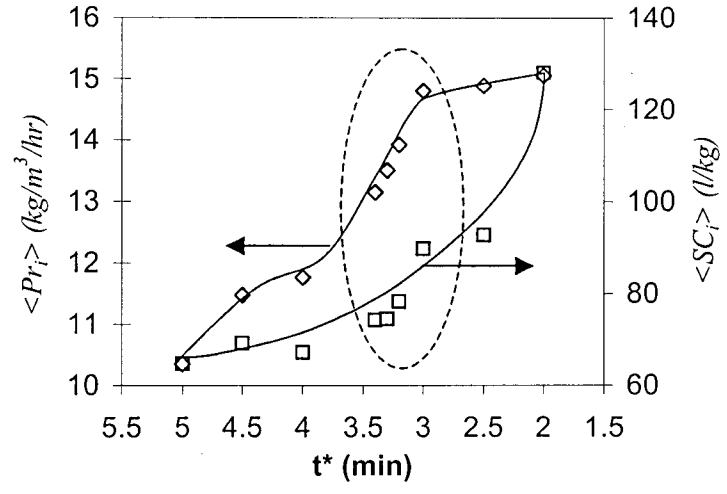

(a)

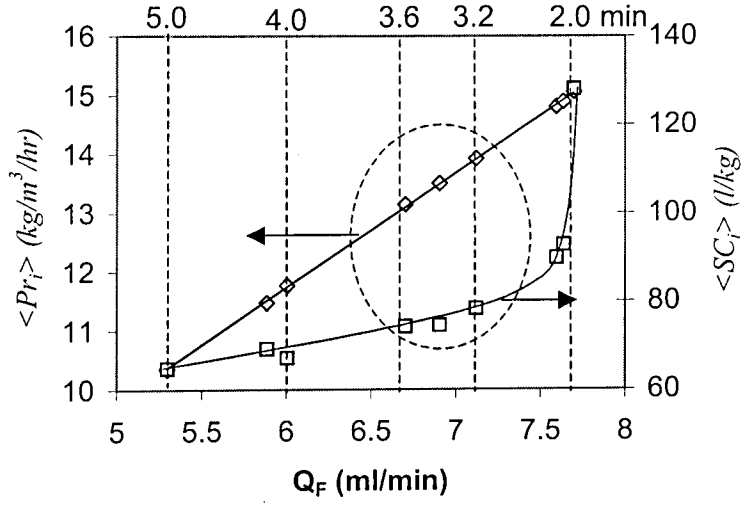

(b)

Figure 3.7 *Optimal performance (productivity and solvent consumption) obtained for different switching times (a) and their respective (maximum) feed flowrate (b)*

Note that the optimal (γ_2,γ_3) pair is (0.385,0.755) in all cases studied in the range 3<t*<4 min. The restriction on γ_2 is slightly violated, which may be attributed to the contamination of 10% allowed for both products. The design problem was repeated for t*=3.2 min and increased column lengths of 40 and 50 cm (plots not shown). All optimized parameters were the same, except for the maximum attainable feed flowrates, which are higher due to the increased adsorbent inventory available.

3.4 Design of Optimal Construction and Operating Parameters for a SMB Adsorber

The design package proposed herein after aims to determine the column dimensions (length and section) and operating conditions that allow a desired purity in the outlet streams with maximum adsorbent productivity and without exceeding given pressure drop limits imposed by the packing material. The number of degrees of freedom in the design problem is, therefore seven: column length and diameter, switching time and the four section velocity ratios γ_j. The optimisation algorithm to be applied is an extension of that developed by Biressi *et al* (2000). However, instead of using a model of equilibrium stages, we have used a detailed TMB steady-state model, as described in Chapter 2.

The flow constraints as stated for an equilibrium model, equations (3.28), (3.29) and (3.30), have been used as general guidelines to provide an initial guess for γ_j. The other pieces of information to be used in our design/optimisation algorithm are:

- A correlation to estimate pressure drop in packed beds, such as the Kozeny-Kárman equation:

$$\frac{\Delta P}{L_c} = 150\frac{(1-\varepsilon)^2}{\varepsilon^3 d_p^2}\mu\upsilon \qquad (3.49)$$

- The detailed TMB model, as proposed in Chapter 2, together with the equivalence relations between a TMB and a SMB (see Table 2.1).

As a first step of the optimisation procedure, the following three assumptions are made:

i. The SMB flowrate in section 1, Q_1, is taken to be 10^3 ml/min, and all other flowrates and column cross section are calculated having this value in mind. After the algorithm calculations are finished, a scale parameter Ω is obtained as the ratio between the desired feed flowrate and the calculated feed flowrate with Q_1=10^3 ml/min, that is, $\Omega = Q_F$ (desired)$/Q_F(Q_1 = 10^3$ ml/min$)$. All other calculated flowrates and section area

may be multiplied by the scale factor to obtain the values necessary to process the desired feed flowrate. Calculated γ_j and L_c values remain unchanged.

ii. Since pressure drop is proportional to the throughput of the plant, we expect that the productivity will be the highest when pressure drop is the highest possible in the plant. Therefore, we set pressure drop in section 1, which is where the fluid velocity is maximum, equal to the allowable upper limit, hence fixing the value of the product $\upsilon_1 \times L_c$ from equation (3.49).

iii. From the adsorption isotherms and using a certain safety margin β, it is possible to predict *a priori* the values of γ_1 and γ_4 which guarantee the proper behaviour of sections 1 and 4, that is, complete regeneration of the adsorbent and eluent, respectively. β is an input parameter to the algorithm so that $\gamma_1 = \beta \times \gamma_1^{eq}$ and $\gamma_4 = \gamma_4^{eq} / \beta$. Design results for different values of β are analysed.

From the items described above, Q_1, $\upsilon_1 \times L_c$, γ_1 and γ_4 are defined. Three from the initially seven degrees of freedom of the design problem are left to be defined: the column length and the velocity ratios γ_2 and γ_3. To define the most adequate values for these variables, an optimisation algorithm is proposed having product purities as constraints. The objective function is adsorbent productivity, which should be maximised. Product purity and adsorbent productivity have been defined in the beginning of this Chapter by equations (3.1) and (3.4), respectively.

The parameter η will be used in the algorithm and is defined as the dimensionless distance of a certain (γ_2, γ_3) pair to the optimum point given by the equilibrium $\left(\nu K_B', \nu K_A'\right)$. In other words:

$$\eta = \frac{\gamma_3 - \gamma_2}{\gamma_3^{eq} - \gamma_2^{eq}} = \frac{\gamma_3 - \gamma_2}{\nu\left(K_{FR}' - K_{GL}'\right)} \tag{3.50}$$

For each value of η, within a certain range defined by the user, the algorithm manages to find the minimum column length and γ_2, which lead to the required product purities. For a given value of η, the algorithm starts with the minimum γ_2 value defined by the equilibrium

theory $\left(\nu K_B'\right)$ and a sufficiently small value for L_c. All information required by the TMB model is available by then and process performance is calculated. Depending on the values of the constraining parameters (product purities), the algorithm makes one of the following decisions:

- Increase column length;
- Increase/decrease γ_2;

The flow sheet describing the decision-making process of the algorithm is shown in Figure 3.8. With the data stored by the design package, plots of η versus column length and adsorbent productivity are constructed. The value of η which maximises productivity is chosen as the adequate operating point. It defines the optimum column length and the scale factor Ω. Multiplying the obtained section area and flowrates by Ω, one is able to re-scale all necessary operating conditions for any desired throughput.

This procedure was applied to the separation of fructose-glucose mixtures under the following conditions:

- Concentration of each sugar = 400 g/l;
- Viscosity = 3 cP;
- Specific mass = 1260 kg/m^3
- Maximum pressure drop = 10 bar/column, 25% of which being due to the column packing itself and 75% being due to piping and fittings connecting columns;
- Adsorbent: Dowex Monosphere 99/Ca, d_p = 320 μm;
- Linear isotherms with K_{GL}'=0.27 and K_{FR}'= 0.53;
- T=50°C;
- 12 columns;
- Purity constraint = 99% for both extract and raffinate;

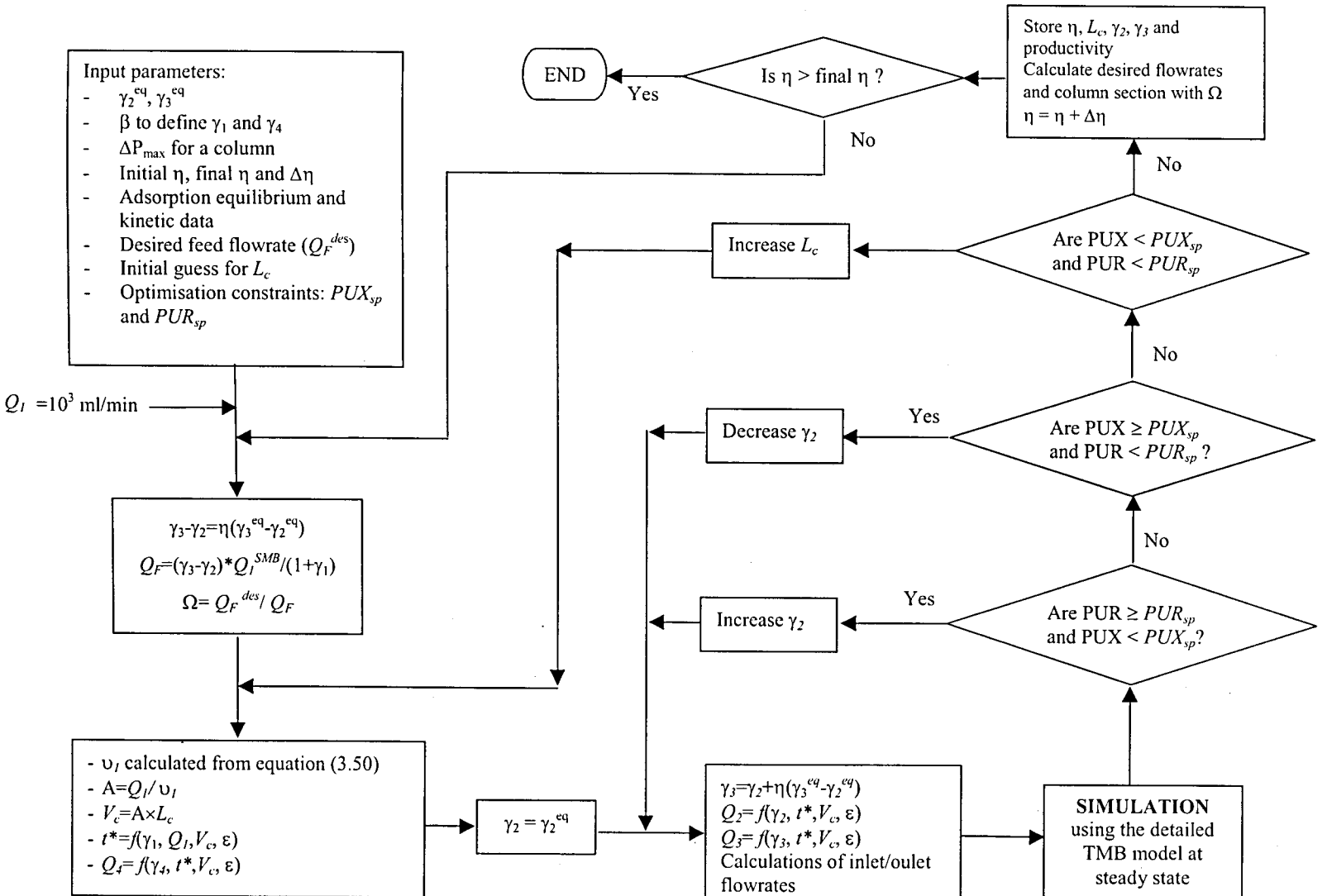

Figure 3.8 Flowsheet describing decision-making process of design algorithm

The results obtained from the design algorithm will be presented as plots showing the minimum column length and adsorbent productivity as a function of parameter η. This parameter is intrinsically related to the amount of feed being treated, that is, the required throughput. Figure 3.9 illustrates the results obtained for increasing safety margins β, so that $\gamma_1 = \beta \times \nu K'_{FR}$ and $\gamma_4 = \nu K'_{GL}/\beta$ were assumed in each case. The degree of subdivision was considered, *a priori*, as 3 columns per section. The axis $<PR_i>$ stands for the average adsorbent productivity calculated from the values of PR_X and PR_R, as defined in equation (3.4). It is clear that an increasing adsorbent inventory becomes necessary as the SMB adsorber is required to treat greater throughputs. This is shown by the rise in the values of L_c obtained, which is initially slow and then becomes steep for $\eta > 0.8$. This may indicate that it is wise to avoid operating a SMB plant close to the theoretical maximum throughput (η=1) because a very large adsorbent inventory would be required. This is further confirmed by the fact that the packing is inefficiently used under this condition. In all plots, the average adsorbent productivity reaches a maximum value at η around 0.6 to 0.7 and it declines abruptly thereafter.

With regard to the effect of the safety margin β, the design algorithm results confirm that shorter columns, or smaller adsorbent inventory, are required as this parameter is increased. The adsorbent productivity also tends to increase for higher values of β. For the sake of comparison, the optimal column length was selected for each value of β as that for which productivity is maximum. Figure 3.10 shows the optimal column lengths as a function of the average adsorbent productivity ($<PR_i>$) and the average solvent consumption ($<SC_i>$). The numbers in the plot stand for the respective values of β. The solvent consumption increases steadily as the safety margin is increased with a steep rise for β>1.3. The adsorbent productivity reaches a new peak at the very same value of β. Therefore, for the present case, the parameters calculated for β=1.3 define the optimal operating conditions for a SMB adsorber with 3 columns per section given a required minimum purity of 99%.

Another interesting point is raised when confronting the optimal (γ_2,γ_3) pairs obtained for each value of η. Figure 3.11 shows the path of points in a $\gamma_2 \times \gamma_3$ parameter space for increasing values of the safety margin β. All "paths" converge to the point

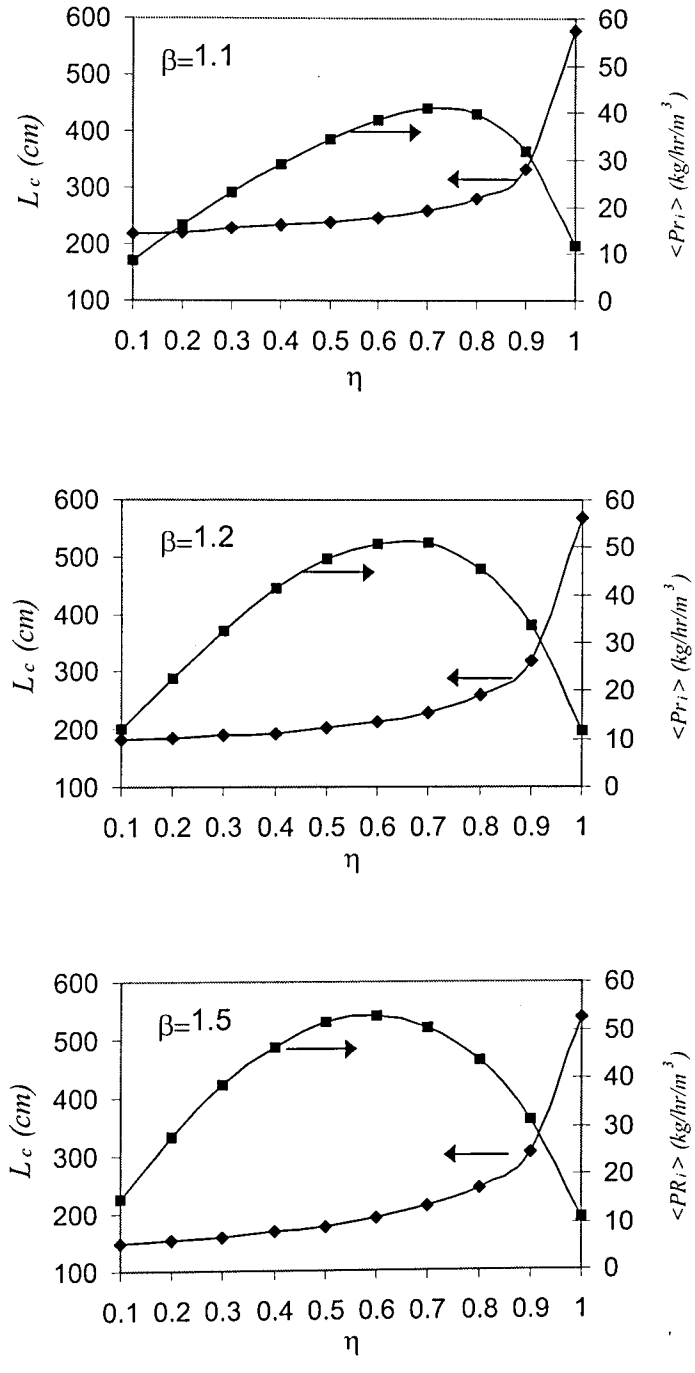

Figure 3.9 Minimum column lengths and corresponding average productivities as a function of required throughput (η) for different safety margins (β) imposed on sections 1 and 4

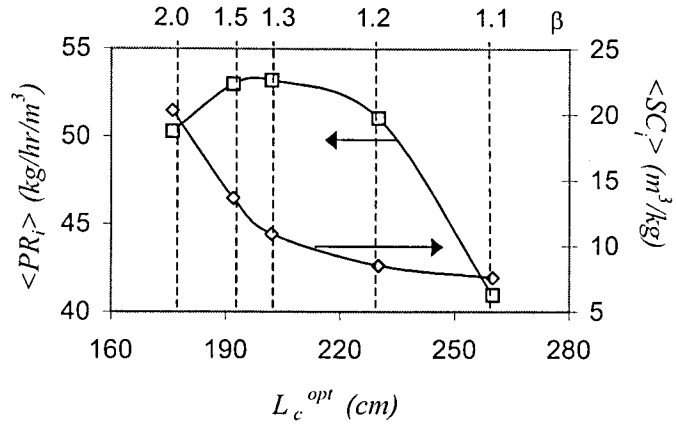

Figure 3.10 Comparison of optimal column length and respective productivity and solvent consumption for different values of parameter β

($\nu K'_{GL}, \nu K'_{FR}$), which is the optimal operating point as predicted by the equilibrium theory. However, from the standpoint of adsorbent productivity, the design algorithm using a detailed model indicates that the optimal operating point is located at η=0.7, rather than at η=1.

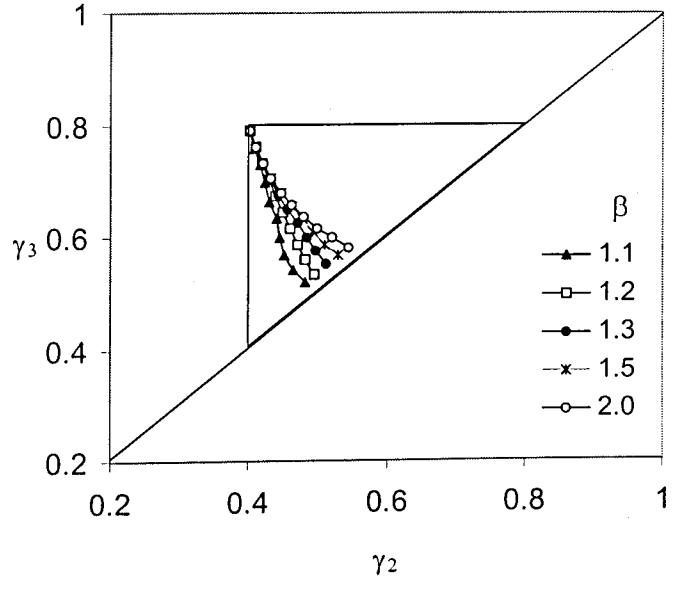

Figure 3.11 Path of optimal operating points in a $\gamma_2 \times \gamma_3$ *parameter space for different safety margins* β.

The same analysis carried out previously was applied to the following SMB column subdivisions: 4-3-3-2; 3-4-3-2 and 3-3-4-2. The purity constraint was kept at 99% and $\beta=1.1$. Little deviations were observed by changing the relative length of the sections. Figure 3.12 shows the results obtained for minimum column length and corresponding productivity, where the lines join the points obtained for the same value of η. Some productivity enhancement is obtained when the size of section 4 is reduced in favour to sections 1 and 3. Yet, the maximum productivity obtained for this configuration is inferior to that obtained for $\beta=1.3$ and 3 columns per section.

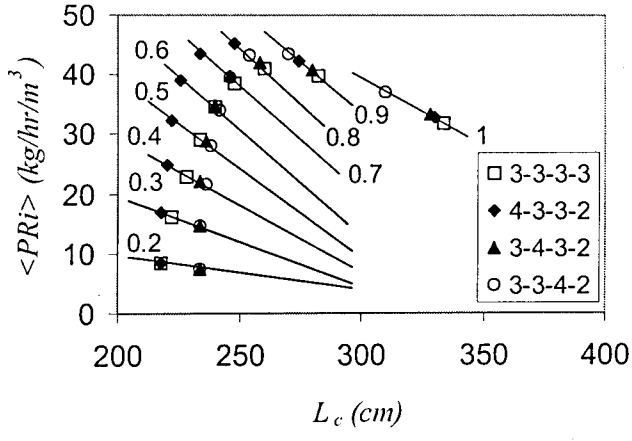

Figure 3.12 Minimum columns lengths and respective productivities obtained for different number of columns per section. Numbers inside plot indicate values of η

Finally, the effect of the requirement on product purity was investigated. For a SMB with 3 columns per section and $\beta=1.3$, the design algorithm was applied for the following minimum product purities: 99.9%, 99%, 95%, 90% and 80%. Figure 3.13 shows the obtained plots of the minimum column lengths (a) and respective productivity (b) as a function of η.

It is interesting to note that, for both plots, the curves obtained for purity requirements below 90% become identical. As lower purities are demanded, the required column length decreases and the adsorbent is more efficiently used. The maximum productivities are obtained for a minimum purity of 90% and no further improvement is obtained with respect to this criterion, even if the constraint is relaxed to 80%, for instance. The same may be said of the minimum column length mandatory to meet a given purity requirement. At 90% requisite purity, a "bottom line" for the column length is found. For the case of glucose-fructose

separation, this is an interesting finding since 90% fructose is a standard concentration for HFCS (high fructose corn syrup). Another commercial standard, 55% HFCS may be obtained by blending 90% HFCS with the raffinate product. Hence, it may not be worth operating a SMB to obtain 99% pure products, if these are mainly intended for use as sweetener syrups.

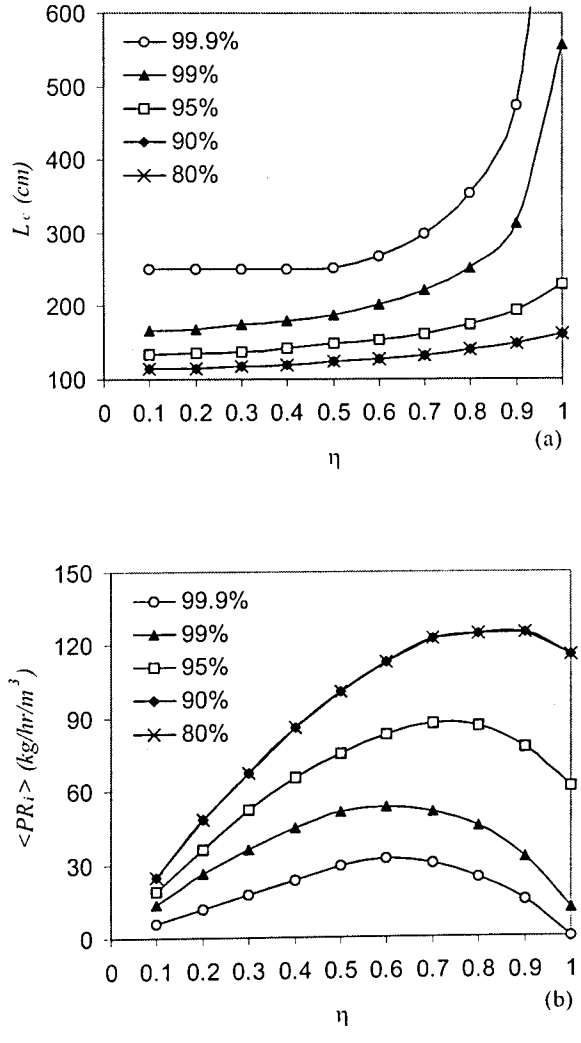

Figure 3.13 Design algorithm results showing the effect of minimum purity required.

3.5 Conclusions

In this Chapter, a package to design the operating conditions of a given SMB plant was presented under the concept of "Separation Volume". The regions of separation in terms of the flowrate ratios in the different SMB sections were plotted in a 3-D parameter space. This way the role of section 1 became more evident in systems with significant mass transfer

effects, that is, for columns with a low number of theoretical stages. For the separation of fructose-glucose solutions using ion-exchange resins, resistance to mass transfer is a major factor in column HETP. By using the separation volume concept, it was possible to predict that a relatively large safety margin β_1 was necessary for section 1 to accomplish the task of adsorbent regeneration. For the simulated equipment dimensions, the separation regions were much narrower than those predicted from the equilibrium theory. The concept of separation volume was generalized in a design algorithm for the purpose of design and optimization of a given SMB plant. By using heuristic rules, it was possible to identify the minimum safety factors in sections 1 and 4, which correspond to a maximum throughput of the plant. Thus, the concept of separation volume may provide a useful way of designing operating conditions of existing SMB equipment.

A design package to define construction and operating parameters of a SMB unit was also described by adapting and improving a previously proposed algorithm. The results were further used for optimization purposes. For a linear system, it has been demonstrated that SMB units operate inefficiently at the vertex of the equilibrium triangle (vK'_B, vK'_A), which is the optimum operating point in the frame of the equilibrium theory. Maximum productivity is achieved at $0.6<\eta<0.8$. A safety margin of 1.3 was found to be ideal in order to obtain optimal performance in terms of adsorbent productivity. Changes in the relative size of one section to another do not significantly alter the obtained results. Superior productivity may eventually be obtained by decreasing the size of section 4 in favour of section 1 or 3. For decreasing purity requirements, required column lengths become shorter and the obtained productivity is higher. The bottom line for these trends was found when the required product purity comes to as low as 90%. A lower constraint on purity does not produce either further improvement in productivity nor a decrease in column length.

3.6 References

D. C. S. Azevedo, A. E. Rodrigues, "Design of a Simulated Moving Bed in the Presence of Mass-Transfer Resistances", *AIChE J.* **45**, 956-966 (1999).

G. Biressi, O. Ludemann-Hombourger, M. Mazzotti, R.-M. Nicoud, M. Morbidelli, "Design and Optimisation of a SMB Unit: Role of Deviations from Equilibrium Theory", *J. Chromatography A* **876**, 3-15 (2000).

F. Charton, R.-M. Nicoud, "Complete Design of a Simulated Moving Bed", *J. Chromatography A* **702**, 97-12 (1995).

C. B. Ching, D. M. Ruthven, "Experimental Study of a Simulated Counter-Current Adsorption System - III. Sorbex Operation", *Chem. Eng. Sci.* **40**, 1411-1417 (1985).

S. Lehoucq, D. Verhève, A. V. Wouwer, E. Cavoy, "SMB Enantioseparation: Process Development, Modeling and Operating Conditions", *AIChE J.* **46**, 247-256 (2000).

O. Ludemann-Hombourger, M. Bailly, R. M. Nicoud, "Design of a Simulated moving bed: Optimal Particle Size of the Stationary Phase", *Sep. Sci. & Technol.* **35**, 1285-1305 (2000).

M. Mazzotti, G. Storti, M. Morbidelli, "Robust Design of Countercurrent Adsorption Separation: 3. Nonstoichiometric Systems", *AIChE J.* **42**, 2784-2796 (1996).

M. Mazzotti, G. Storti, M. Morbidelli, "Optimal Operation of Simulated Moving Bed Units for Nonlinear Chromatographic Separations", *J. Chromatography A* **769**, 3-24 (1997).

M. Migliorini, A. Gentilini, M. Mazzotti, M. Morbidelli, "Design of Simulated Moving Bed Units under Nonideal Conditions", *Ind. Eng. Chem. Res.* **38**, 2400-2410 (1999).

R.-M. Nicoud, "The Simulated Moving Bed: A Powerful Chromatographic Process", *LC-GC Intl.* **5**, 43-47 (1992).

L. S. Pais, J. M. Loureiro, A. E. Rodrigues, "Modeling, Simulation and Operation of a Simulated Moving Bed for Continuous Chromatographic Separation of 1,1'-bi-2-naphtol Enantiomers", *J. Chromatography A* **827**, 215-233 (1997).

L. S. Pais, J. M. Loureiro, A. E. Rodrigues, "Separation of Enantiomers of a Chiral Epoxide by Simulated Moving Bed Chromatography", *J. Chromatography A* **827**, 215-233 (1998).

H.-K. Rhee, R. Aris, N. Amundson, "Multicomponent Adsorption in Continuous Countercurrent Exchangers", *Phil. Trans. Roy. Soc. London* **A269**, 187-205 (1971).

G. Storti, M. Mazzotti, M. Morbidelli, S. Carrá, "Robust Design of Binary Countercurrent Adsorption Separation Processes", *AIChE J.* **39**, 471-492 (1993).

4. Operation of a SMB Adsorber

4.1 Introduction

This Chapter describes the experimental work performed with respect to the separation of fructose-glucose mixtures by simulated moving bed chromatography. Experimental results are shown to support the concept of separation volume and illustrate some of the findings from the previous chapters. In section 4.2, we recapitulate the materials and methods employed in order to determine experimentally the pertinent parameters required for the process models formulated in Chapter 2. Section 4.3 shows experimental data for the separation of glucose from fructose using a simulated moving-bed (SMB) pilot plant. A design procedure based on the concept of "Separation Volume" was applied so as to overcome the inherent strong mass transfer resistance present in ion-exchange resins. The fluid/solid velocity ratios in SMB sections 1,2 and 3 leading to at least 90% product purity were pursued by simulation and plotted in a 3-D parameter space. The design methodology also took into consideration the geometric parameters and allowable working flowrates, temperature and pressure of the plant. Operating conditions obtained from this procedure were used to operate the SMB unit and the expected performance was achieved experimentally. Simulation strategies based on a true countercurrent (TMB) and a real simulated moving bed (SMB) were used and either predicted performance agreed well with experimental data.

4.2 Fundamental Experimental Data for Fructose-Glucose Separation

The process model parameters were all determined by performing experiments with the packed columns to be used in the SMB pilot plant. A set of twelve Superformance® glass columns SP 300x26 (Götec Labortechnik, Mühltal) was used. They may withstand pressures up to 60 bar and are equipped with thermostated jackets. Their internal diameter is 26 mm and screwed piston heads in both ends allow the adjustment of bed length in the range of 25-30 cm. The columns were packed with a cation-exchange resin Dowex Monosphere 99/Ca (d_p=320 μm) of gel type (Supelco) by the slurry method. The resin was immersed in deionized and distilled water and gently stirred so as to obtain a slurry, which was carefully poured into the column. With the aid of a tool, especially designed for this purpose, the resin was gently compacted to allow the release of air bubbles. The average packing length was 29 cm. Each column was further submitted to a flowrate of 30 ml/min. A 30-bar back pressure was maintained by placing a valve at the exit of the column for 30 minutes so as to ensure complete settling of the packing and eliminate any dead volume there might be. The following determinations were carried out in order to estimate required parameters for the SMB/TMB model:

- Pulse experiments with a tracer;
- Determination of Equilibrium Isotherms for fructose and glucose;
- Breakthrough and desorption curves with pure fructose and glucose solutions;
- Pulse experiment for a binary mixture;

4.2.1 Pulse experiments with a tracer

Each of the twelve columns was subjected to tracer experiments in order to verify the homogeneity of packing and determine bed porosity. The tracer was blue dextran (5 g/l solution), which is a polymer whose molecule is large enough (M.W.=2,000,000) to diffuse only in the bulk fluid phase between resin particles. Deionized and distilled water was pumped through the column under the flowrates of 25-40 ml/min. Samples of 0.2 ml blue dextran were injected and the column response was monitored by using a UV detector. If

$C(t)$ is the recorded detector signal, the bed porosity ε may be calculated from the stoichiometric time, t_{st}, of the experimental curves by using the following relation:

$$t_{st} = \frac{\varepsilon V_c}{Q} = \int_0^\infty tE(t)dt \tag{4.1}$$

$$\text{where} \quad E(t) = \frac{C(t)}{C^o t_{st}} = \frac{C(t)}{\int_0^\infty C(t)dt} \tag{4.2}$$

In the above equations, V_c is the column volume, Q is the volumetric flowrate and C^o is the mass injected divided by the intraparticle void volume in the column. By calculating the variance (σ^2) of the experimental curve, axial mixing within the packing may be quantified by calculation of the Peclet number (Levenspiel and Bischoff, 1963). The Peclet number is the positive root of the following equation:

$$\frac{2}{Pe} - \frac{2}{Pe^2}\left(1 - e^{-Pe}\right) = \frac{\sigma^2}{t_{st}^2} \tag{4.3}$$

$$\text{where} \quad \sigma^2 = \int_0^\infty (t - t_{st})^2 E(t)dt \tag{4.4}$$

The mean value obtained for porosity was 0.4 with a relative error of ± 2%. Axial mixing did not vary significantly from column to column and in the flow range studied. The mean value obtained for the Pe number was 500. Figure 4.1 shows the obtained experimental pulse for one of the columns as compared to its theoretical simulation using Pe=500. Agreement is very good, even though the asymmetry of the peak may evidence either some degree of radial dispersion or surface adsorption. For the sake of simplicity, the columns were all assumed to be homogeneously packed with axial mixing accounted for by assigning Pe=500 in the range of flowrates to be used in the SMB.

The same methodology as described above was applied using sucrose as a tracer. This time the column was connected to a refractive index (RI) detector. Sucrose is not appreciably adsorbed in cation-exchange resins of Ca^{2+} form, but its molecular size is small enough to penetrate in the major pores of the resin. By using equation (4.1), a total porosity (ε_T) may be calculated, which includes the bed (ε) and resin (ε_p) void fraction, so that:

$$\varepsilon_T = \varepsilon + (1-\varepsilon)\varepsilon_p \tag{4.5}$$

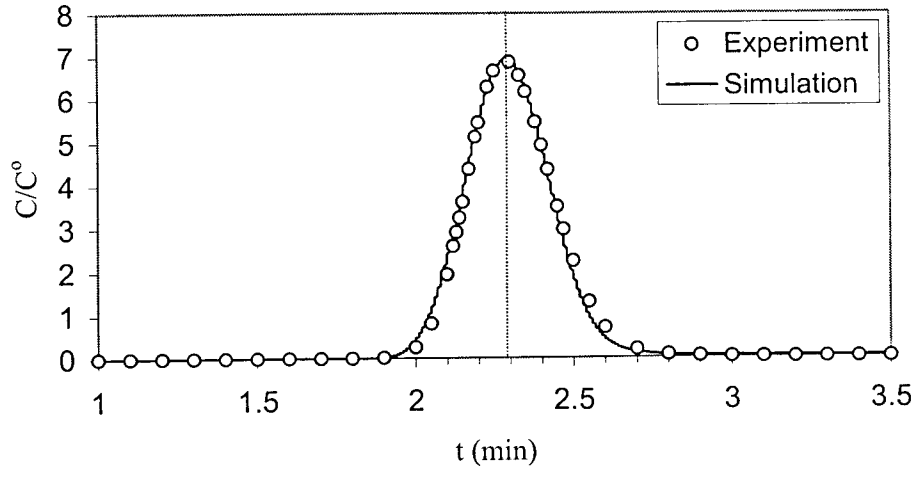

Figure 4.1 *Pulse curve of a tracer (blue dextran) in a Superformance column: comparison between experiment and simulation*

By using this procedure a particle void fraction of 0.1 was obtained. Figure 4.2 shows the obtained curve for a pulse of 200 µl of sucrose injected into a Superformance column under a flowrate of 9.6 ml/min.

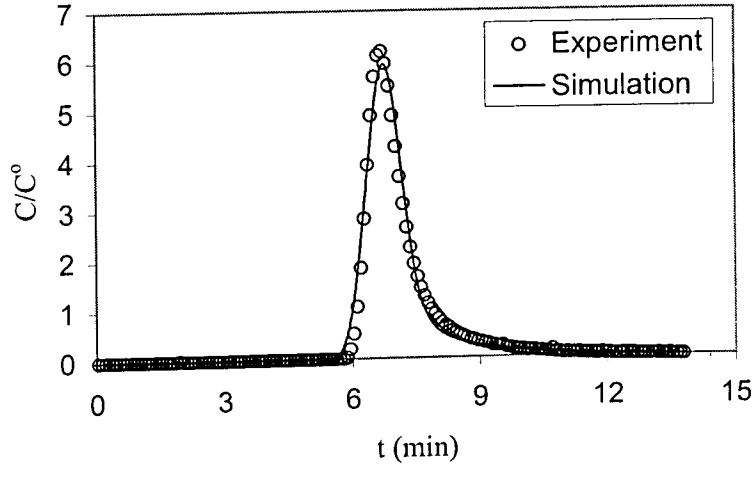

Figure 4.2 *Pulse curve of a sucrose in a Superformance column: comparison between experiment and simulation (Q=9.6 ml/min)*

4.2.2 Determination of equilibrium isotherms for fructose and glucose

Equilibrium isotherms for binary mixtures of fructose and glucose onto the cation-exchange resin were determined according to the following steps:

i. A solution of fructose-glucose of known composition (C_{i_o}) is pumped through the column for enough time to ensure complete saturation of the adsorbent. This may be done by monitoring the outlet concentration with a RI detector.

ii. Then, fresh eluent (deionized water) is pumped through the previously saturated column until the RI signal comes to the initial baseline. The eluate must be collected in a previously weighed reservoir.

iii. The concentration of the eluate (C_i^{el}) must be measured for both fructose ($i = FR$) and glucose ($i = GL$).

iv. Knowing the initial solution concentration (C_{i_o}), the volume of eluate (V_{el}), the column void fraction (ε), the column volume (V_c), any extra-column volume (V_{ex}) and the concentration of the eluate (C_i^{el}), the adsorbed phase concentration (q_i^*) in equilibrium with C_{i_o} is given by the following equation:

$$q_i^* = \frac{V_{el}C_i^{el} - C_{i_o}(\varepsilon V_c + V_{ex})}{(1-\varepsilon)V_c} \qquad i = FR, GL \tag{4.6}$$

v. The procedure described in items (i) through (iv) is repeated for another fluid phase concentration C_{i_o}

The isotherms were measured in the range of 0 to 30 g/l at 30°C. They are illustrated in Figure 4.3. Both sugar are linearly adsorbed in this concentration range with equilibrium constants equal to 0.29 and 0.55 for glucose and fructose, respectively, assuming the adsorbent to be a homogeneous solid.

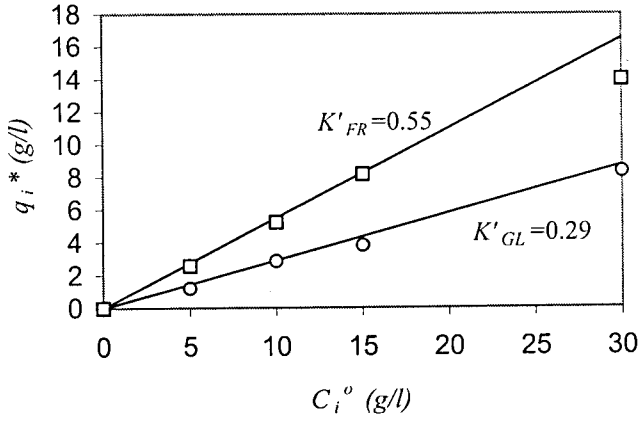

Figure 4.3 Adsorption isotherms for fructose (F) and glucose (G) at 30°C.

4.2.3 Breakthrough and desorption curves with pure fructose and glucose solutions

Breakthrough and elution experiments with fructose and glucose pure solutions were performed by applying step changes in the concentration of these sugars at the inlet of a column. Figure 4.4 depicts the scheme used in these experiments as well as the obtained response curves. The curves show concentration histories at the outlet of the column, as detected by a RI detector, compared to simulated curves. The theoretical model used in the simulations included the bi-linear driving approximation so as to allow the estimation of pertinent model parameters. The linear equilibrium constant ($K_i^{'}$) was estimated from the stoichiometric time of the curves using the following expression:

$$t_{st_i} = \int_0^\infty tE_i(t)dt = \frac{V_c}{Q}\left(\varepsilon + (1-\varepsilon)K_i^{'}\right) \tag{4.7}$$

$$\text{where} \quad E_i(t) = \frac{d}{dt}\left[\frac{C_i(t)}{C_{i_o}}\right] \qquad i = FR, GL \tag{4.8}$$

C_{i_o} is the step concentration and C_i, the concentration detected at the exit of the column. The parameter k_p was calculated from the Glueckauf (1955) correlation ($15D_{p_e}/R_p^2$) and k_μ was found from a "best-fit" procedure.

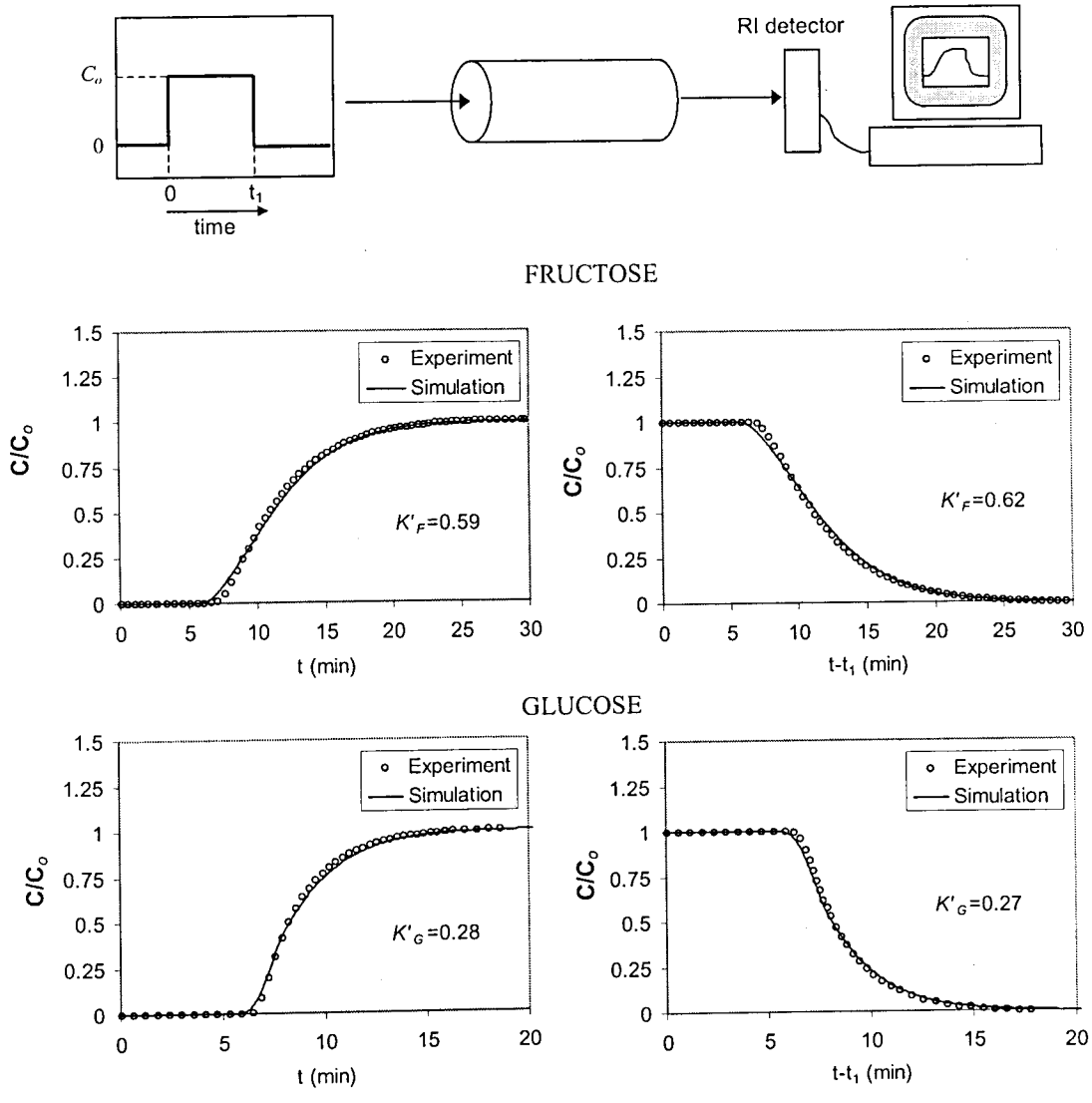

Figure 4.4 *Procedure and response curves obtained for breakthrough and desorption experiments using pure fructose and glucose solutions.*

Since glucose and fructose have the same molecular size, and hence the same molecular diffusivity, these kinetic parameters are assumed to be identical for both sugars. Table 4.1 summarizes the various kinetic and equilibrium parameters obtained from the experiments described so far.

Table 4.1 Summary of SMB model parameters obtained experimentally

Experiment described in subsection:	ESTIMATED PARAMETER						
	Pe	ε	ε_p	K'_{FR}	K'_{GL}	k_p, min^{-1}	k_μ, min^{-1}
4.2.1	500	0.4	0.1	---	---	---	---
4.2.2	---	---	---	0.55	0.29	---	---
4.2.3[a]	500 [c]	0.4 [c]	0.1 [c]	0.59	0.28	2	0.8
4.2.3[b]	500 [c]	0.4 [c]	0.1 [c]	0.62	0.27	2	0.8
Average	500	0.4	0.1	0.6	0.28	2	0.8

[a] Breakthrough experiments
[b] Desorption experiments
[c] Input to the simulation of experimental data

4.2.4 Pulse experiment for a binary mixture

In order to have a final confirmation of the dispersion, equilibrium and kinetic parameters obtained through the previously described experiments, a pulse experiment was conducted in the SMB columns placed in series using a binary glucose and fructose solution. A sample of 300 ml and 20 g/l was injected into the set of columns and then eluted under a flowrate of 30 ml/min. This experiment was not used to estimate any model parameters. Figure 4.5 shows the exit concentration histories obtained experimentally as compared with the simulated curves. The simulations were able to predict the experimental curves quite accurately by using the average values shown in Table 4.1. Film mass transfer (Bi_m=20)

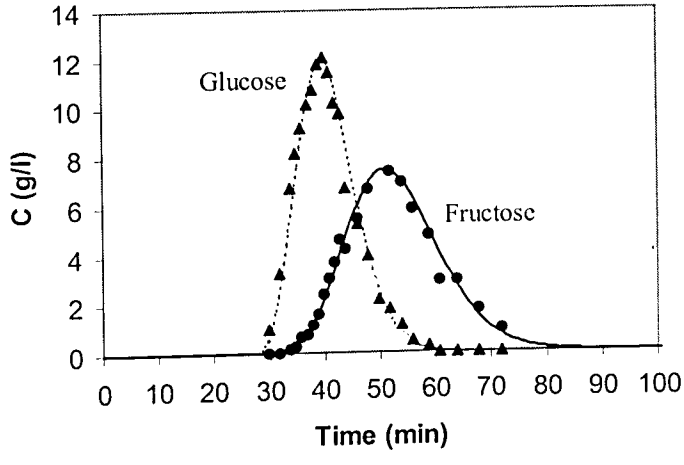

Figure 4.5 Concentration history for a pulse of fructose-glucose mixture injected in SMB columns placed in series

was accounted for by evaluating k_f from the Thoenes and Kramers' correlation (1958) for flow in packed beds.

4.3 SMB Experiments for Fructose-Glucose Separation

All SMB experiments described in this thesis were performed in a pilot unit LICOSEP 12-26 by Novasep (Vandoeuvre-dès-Nancy, France). Twelve columns Superformance SP 300 x 26 (length x i.d., mm), by Götec Labortechnik (Mühltal, Germany), packed with the cationic resin Dowex Monosphere 99/Ca (Supelco) were connected to the SMB pilot unit. Each column is jacketed to ensure temperature control and the jackets are connected to one another by silicone hoses and to a thermostat bath (Lauda). Operating temperatures may be set within the range of 20°C to 60°C. Between every two columns there is a four-port valve actuated by the control system. When required, the valves allow either pumping of feed/eluent into the system or withdrawal of extract/raffinate streams. Each of the inlet (feed and eluent) and outlet (extract and raffinate) streams is pumped by means of Merck-Hitachi HPLC pumps. The recycling pump is a positive displacement Milton Roy diaphragm pump, which may deliver flowrates as low as 20 ml/min up to 120 ml/min. The maximum allowable pressure is 60 bar. Between the twelfth and the first column there is a six-port valve, which is used to collect samples for internal concentration profile measurements. Figure 4.6 shows a side view of the pilot unit, where six columns are placed. The other six columns used in most experiments are placed on the other side. The equipment has its own process control software, which is able to accomplish the following tasks:

- Switch the inlet and outlet streams at regular time intervals (as assigned by user) by opening and closing on-off pneumatic valves;
- Keep steady and constant section flowrates as assigned;
- Keep suction pressure at the recycling pump around a setpoint assigned by the user (usually 1.5 bar);

All piping between columns consists of 1/16" i.d. tubing in order to minimize the dead volumes. The dead volume represented by the recycling pump accounts for 21 cm^3. Its adverse effects on the unit performance are overcome by desynchronising the switches of the

was accounted for by evaluating k_f from the Thoenes and Kramers' correlation (1958) for flow in packed beds.

4.3 SMB Experiments for Fructose-Glucose Separation

All SMB experiments described in this thesis were performed in a pilot unit LICOSEP 12-26 by Novasep (Vandoeuvre-dès-Nancy, France). Twelve columns Superformance SP 300 x 26 (length x i.d., mm), by Götec Labortechnik (Mühltal, Germany), packed with the cationic resin Dowex Monosphere 99/Ca (Supelco) were connected to the SMB pilot unit. Each column is jacketed to ensure temperature control and the jackets are connected to one another by silicone hoses and to a thermostat bath (Lauda). Operating temperatures may be set within the range of 20°C to 60°C. Between every two columns there is a four-port valve actuated by the control system. When required, the valves allow either pumping of feed/eluent into the system or withdrawal of extract/raffinate streams. Each of the inlet (feed and eluent) and outlet (extract and raffinate) streams is pumped by means of Merck-Hitachi HPLC pumps. The recycling pump is a positive displacement Milton Roy diaphragm pump, which may deliver flowrates as low as 20 ml/min up to 120 ml/min. The maximum allowable pressure is 60 bar. Between the twelfth and the first column there is a six-port valve, which is used to collect samples for internal concentration profile measurements. Figure 4.6 shows a side view of the pilot unit, where six columns are placed. The other six columns used in most experiments are placed on the other side. The equipment has its own process control software, which is able to accomplish the following tasks:

- Switch the inlet and outlet streams at regular time intervals (as assigned by user) by opening and closing on-off pneumatic valves;
- Keep steady and constant section flowrates as assigned;
- Keep suction pressure at the recycling pump around a setpoint assigned by the user (usually 1.5 bar);

All piping between columns consists of 1/16" i.d. tubing in order to minimize the dead volumes. The dead volume represented by the recycling pump accounts for 21 cm^3. Its adverse effects on the unit performance are overcome by desynchronising the switches of the

ports which are about to or have been shifted across the pump at each cycle. In such cases, the switch is delayed t_d minutes, as calculated from the following equation:

$$t_d(\text{min}) = \frac{21}{\overline{Q}(\text{ml/min})} \quad \text{where} \quad \overline{Q} = \frac{\sum_1^4 Q_j}{4} \tag{4.9}$$

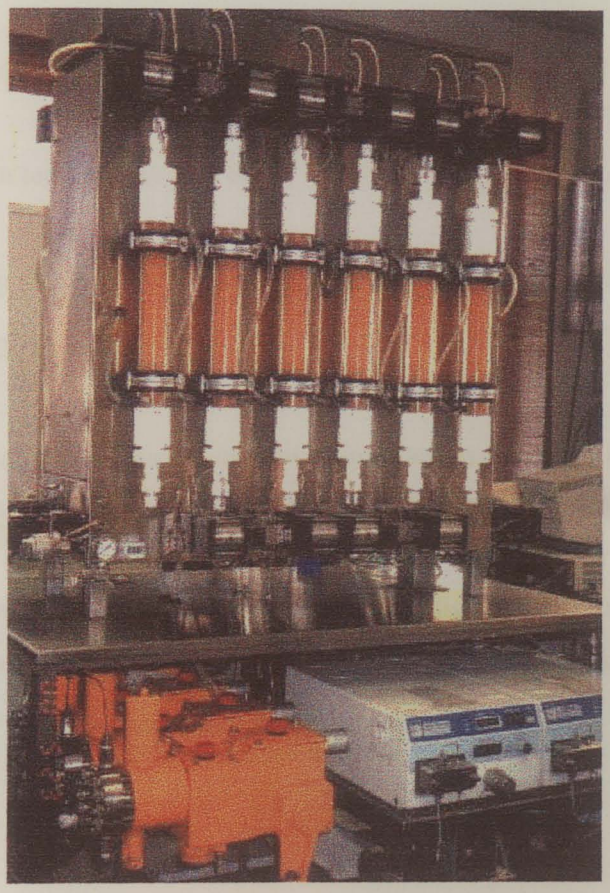

Figure 4.6 SMB pilot unit LICOSEP 12-26.

This feature is also built in the control software, so that the behaviour of the unit is identical to that of an ideal SMB with no dead volumes. Therefore, the experimental results obtained with this piece of equipment were always confronted to the results of simulations neglecting dead volumes, even though these significantly affect the performance of SMB processes (Azevedo *et al*, 1998; Migliorini *et al*, 1999).

4.3.1 Choice of operating conditions

The operating conditions under which the SMB unit was operated were selected with the aid of the Separation Volume Analysis. However, some of the equipment limitations had to be taken into account, such as:

a) Total pressure drop across columns, including piping, could not exceed 60 bar;

b) Maximum temperature was 60°C;

c) Recycling pump could be calibrated to deliver flowrates with precision within the range of 20 to 120 ml/min

Due to the high mass transfer limitations imposed by the resin, it was desirable to have as low flowrates (as high column residence times) as possible, which was confirmed from preliminary simulations. The equipment recycling pump could deliver a minimal flowrate of 20 ml/min with accuracy. Therefore, we arbitrarily assigned 24 ml/min as the flowrate of section 4, which is where flowrate is the lowest. By imposing a safety margin β of 1.4 on γ_4, the rotation period t* could be calculated from the following equation:

$$\gamma_4 = \frac{\nu K'_{GL}}{1.4} = \frac{Q_4 t^*}{\varepsilon V_c} - 1 \qquad (4.10)$$

Operating the SMB at higher temperatures was also considered. Following the methodology described in section 4.2, model parameters were measured/estimated at 50°C. Although adsorption capacity tends to decrease at higher temperatures, mass transfer could be enhanced and microbial growth on the resin could be inhibited. Table 4.2 summarizes the model parameters found at 50°C and compares them to those obtained at 30°C. These parameters were used in the search of the respective separation volumes for the SMB pilot unit at these temperatures.

Since the adsorption constant for glucose did not vary much for the two temperatures examined, the switching time calculated from equation (4.10) was taken to be 3.3 minutes for both cases. Having fixed the value of γ_4, the operating points $(\gamma_1, \gamma_2, \gamma_3)$ which result in product purities greater than 90% were searched according to the analysis of separation

volumes for both temperatures. For increasing values of γ_1, starting from the minimum equilibrium bound (see Table 4.2), the region of separation (both product purities above 90%) was determined by simulation in $\gamma_2 \times \gamma_3$ planes. The separation volumes obtained at 30°C and 50°C are shown in Figure 4.7. They are shown as polygons obtained for various distinct values of γ_1 starting from 0.8, which is the minimal equilibrium bound at 50°C. It may be

Table 4.2 Summary of model parameters measured/estimated at 30 and 50°C.

PARAMETER	T = 30°C		T = 50°C	
	Glucose	Fructose	Glucose	Fructose
Pe/column	500			
Bi_m	20		30	
ε	0.4			
ε_p	0.1			
K	0.18	0.5	0.17	0.43
$K' = K + \varepsilon_p$	0.28	0.6	0.27	0.53
$\frac{(1-\varepsilon)}{\varepsilon} K'$	0.42	0.9	0.405	0.795
k_p, min^{-1}	2	2	2.5	2.5
k_μ, min^{-1}	0.8	0.8	1.5	1.5
k_h, min^{-1}	1.06	0.75	1.89	1.33

verified that the separation volume obtained at 50°C is much larger than that obtained at 30°C. The same color indicates the same γ_1 value. For the sake of clarity, these separation volumes are also represented in 2-D $\gamma_2 \times \gamma_3$ plots for different values of γ_1 in Figure 4.8 (a) and (b). The highest value of γ_1 in each plot is that above which the area of separation has an unchanging shape. In practice, increasing γ_1 means using larger eluent flowrates, which enables more combinations of operating conditions so as to achieve the desired purities. However, higher eluent flowrates also lead to more diluted products, which is undesirable if one intends to obtain fructose syrups, for instance. From a certain point on, further increases in eluent flowrate do not contribute to the expansion of the area of separation and that is an appropriate condition to carry out an experiment. By comparing the plots obtained at 30°C and 50°C, it is clear that better performances may be achieved at 50°C at the expense of less

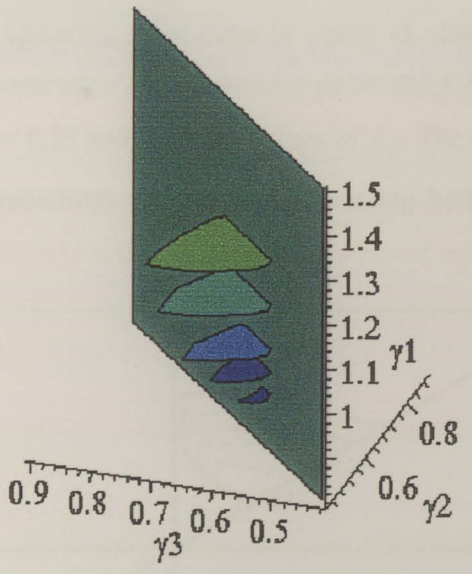

(a)

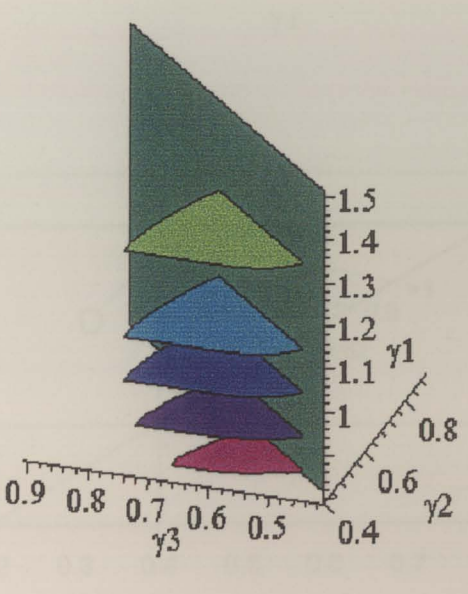

(b)

Figure 4.7 Separation volumes for a desired product purities of 90% at 30°C (a) and 50°C (b).

eluent. Moreover, by using temperatures up to 70°C, microbial growth is inhibited and fluid viscosity is decreased. These may be appropriate factors when working in a high sugar concentration range. Hence, we have chosen to operate the SMB unit at 50°C. As for the

choice of the (γ_2,γ_3) operating point, it is desirable to have as high throughputs as possible. This means choosing an operating point close to vertex O, shown in Figure 4.8, but yet far enough to ensure robust operation. The operating point (0.5,0.68) was selected to carry out SMB experiments for γ_4 = 0.29 and different values of γ_1. The obtained experimental results were compared to the predictions from simulations using both TMB and SMB strategies.

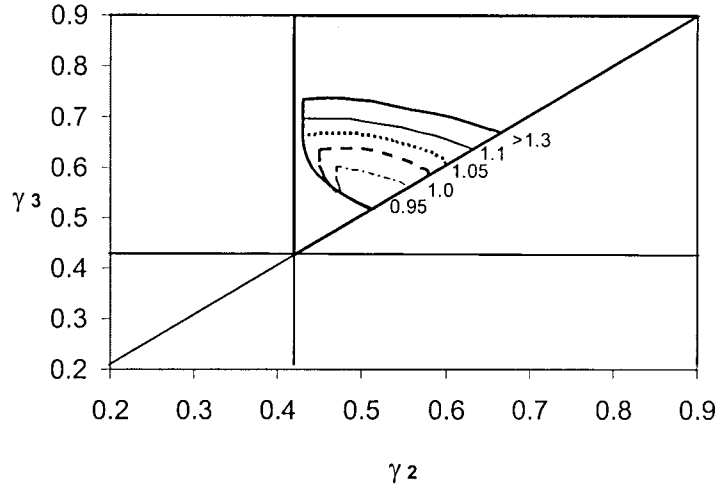

(a)

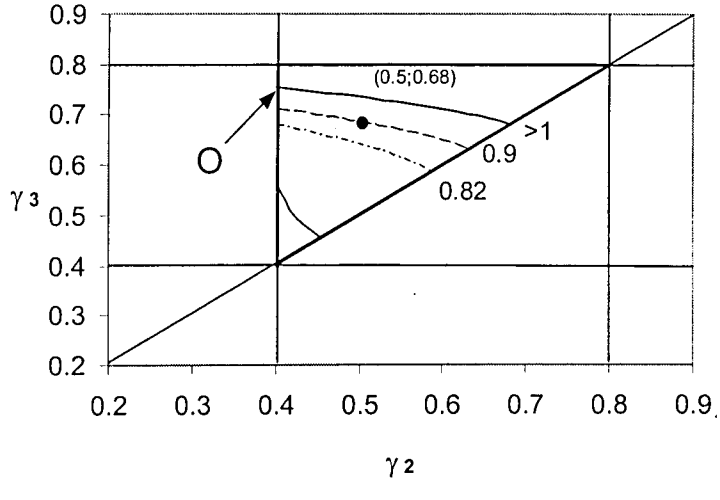

(b)

Figure 4.8 Regions of desired separation in a 2-D parameter space as a function of γ_1 obtained for model parameters measured/estimated at 30°C (a) and 50°C (b).

4.3.2 SMB Experimental Results

Four experiments were carried out for the separation of fructose-glucose mixtures in a SMB. The operating conditions of these experiments, identified as runs A, B, C and D, are summarized in Table 4.3. Each table also compares performance parameters obtained experimentally with those predicted from simulation. In all cases, the predicted parameters were obtained by numerical simulation using the TMB model, except for experiment D, which also shows predicted results from the real SMB model (inside brackets).

In all experiments, the feed concentration was 40 g/l for each sugar. Switching time, feed and raffinate flowrates were the same and equal to 3.3 min, 3.36 and 7.26 ml/min, respectively. There were three columns per section. By varying γ_1, different eluent and extract flowrates were tested. In all experiments, the system reached its periodic steady state in the 10th cycle. From that point on, the average product concentration collected for a whole cycle remained unchanged. Global mass balances of both sugars were verified, that is, after cyclic steady state the amount of fructose and/or glucose that entered the unit was the same as that which left it in a time period.

In run A, the velocity ratio in section 1 is 0.82, which is very close to the minimum equilibrium bound of 0.795 ($= \nu K'_{FR}$). In fact, by examining Figure 4.8 (b), one may verify that at γ_1=0.82, the point (0.5,0.68) lies in the region of pure extract only (purity above 90%). The obtained experimental purities confirm this. As shown in Table 4.3, there is good agreement between theoretical and experimental performance. Figure 4.9 shows the concentration profile measured at the 15th cycle. Each point (white) was sampled at 50% of each of the 12 periods of a cycle. The simulated profile obtained from the steady-state TMB model, represented by continuous lines, predicts well the experimental data. The black-ink points represent the average concentration of extract and raffinate collected for the whole 15th cycle.

The following experiment, run B, was carried out using a larger eluent flowrate. The velocity ratio γ_1 was increased to 0.9, as may be seen in Table 4.3. The Table also shows the other operating conditions and the performance parameters obtained. The raffinate purity is increased as compared to run A, however it is still below 90%. In this situation, the pair (0.5,0.68) in a $\gamma_2 \times \gamma_3$ plane lies right on the border of the separation region, as may be

Table 4.3 Summary of SMB experimental operating conditions and performance

SMB operating flowrates (ml/min)		Performance parameter	Experimental	Predicted
EXPERIMENT A				
$Q_1 = 34.02$	$\gamma_1 = 0.82$	PU_X, %	95.7	97.9
$Q_2 = 27.90$	$\gamma_2 = 0.50$	PU_R, %	85.5	86.1
$Q_3 = 31.26$	$\gamma_3 = 0.68$	PR_X, kg/m^3 h	5.74	5.76
$Q_4 = 24.00$	$\gamma_4 = 0.29$	PR_R, kg/m^3 h	6.68	6.82
$Q_E = 10.02$	$Q_F = 3.36$	C_F^X, kg/m^3	17.43	17.41
$Q_X = 6.12$	$Q_R = 7.26$	C_G^R, kg/m^3	16.99	17.28
EXPERIMENT B				
$Q_1 = 35.46$	$\gamma_1 = 0.90$	PU_X, %	96.9	97.9
$Q_2 = 27.90$	$\gamma_2 = 0.50$	PU_R, %	87.8	90.2
$Q_3 = 31.26$	$\gamma_3 = 0.68$	PR_X, kg/m^3 h	6.14	6.27
$Q_4 = 24.00$	$\gamma_4 = 0.29$	PR_R, kg/m^3 h	7.00	7.06
$Q_E = 11.46$	$Q_F = 3.36$	C_F^X, kg/m^3	14.88	15.27
$Q_X = 7.56$	$Q_R = 7.26$	C_G^R, kg/m^3	17.78	17.89
EXPERIMENT C				
$Q_1 = 37.26$	$\gamma_1 = 1.00$	PU_X, %	94.9	98
$Q_2 = 27.90$	$\gamma_2 = 0.50$	PU_R, %	92.7	92.1
$Q_3 = 31.26$	$\gamma_3 = 0.68$	PR_X, kg/m^3 h	6.66	6.58
$Q_4 = 24.00$	$\gamma_4 = 0.29$	PR_R, kg/m^3 h	6.54	6.68
$Q_E = 13.26$	$Q_F = 3.36$	C_F^X, kg/m^3	13.00	12.99
$Q_X = 9.36$	$Q_R = 7.26$	C_G^R, kg/m^3	16.19	16.93
EXPERIMENT D				
$Q_1 = 38.28$	$\gamma_1 = 1.05$	PU_X, %	95.7	98.0 (96.2)
$Q_2 = 27.90$	$\gamma_2 = 0.50$	PU_R, %	91.2	93.2 (91.5)
$Q_3 = 31.26$	$\gamma_3 = 0.68$	PR_X, kg/m^3 h	6.47	6.74 (6.80)
$Q_4 = 24.00$	$\gamma_4 = 0.29$	PR_R, kg/m^3 h	7.10	7.12 (7.23)
$Q_E = 14.28$	$Q_F = 3.36$	C_F^X, kg/m^3	11.44	11.99 (11.76)
$Q_X = 10.38$	$Q_R = 7.26$	C_G^R, kg/m^3	18.71	18.05 (17.82)

checked in Figure 4.8 (b). Should any fluctuations in section flowrate happen and the desired performance is not likely to be achieved. Besides, the area of separation was defined using a TMB steady-state model, which usually result in more optimistic predictions than the SMB transient model.

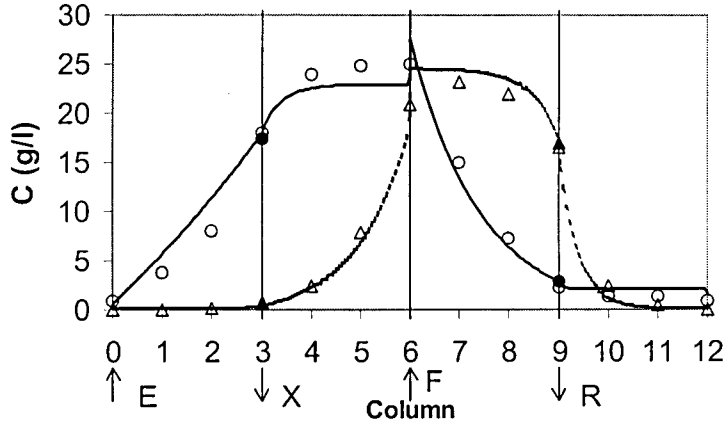

Figure 4.9 Experimental concentration profile for glucose (triangles) and fructose (circles) in a SMB adsorber obtained after periodic steady state has been reached. Operating conditions are those stated for experiment A in Table 4.3. Curves were obtained from simulation using the TMB strategy.

Figure 4.10 illustrates the experimental concentration profile of fructose and glucose sampled at 50% of each period of the 15th cycle. The dotted lines are simulated using the steady state TMB model. Like the plot shown in Figure 4.9, there is very good agreement between theory and experiment. The continuous lines depict simulated profiles obtained from a SMB strategy, calculated at a half cycle after periodic steady state has been reached. A better agreement for the experimental points from sections 2 and 3 is observed. However, from Table 4.3, some discrepancy between experimental and predicted product purities may be observed. This is due to the underestimation of the contaminant species in both extract and raffinate. Figure 4.11 (a) and (b) show this effect. The dark points represent the measured concentration of the products collected for a whole cycle at the 3rd, 5th and 7th cycle. The circles stand for fructose and the triangles stand for glucose. The thin lines were obtained from simulation using the transient SMB model and they represent local concentrations measured in the product ports. The white symbols represent the average cycle concentrations, as calculated by the simulator. For both extract and raffinate, the amount of contamination is

actually greater than that predicted. The cause of such discrepancy may be a common piece of tubing, which is part of the four-port valve located between every two columns. Every time extract leaves a column, it mixes with a 0.1 ml volume of raffinate and vice-versa. Therefore, this discrepancy tends to be negligible the longer the cycle is and the larger product flowrates are.

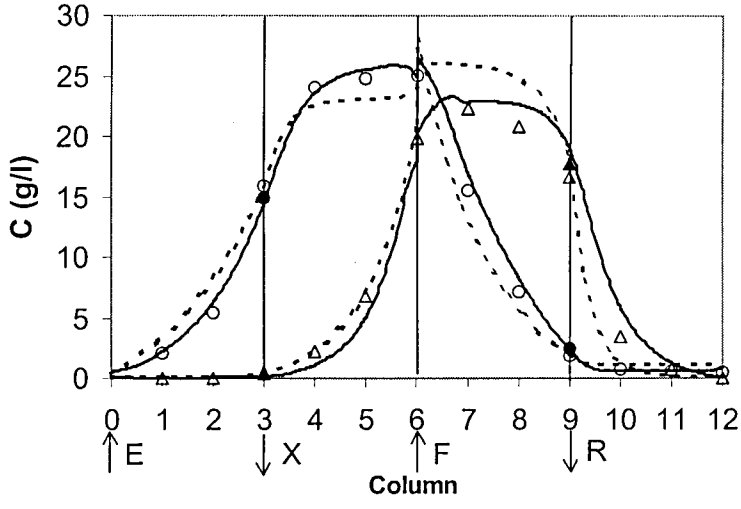

Figure 4.10 Experimental concentration profile for glucose (triangles) and fructose (circles) in a SMB adsorber obtained after periodic steady state has been reached. Operating conditions are those stated for experiment B in Table 4.3. Dotted and continuous curves were obtained from simulations using the TMB and SMB strategies, respectively.

In runs C and D, γ_1 is further increased to 1 and 1.05. The plot on Figure 4.8 (b) shows that the separation area predicted for these cases should be identical. As expected, both product purities are above 90%. This is shown in Table 4.3, which summarizes the main performance parameters obtained in the two runs. In general, all performance parameters in these two runs are very similar. Since fructose has a higher added value than glucose, the latter usually being recycled for isomerization, there are no advantages in further increases in γ_1. Using larger eluent flowrates would slightly raise extract purity but, all the same, cause undesired dilution.

Figure 4.12 shows the experimental concentration profile obtained for run C as compared with the theoretical curves as calculated from a TMB model. Unlike the previous profiles shown in Figure 4.9 and 4.9, concentration of both species in sections 1 and 4 is nearly zero. In other words, eluent and adsorbent are both regenerated and cross

contamination is decreased. Again, experimental process performance is somewhat poorer than predicted from a TMB model. Figure 4.13 shows experimental profiles sampled at 25%, 50%, 75% and 100% of each period of the 15th cycle under the operating conditions described for run D. The axial movement of concentration fronts may be verified. The curves were obtained from simulation using a transient SMB model after periodic steady state had been reached. Experimental data agrees closely with that predicted from simulation.

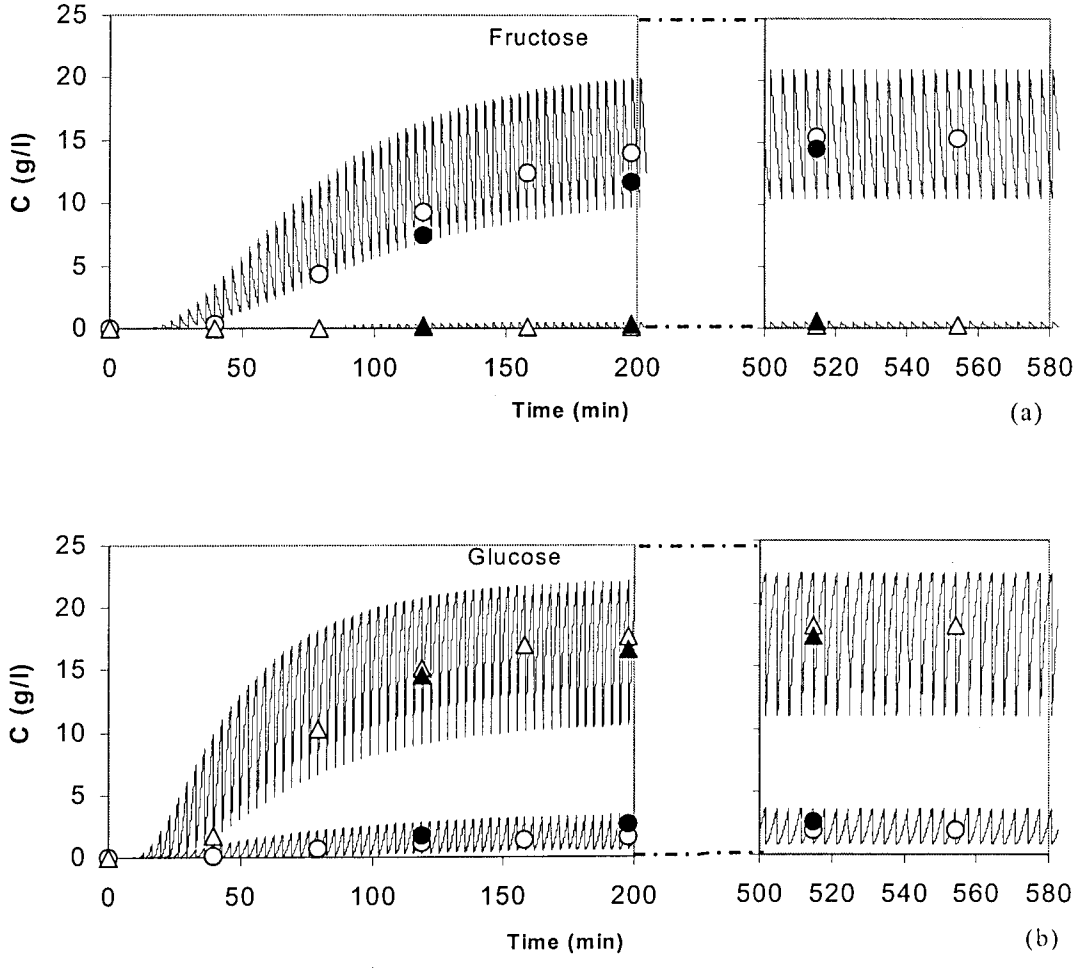

Figure 4.11 *Extract (a) and raffinate (b) concentration histories as calculated from a SMB dynamic model. Black points are experimental product concentrations collected for a whole cycle. White points are average cycle concentration as calculated by simulator.*

The compatibility between theory and experiment may also be verified in Table 4.3 for run D. Predicted parameters include those obtained both by the TMB and the SMB models. Product purities obtained from the SMB model are only slightly lower to the ones predicted by the TMB model and they were closer to the experimental values. Therefore,

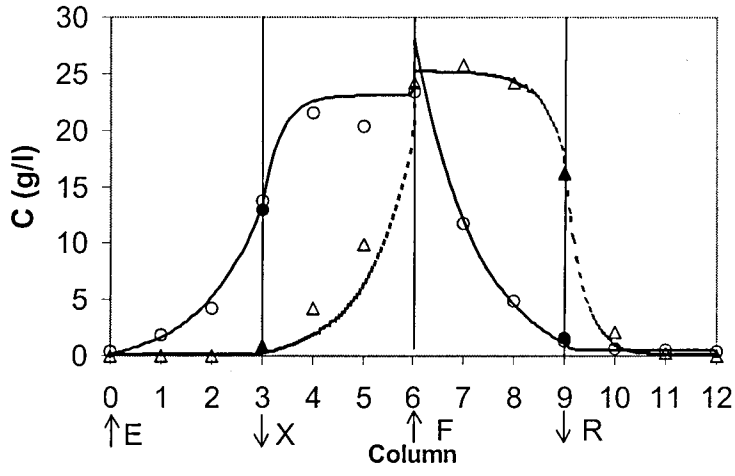

Figure 4.12 Experimental concentration profile for glucose (triangles) and fructose (circles) in a SMB adsorber obtained after periodic steady state has been reached. Operating conditions are those stated for experiment C in Table 4.3. Curves were obtained from simulation using the TMB strategy.

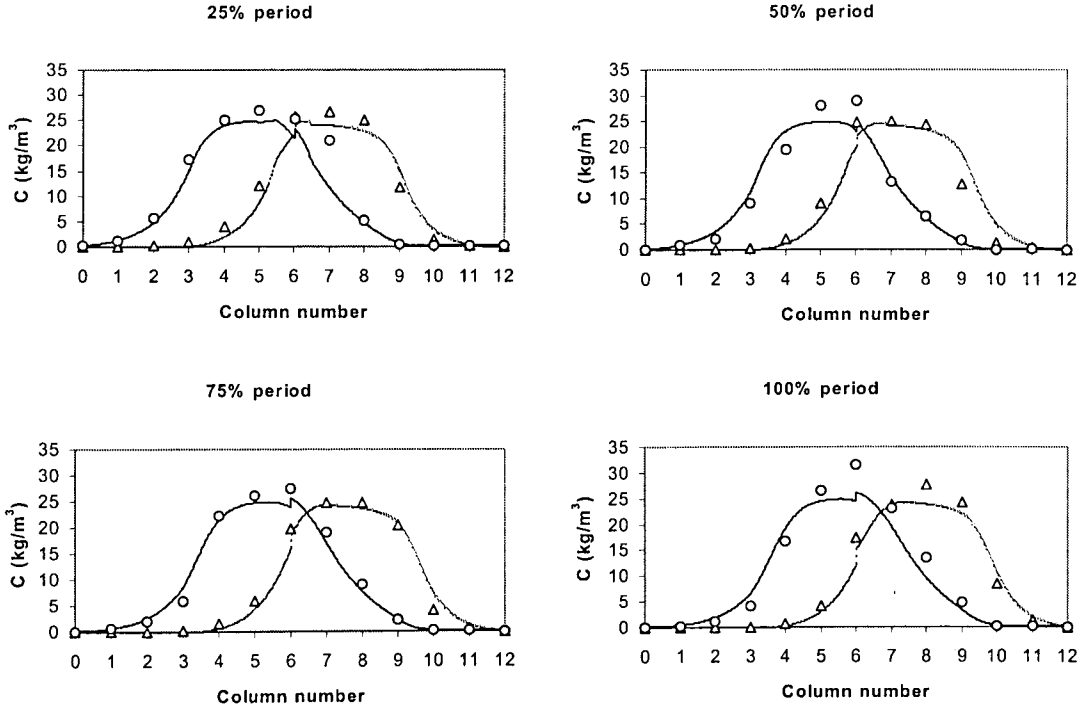

Figure 4.13 Experimental and simulated concentration profiles obtained for different period fractions at periodic steady state.

the TMB model provides a fast and relatively accurate prediction of the steady-state performance of a given SMB plant, which is enough to define its separation volume.

4.4 Conclusions

The present chapter showed experimental data for the SMB separation of a glucose-fructose mixture in a pilot unit LICOSEP 12-26. The methodology and materials employed were described in order to determine pertinent model parameters experimentally. The agreement observed between experiments and simulations for various chromatographic operation modes (pulse, breakthrough, elution) evidences the accuracy of the obtained data. A design methodology based on the concept of "Separation Volume", addressed in a previous publication (Azevedo and Rodrigues, 1999), was used to select appropriate operating conditions for the SMB pilot plant. The plant operating limitations were taken into consideration and a constraint on the purity of both products (extract and raffinate) was set at a minimum of 90%. The effect of temperature on the kinetic and equilibrium parameters was also examined. Results of this methodology were presented in terms of $\gamma_2 \times \gamma_3$ plots for various values of γ_1. Operating points that fulfilled the purity restrictions were chosen as conditions to operate the SMB. The experimental results obtained at conditions chosen from this methodology agreed quite well with theoretical predictions. Detailed mathematical models based on a true moving bed (TMB) and a real simulated moving bed (SMB) were used and simulated results were in accordance with experimental data. As a conclusion, the "Separation Volumes" methodology was validated as a useful SMB design tool in achieving desired product purity and dilution requirements.

4.5 References

D. C. S. Azevedo, S. B. Neves, S. P. Ravagnani, C. L. Cavalcante Jr., A. E. Rodrigues, "The Influence of Dead Zones on Simulated Moving bed Units", F. Meunier, Ed., 6th Conference on Fundamentals of Adsorption, Gien (Elsevier, 1998).

D. C. S. Azevedo, A. E. Rodrigues, "Design of a Simulated Moving Bed in the Presence of Mass-Transfer Resistances", *AIChE J.* **45**, 956-966 (1999).

E. Glueckauf, "Theory of chromatography. Part 10. Formulae for Diffusion into Spheres and Their Application to Chromatography", *Trans. Faraday Soc.* **51**, 1540-1551 (1955).

O. Levenspiel, K. Bischoff, "Patterns of Flow in Chemical Process Vessels", *Adv. Chem. Eng.* **4**, 95-198 (1963).

C. Migliorini, M. Mazzotti, M. Morbidelli, "Simulated Moving-Bed Units with Extra-Column Dead Volume", *AIChE J.* **45**, 1411-1421 (1999).

D. Thoenes Jr., H. Kramers, "Mass Transfer from Spheres in Various Regular Packings to a Flowing Fluid", *Chem. Eng. Sci.* **8**, 271-283 (1958).

5. Obtainment of Fructose from Cashew Apple Juice by SMB Chromatography

5.1 Introduction

This chapter is intended to demonstrate the possibility of using the SMB technology in order to obtain high-fructose solutions from the cashew apple juice, which may represent an attractive economic alternative for its industrial exploitation. The cashew tree is a native tropical plant abundant in Northeastern Brazil, whose commercial value relies mainly on the processing of its nut. Despite the high nutrition value of the penduncle of the fruit, the cashew apple, more than 90% of the crop is left behind to rot when the nut is harvested. In this chapter, the chemical composition of the aqueous phase of cashew apple juice was determined by HPLC analysis. The actual juice, as sold commercially, was fed into a SMB adsorber after being filtered for coarse solids removal. Empirical steady state process performance for SMB operation at 55°C followed closely the predictions from simulation packages. Purity around 90% was obtained for the fructose-enriched extract. However, the transient history of product concentrations and internal band profiles showed an unexpected behaviour for the first time

the resin was contacted with the juice. Concentrations of carbohydrates went beyond the values of the periodic steady state temporarily. Follow-up experiments seem to suggest that the phenomena is caused by irreversible adsorption of larger molecules such as tannins.

To increase the added value and versatility of the products, either a step of isomerization of the raffinate or diverse SMB fluid-solid flowrate ratios may be applied. This way, a wide range of products may be obtained, from nearly pure fructose to 42%, 55% and 90% solutions, which are the standard concentrations of high-fructose syrup. If solids content is conveniently raised to the standards of commercial high-fructose syrups, these products may be used as food additives, thus confirming a potentially attractive use of the cashew apple juice.

5.2 Literature Review

The cashew tree (*Anacardium Occidentale, L.*) is a Brazilian tropical native plant that is cultivated in sandy fields on the north-eastern coast of the country, the state of Ceará being its major producer (Lima, 1988). It was originally found in Brazil by the Europeans in the sixteenth century and further taken to India and East Africa. The world production in 1994, as estimated by FAO, was around 614 billion tons from which Brazil's production accounted for 32% (see http://www.uga.edu/hortcrop/rieger/cashew.htm). This was the year when Brazil's production exceeded that of India and it has been the world's leading producer since then. Other great world producers are Mozambique, Guinea-Bissau, Indonesia and Tanzania. The cashew agroindustry has an outstanding role in the economic and social context of these places since it is a highly labour intensive activity which offers one of the few, if not only, job opportunities in such under-developed areas. Of the 30-35 products from the cashew tree, the nut is the most valuable one. In Brazil alone cashew generates 16,000 jobs in nut processing, 43,000 jobs in farm management and 280,000 temporary jobs during the harvest period (Pessoa *et al*, 1995). At present, the cashew nut is the most largely exported agroproduct in the state of Ceará (Leite, 1994).

Botanically speaking, the kidney-shaped shells depicted in Figure 5.1 are the actual fruit of the tree. The nut kernel inside is covered with an inner shell and between the two shells there is a thick caustic toxic oil consisting of a mixture of phenolic acids. The shells are topped by a swollen fleshy penduncle, the cashew apple or pear, whose colour varies from yellow to intense red. The nutritious and therapeutic properties of the different parts of the

cashew tree have long been acknowledged (Campos, 1946). In various sites of the world, parts of the cashew tree are claimed to heal a great variety of illnesses, which are summarized in Table 5.1. Fruits or seeds are consumed by roasting, shelling and salting the nuts, with Madeira wine or mixed in chocolates. The black, acrid, powerful vesicant oil may be extracted from the shells, which has been used as preservative and waterproofing agent in brake linings, lubricant in airplane armatures and termite-proofing timbers. Timber from cashew tree may be used in building and furniture making. The bark exudate may be used in pharmaceuticals and as a substitute for gum arabic.

Figure 5.1 The cashew shells, topped by their hypertrophied penduncles.

The apples may be consumed *in natura* or they may be processed industrially into a wide range of products from concentrated juice to body care products. The juice expressed from the apples may be made into a beverage or fermented into wine. The local market, basically, consumes these goods and such industry does not play an important role to the economy of the region. Furthermore, sadly enough, the majority of the cashew apple production rottens in the soil since the nut is harvested after fruit and penduncle have fallen on the ground. In the state of Ceará, for instance, according to Vieira *et al* (1982), no more than 2% of the annual production of cashew apples is estimated to have been explored industrially. This scenario is also confirmed by Lopes Neto (1981), who reports that the industrial exploration of the cashew apple ranges from 2 to 6%.

The high degree of waste of the cashew apple crop is mainly due to its quick degradability and to the lack of convenient preservation procedures. Moreover, the extreme adstrigency of the (pseudo-)fruit, caused by the presence of polyphenols, and the formation of two phases within the juice bottles seem to impair its acceptance by foreign markets. In Brazil, there has been a strong governmental effort to overcome these drawbacks (see

http://www.cnpat.embrapa.br/) by improving handling and manufacture techniques (Filgueiras *et al*, 1997) and by sponsoring agriculture research programs to develop new

Table 5.1 World wide claimed therapeutic uses of the cashew tree

Africa	Intoxicant, Tattoo
Brazil	Analgesic, Aphrodisiac, Asthenia, Asthma, Bronchitis, Callosity Corn, Cough, Diabetes, Diuretic, Dyspepsia, Eczema, Gargle, Genital, Impotency, Intestinal Colic, Leishmaniasis, Mouthwash, Muscular Debility, Psoriasis, Scrofula, Stimulant, Syphilis, Throat, Tonsillitis, Ulcers (mouth), Urinary, Venereal, Vesicant, Wart, Wounds
Elsewhere	Asthma, Adstrigent, Cold, Corn, Congestion, Cough, Debility, Diabetes, Dysentery, Liqueur, Piscicide, Purgative, Scurvy, Tumour, Vesicant, Wart
Guatemala	Liqueur, Poison, Skin, Wart
Haiti	Caries, Toothache, Wart, Stomatitis, Diabetes
Malaya	Diarrhoea, Thrush, Catarrh, Dermatitis, Nausea, Constipation
Mexico	Caustic, Diabetes, Diarrhoea, Freckle, Leprosy, Liqueur, Poison, Skin, Swelling, Syphilis, Ulcer, Wart
Panama	Asthma, Cold, Congestion, Diabetes, Diarrhoea, Hypertension, Inflammation
Peru	Antiseptic, Diarrhea, Douche, Infection (skin)
Trinidad	Ache (stomach), Asthma, Cough, Diarrhoea, Dysentery, Dyspepsia
Turkey	Diarrhoea, Fever, Poison, Wart
Venezuela	Dysentery, Gargle, Leprosy, Sore (throat)

Source: http://www.rain-tree.com/cajueiro.htm

breeding varieties. With respect to this latter aspect, one of the recent breakthroughs in cashew agronomic research was the development of the *precocious dwarf* cashew tree, shown in Figure 5.2. Clones of the dwarf type have been selected which produce non-adstrigent, high vitamin C content and high-sugar cashew apples (Montealegre *et al*, 1999). The average height of the trees is no more than 3 m, which enhances hand harvesting without the use of ladders. Flowering and fruit set is obtained in the first year after seeding and economic production may be achieved in the 3rd year, a much shorter time than the usual 8 years that a conventional tree takes to reach the same status. On the other hand, the reduction of the juice adstrigency and improvement of its stability has been addressed by various authors (Cavalcante *et al*, 1986; Souza Filho *et al*, 1991; Dubuc, 1995; Fonseca, 1995). The main objective of these works is to investigate methods of juice clarification, that is, removal of tannins and polyphenols so as to raise the marketing potential of the juice as a soft drink either in the whole or pasteurised form (cajuína).

Figure 5.2 Precocious Dwarf Cashew Tree

In such context, the use of the cashew apple as a source of high added-value sugars may point out to attractive economic alternatives in cashew producing regions. The following sections investigate the technical feasibility of producing high-fructose solutions from cashew apple juice by using the simulated moving bed technology, in a similar way to the industrial high fructose corn syrup (HFCS) widely used in beverage and food industry.

5.3 Chemical Composition of Cashew Apple Juice

The chemical composition of the cashew apple juice has been the subject of investigation by a number of authors (Pereira Jr. *et al*, 1966; Lopes, 1972; Moura Fé, 1972; Cecchi and Rodriguez-Amaya, 1981). They all agree that the main constituents of the aqueous juice are carbohydrates (glucose and fructose), proteins, organic acids, ascorbic acid, mineral salts (calcium, iron and phosphorus), polyphenols (tannins) and pigments. The extracted juice is usually obtained through squeezing and sieving processes. It is composed of two phases: a solid phase, which is usually yellow and contains polysaccharides, insoluble pigments and tannins, and an aqueous colourless phase, which is rich in carbohydrates and may be somewhat turbid due to tannins in suspension.

In this work, the sugar content of the aqueous phase of the juice was determined by HPLC analysis. Due to the difficulty in obtaining fresh fruit, two well-known brands of commercial cashew apple juice were analysed. They will be referred to as A and B. Samples of the supernatant liquid which was above the solid phase inside the bottles were collected and centrifuged (5000 rpm in a centrifuge Sigma 203) until a clear supernatant was obtained. These clarified samples were diluted (1:1) and injected into a chromatographic ion-exchange column connected to a refractive index detector Gilson model 131. The analytical equipment is shown in Figure 5.3. The analysis conditions were the following:

- Mobile phase: 0.005 N H_2SO_4 solution;
- Mobile phase flowrate: 0.3 ml/min;
- Pressure: 80 bar;
- Column: Organic acids column Interaction ION-300, 300x7.8 mm;
- Sample volume: 20 μl;

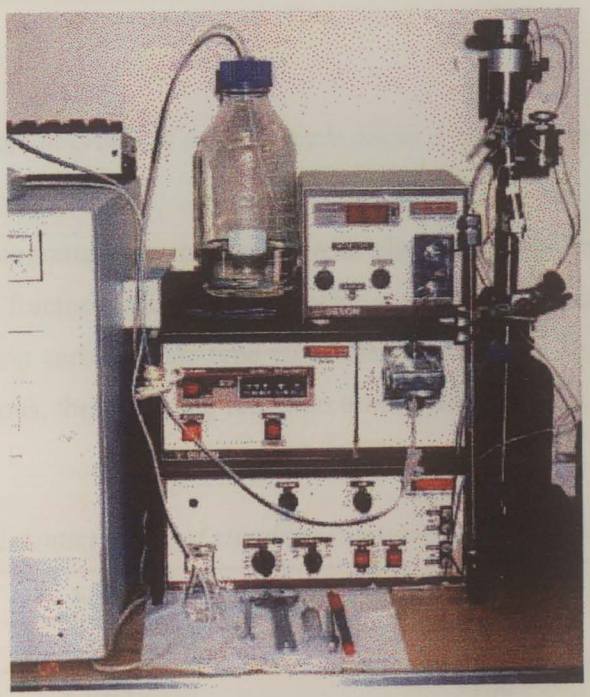

Figure 5.3 Equipment for HPLC analysis.

Figure 5.4 shows chromatograms of samples of the two brands of cashew apple juice labelled as A and B. Good reproducibility between the two commercial brands was observed.

A significant amount of ascorbic acid was verified confirming long-term literature records (Campos, 1946) about the nutritious value of the fruit. However, the amount of vitamin C is nearly a third of that measured for the fresh fruit due to oxidation caused by light and oxygen.

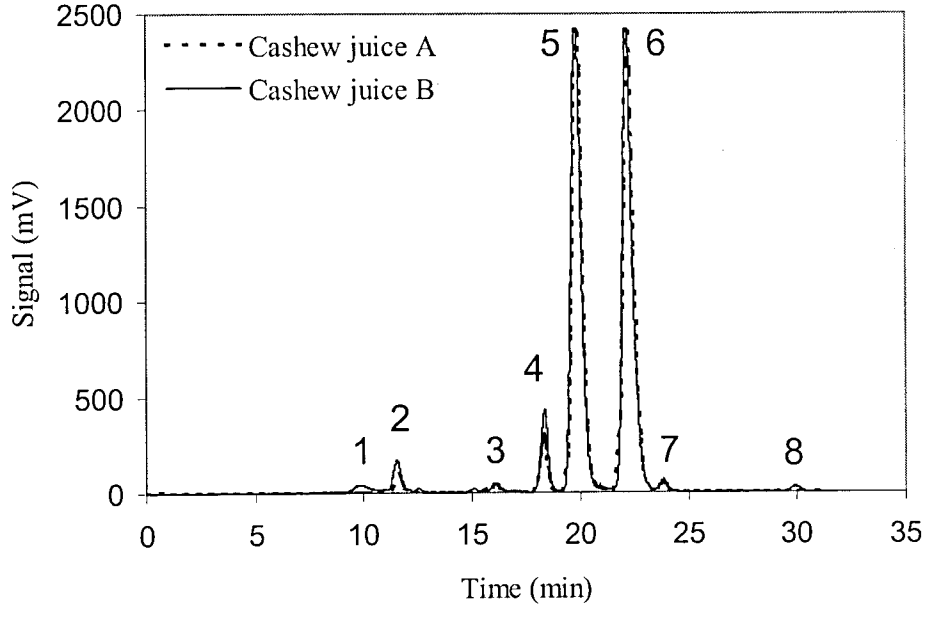

Figure 5.4 *Chromatograms of cashew apple juices A and B under the HPLC analysis conditions stated previously.*

These chromatograms were compared with chromatograms (not shown) of standard solutions of glucose, fructose, sucrose, citric acid, malic acid and ascorbic acid, which are reported to be the main carbohydrate-type constituents of cashew apple juice. By using the same analysis conditions, the following retention times were obtained, which are summarized in Table 5.2.

Table 5.2 *Retention times of standard solutions obtained from HPLC analysis*

Standard	Retention time (s)
Sucrose	976
Citric Acid	1134
Glucose	1209
Fructose	1355
Malic Acid	1380
Ascorbic Acid	1439

Comparison of data illustrated in Table 5.2 and Figure 5.4, aided by literature records, allowed us to propose the identification of the peaks as presented in Table 5.3. Peaks 1, 2 and 8 could not be identified and may be pigments, polysaccharides or tannins. The peak for malic acid is probably overlapped with that of fructose since the former occurs in a much lower concentration than the latter and both species have about the same retention time in the analytical column in question. The average sugar content found in both samples of juice is around 40 g/l for each of the sugars (glucose and fructose), or 4 g/100g juice. This figure is in accordance with literature records (Lopes, 1972; Moura Fé, 1972), which mention a total reducing sugar content (fructose +glucose) of 4-11.9 g/100g present in the aqueous phase of cashew apple juice. Citric acid is present because it is a commonly used anti-oxidant, which is added to industrialised juice in order to prevent vitamin C from decaying.

Table 5.3 Probable composition of cashew apple juice

Peak	Component	Reported concentration (g/100g)[a]	Cashew juice A		Cashew Juice B	
			Retention time (s)	Concentration (g/100g)	Retention time (s)	Concentration (g/100g)
1	(unknown)	---	---	---	597	---
2	(unknown)	---	694	---	694	---
3	Sucrose	0.08	967	0.051	964	0.042
4	Citric acid	0.224 – 0.828	1100	0.64	1102	0.42
5	Glucose	4.0 - 11.9 (gluc + fruc)	1208	3.99	1212	3.92
6	Fructose		1345	3.85	1344	3.90
7	Ascorbic Acid	0.121 – 0.231	1430	0.052	1430	0.056
8	(unknown)	---	---	---	1795	---

[a] Source: (Lima, 1988)

Following the same treatment as described previously, cashew apple juice was injected in a gel-permeation chromatographic column (Macherey-Nagel) connected to a UV detector with wave length set at 280 nm, which is a suitable value for protein detection. The analysis conditions were the following:

- Mobile phase: deionized and distilled water;
- Mobile phase flowrate: 1 ml/min;

- Pressure: 30 bar;
- Column: Gel permeation column Nucleogel GFC 4000-8;
- Sample volume: 10 μl;

A unique peak was detected. Since none of the compounds identified in the previous HPLC analysis are resolved by ultra-violet light, one may conclude that this peak accounts for a chemical species or group of chemical species not included in Table 5.3. Examination of literature records indicates that the peak may stand for proteins, polyphenols or pigments (carotenoids).

5.4 Design of SMB Operating Conditions

In the previous section, it has been shown that the aqueous phase of cashew apple juice is essentially a carbohydrate multicomponent mixture. The design of operating conditions under which a SMB adsorber will separate fructose from this mixture must take into account the adsorption and kinetic data of the individual chemical species present in the mixture. Since all species, other than fructose and glucose, are present in much lower concentrations, linear uncoupled equilibria onto the SMB packing (cation-exchange resin) were assumed. The linear adsorption constants of individual cashew apple constituents were determined according to the following procedure:

- Standard solutions of the following chemical species were prepared: sucrose, citric acid, glucose, fructose and malic acid. The concentrations were nearly those present in the juice and shown in Table 5.3. Ascorbic acid was neglected since it decays quite fast after being exposed to oxygen and light.
- Samples of the solutions were injected into a SMB column (as those previously used for fructose-glucose separation) with the aid of an injecting loop (500μl) and the column response was monitored by a RI detector.
- The linear equilibrium constant (K_i') of each of the chemical species investigated was calculated from the stoichiometric time of the respective experimental curve according to equation (4.7).

The linear adsorption constants (K_i') obtained at 55°C were 0.12; 0.26; 0.27; 0.42; 0.51 for sucrose, citric acid, glucose, malic acid and fructose, respectively. Note that we have chosen to increase operating temperature to 55°C in order to further inhibit bacterial growth and not to reach the limiting temperature of the equipment (60°C). The equilibrium theory has been successfully applied to multicomponent mixtures (Chiang, 1998; Migliorini *et al*, 2000) in order to predict the distribution pattern in the extract and raffinate of the chemical species involved. For linear systems, the theory is readily applicable, following the concepts introduced in Chapter 2. In the case of cashew apple juice, the different separation zones, found in the frame of equilibrium theory, are shown in Figure 5.5.

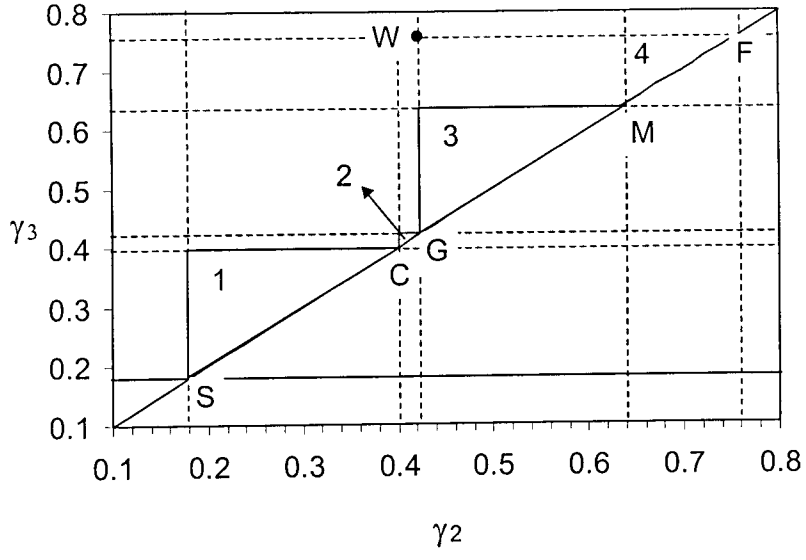

Figure 5.5 *Separation regions for a multicomponent mixture according to the equilibrium theory applied to linear adsorption isotherms*

The points F, M, G, C and S are located on the diagonal line ($\gamma_2 = \gamma_3$) and their co-ordinates are ($\nu K_i', \nu K_i'$), which refer to the equilibrium data obtained for fructose ($i = F$), malic acid ($i = M$), glucose ($i = G$), citric acid ($i = C$) and sucrose ($i = S$) respectively. Four distinct triangles may be observed in Figure 5.5, which define operating points under which the SMB adsorber may be operated in order to achieve different distributions of the mixture components in the extract and raffinate products. For, instance, if one chooses to use a (γ_2, γ_3) point located inside triangle 2, the extract will collect glucose, malic acid and fructose, whereas the raffinate will contain sucrose and citric acid. If the SMB is operated

within the (γ_2,γ_3) parameter space just above triangle 4, nearly pure fructose may be obtained in the extract and all other species, plus some traces of fructose, will be obtained in the raffinate. Table 5.4 summarizes the implications of operating a SMB adsorber under (γ_2,γ_3) pairs located in triangles depicted in Figure 5.5. Inside all of them, within the frame of equilibrium theory, there is no cross contamination and the products collected in each product are 100% pure.

Table 5.4 *Species collected in the extract and raffinate products of a SMB operated under different section flow conditions.*

Triangle	Conditions on γ_2 and γ_3	Species in extract	Species in raffinate
1	$\gamma_1 > \nu K_C'$ and $\gamma_4 < \nu K_S'$ $\nu K_S' < \gamma_2 < \gamma_3 < \nu K_C'$	*C, G, M, F*	*S*
2	$\gamma_1 > \nu K_G'$ and $\gamma_4 < \nu K_C'$ $\nu K_C' < \gamma_2 < \gamma_3 < \nu K_G'$	*G, M, F*	*S,C*
3	$\gamma_1 > \nu K_M'$ and $\gamma_4 < \nu K_G'$ $\nu K_G' < \gamma_2 < \gamma_3 < \nu K_M'$	*M, F*	*S, C, G*
4	$\gamma_1 > \nu K_F'$ and $\gamma_4 < \nu K_M'$ $\nu K_M' < \gamma_2 < \gamma_3 < \nu K_F'$	*F*	*S, C, G, M*

Note that these statements are strictly valid only if mass transfer effects are neglected, which is an applicable assumption if column HETP is low enough. Experience has shown us that this is not the case of the columns used in the previously described experiments of glucose-fructose separation. Furthermore, it is desirable to obtain a fructose-enriched extract with high recovery of this sugar from the feed. Therefore, we have chosen to operate inside the triangle CWF, which includes triangles 3 and 4. If we were to obtain "malic-free fructose", very low throughputs would be processed and mass transfer effects would eventually forbid the operation of our present equipment to reach this purity requirement. This decision also implies that some contamination of malic acid in both extract and raffinate may be tolerated.

5.5 Separation of Fructose by SMB Chromatography

Before using the actual juice as feed, we have performed a SMB experiment using a synthetic mixture of glucose, fructose and malic acid. Besides glucose and fructose, citric acid and malic acid are the two organic acids in larger quantities that would potentially pose any problem concerning the change of the resin ionic form. Note that citric acid is an antioxidant added to the industrial juice and would not be present in freshly expressed juice. Hence, we decided to verify fructose-glucose SMB separation in the presence of malic acid. Table 5.5 summarizes the operating conditions used in this experiment. We assigned values to γ_2 and γ_3 nearly equal to the coordinates of triangle 4 (see Figure 5.5), which is the equilibrium triangle for complete separation of fructose (collected in the extract) from the other cashew juice components (collected in the raffinate). At this point, the equipment could be operated at maximum throughput. Nonetheless, some contamination of malic acid in the extract was to be expected due to the well-known mass transfer limitations of the resin.

Table 5.5 Operating conditions used to operate a SMB pilot unit in order to separate fructose from a synthetic mixture of fructose, glucose and malic acid.

Operating conditions		**Columns**
T=55°C	Feed concentration: 40 g/l for FR/GL 5 g/l for malic acid	D_b = 2.6 cm
t* = 3.3 min		L_b = 29 cm
$Q_R = Q_4$ = 24 ml/min		Configuration: 3-3-3-3
Q_E = 11.00 ml/min	γ_1 = 0.88	Zone length:
Q_X = 4.59 ml/min	γ_2 = 0.63	87 cm for sections 1 to 4
Q_F = 2.43 ml/min	γ_3 = 0.76	
Q_R = 8.84 ml/min	γ_4 = 0.29	

Figure 5.6 shows the internal concentration profiles of fructose, glucose and malic acid at cyclic steady state. The points were collected at 50% of each period of cycle 15. The dark points are the average extract and raffinate concentrations measured from the products collected for a whole cycle. The curves are the simulated from a TMB-based model. A good agreement may be observed and the presence of malic acid does not seem to have altered the resin adsorption and mass transfer characteristics. As expected, malic acid contaminates the

extract since it is not completely desorbed in section 2 due to the slow mass transfer. In the following experiment, actual cashew apple juice was used.

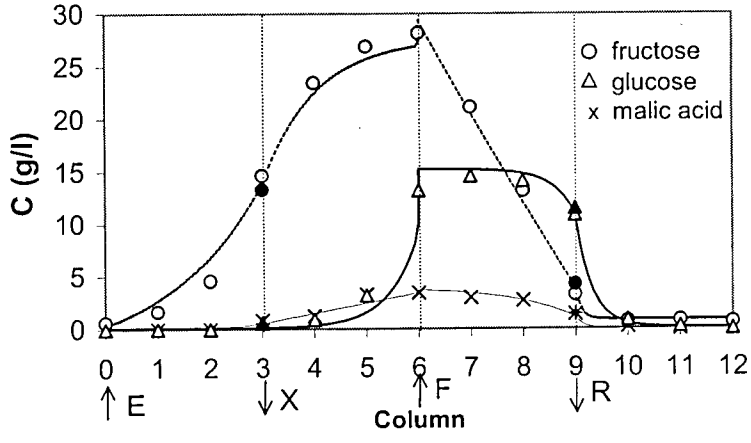

Figure 5.6 *Concentration profiles at cyclic steady state for the separation of synthetic fructose and glucose in the presence of malic acid. Symbols are experimental data and curves are simulated using a TMB model.*

The cashew apple juice, as found in commercial brands, had to undergo a filtration step before being fed into the SMB. The eluent was distilled deionized water, which was filtered and degassed prior to SMB operation. Both feed and eluent pumps made use of online filters before and after the pump heads. Eluent and feed reservoirs were kept in a thermostat bath at 55°C throughout the experiment. The operating conditions under which the SMB was operated in order to separate fructose from cashew apple juice are summarized in Table 5.6.

Table 5.6 *Operating conditions used to operate a SMB pilot unit in order to separate fructose from cashew apple juice*

Operating conditions		**Columns**
T=55°C Feed concentration as in Table 5.3		D_b = 2.6 cm
t* = 3.3 min		L_b = 29 cm
$Q_R = Q_4$ = 24 ml/min		Configuration: 3-3-4-2
Q_E = 10.91 ml/min	γ_1 = 0.87	Zone length:
Q_X = 7.04 ml/min	γ_2 = 0.49	87 cm for sections 1 and 2
Q_F = 2.90 ml/min	γ_3 = 0.65	116 cm for section 3
Q_R = 6.77 ml/min	γ_4 = 0.29	58 cm for section 4

The extract and raffinate streams were collected for a complete cycle at the 2nd, 3rd, 5th, 6th, 8th, 10th and 15th cycles. Their average cycle concentration was determined by HPLC analysis. By decreasing the mobile phase flowrate in the conditions of analysis, it was possible to resolve the peak of malic acid and calculate its concentration in the sample. However, for the sake to clarity, only fructose and glucose concentrations will be shown in some plots since they are present in a much higher content. Figure 5.7 shows the experimental histories of the average extract and raffinate concentrations. The curves do not represent simulated results, but simply the best smooth lines that link the experimental points. An unexpected behaviour is observed. The product concentrations surpass the values expected to be reached at steady state. The concentrations at steady state, as calculated from the equivalent TMB model, are shown as dot-dashed lines in the plot. The internal profiles were also sampled at 50% of each of the periods of the 5th, 10th and 15th cycles. Figure 5.8 shows the profiles obtained at the 5th and 10th cycles, as compared with the predictions from a model using a real SMB strategy. The same anomalous behaviour is observed, being more pronounced at the 5th cycle. In sections 2 and 3, fructose and glucose concentrations go far beyond those expected assuming linear uncoupled isotherms and mass transfer described by the LDF expression.

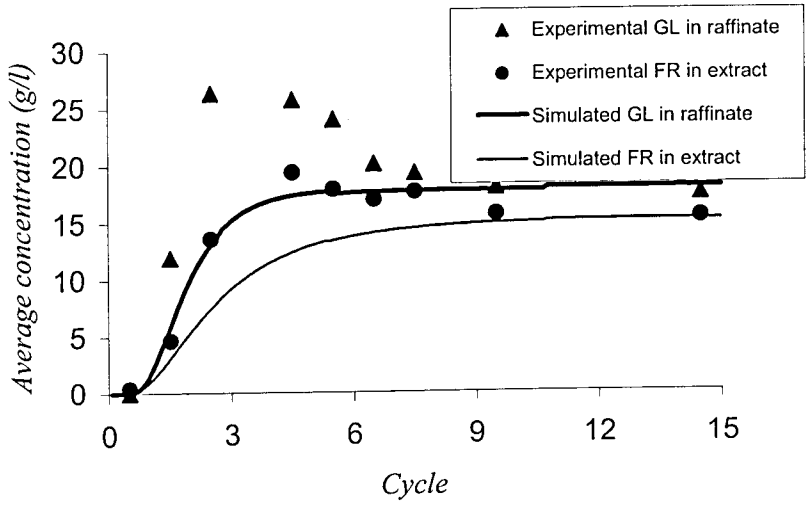

Figure 5.7 Histories of average extract and raffinate concentration for SMB experiment with cashew apple juice.

This behaviour, observed in Figure 5.7 and Figure 5.8, is not usual in systems with linear equilibria. No such phenomenon was observed for the fructose-glucose experiments described in Chapter 4. Therefore, it may be due to other chemical species present in the feed

(and not identified by the previous HPLC analysis), which induced non-linear effects either in the equilibrium isotherms of the sugars or in their diffusion mechanisms. The periodic steady state was assumed to have been achieved in the 15th cycle. This was confirmed by measuring unchanging average product concentrations and by checking glucose and fructose global mass balances. The profile obtained at a half period of the 15th cycle is illustrated in Figure 5.9. The curves stand for simulations: the thick ones were obtained from a SMB strategy and the thin ones, from a TMB strategy. There is very good agreement among simulation results using

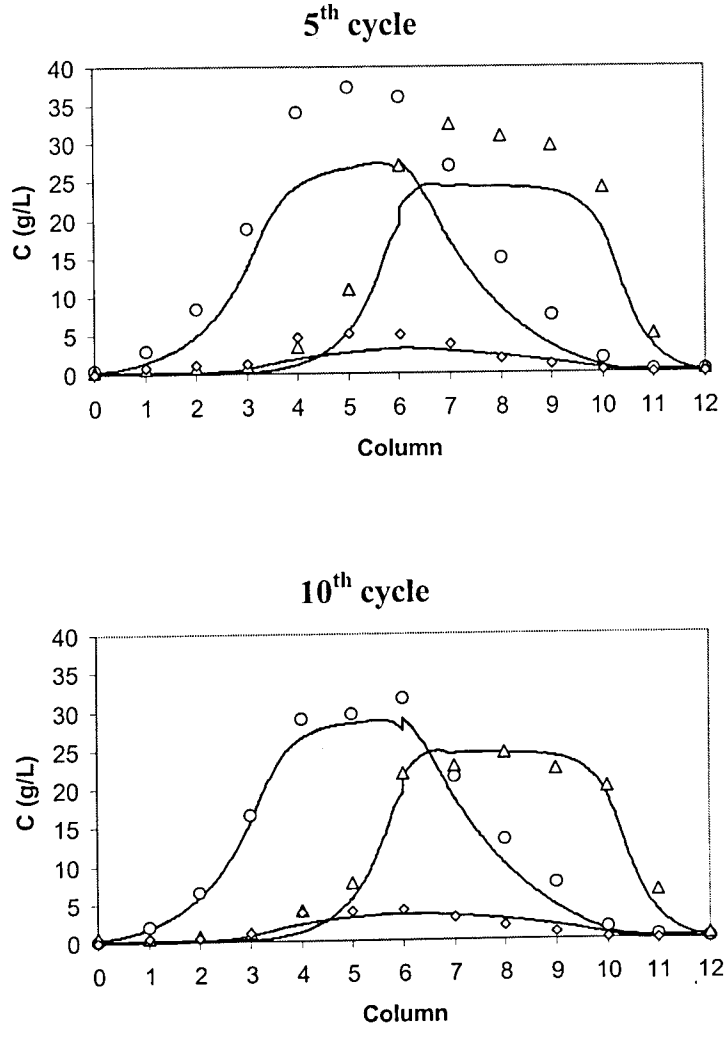

Figure 5.8 *Experimental concentration profiles for fructose (circles), glucose (triangles) and malic acid (diamonds), sampled at 50% of each of the periods of the 5th and 10th cycles. Lines are simulations using SMB strategy.*

both strategies and experimental data. This seems to indicate that the anomalous behaviour is only restricted to the transient phase of SMB operation and, hence, it should be related to a

diverse mass transfer mechanism, rather than to the occurrence of non-linear isotherms.

Another point that may be raised is that related to the ionic form of the resin throughout the experiment. The cashew apple juice contains organic acids and dissolved cations (pH = 4-4.5), which may exchange the Ca^{2+} ions present in the resin and alter its selectivity for fructose. Nevertheless, organic acids usually have low dissociation factors and ions H^+ are not expected to appreciably change the resin cationic form. As for the dissolved cations present in the juice, they are reported to be calcium, iron and phosphorus (P_2O_5). Out of these, iron would be most likely to cause problems; yet, its concentration is reported to be 0.35 mg/100g, compared to 14.5 mg/100g for Ca (Moura Fé, 1972). The most irrefutable proof to support that the resin selectivity remains essentially unchanged is the profile

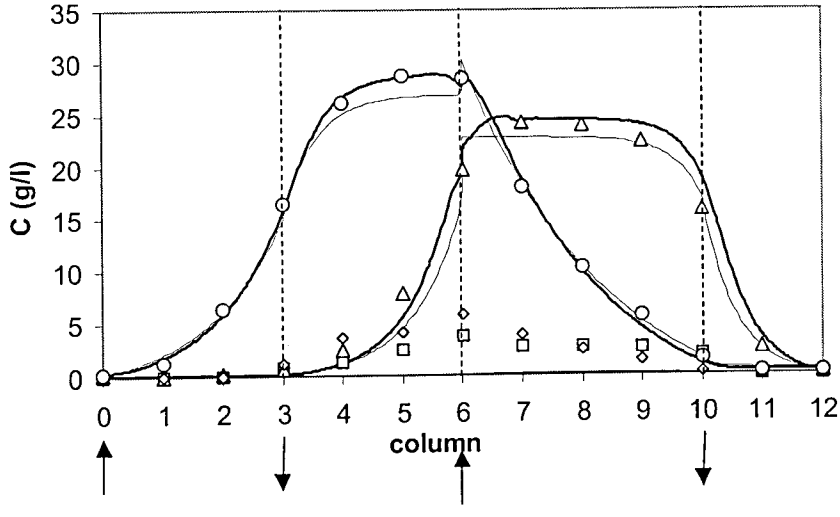

Figure 5.9 *Experimental concentration profiles for fructose (circles), glucose (triangles), malic acid (diamonds) and citric acid (squares) obtained at half period in the 15th cycle. Curves stand for simulation results.*

obtained at the periodic steady state, as shown in Figure 5.9. The performance criteria obtained experimentally agree reasonably well with those predicted from simulation using both TMB and SMB strategies, as may be verified in Table 5.7. Even though experimental purities are below the predicted ones, the concentration of the key products (fructose and Glucose) obtained in the extract and raffinate follow closely those calculated from numerical simulation.

Table 5.7 Comparison of performance criteria obtained experimentally and through simulations using a TMB and SMB strategies.

Performance Criteria	Experimental	Simulated from TMB strategy	Simulated from SMB strategy
PU_X (%)	90.2	92.3	94.5
PU_R (%)	88.4	91.8	93.6
Average PR_i (kg/hr/m^3)	6.4	6.2	6.5
Fructose in extract (g/l)	15.5	14.8	15.9
Glucose in raffinate (g/l)	18.0	17.0	18.0

In order to acquire a better understanding of the behaviour reported in Figure 5.7 and Figure 5.8, a pulse experiment was performed with the 12 SMB columns placed in series. At $t = 0$, a step of cashew apple juice was applied for 10 minutes under a flowrate of 30 ml/min. Samples were collected at the exit of the twelfth column from $t = 30$ to $t = 65$ min. The samples were analysed by HPLC to assess their sugar content. The scheme of this experiment, together with the measured column response, is depicted in Figure 5.10.

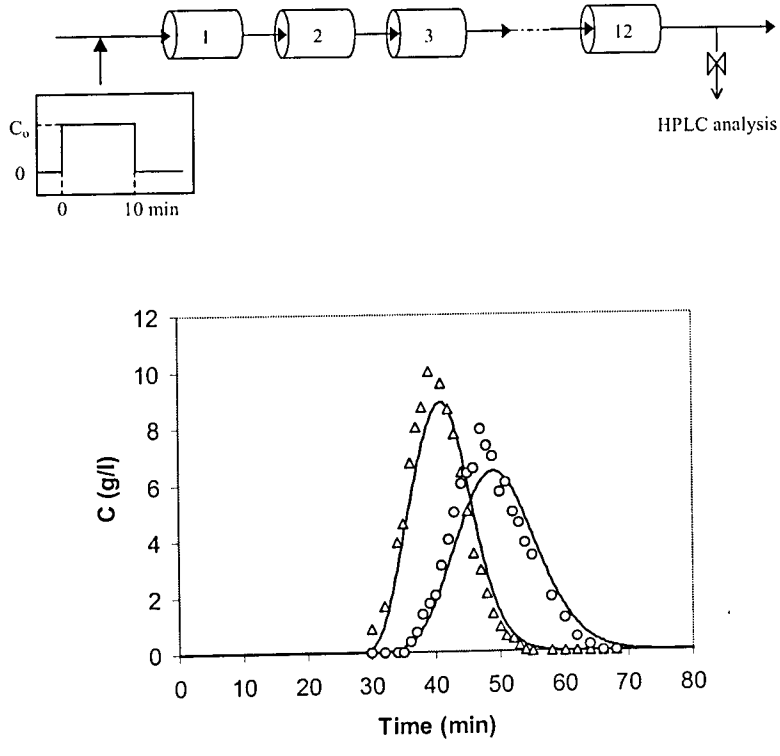

Figure 5.10 Scheme for pulse experiment with cashew juice using the 12 SMB columns and the obtained response curve. Triangles are experimental data for glucose and circles, for fructose

The resin selectivity seems not to have changed much, which is evidenced by the fair agreement between experimental and simulated data. However, some shifting of the curves to the left may point out to a decrease in the adsorption capacities. The maximum height of the experimental peaks is also somewhat greater than that calculated for the simulated curves.

A second experiment in the simulated moving bed was performed using cashew apple juice as feed, which will be referred to as "experiment 2" in contrast to "experiment 1". The operating conditions were the same as in the first experiment (see Table 5.6). Between experiment 1 and experiment 2, no special procedure was employed to "clean" the columns. The equipment was run for several cycles with only water as both feed and eluent in order to rinse the resin and elute all sugars.

In experiment 2, the raffinate and extract were collected for a whole cycle in the 2nd, 4th, 5th, 8th, 10th, 12th and 15th cycles. The surpassing of steady state product concentrations previously reported for experiment 1 was not observed. Figure 5.11 shows the concentrations of fructose in the extract and glucose in the raffinate as compared to the simulated curves of the respective concentrations averaged at each period and to those concentrations obtained in experiment1.

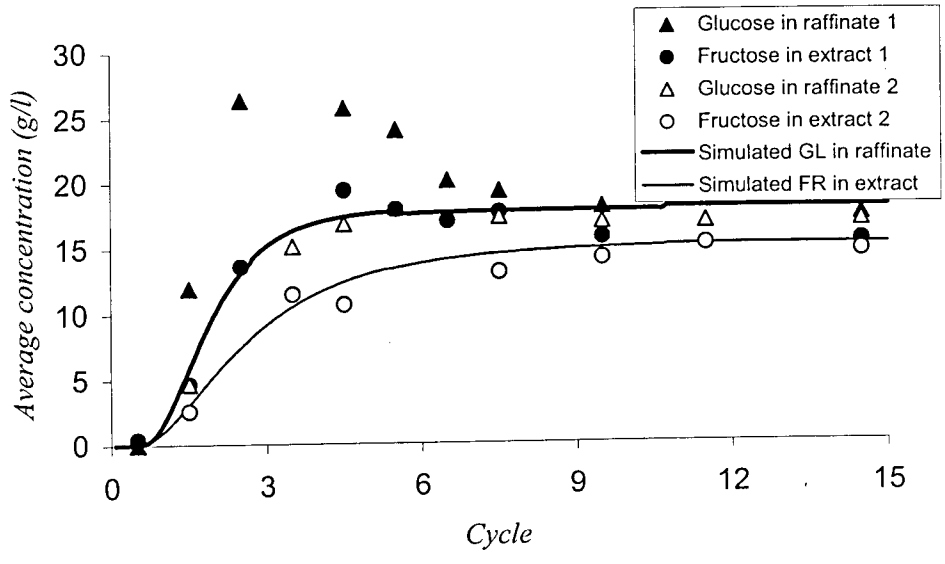

Figure 5.11 *Concentration histories of fructose in the extract and glucose in the raffinate. The curves are simulated (SMB model) and represent the average concentrations at each period. The symbols are concentrations measured from the products collected for a whole cycle.*

The internal concentration profiles were also sampled at 50% of each of the switching times of the 5th and the 10th cycle. The results are shown in Figure 5.12. For the sake of clarity, the profiles of the other species are omitted. The black symbols stand for the concentrations obtained in experiment 1 whereas the white symbols are those obtained in experiment 2.

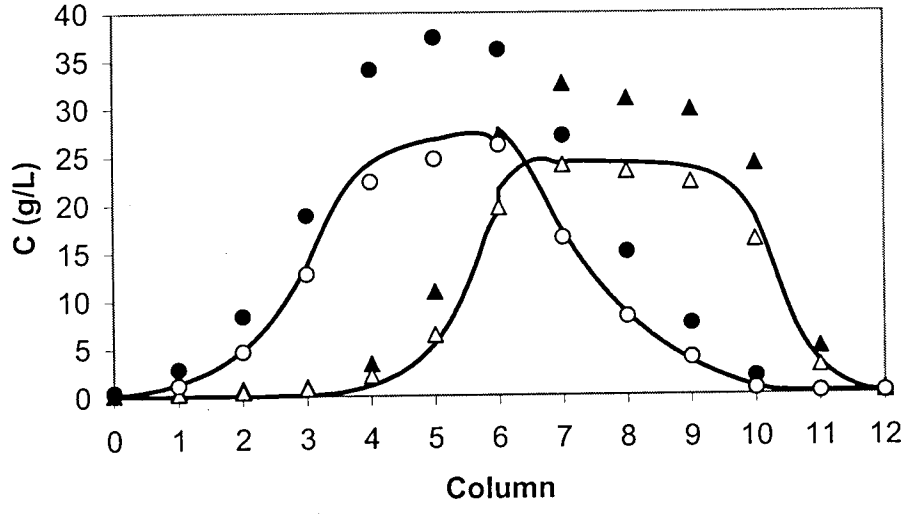

(a)

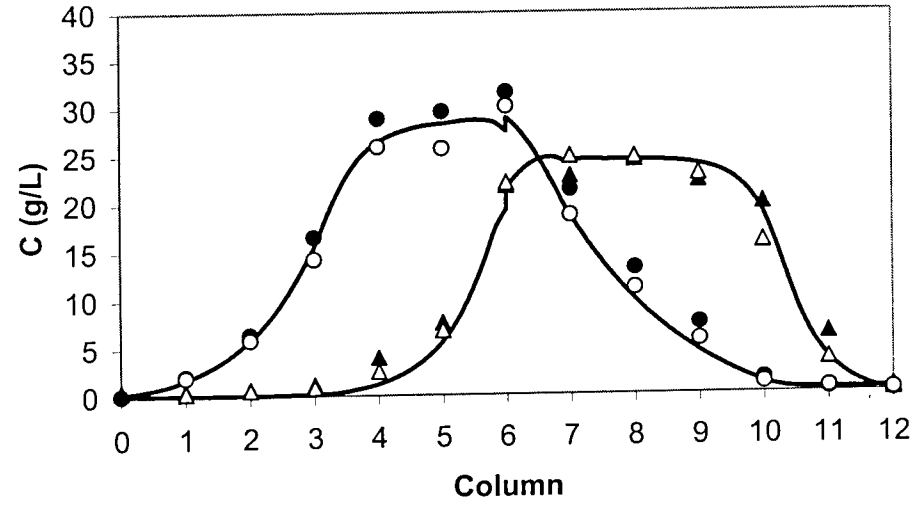

(b)

Figure 5.12 Internal concentration profiles for glucose (triangles) and fructose (circles) sampled at the 5th (a) and 10th (b) cycles. Black symbols refer to experiment 1 and white ones refer to experiment 2. Curves are simulated (SMB model).

It is clear that, in experiment 2, the transient behaviour of sugar concentrations follows closely the fashion predicted by the process simulator for a synthetic mixture. Both mass transfer phenomena and equilibrium parameters seem to have been preserved despite the anomalous behaviour detected in experiment 1. This "overshoot" pattern was also observed for breakthrough curves in a fixed bed packed with fresh resin. This experiment and some others are described in Appendix B. They support the hypothesis that the overshoot pattern may be caused by kinetic hindrances posed by larger molecules (tannins, pigments, enzymes, etc.) being adsorbed irreversibly on the surface of the resin. After these macromolecules have "sat on" the resin particles, the sugars may diffuse and adsorb by the standard well known mechanisms. In the long run, however, these molecules adsorbed on the resin may affect the separation by promoting microbial growth and sugar degradation. This aspect is suggested as a topic for future research.

5.6 Optimized Production of Fructose from Cashew Apple Juice

In this section, the design-optimization algorithm, as presented in Chapter 3, is applied to the separation of fructose from cashew apple juice by SMB. The results are presented in terms of optimal equipment dimensions and operating conditions. The design of SMB equipment to process cashew apple juice in order to obtain high-fructose solutions has some key differences from the conventional SAREX process to produce HFCS from dextrose syrup from corn. They are listed as follows:

- The feed is already a 1:1 binary mixture of fructose and glucose, whereas the SAREX feed comes from a isomerization reactor.

- The feed is very diluted, around 10 times as much as in the SAREX process. If the product is to be made into a syrup, the energy costs of a concentration step must be taken into account in the economic evaluation of the process.

- A step of isomerization of the raffinate stream may be included to obtain a 1:1 fructose-glucose mixture, which may either be recycled to the feed or be concentrated into 50% fructose syrup.

As far as this work is concerned, results will be presented for the design of a SMB plant and optimization of its operation in order to achieve the highest productivity and lowest dilution possible. The economic evaluation of the process taking energy and feedstock costs into account is out of the scope of the present section. The design and optimization package, as described in Chapter 3, was applied to the case of cashew apple juice under the following conditions:

- Minimum purity required = 95% for both extract and raffinate;
- Safety margin of 1.1 and 1.3 was assumed for flowrate ratios in sections 1 and 4;
- Maximal pressure drops per column were allowed to be 10, 5, 1, 0.2 and 0.1 bar;
- Instead of using the adsorbent productivity as the objective function to be maximized, the ratio between solvent consumption and adsorbent productivity was used instead. This decision was taken because dilution of products is a crucial aspect in this case. The algorithm attempted to minimize this new objective function, named as SC/PR.

Figure 5.13 shows the obtained results for a safety margin of 1.3 in terms of minimal required columns lengths to process a certain throughput (a) and the corresponding process parameter SC/PR (b). Plot (c) magnifies the region where the parameter SC/PR reaches a minimal value. It is desirable to operate under as high pressure drop as possible because enhanced productivity may be achieved. Minimal SC/PR is achieved at 5 bar and no further decrease is obtained by raising the pressure drop limit to 10 bar. Since the objective function should be minimized, while keeping high productivity, the optimal operating point seems to be located at a feed flowrate of 140 ml/min, value at which SC/PR is below 11. The optimal equipment dimensions, operating conditions and corresponding performance are summarized in Table 5.8.

Note that the optimized data shown in Table 5.8 were obtained assuming $Q_I = 10^3$ ml/min. Nevertheless, the results apply for any desired throughput by using a scale factor Ω. If one wishes to process a feed flowrate Q_F^{des}, the scale factor is defined as the ratio between the desired flowrate and the optimal feed flowrate obtained from the design algorithm. Then, the cross section area and all other flowrate may be multiplied by this scale factor. Required column length, as well as performance parameters, remain the same.

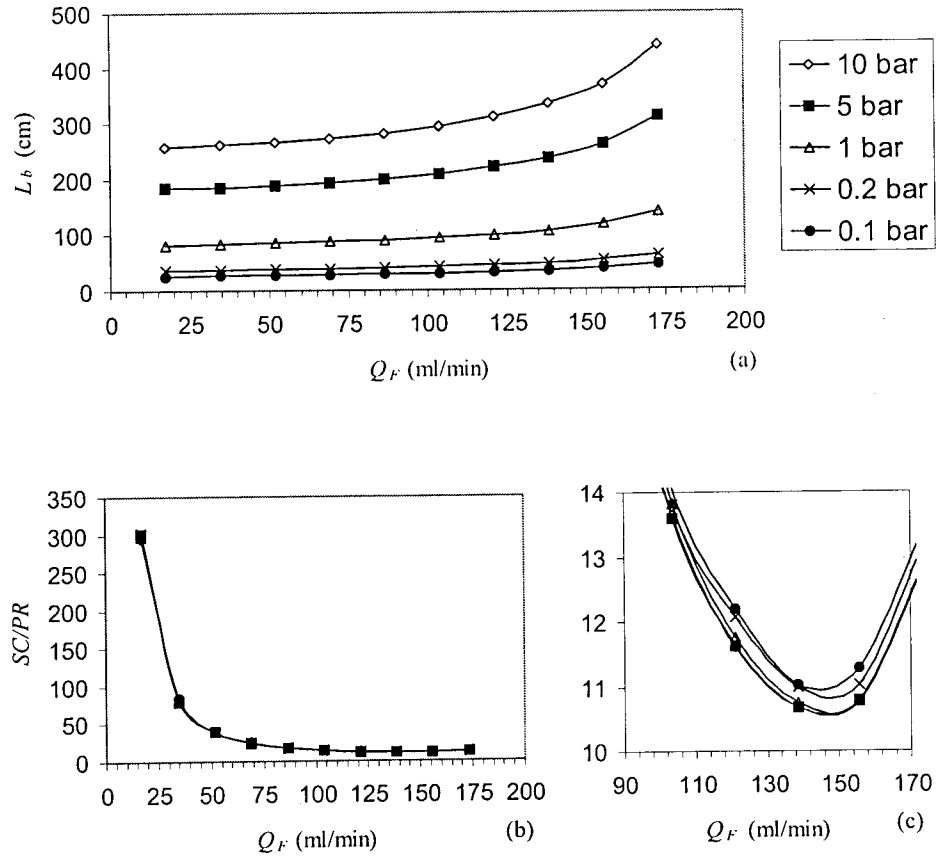

Figure 5.13 Results from SMB design package with β =1.3. (a) Minimum column lengths required to process given throughputs and (b) respective obtained performance. (c) Magnification of plot (b) to observe minimum of curves.

Table 5.8 Data for optimized SMB to separate fructose from cashew apple juice (β =1.3)

Equipment dimensions	Operating conditions	Performance parameters
L_b = 236 cm	$Q_R = Q_4$ =693 ml/min	PU_X = 95.0%
D_b = 5.45 cm	Q_E = 307 ml/min	PU_R = 95.0%
A = 23.3 cm^2	Q_X = 283 ml/min	PR_X = 8 kg/m^3 h
ΔP_{max} =5 bar/column	Q_F = 138 ml/min	PR_R = 8 kg/m^3 h
(25% packing; 75% piping)	Q_R = 162 ml/min	C_F^X = 18.5 kg/m^3
	t^* = 4.4 min	C_G^R = 32.3 kg/m^3

The extract dilution is quite severe, the concentration of fructose being less than half of its value in the feed. Therefore, the same approach as described previously was applied for

a lower safety margin β equal to 1.1. Under this condition, longer columns than for β=1.3 may be required, but less eluent is expected to be used; hence, the extract is supposed to be less diluted. Figure 5.14 illustrates the results obtained for this case. Plot (a) confirms that

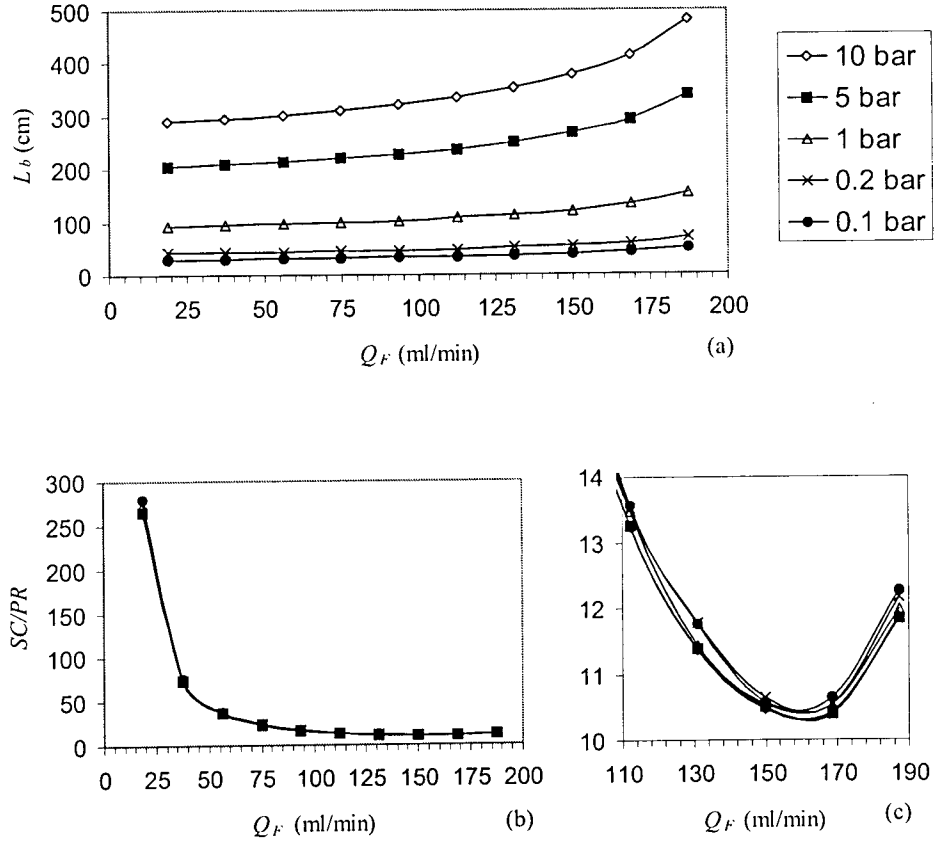

Figure 5.14 Results from SMB design package with β =1.1. (a) Minimum column lengths required to process given throughputs and (b) respective obtained performance. (c) Magnification of plot (b) to observe minimum of curves.

longer columns are necessary to overcome the decrease in the safety margin β. A similar behaviour is obtained for parameter SC/PR. For higher restrictions on pressure drop, SC/PR decreases until itbecomes nearly stationary at ΔP = 1 bar and higher. However, the absolute value of the minimal SC/PR is below that obtained for β=1.3. The corresponding optimal feed flowrate is around 160 ml/min, which is higher than the 140 ml/min obtained in the previous case. These findings indicate that more concentrated products are likely to be obtained. Table 5.9 summarizes the optimized data obtained for β=1.1 in terms of equipment dimensions, operating conditions and expected performance parameters. As expected, more concentrated products are obtained. Despite the somewhat lower product productivity,

operating under the conditions stated in Table 5.9 may be advantageous, since the cost of the stationary phase is not high and dilution is significantly reduced. The choice on whether to operate under a pressure drop of 1, 5 or 10 bar depends on an economic evaluation of the pumping costs. The figures printed in brackets are the results obtained for optimal SMBR operation if the particle size were reduced two-fold. Mass transfer would be enhanced and much shorter columns would be required with improved productivity. The optimal operating flowrates and obtained product concentrations remain essentially the same.

In order to obtain syrups of commercial interest, the extract stream must undergo a step of concentration to raise its concentration to 50 Brix (20 fold concentration). To raise the added value of raffinate, it may undergo a isomerization step to produce a 1:1 fructose-glucose solution, which in turn may be either recycled back to the feed stream or concentrated into a syrup.

Table 5.9 Data for optimized SMB to separate fructose from cashew apple juice (β =1.1)

Equipment dimensions	Operating conditions	Performance parameters
L_b = 268 cm (120)	$Q_R = Q_4$ =750 ml/min	PU_X = 95.1%
D_b = 5.8 cm (7.8)	Q_E = 250 ml/min	PU_R = 95.1%
A = 26.4 cm^2 (47.8)	Q_X = 228 ml/min	PR_X = 6.7 kg/m^3 h (8.32)
ΔP_{max} =5 bar/column	Q_F = 150 ml/min	PR_R = 6.7 kg/m^3 h (8.34)
(25% packing; 75% piping)	Q_R = 172 ml/min	C_F^X = 25 kg/m^3
	t^* = 5.2 min (4.2)	C_G^R = 33 kg/m^3

5.7 Conclusions

This section examined the potential use of cashew apple juice as a source of fructose to be separated by SMB chromatography. The chemical analysis of the aqueous phase of cashew apple juice by HPLC revealed the presence of glucose and fructose in equal amounts (40 kg/m^3). The steady state performance of a SMB pilot plant using cashew apple juice as feed agreed quite well with the theoretical predictions, as obtained from the models described in Chapter 3. Interesting anomalous behaviour was obtained at the transient state for the first time that the adsorbent resin was contacted with the juice. We believe that larger molecules, yet to be identified, are strongly and irreversibly adsorbed on the resin. During the transient period, the concentration of such molecules at the vicinity of the resin particles may impair

the diffusion of sugar molecules. As the "macromolecules" reach a state of equilibrium of adsorption, the sugar molecules may diffuse, adsorb and desorb in the different SMB section by the conventional well-known mechanisms. Appendix B describes further experimental work carried out in fixed bed mode and the obtained results support this theory. Further investigation into the long-term life of the resin is strongly recommended for future research. The design algorithm proposed previously in this thesis was applied to find optimal equipment dimensions and operating conditions by considering both the adsorbent productivity and solvent consumption as objective functions. The results indicate that optimal performance in terms of product dilution and productivity may be achieved at dimensionless throughputs η around 0.8. The newly defined parameter SC/PR is minimized by operating at a minimal pressure drop limit of 1 bar/column and applying low safety margins to sections 1 and 4.

5.8 References

F. A. M. Campos, "Virtudes Nutritivas do Caju", *Anais Fac. Med. Univ. São Paulo* **22**, 79-94 (1946).

M. N. Cavalcante, G. A. Maia, H. F. Oriá, R. W. Figueiredo, Z. B. L. Guedes, "Estudo do processamento e Estabilidade da Cajuína a Partir do Suco de Caju (Anacardium occidentale, L.)", *Ciên. Agron.* **17**, 105-109 (1986).

H. M. Cecchi, D. B. Rodriguez-Amaya, "Carotenoid Composition and Vitamin A Value of Fresh and Pasteurized Cashew-Apple (Anacardium occidentale L.) Juice", *J. Food Sci.* **46**, 147-149 (1981).

A. S. T. Chiang, "Equilibrium Theory for Simulated Moving Bed Adsorption Processes", *AIChE J.* **44**, 2431-2441 (1998).

B. Dubuc, "Cashew Apple Juice, Anyone?", . (IDRC: Resources: Books: Reports: Vol. 23, No. 1, 1995), www page, http://www.idrc.ca/books/reports/V231/cashew.html.

H. A. C. Filgueiras, R. E. Alves, J. L. Mosca, J. B. Menezes, "Cashew Apple for Fresh Consumption: Research on Harvest and Postharvest Technology in Brazil", W. Plocharski, Ed., International Symposium On Effect of Pre- and Post Harvest Factors on Storage of Fruit, Warsaw, Poland (1997).

I. L. M. Fonseca, G.A.; Júnior, J.C.G.; Rodrigues, M.C.P.; Monteiro, J.C.S.; Oriá, H.F. and Guedes, Z.B.L., "Obtenção de Bebida Dietética a Base de Caju (Anacardium occidentale, L.)", *Ciên. Agron.* **26**, 79-84 (1995).

L. A. S. Leite *The Cashew Agroindustry in Brazil.* EMBRAPA-CNPAT, Fortaleza, 195 p. (1994).

V. P. M. S. Lima *The Cashew Crop in Northeastern Brazil (in Portuguese).* BNB-ETENE, Fortaleza, 486 p. (1988).

M. H. C. Lopes, "Composição Química e Aproveitamento da "Pêra" de Caju de Moçambique", *Agron. Moçamb.* **6**, 119-131 (1972).

A. Lopes Neto *A Agroindústria do Caju no Nordeste e em outros Grandes Países Produtores.* Banco do Nordeste do Brasil, Fortaleza, 472 p. (1981).

C. Migliorini, M. Mazzotti, M. Morbidelli, "Design of Simulated Moving bed Multicomponent Separations: Langmuir Systems", *Sep. Pur. Technol.* **20**, 79-96 (2000).

J. C. Montealegre, N. F. Childers, S. A. Sargent, L. M. Barros, R. E. Alves, "Cashew (Anacardium occidentale, L.) Nut and Apple: a Review of Current Production and Handling Recommendations", *Fruit Varieties Journal* **53**, 2-9 (1999).

J. A. Moura Fé, "Características Químicas do Hipocarpo do Caju (Anacardium occidentale, L.)", *Ciênc. Agron.* **2**, 103-108 (1972).

A. Pereira Jr., J. B. Graça, J. Pereira, M. M. A. Pereira, "Estudo do Suco da Maçã de Caju (Anacardium occidentale L.) da Guiné Portuguesa", *Estud. Agron.* **7**, 35-41 (1966).

P. F. A. P. Pessoa, L. C. S. Leite, C. R. M. Pimentel, "Situação Atual e Perspectivas da Agroindústria Tropical", in *Cajucultura, modernas técnicas de produção* J. P. P. Araújo, V. V. Silva, Eds. (EMBRAPA/CNPAT, Fortaleza, 1995) pp. 23-42.

M. S. M. Souza Filho, et al., "Clarificação Enzimática do Suco de Caju", *Pesq. Agropec. Bras.* **26**, 1647-1653 (1991).

R. Vieira, N. Woolfe, E. Pires, W. J., N. B. Guerra, "Produção de suco concentrado de caju", *Boletim SBCTA (Campinas-SP)* **2**, 222-232 (1982).

6. Inversion of Sucrose and Fructose-Glucose Separation in a Simulated Moving Bed Reactor (SMBR)

6.1 Introduction

When a chemical reaction occurs within a chromatographic column, simultaneous reaction and separation are usually promoted. The combination of reaction and separation in a single piece of equipment has the obvious economical advantage of reducing the cost of unit operations for downstream purification steps. In preparative and production-scale applications, there are other scientific factors in favour of the use of this type of reactors as compared to conventional batch, plug flow and stirred-tank reactors. In the case of reversible reactions, removal of products as they are formed allows achieving conversions well beyond equilibrium values. When a reaction product has an inhibiting or poisoning effects, its removal from the reaction medium also promotes enhanced yield. For reactions in series or in parallel, it may be possible to separate selectively desired intermediate species. In many biochemical reactions, where excess substrate has an inhibiting effect, it may be possible to achieve higher yields at the expense of lower enzymatic activity.

The basic operation principles of a batch chromatographic reactor may be illustrated in Figure 6.1. The figure shows a chromatographic column packed with a selective adsorbent subjected to a constant eluent flow. The reaction catalyst may be introduced in free form (dissolved in the eluent), supported within the adsorbent bed or homogeneously mixed in the packing. Let us assume that the reversible chemical reaction $A \leftrightarrow B + C$ is to occur in the chromatographic reactor by injecting a sharp pulse of reagent A. Consider that A, B and C have different affinities for the packing expressed by their respective linear adsorption constants K_A', K_B' and K_C'. If $K_C' < K_A' < K_B'$, the pulse of A will decrease in size as it forms the products B and C, which move at different speeds within the column. As time goes by, B is retarded as compared to C and reagent A may eventually disappear. Since B and C are segregated, the reverse reaction is inhibited and reaction conversion may go beyond the equilibrium values. Both products may be collected at high purity with nearly complete conversion.

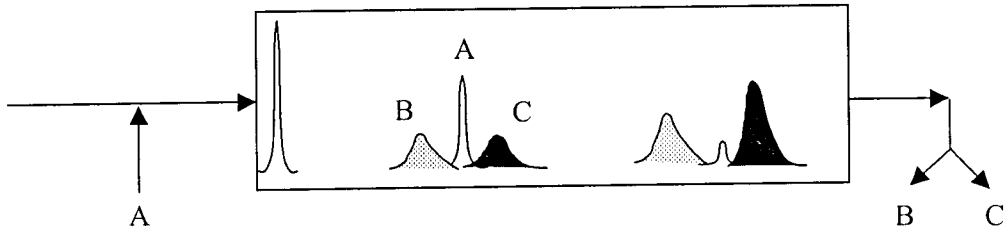

Figure 6.1 Principle of operation of a batch chromatographic reactor.

The major drawbacks of this type of reactor are those aspects common to batch chromatography: low yields, high product dilution, poor use of the packing and inherently discontinuous operation. Because of these factors, batch chromatographic reactors have limited use for preparative scale applications. Instead, they have been frequently used in analytical scale. In the absence of mass transfer resistances and other dispersive effects, the reaction chromatogram provides a useful means of obtaining information on the reaction rate expression.

For the last thirty years, the concept of chromatographic reactors has been extended to continuous processes in order to benefit from those features as enhanced productivity and decreased solvent consumption. Continuous mode of operation has been achieved by means of moving the adsorbent bed or simulating its motion. This is possible by such equipment configurations as simulated moving bed (Hashimoto *et al*, 1983), countercurrent moving-bed

(Fish and Carr, 1989; Petroulas *et al*, 1985), rotating annular chromatograph (Sarmidi and Barker, 1993) and semicontinuous countercurrent chromatographic reactor-separator (Ganetsos *et al*, 1993).

Continuous chromatographic reactors have found quite interesting applications in biochemical reactions and separations (Cen and Tsao, 1993). Among these, the inversion of sucrose and separation of fructose from glucose is an illustrative example due to the following aspects:

- Sucrose is probably the most abundant saccharide, which may be either found in nature or readily obtained from degradation of starch;
- Invertase, the enzyme which promotes sucrose inversion, is relatively stable and cheap to be obtained in quite pure form;
- The reaction rate law of sucrose inversion is well described by the Michaelis-Menten expression;
- The adsorption and diffusion of carbohydrates in cation-exchange resins is well-known in terms of equilibrium isotherms and mass transfer mechanisms:

Hence, enzymatic sucrose inversion is an excellent test reaction to be used as an application for the purposes of modeling, design and optimization of continuous chromatographic reactor-separators, especially those of simulated moving bed type. This chapter describes the principles of inversion of sucrose and glucose-fructose separation in a simulated moving bed reactor. The state of the art of continuous chromatographic reactors is addressed in the following section. Then, the proposed mathematical models for the process are described. Experimental results are presented and confronted with predictions from theoretical simulations. The role of the enzyme strength is investigated taking into account that reaction occurs both in the bulk liquid phase and on the adsorbent resin surface.

6.2 Literature Review

The first attempts to combine reaction and chromatographic separation in a continuous mode are reported (Ganetsos *et al*, 1993) to date back to the early 70's. The first continuous chromatographic reactors worked in gas phase and employed falling moving bed schemes to promote surface-catalysed chemical reactions. A stream of fine catalyst particles falls

downwards against an upward flowing current of gas. Throughout the decades of 70's and 80's, the main applications investigated for gas-phase moving bed reactors were the catalytic oxidation of carbon monoxide (Takeuchi and Late Uraguchi, 1977; Takeuchi *et al*, 1978; Takeuchi and Uraguchi, 1976) and the hydrogenation of mesitylene (Fish and Carr, 1989; Petroulas *et al*, 1985).

Well-known problems associated with solids movement are attrition and the resulting requirement for fines removal, inclusion of a solids handling system for recycling and the maintenance of a uniform flow of solids. All these factors led Prof. Carr to innovate the scenario of continuous chromatographic reactors (Ray *et al*, 1990) by proposing an equipment configuration resembling the SORBEX process (by UOP) for continuous adsorptive separation of binary mixtures. Solids countercurrent motion was simulated by periodically changing the feed positions sequentially along a fixed bed. Prof. Carr research group has successfully used the simulated moving bed reactor in gas phase applied to the hydrogenation of 1,3,5-trimethylbenzene (Ray *et al*, 1994) and to the oxidative coupling of methane (Tonkovich and Carr, 1994). These applications, together with others in liquid phase, are summarized in Table 6.1.

For most of the applications developed up to the mid 90's, catalyst and adsorbent are essentially different materials, which may be mixed or arranged in alternate columns. An additional problem arises when reaction and separation occur at different temperatures so that temperature gradients must be conveniently handled within the chromatographic reactor. Mazzotti et al (1996) investigated the esterification of acetic acid on a simulated moving bed reactor as a model reaction for which these effects are overcome. Esterification reactions are reversible and may be catalysed by acid sites promoted by sulphonic groups present in crosslinked polystyrene-based resins. Moreover, the resin may selectively adsorb the chemical species involved and enhance the separation of reaction products. This remarkable property from a class of ion-exchange resins has motivated the study of other reactions in a simulated moving bed reactor such as the esterification of acetic acid by β-phenethyl alcohol (Kawase *et al*, 1996) and the production of bisphenol A (Kawase *et al*, 1999).

In Table 6.1, a marked contribution may be observed from the biochemical field in the development of applications to continuous chromatographic reactors. Some ingenious arrangements that implement the principle of the continuous chromatographic reaction-separation principle have been reported. Barker *et al* (1992) have successfully used a

Table 6.1 Applications of continuous chromatographic reactor-separators

APPLICATION	TYPE OF REACTOR	PHASE	REFERENCE
Catalytic oxidation of carbon monoxide on activated alumina	Moving (falling) bed reactor	Gas	(Takeuchi and Late Uraguchi, 1977)
Production of higher-fructose syrup from isomerization of glucose by action of immobilised isomerase	SMBR with alternate fixed beds packed with enzyme and adsorbent in the reaction zone	Liquid	(Hashimoto *et al*, 1983)
Hydrogenation of 1,3,5-trimethyl benzene by Pt supported on alumina	Moving (falling) bed reactor	Gas	(Fish and Carr, 1989)
	SMBR	Gas	(Ray *et al*, 1994)
Inversion of sucrose by action of enzyme invertase and glucose-fructose separation	Simulated moving column continuous countercurrent chromatographic reactor-separator (SCCR-S)	Liquid	(Barker *et al*, 1992)
	Continuous rotating annular chromatographic (CRAC) reactor		(Sarmidi and Barker, 1993)
	SMBR		(Azevedo and Rodrigues, 2001; Meurer *et al*, 1996)
	SMBR without liquid recycle		(Ching and Lu, 1997)
Biosynthesis of dextran from sucrose by action of enzyme dextranosucrase	SCCR-S	Liquid	(Ganetsos *et al*, 1993)
Repeated use of coenzyme ATP in the enzymatic conversion of glucose to glucoe-6-phosphate	2-section SMBR	Liquid	(Hashimoto *et al*, 1993)
Methanol synthesis from syngas by action of metal catalysts	SMBR	Gas	(Kruglov, 1994)
Oxidative coupling of methane by action of oxide-type catalysts	SMBR	Gas	(Tonkovich and Carr, 1994)
Esterification of acetic acid with β-phenethyl alcohol by action of proton-type ion-exchange resins	SMBR	Liquid	(Kawase *et al*, 1996)
Esterification of acetic acid with methanol by action of proton-type ion-exchange resins	SMBR	Liquid	(Mazzotti *et al*, 1996)
Synthesis of bisphenol A from acetone and excess phenol over ion-exchange catalyst	3-section SMBR	Liquid	(Kawase *et al*, 1999)
Production of lactosucrose by action of enzyme β-fructofuranosidase	SMBR	Liquid	(Kawase *et al*, 2001)

semicontinuous countercurrent chromatographic reactor-separator (SCCR-S) for the inversion of sucrose and biosynthesis of dextran from sucrose. Sarmidi and Barker (1993) were the first authors to carry out the inversion of sucrose and separation of fructose from glucose using a continuous rotating annular chromatograph (CRAC). Hashimoto and co-workers (1983) studied the use of a continuous moving-column chromatographic separator for the production of high-fructose syrups by combining the adsorption of fructose and isomerization of the separated glucose fraction on alternatively arranged adsorption and bio-reaction columns.

The inversion of sucrose and subsequent separation of produced glucose and fructose by continuous chromatographic reactor-separators have been studied mainly by the group from the University of Aston (Barker *et al*, 1992; Ganetsos *et al*, 1993; Sarmidi and Barker, 1993) and, to a lesser extent, by the University of Dortmund (Meurer *et al*, 1996) and Singapore (Ching and Lu, 1997). There are few experimental results published except for the reactors of CRAC and SCCR-S types. The inversion of sucrose by enzyme invertase, represented below, is an irreversible reaction, and thus the reaction rate is not influenced by product accumulation.

$$\textbf{Sucrose} \xrightarrow{\text{invertase}} \textbf{Fructose} + \textbf{Glucose}$$

However, it has been shown that, even for irreversible reactions, the use of a SMBR increases conversion and product purity as compared to the performance of conventional processes (Meurer *et al*, 1997). Barker *et al* (1992) have also shown that simultaneous inversion and product separation makes it possible to overcome problems associated with substrate inhibition. Hence, the authors report using feed concentrations up to 55% (w/v), having achieving complete conversion and product purities over 90% in a SCCR-S. An optimum enzyme/sucrose ratio was found to be around 600 U/g for this reactor, with a corresponding adsorbent productivity of 16 kg sugar per m^3 resin per hour. These performance parameters will be compared with those obtained in this work.

The design and optimisation of an SMBR to carry out simultaneous and continuous bio-reaction and separation are essential to define the feasibility of implementation of the process at industrial scale. The number of publications focusing on the design of non-reactive SMB's is quite large, as discussed in Chapter 3. Nevertheless, the same may not be said of SMBR design (Dünnebier *et al*, 2000; Fricke *et al*, 1999; Migliorini *et al*, 1999). Design will define geometric and operating parameters that should lead not only to product separation but also to high reagent conversions. If the reaction is to be catalysed, and this is the case in bio-

reactions, the amount of catalyst is an additional degree of freedom to the optimisation problem. These aspects will be addressed in detail in the following chapter.

6.3 Modeling of a SMBR

In this section, a simulated moving bed reactor with four sections will be considered for the enzymatic inversion of sucrose and separation of fructose from glucose. Figure 6.2 shows the column arrangement of our theoretical modeling object. A set of packed columns is arranged in a closed circuit having two ports for liquid introduction (feed and eluent) and two ports for liquid withdrawal (extract and raffinate). A sucrose solution is used as feed and the enzyme is introduced in the system diluted in the eluent (buffer solution). Fructose, which is more strongly retained in the cation-exchange resin, is collected in the extract port. The raffinate port collects the glucose-enriched product. At regular time intervals, the introduction and withdrawal points are advanced one bed ahead in the direction of fluid flow. A cycle is completed when the number of switches is equal to the number of columns. This way, the countercurrent motion of the solid adsorbent is simulated under a velocity equal to the length of a column divided by the switching time.

The relative motion of the chemical species present in a SMBR may be more clearly understood by considering the equivalent representation of a true countercurrent moving bed reactor (TMBR). Inlet and withdrawal points are kept stationary and the solid adsorbent moves in the opposite direction to the fluid phase. The TMBR representation provides not only a clearer picture of the equipment operation but also a simpler model to implement for the purposes of process prediction, design and optimization.

We have proposed mathematical models using both SMBR and TMBR strategies. The TMBR strategy was employed in steady-state calculations for design and optimization purposes. Due to the higher computational effort required in its solution, the SMBR strategy was used only to assess the history of product concentrations and to examine transient concentration profiles. Since both models convey essentially the same information at steady state, the TMBR strategy has been our model of choice as far as performance prediction is concerned.

For each of the four countercurrent sections of a TMBR (denoted by subscript j), the differential mass balance equations for chemical species i at steady-state would be the following:

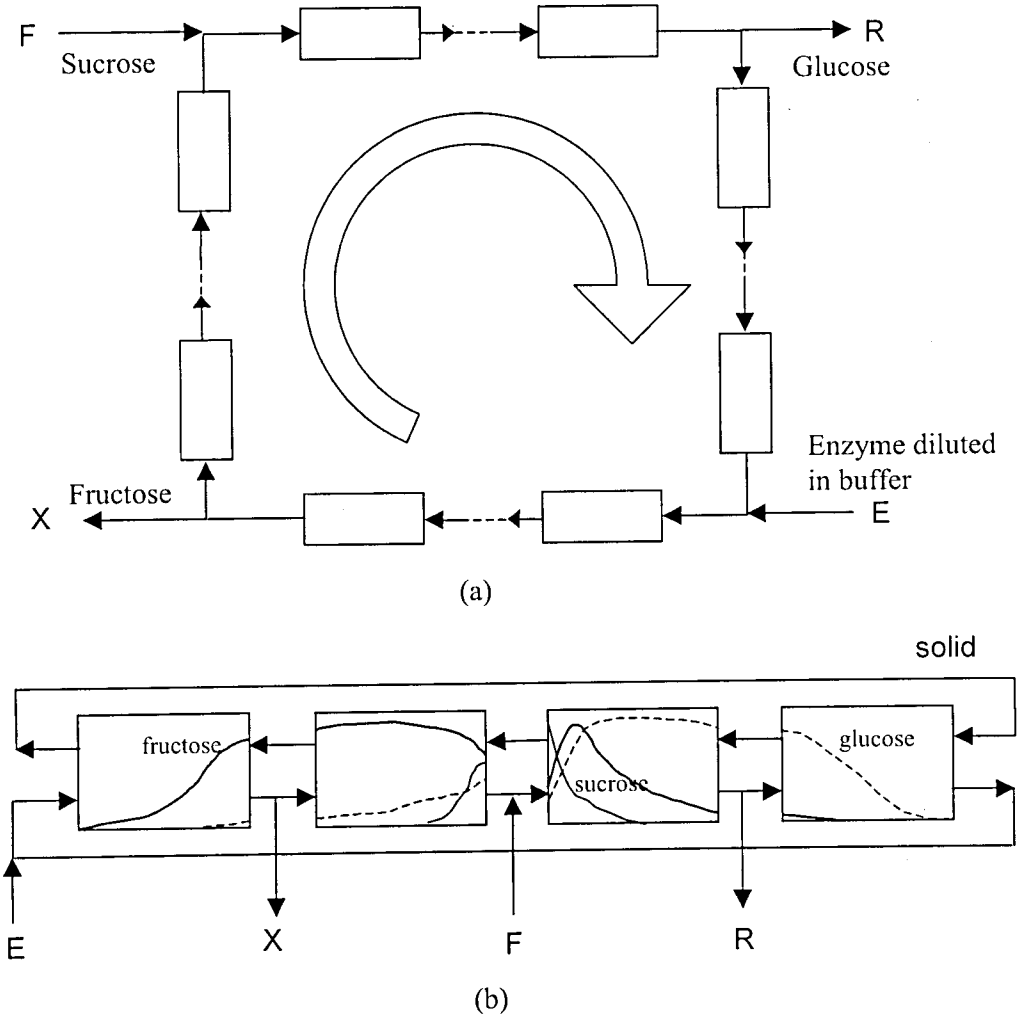

Figure 6.2 *Representation of a simulated moving bed reactor (a) and the equivalent true moving bed reactor (b). The latter shows an illustrative concentration profile.*

– For the bed fluid phase between adsorbent particles:

$$\frac{\gamma_j}{Pe_j}\frac{d^2C_{i,j}}{dx^2}-\gamma_j\frac{dC_{i,j}}{dx}-\nu\frac{Bi_{m_j}}{Bi_{m_j}+5}\alpha_{p_{i,j}}\left(C_{i,j}-<C_p>_{i,j}\right)+\alpha_{r_j}\left(1+\nu K_{enz}\right)\left(\frac{\sigma_i R_j}{k_r}\right)=0$$

i = glucose or fructose (6.1)

$$\frac{\gamma_j}{Pe_j}\frac{d^2C_{i,j}}{dx^2}-\gamma_j\frac{dC_{i,j}}{dx}+\alpha_{r_j}\left(1+\nu K_{enz}\right)\left(\frac{\sigma_i R_j}{k_r}\right)=0 \qquad i = \text{sucrose} \qquad (6.2)$$

$$\frac{1}{Pe_j}\frac{d^2C_{i,j}}{dx^2}-\frac{dC_{i,j}}{dx}=0 \qquad i = \text{enzyme} \tag{6.3}$$

$$\text{where } R_j = k_r \frac{C_{s,j}\times C_{e,j}}{K_{mm}+C_{s,j}};\ \sigma_i = \begin{cases} -1 \text{ if } i \text{ is sucrose} \\ +0.526 \text{ if } i \text{ is fructose or glucose} \end{cases} \tag{6.4}$$

and K_{enz} = linear adsorption constant of enzyme onto resin surface

– For the fluid phase within particle pores (i = glucose or fructose, only):

$$\frac{\partial < C_p >_{i,j}}{\partial x}+\frac{Bi_{mj}}{5+Bi_{mj}}\frac{\alpha_{pj}}{\varepsilon_p}\left(C_{i,j}-< C_p >_{i,j}\right)-\frac{\alpha_{\mu j}}{\varepsilon_p}\left[K_i < C_p >_{i,j} - << q >>_{i,j}\right]=0 \tag{6.5}$$

– For the solid phase within the resin particles (i = glucose or fructose, only):

$$\frac{\partial << q >>_{i,j}}{\partial x}+\alpha_{\mu_j}\left[K_i < C_p >_{i,j} - << q >>_{i,j}\right]=0 \tag{6.6}$$

The corresponding boundary conditions for a given section j are:

$$C_{i,j}^{in} = C_{i,j}(0)-\frac{1}{Pe_j}\frac{\partial C_{i,j}}{\partial x} \quad \text{for any } i \tag{6.7}$$

$$\frac{\partial C_{i,j}}{\partial x}(1)=0 \qquad \text{for any } i \tag{6.8}$$

$$< C_p >_{i,j}(1) =< C_p >_{i,j+1}(0) \qquad \text{for } i = \text{glucose or fructose} \tag{6.9}$$

$$<< q >>_{i,j}(1) =<< q >>_{i,j+1}(0) \qquad \text{for } i = \text{glucose or fructose} \tag{6.10}$$

The dimensionless space variable is $x = z/L_j$, where L_j is the length of section j. The dimensionless numbers present in the model equations are:

$$\gamma_j = \frac{U'_{Fj}}{U_S} \qquad \text{Fluid/solid intersticial velocity ratio} \tag{6.11}$$

$$Pe_j = U'_{F_j} L_j / D_{ax_j} \quad \text{Peclet number} \quad (6.12)$$

$$\nu = \frac{(1-\varepsilon)}{\varepsilon} \quad \text{Solid/fluid phase ratio} \quad (6.13)$$

$$\sigma_i = \frac{\text{Mol. weight of species } i}{\text{Mol. weight of sucrose}} \quad \text{Molecular weight ratio} \quad (6.14)$$

$$\alpha_{pj} = \frac{k_p L_j}{U_S} \quad \text{Number of macropore mass transfer units} \quad (6.15)$$

$$\alpha_{rj} = \frac{k_r L_j}{U_S} \quad \text{Number of reaction units} \quad (6.16)$$

$$\alpha_{\mu j} = \frac{k_\mu L_j}{U_S} \quad \text{Number of microparticle mass transfer units} \quad (6.17)$$

$$Bi_{mj} = \frac{k_{fj} R_p}{D_{pe}} \quad \text{Mass Biot number} \quad (6.18)$$

$C_{i,j}^{in}$, present in the boundary condition at the section inlet, can be found from the node balances. The following equations are valid for all i (glucose, fructose, sucrose and enzyme)

Eluent node:

$$C_{i,1}^{in} = \frac{Q'_4}{Q'_1} C_{i,4}(1) + \frac{Q_E}{Q'_1} C_{i,E} \quad (6.19)$$

Extract node:

$$C_{i,2}^{in} = C_{i,1}(1) \quad (6.20)$$

Feed node:

$$C_{i,3}^{in} = \frac{Q'_2}{Q'_3} C_{i,2}(1) + \frac{Q_F}{Q'_3} C_{i,F} \quad (6.21)$$

Raffinate node:

$$C_{i,4}^{in} = C_{i,3}(1) \tag{6.22}$$

The reaction of inversion of sucrose was described by the Michaelis-Menten equation, with substrate inhibition, as stated in equation (6.4). Since all mass balance equations are written in terms of mass rather than moles, the "stoichiometric" parameter σ_i is calculated as the ratio between the molecular weight of species i and that of sucrose.

Sucrose is assumed to react in inter-particle fluid phase and at the surface of the resin due to immobilized enzyme adsorbed at its exterior surface. This is accounted for by the term $(1+\nu K_{enz})$, present in equations (6.1) and (6.2). Reaction products glucose and fructose are assumed to have linear isotherms, as measured in the experiments summarized in Chapter 4. Their diffusion within the adsorbent particle is described by means of a bi-linear driving force approximation, as shown in Chapter 3. Sucrose adsorption into the adsorbent particles was not considered in the model, since it has been observed experimentally that the adsorption constant of sucrose is nearly equal to the particle porosity (Santos, 1999). Diffusion of sucrose into the adsorbent was not considered as well since the reaction characteristic time constant (50.32 min^{-1}), as measured by Santos (1999), is much larger than the pore diffusion characteristic time (1.44 min^{-1}), as calculated from the Glueckauf correlation (1955).

The system of ordinary differential equations that describes the process was solved numerically, using the ODE solver package COLNEW (Ascher *et al*, 1981). Spatial discretization was performed by modified B-splines assuming 150 elements per section with 2 collocation points in each element. The integrator tolerance was set at 10^{-9}. Solution was pursued by consecutive iterations, each new iteration taking the solution calculated from the previous one as an initial guess. This iterative process went on until the sum of the following absolute errors was less 1%:

- Sum of relative differences between extract and raffinate concentrations of two consecutive iterations;
- Global molar balance between sucrose and invert sugar (for each mole of sucrose that enters the SMBR, one mole of glucose and one mole of fructose must leave);
- Global mass balance for enzyme (amount that enters = amount that leaves);

The solver took an average of 15 iterations to solve the system of ODE's. Run times were typically 5 minutes in a Pentium II 300 MHz processor.

A transient model for the simulated moving bed reactor was proposed based on the actual switching of inlet and outlet ports. This approach consists in writing the proper mass balance equations for each of the fixed beds present in the SMBR. The mass balance equations for a species i in bed k are:

- For the bed fluid phase between adsorbent particles:

$$\frac{\partial C_{i,k}}{\partial \tau} = \frac{\psi_k}{Pe_k}\frac{\partial^2 C_{i,k}}{\partial \chi^2} - \psi_k \frac{\partial C_{i,k}}{\partial \chi} - \nu \frac{Bi_{m_k}}{Bi_{m_k}+5}\alpha_i\left(C_{i,k} - < q >_{i,k}\right) + \alpha_{r_k}\left(1+\nu K_{enz}\right)\left(\frac{\sigma_i R_k}{k_r}\right)$$

i = glucose or fructose (6.23)

$$\frac{\partial C_{i,k}}{\partial \tau} = \frac{\psi_k}{Pe_k}\frac{\partial^2 C_{i,k}}{\partial \chi^2} - \psi_k \frac{\partial C_{i,k}}{\partial \chi} + \alpha_{r_k}\left(1+\nu K_{enz}\right)\left(\frac{\sigma_i R_k}{k_r}\right) \qquad i = \text{sucrose} \quad (6.24)$$

$$\frac{\partial C_{i,k}}{\partial \tau} = \frac{\psi_k}{Pe_k}\frac{\partial^2 C_{i,k}}{\partial \chi^2} - \psi_k \frac{\partial C_{i,k}}{\partial \chi} \qquad i = \text{enzyme} \quad (6.25)$$

- For the solid phase within the resin particles (i = glucose or fructose, only):

$$\frac{\partial < q >_{i,k}}{\partial \tau} = \alpha_i\left[K_i' C_{i,k} - < q >_{i,k}\right] \quad (6.26)$$

The corresponding boundary conditions for a given bed k are:

$$C_{i,k}^{in} = C_{i,k}(0) - \frac{1}{Pe_k}\frac{\partial C_{i,k}}{\partial \chi} \qquad \text{for any } i \quad (6.27)$$

$$\frac{\partial C_{i,k}}{\partial \chi}(1) = 0 \qquad \text{for any } i \quad (6.28)$$

The initial conditions are:

$$C_{i,k}\big|_{\tau=0} = 0 \qquad \text{for all } i \text{ and all } k, \text{ except for } i = \text{enzyme} \quad (6.29)$$

$$C_{i,k}\big|_{\tau=0} = C_{enz}^{o} \qquad \text{for } i = \text{enzyme} \quad (6.30)$$

The dimensionless variables are $\chi = z / L_c$ and $\tau = t / t^*$, where L_c is the length of a column and t^* is the switching time. The parameters are defined as for the TMBR strategy using the column length, L_C, instead of the section length, where pertinent. The new dimensionless numbers present in the model equations are:

$$\psi_k = \frac{U_{F_k}}{L_k} t^* = \frac{U_{F_k}}{U_S'} \qquad \text{Fluid/solid interstitial velocity ratio} \qquad (6.31)$$

$$\alpha_i = k_{h_i} t^* \qquad \text{Number of intraparticle mass transfer units} \qquad (6.32)$$

$C_{i,k}^{in}$, present in the boundary condition at the column inlet, is ordinarily equal to the concentration of such species leaving the previous column. For NC columns:

$$C_{i,k}^{in} = C_{i,k-1}(1,\tau) \qquad (6.33)$$

except if column k is where either eluent or feed are introduced. In such cases:

- Eluent node:

$$C_{i,k}^{in} = \frac{Q_4}{Q_1} C_{i,k-1}(1,\tau) + \frac{Q_E}{Q_1} C_{i,E} \qquad \text{if } i = \text{enzyme} \qquad (6.34)$$

$$C_{i,k}^{in} = \frac{Q_4}{Q_1} C_{i,k-1}(1,\tau) \qquad \text{if } i = \text{sucrose, glucose or fructose} \qquad (6.35)$$

- Feed node:

$$C_{i,k}^{in} = \frac{Q_2}{Q_3} C_{i,k-1}(1,\tau) + \frac{Q_F}{Q_3} C_{i,F} \qquad \text{if } i = \text{sucrose} \qquad (6.36)$$

$$C_{i,k}^{in} = \frac{Q_2}{Q_3} C_{i,k-1}(1,\tau) \qquad \text{if } i = \text{enzyme, fructose or glucose} \qquad (6.37)$$

In the equations above (6.33-6.37), if k =1, then $k-1$ =NC

The system of partial differential equations that describes a transient SMBR was solved numerically, using the PDE solver package PDECOL (Madsen and Sincovec, 1979). Spatial discretization was performed by modified B-splines assuming 30 elements per column

with 2 collocation points in each element. The integrator tolerance was set at 10^{-9} and the integration time step was 10^{-10} units of dimensionless time. Transient evolution of concentration profiles was calculated and went on until the sum of the following absolute errors was less 1%:

- Sum of relative differences between average extract and raffinate concentrations of two consecutive cycles;
- Global molar balance error between sucrose and invert sugar (for each mole of sucrose that enters the SMBR, one mole of glucose and one mole of fructose must leave);
- Global mass balance error for enzyme (amount that enters = amount that leaves);

The solver is quite time-consuming, like the transient SMB solver described in Chapter 2. In a Pentium II 300-MHz processor, it takes about 25 hours to solve 15 cycles, which is the time where experiments show that steady state has been reached.

6.4 Operation of a SMBR for sucrose inversion

Experiments for the inversion of sucrose and simultaneous product separation were performed in SMBR equipment, which was the same pilot unit described in Chapter 4 and used for the SMB experiments. The columns were packed with the cation-exchange resin DOWEX Monosphere 99/Ca, by Sigma, with a particle diameter of 320μm. The chosen section configuration was 3, 2, 5 and 2 columns for sections 1, 2, 3 and 4, respectively. This choice was made based on previous experimental work conducted by LSRE (Santos, 1999). Section 3, where reaction and adsorption of one of the reaction products take place, should be longer than the other sections. Sections 2 and 4, where the weakly adsorbed component is desorbed and adsorbed, respectively, may be shorter than the other sections.

The feed was a diluted sucrose solution (8 g/100ml), since the Michaelis-Menten equation has been shown to apply at this concentration (Santos, 1999). Besides, the available SMB equipment could not withstand the high pressure drops that would result from the high viscosity of concentrated sucrose syrups due to the small diameter of tubing (1/16'') connecting columns. The enzyme invertase, which catalyses the inversion of sucrose, was fed to the SMBR diluted in the eluent. Its maximum activity is observed at 55°C and pH 4.5, according to the supplier. Therefore, the eluent consisted of a pH-4.5 buffer prepared from

acetic acid (0.28% v/v) and calcium acetate (0.5% w/v). Calcium acetate was used instead of other buffering salts not to alter the adsorbent resin ionic form and maintain its adsorption properties. The sucrose solution used as feed was also prepared with this buffer, so that the pH of the whole mobile phase present in the SMBR would be 4.5 throughout the experiment. Temperature was kept at 55°C, by keeping the eluent and feed reservoirs in a thermostatic bath and by circulating bath water through the column jackets. Eventual acid hydrolysis in the feed reservoir was monitored by HPLC analysis of samples of feed in the beginning and at the end of the experiment. No appreciable sucrose degradation was observed.

Adsorption equilibrium data, mass transfer and reaction parameters for sucrose inversion and glucose-fructose adsorptive separation are shown in Table 6.2. Reaction kinetics was determined by Santos (Santos, 1999), all the other parameters being measured in our laboratory, according to the methodology described in Chapter 4. The external mass transfer coefficient (used to calculate Bi_m) was estimated from literature correlations for fixed beds (Thoenes Jr. and Kramers, 1958). The linear adsorption constant of the enzyme on the resin, K_e, was measured experimentally according to the procedure described in Appendix A.

Table 6.2 Model input parameters used in SMBR experiments

Model parameters	**Operating conditions**	**Columns**
Pe =500/column	T=55°C pH = 4.5	D_b = 2.6 cm
Bi_m =500	Feed concentration,	L_b = 29 cm
k_r = 50.32 min^{-1}	C_F = 80 g sucrose/l buffer	Configuration: 3-2-5-3
K_{mm} = 23 g/l	C_{enz} = 40-250 mg/l buffer	d_p = 320 μm
k_p = 2.5 min^{-1}	t*= 3.4 min	
k_μ = 1.5 min^{-1}	Q_{Rec}= Q_4 = 24 ml/min	
K_{FR}= 0.43 K_{GL}= 0.18		
K_{enz} = 4 ε_p=0.1		

Four experiments were performed under the conditions summarized in Table 6.3. Operating flowrates and switching time were cautiously selected so as to provide a high conversion and good separation of products. By comparing the reaction time constant, k_r, with the mass transfer time constants, k_p and k_μ, one may foresee that reaction is much faster than the diffusion of products (glucose and fructose) in the resin. Hence, the

Table 6.3 Operating conditions used in experiments of SMBR for sucrose inversion

	Experiment 1	Experiment 2	Experiment 3	Experiment 4
Switching time, min	3.4	3.4	3.4	3.4
Flowrates, ml/min:				
Eluent	11.38	11.38	11.38	11.04
Extract	9.11	9.47	9.49	9.94
Feed	3.62	3.62	4.6	4.6
Raffinate	5.89	5.53	6.5	5.7
Recycle	24	24	24	24
$\gamma_1, \gamma_2, \gamma_3, \gamma_4$	0.95, 0.45, 0.65, 0.33	0.95, 0.43, 0.63, 0.33	0.95, 0.43, 0.68, 0.33	0.93, 0.39, 0.64, 0.33
Enzyme concentration in the eluent (mg/l)	250	40	50	50
Enzyme/sucrose ratio	450U/g	73 U/g	71 U/g	69U/g
Productivity (kg/m^3/hr)	16	16	20	20
Performance parameters, experimental/TMBR model prediction/SMBR model prediction				
Extract purity (%)	89.6/92.6/90.0	86.6/93.4/92.8	87.7/93.8/89.1	86.4/92.7/89.1
Raffinate purity (%)	97.0/96.6/96.5	96.9/95.7/96.4	94.0/94.1/94.4	95.3/96.5/95.9
FR in the extract (g/l)	16.0/16.1/15.8	15.9/15.3/15.3	17.8/18.6/18.8	17.2/18.7/18.5
GL in the raffinate (g/l)	21.2/24.0/22.9	22.6/25.8/25.3	26.7/27.9/27.1	29.8/31.5/29.0

equilibrium model concept, formulated for linear equilibrium non-reactive systems (Ruthven, 1984), was used as an initial guess to provide adequate values for the TMBR section velocity ratios according to the following equations:

$$\gamma_1 > \nu\left(K_{FR} + \varepsilon_p\right) = 0.80 \tag{6.38}$$

$$\nu\left(K_{GL} + \varepsilon_p\right) = 0.42 < \gamma_2 < \gamma_3 < 0.80 = \nu\left(K_{FR} + \varepsilon_p\right) \tag{6.39}$$

$$\gamma_4 < \nu\left(K_{GL} + \varepsilon_p\right) = 0.42 \tag{6.40}$$

The recycling pump of the SMB unit could deliver flowrates in the range of 20 to 120 ml/min. The adsorbent inventory being much smaller than that usually reported for fructose-glucose SMB separations, lower flowrates were required in order to overcome mass transfer resistance. A flowrate of 24 ml/min was assumed for section 4, the zone having the lowest flowrate. Having set γ_4 as 0.33, which is in accordance with equation (6.40), the switching time t^* may be calculated from the following expression:

$$\gamma_j = \frac{Q_j \times t^*}{\varepsilon \times V_c} - 1 \tag{6.41}$$

All the other section flowrates were calculated using equation (6.41) and choosing convenient values for γ_j, so as to conform to equations (6.38) and (6.39) The inlet and outlet streams were calculated from the differences between neighbouring section flowrates. The amount of enzyme necessary to completely convert the feed was calculated based on the activity information provided by the supplier. Each mg of enzyme contains 46 units (U). One enzyme unit is defined as the amount necessary to invert 1 μmole of sucrose per minute at 55°C and pH 4.5. The feed flowrate is 3.62 ml/min for the first experiment and sucrose concentration is 80 g/l, which means a throughput of 846.8 μmoles/min. To invert such amount, 846.8 enzyme units or 18.4 mg would be necessary within the SMBR void volume. The total SMBR void volume is 12×0.4×154 ≈ 740 ml, thus the enzyme concentration must be 0.025 g/l. The definition of enzyme activity is usually calculated for a condition in which the substrate concentration is much larger than the Michaelis Menten constant. In such condition, the rate of reaction is constant and maximum. Since concentrations of sucrose comparable to the Michaelis-Menten constant (23 g/l) were used in the SMBR, the enzyme activity at such condition will probably be lower and more enzyme will be required to achieve

the same conversion rate. That is why we arbitrarily set the amount of enzyme 10 times as much as the theoretical value for experiment 1. To address the effect of enzyme strength- on the performance of a SMBR, lower enzyme concentrations were tested.

During the first cycle of operation, enzyme with diluted buffer was pumped into the SMBR by both eluent and feed pumps in order to make sure that mobile phase and resin were saturated with catalyst. From the second cycle on, the feed pump started delivering sucrose solution. At each cycle, raffinate and extract were collected and analysed by HPLC for sugar content assessment in order to monitor the steady state attainment. Stationary average product concentrations were obtained at the 10^{th} cycle. In the fifteenth cycle, 1-ml samples were collected at 50% of each of the 12 periods with the aid of a 6-port valve. The samples were immersed in boiling water for 1 minute in order to ensure the inactivation of the enzyme and stop reaction. Figure 6.3 (a) shows the experimental profile (points) obtained for experiment 1 as compared with the simulated curves. Good agreement was found between theory and experiment. Sucrose is completely converted within the first of the five columns that make up section 3. One would think that such a long section is not necessary to achieve 100% conversions. However, fructose, one of the reaction products which is preferentially adsorbed, diffuses slowly within the resin. Thus, it takes the whole section length for fructose concentration to decrease to nearly zero, so as not to contaminate the raffinate stream. At the raffinate and extract nodes, the filled points indicate the average concentrations measured for both products collected for a whole cycle (15^{th} cycle).

Table 6.3 compares the performance parameters obtained experimentally with those predicted by the numerical simulation. Experimental performance is slightly different from the predicted ones by both modeling strategies. This may be due to small deviations in the flowrates delivered by the recycling pump and to unpredicted nonlinearities in the sugar isotherms introduced by the adsorption of enzyme on the resin surface. However, such error may be accepted if the model is to be used for design/optimisation purposes, especially for the TMBR-based model given its simplified solution.

Another experiment (2) was performed using a lower enzyme concentration, 40 mg/l, in order to make more effective use of section 3 as a reactor. The operating conditions are nearly the same as described in Table 6.3, except for the extract and raffinate flowrates, which were equal to 9.47 and 5.53 ml/min, respectively. Hence, γ_2=0.43 and γ_3=0.63. Figure 6.3 (b) shows the steady state experimental axial profile as compared with the model predictions. The decrease in enzyme concentration caused the sucrose concentrations to be positive for three

columns of section 3. It is possible to verify the adequate description of the reaction rate from the nice agreement between theory and experiment.

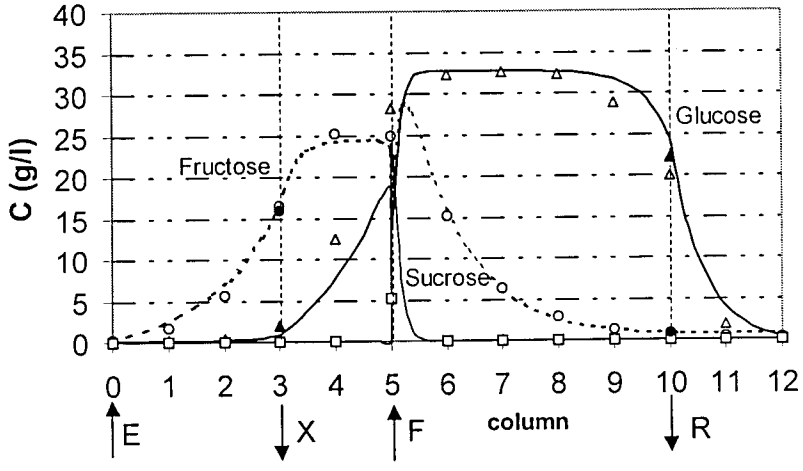

(a)

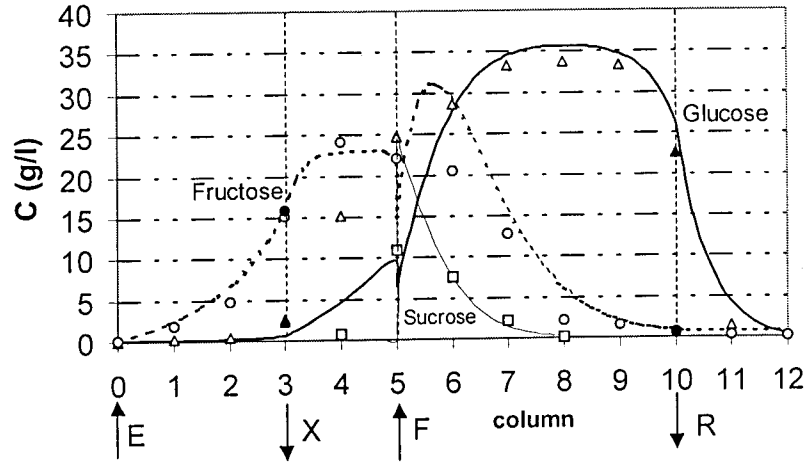

(b)

Figure 6.3 Concentration profiles for a SMBR obtained at steady state referring to experiment 1 (a) and experiment 2 (b). The symbols are experimental and the curves are simulated using a TMBR model.

In experiment 2, one may also verify that the value of γ_2 approaches the minimum bound defined by the equilibrium theory ($\gamma_2 = 0.42$), below which the extract product becomes impure. This trend may be noticed by the decrease in extract purity.

In the following experiments, the feed flowrate was further increased as well as the enzyme concentration (50 mg/l) to prevent any unconverted substrate from contaminating the products. In experiment 3, γ_2 was kept at 0.43 and γ_3 was increased to 0.68, thus coming closer to the upper bound (0.80) defined by the equilibrium theory. This was reflected in a decrease in raffinate purity. By observing the steady state internal profile, shown in Figure 6.4, it is clear that the increase in enzyme concentration surpassed the required amount necessary to make up for the increase in feed concentration. Only two out of the five beds of section 3 are enough to achieve complete conversion.

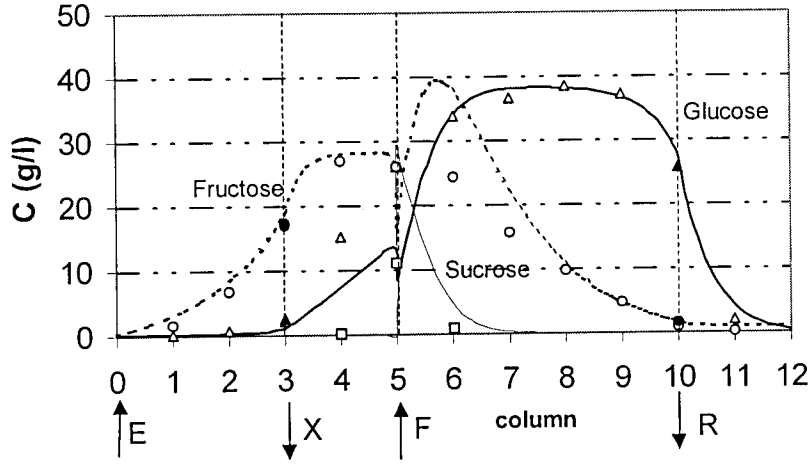

Figure 6.4 Concentration profiles for a SMBR obtained at steady state referring to experiment 3. The symbols are experimental and the curves are simulated using a TMBR model.

In experiment 4, the lowest extract concentration from all experiments was obtained. This is a consequence of the value assigned for γ_2 (0.39), which is lower than the minimum equilibrium bound (0.42). Likewise, the concentration of glucose in the raffinate is the highest due to the low raffinate flowrate. In all experiments described, there is some discrepancy between experimental purities and those obtained from simulation. The simulator fails to predict the correct degree of contamination in both products. This error has probably the same causes as those described in Chapter 4 for SMB experiments. Fluctuations in flowrate and common piping to exit products are some of the factors that were not taken into account in our models for the sake of simplicity. The TMB-based simulator also fails to fit experimental data close to the feed port, especially for the fructose profile in section 3. This agreement is improved by comparing the simulations from a SMB strategy with the experimental results. This is shown in Figure 6.5 for experiment 4. Nevertheless, the good agreement between

experimental and simulated steady state profile in the four situations examined and the conformity with trends from the equilibrium theory build reliability to the models proposed herein.

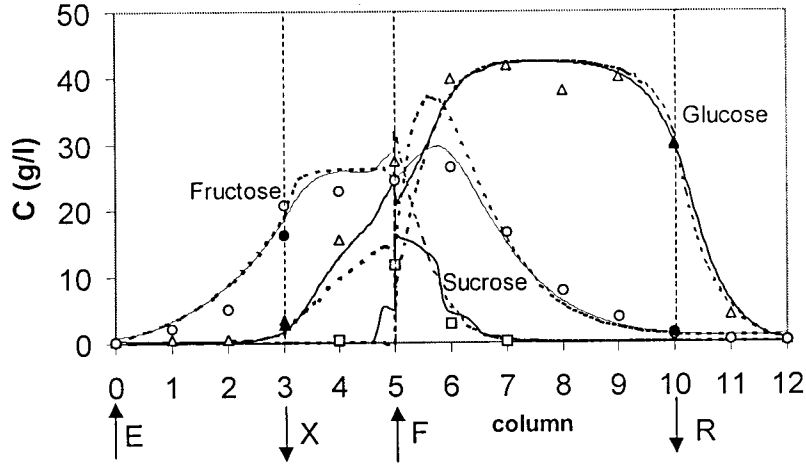

Figure 6.5 *Concentration profiles for a SMBR obtained at steady state referring to experiment Points are experimental, curves are simulated using a TMBR strategy (dotted) and a SMBR strategy (continuous).*

Some of the performance parameters obtained in our experiments for the inversion of sucrose in a SMBR were compared with those obtained by Barker *et al* (1992) for the same reaction conducted in a semicontinuous countercurrent chromatographic separator-reactor (SCCR-S) system. These data are summarized below in Table 6.4.

Table 6.4 *Comparison of experimental results obtained for a semicontinuous countercurrent chromatographic separator-reactor (SCCR-S) and a SMBR*

	Barker *et al* (1992)	This work
Number of columns	12	12
Column volume (cm^3)	1700	152
No. columns per section	6-5[a]-1	3-2-5[a]-2
Feed flowrate (ml/min)	9	3.62-4.6
Feed concentration (g/l)	200-550	80
Maximum Productivity (kg sucrose/m^3 resin/hr)	16	20
Minimum enzyme/sucrose ratio (U/g)	600	70
FR in extract (g/l)	9-29	16-17
GL in raffinate (g/l)	23-50	21-30

[a] Reacting zone

Even though, much higher feed concentrations were employed by Barker *et al*, the product concentrations obtained by them in some experiments are comparable to the ones reported in this work. This indicates that the SCCR-S requires a much higher solvent consumption. The minimum enzyme/sucrose ratio used in this work is substantially lower than that reported by the group of Aston, which in turn is reported by the authors as 20% of the enzyme requirements in a batch reactor. Thus, the use of a simulated moving bed reactor represents major savings in enzyme requirements. Despite the differences in equipment size and treated throughputs, the maximum adsorbent productivity (sucrose-based) reported by Barker *et al* is lower than that obtained in this work. These findings illustrate the need of an optimization tool to define ideal construction and operating parameters as those which maximise the use of the reaction zone as both a reactor and separator while keeping eluent and enzyme requirements as low as possible. A design and optimization algorithm for this test reaction-separation is fully described in the next chapter. As an example of the type of results brought about by this algorithm, it was applied to find optimal operating conditions for the LICOSEP pilot unit with column section area of 5.3 cm^2 with a feed concentration of 80 g/l. Constraints on product purities were assigned as 95% and as 99% on conversion. Table 6.5 summarizes the optimization package output. Actually, longer columns would be required and the enzyme concentration could be decreased down to 45 mg/l. As far as the optimal performance operation parameters are concerned, though, the values of enzyme and adsorbent productivity are very close to those obtained in our experiments.

Table 6.5 Output for an optimization algorithm of a SMBR plant such as Licosep (column section area of 5.3 cm^2) treating a feed concentration of 80 g/l.

Operating conditions		**Expected performance**	
Column length, L_c =	35 cm	Enzyme/sucrose ratio	80 U/g
Enzyme concentration =	45 mg/l	Adsorbent productivity	17 kg sucrose/ m^3 resin/hr
Switching time, t^* =	3.2 min		
Recycle flowrate, Q_4 =	30.8 ml/min		
Feed flowrate, Q_F =	4.6 ml/min	FR in extract	15.5 g/l
Eluent flowrate, Q_E =	14.7 ml/min	GL in raffinate	25.7 g/l
γ_2, γ_3	0.44,0.64		

6.5 Conclusions

In this Chapter, the principles, modeling and operation of a simulated moving bed were investigated under the application of the inversion of sucrose and simultaneous separation of fructose and glucose. Detailed mathematical models to describe process performance were proposed following the strategies of a true moving bed and simulated moving bed reactors. Experimental data for SMBR operation were obtained in a SMB pilot unit Licosep. Comparison with simulated data reveals that the enzyme, introduced in free form together with the eluent, is actually adsorbed onto the surface of the separating resin. In spite of being a heterogeneous reaction, the description of reaction rate law by an expression of pseudo-homogeneous type led to good agreement between experimental and theoretical results.

Comparison of the experimental results obtained in this work with those reported by Barker et al (1992) for a reactor of SCCR-S type showed significant savings in enzyme requirements and productivity enhancement. The experiments described herein were also found to have been performed in nearly optimized conditions. The issues of design and optimization of construction and operating parameters in a SMBR will be addressed in the following chapter.

6.6 References

U. Ascher, J. Christiansen, R. D. Russel, "Collocation Software for Boundary-Value ODEs", *ACM Trans. Math. Software* **7**, 209-222 (1981).

D. C. S. Azevedo, A. E. Rodrigues, "Design Methodology and Operation of a Simulated Moving Bed Reactor for the Inversion of Sucrose and Glucose-Fructose Separation", *Chem. Eng. J.* **82**, 95-107 (2001).

P. E. Barker, G. Ganetsos, J. Ajongwen, A. Akintoye, "Bioreaction-separation on continuous chromatographic systems", *Chem. Eng. J. Biochem. Eng. J.* **50**, B23-B28 (1992).

P. Cen, G. T. Tsao, "Recent Advances in the Simultaneous Bioreaction and Product Separation Processes", *Sep. Technol.* **3**, 58-75 (1993).

C. B. Ching, Z. P. Lu, "Simulated Moving-Bed Reactor: Application in Bioreaction and Separation", *Ind. Eng. Chem. Res.* **36**, 152-159 (1997).

G. Dünnebier, J. Fricke, K.-U. Klatt, "Optimal Design and Operation of Simulated Moving Bed Chromatographic Reactors", *Ind. Eng. Chem. Res.* **39**, 2290-2304 (2000).

B. B. Fish, R. W. Carr, "An Experimental Study of the Countercurrent Moving-Bed Chromatographic Reactor", *Chem. Eng. Sci.* **44**, 1773-1783 (1989).

J. Fricke, M. Meurer, H. Schmidt-Traub, "Design and Layout of Simulated-Moving-Bed Chromatographic Reactors", *Chem. Eng. Technol.* **22**, 835-839 (1999).

G. Ganetsos, P. E. Barker, J. N. Ajongwen, "Batch and Continuous Chromatographic Systems as Combined Bioreactor-Separators", in *Preparative and Production Scale Chromatography* G. Ganetsos, P. E. Barker, Eds. (Marcel Dekker, New York, 1993) pp. 375-394.

E. Glueckauf, "Theory of chromatography. Part 10. Formulae for Diffusion into Spheres and Their Application to Chromatography", *Trans. Faraday Soc.* **51**, 1540-1551 (1955).

K. Hashimoto, S. Adachi, H. Noujima, H. Maruyama, "Models for the Separation of Glucose/Fructose Mixture using a Simlated Moving-Bed Adsorber", *J. Chem. Eng. Jpn.* **16**, 400-406 (1983).

K. Hashimoto, S. Adachi, H. Noujima, Y. Ueda, "A New Process Combining Adsorption and Enzyme Reaction for Producing Higher-Fructose Syrup", *Biotechnol. & Bioeng.* **25**, 2371-2393 (1983).

K. Hashimoto, S. Adachi, Y. Shirai, "Development of New Bioreactors of a Simulated Moving-Bed Type", in *Preparative and Production Scale Chromatography* G. Ganetsos, P. E. Barker, Eds. (Marcel Dekker, New York, 1993) pp. 395-419.

M. Kawase, Y. Inoue, K. Hashimoto, "The Simulated Moving Bed Reactor for the Production of Bisphenol A", *Catalysis Today* **48**, 1-4 (1999).

M. Kawase, A. Pilgrim, T. Araki, K. Hashimoto, "Lactosucrose production using a simulated moving bed reactor", *Chem. Eng. Sci.* **56**, 453-458 (2001).

M. Kawase, T. B. Suzuki, K. Inoue, K. Yoshimoto, K. Hashimoto, "Increased Esterification Conversion by Application of the Simulated Moving-Bed Reactor", *Chem. Eng. Sci.* **51**, 2971-2976 (1996).

A. Kruglov, "Methanol Synthesis in a Simulated Countercurrent Moving-Bed Adsorptive Catalytic Reactor", *Chem.Eng. Sci.* **49**, 4699-4716 (1994).

N. K. Madsen, R. F. Sincovec, "PDECOL: General Collocation Software for Partial Differential Equations", *ACM Trans. Math. Software* **5**, 326-351 (1979).

M. Mazzotti, A. Kruglov, B. Neri, D. Gelosa, M. Morbidelli, "A Continuous Chromatographic Reactor: SMBR", *Chem. Eng. Sci.* **51**, 1827-1836 (1996).

M. Meurer, U. Altenhöner, J. Strube, H. Schmidt-Traub, "Dynamic Simulation of Simulated-Moving-Bed Chromatographic Reactors", *J. Chromatography A* **769**, 71-79 (1997).

M. Meurer, U. Altenhöner, J. Strube, A. Untiedt, H. Schmidt-Traub, "Dynamic Simulation of a Simulated-Moving-Bed Chromatographic Reactor for the Inversion of Sucrose", *Starch* **48**, 452-457 (1996).

C. Migliorini, M. Fillinger, M. Mazzotti, M. Morbidelli, "Analysis of Simulated Moving-Bed Reactors", *Chem. Eng. Sci.* **54**, 2475-2480 (1999).

T. Petroulas, R. Aris, R. W. Carr Jr., "Analysis and Performance of a Countercurrent Moving-Bed Chromatographic Reactor", *Chem. Eng. Sci.* **40**, 2233-2240 (1985).

A. Ray, A. L. Y. Tonkovich, R. Aris, R. W. Carr, "The Simulated Countercurrent Moving Bed Chromatographic Reactor", *Chem. Eng. Sci.* **45**, 2431-2437 (1990).

A. K. Ray, R. W. Carr, R. Aris, "The Simulated Countercurrent Moving Bed Chromatographic Reactor: A Novel Reactor-Separator", *Chem. Eng. Sci.* **49**, 469-480 (1994).

D. M. Ruthven *Principles of Adsorption and Adsorption Processes*. Wiley, New York, 464 p. (1984).

M. M. L. Santos, "Produção de Dextrano e Frutose a partir da Sacarose com Leuconostoc mesenteroides NRRL B512 (f)", PhD thesis, University of Porto (1999).

M. R. Sarmidi, P. E. Barker, "Simultaneous Biochemical Reaction and Separation in a Rotating Annular Chromatograph", *Chem. Eng. Sci.* **48**, 2615-2623 (1993).

K. Takeuchi, Y. Late Uraguchi, "Experimental Studies of a Chromatographic Moving-Bed Reactor - Catalytic Oxidation of Carbon Monoxide on Activated Alumina as a Model Reaction", *J. Chem. Eng. Jpn.* **10**, 455-460 (1977).

K. Takeuchi, T. Miyauchi, Y. Late Uraguchi, "Computational Studies of a chromatographic Moving-Bed Reactor for Consecutive and Reversible Reactions", *J. Chem. Eng. Jpn.* **11**, 216-220 (1978).

K. Takeuchi, Y. Uraguchi, "Separation Conditions of the Reactant and the Product with a Chromatographic Moving Bed Reactor", *J. Chem. Eng. Jpn.* **9**, 165-166 (1976).

D. Thoenes Jr., H. Kramers, "Mass Transfer from Spheres in Various Regular Packings to a Flowing Fluid", *Chem. Eng. Sci.* **8**, 271-283 (1958).

A. L. Y. Tonkovich, R. W. Carr, "A Simulated Countercurrent Moving-Bed Chromatographic Reactor for the Oxidative Coupling of Methane: Experimental Results", *Chem. Eng. Sci.* **49**, 4647-4656 (1994).

7. Design and Optimization of a SMBR

7.1 Introduction

This Chapter describes a design algorithm for a simulated moving bed reactor applied to the case of sucrose inversion and fructose-glucose separation. The objective of the strategy is to calculate the minimum adsorbent inventory and enzyme concentration required to treat increasing feed flowrates. Performance constraints are set on the reaction conversion, which should be no less than 99% and on minimum purities of no less than 95% for both extract and raffinate products. An optimisation step is included by defining the enzyme productivity as the objective function to be maximised. Design algorithm results are shown for different values of fluid/solid velocity ratios on sections 1 and 4. This way, the effects of the safety margin applied to γ_1 and γ_4 have been investigated on the reaction conversion and separation performance. The results have been compared with predictions from the equilibrium theory for a non-reactive SMB system in a $\gamma_2 \times \gamma_3$ parameter space. Interesting deviations have been observed and discussed.

7.2 Literature Review

The design and optimization of chromatographic reactors of simulated moving bed type has been the subject of few publications. It is common sense to use the equilibrium theory applied to the separation of the reaction products in a non-reactive SMB. It provides a useful starting point in defining adequate operating conditions. However, reaction kinetics is an ignored aspect in this approach, which must be taken into account in order to ensure high conversions. Migliorini *et al* (1999) have proposed a modeling analysis to design the operating conditions of a SMBR. The procedure was illustrated for the esterification of acetic acid and ethanol catalysed by resin Amberlyst 15. The region of complete separation of products ($m_2 \times m_3$), as defined by the equilibrium theory, was spanned by consecutive simulation using a detailed model that included the reaction kinetics. Points that satisfied the constraints of complete conversion of acetic acid and complete separation of products were searched in order to shape a new region of both complete separation and reaction. It was found that the complete reaction/separation region has a triangular shape similar to that found for the non-reactive case, the size being significantly reduced. The authors also analysed the case of inversion of sucrose and fructose-glucose separation reported by Ching and Lu (1997). They located the operating points corresponding to the experiments performed by Ching and Lu in an operating parameter space ($m_2 \times m_3$). It was observed that the use of the non-reactive equilibrium triangle applied to the reaction products provides clear insight into the SMBR process behaviour and guidelines for process optimization.

Dünnebier *et al* (2000) presented a novel optimisation and design strategy for a SMBR based on mathematical optimization, a rigorous process model and a detailed cost function. The procedure was illustrated for two applications: enzymatic inversion of sucrose and esterification of acetic acid with β-phenethyl alcohol. Potential savings in operating cost of up to 20% and in desorbent consumption of up to 60% were identified. The optimal operating point in terms of the velocity ratio in section 2, γ_2, was quite different from that expected if a non-reactive SMB were analysed in the frame of equilibrium theory.

Nevertheless, the results provided by the analysis of both Migliorini *et al* and Dünnebier *et al* are restricted to given SMBR equipment with fixed geometric parameters (column length and diameter). When it comes to the design of the physical configuration of a new unit, another approach must be followed. Concerning this matter, we have adapted the

algorithm proposed by Biressi *et al* (2000) to design not only operating but also geometric parameters for SMB adsorbers. The main differences introduced in this algorithm are the inclusion of the reaction conversion as a design constraint, the use of a detailed model for the SMBR process and adaptation of the heuristic rules built in the algorithm in order to include reactor performance criteria.

7.3 The Design Algorithm

The design strategy proposed herein consists in determining the adsorbent inventory (column length and section), enzyme concentration and operating conditions that allow a desired substrate conversion and purity in the outlet products without exceeding given pressure drop limits imposed by the packing material. The number of degrees of freedom in the design problem is, therefore, eight: column length and diameter, enzyme concentration, switching time and the four section velocity ratios γ_j's. We have used a rigorous process model based on a TMBR strategy, as shown and validated in Chapter 6.

The equations from an equilibrium model that define separation for a non-reactive linear SMB will be used as general guidelines to define starting values for γ_j's. Those equations are:

$$\gamma_1 > \nu K'_{FR} \tag{7.1}$$

$$\nu K'_{GL} < \gamma_2 < \gamma_3 < \nu K'_{FR} \tag{7.2}$$

$$\gamma_4 < \nu K'_{GL} \tag{7.3}$$

where $\nu = (1-\varepsilon)/\varepsilon$ and $\gamma_j = \left.\frac{Q_j t^*}{\varepsilon V_c}\right|_{SMBR} - 1$.

As shown by Migliorini *et al* (1999), a complete conversion/separation region has a more reduced triangular shape, similar to that found for non-reactive SMB's. This was said of non-linear adsorption system in which feed concentration is a key optimisation parameter. We have assumed this conclusion to be true for our reaction/separation system. Therefore, the design algorithm scans (by consecutive numerical simulation) the region defined by the

equilibrium theory for non-reactive SMB in search for operating points which minimally fulfill required constraints for reaction conversion and product purity.

The pieces of information to be used by the algorithm are:

a) A correlation to estimate pressure drop in packed beds, such as the Kozeny-Kárman equation:

$$\frac{\Delta P}{L_c} = 150\frac{(1-\varepsilon)^2}{\varepsilon^3 d_p^2}\mu\upsilon \qquad (7.4)$$

b) The separation region for a non-reactive SMB in the operating parameters space as defined by the equilibrium theory (equations 7.1 to 7.3);

c) The detailed TMBR model as proposed in Chapter 6, together with the equivalence relations between a TMBR and a SMBR;

d) The theoretical calculation of the necessary amount of enzyme within the SMBR volume, according to the supplier's information about the enzyme activity.

As a first step of the design procedure, the following three statements are made, as adapted from the work of Biressi *et al* (2000):

i. The SMBR flowrate in section 1, Q_1, is taken to be 10^3 ml/min, and all other flowrates and column cross section are calculated having this value in mind. After the algorithm calculations are finished, a scale parameter Ω is obtained as the ratio between the desired feed flowrate and the calculated feed flowrate with Q_1=10^3 ml/min, that is, $\Omega = Q_F\big|^{desired} / Q_F\big|^{Q_1=10^3 ml/min}$. All other calculated flowrates and section area may be multiplied by the scale factor to obtain the values necessary to process the desired feed flowrate. Calculated γ_j and L_c values remain unchanged.

ii. Since pressure drop is proportional to the throughput of the plant, we expect that the productivity will be the highest when pressure drop is the highest possible. Therefore, we set pressure drop in section 1, which is where the fluid velocity is maximum, equal to the allowable upper limit, hence fixing the value of the product $\upsilon_1 \times L_c$.

iii. From the adsorption isotherms and using a certain safety margin β, it is possible to predict *a priori* the values of γ_1 and γ_4 that ensure the proper behaviour of sections 1 and 4, that is, complete regeneration of the adsorbent and eluent, respectively. β is an input parameter to the algorithm so that $\gamma_1 = \beta \times \gamma_1^{eq}$ and $\gamma_4 = \gamma_4^{eq}/\beta$. Design results for different values of β are analysed.

From the items described above, Q_1, $\upsilon_1 \times L_c$, γ_1 and γ_4 are defined. Four from the initially eight degrees of freedom of the design problem are left to be defined: the column length, enzyme concentration and the velocity ratios γ_2 and γ_3.

The parameter η will be used in the algorithm and is defined as the dimensionless distance of a certain (γ_2, γ_3) pair to the optimum point given by the equilibrium theory $(\gamma_2^{eq}, \gamma_3^{eq})$. In other words:

$$\eta = \frac{\gamma_3 - \gamma_2}{\gamma_3^{eq} - \gamma_2^{eq}} = \frac{\gamma_3 - \gamma_2}{\nu\left(K'_{FR} - K'_{GL}\right)} \tag{7.5}$$

For each value of η, within a certain range defined by the user, the algorithm manages to find the minimum column length, minimum enzyme concentration and γ_2, which lead to the required reaction conversion and product purities. For a given value of η, the algorithm starts with the minimum (γ_2, γ_3) pair defined by the non-reactive equilibrium triangle and sufficiently small values for L_c and C_{enz}. All information required by the TMBR model is available by then and process performance at steady state is calculated. Depending on the values of the constraining parameters (reaction conversion and product purities), the algorithm makes one of the following decisions:

- Increase enzyme concentration;
- Increase column length;
- Increase/decrease (γ_2, γ_3)

After all the assigned values for η have been tested and design parameters have been found for each case, an optimisation step may be performed in order to select an optimal η.

The objective function is enzyme productivity, which should be maximised. The objective function enzyme productivity and the constraints reaction conversion (X), extract purity (PUX), raffinate purity (PUR) are defined as follows:

$$\text{Enzyme productivity (kg suc/g enz)} = \frac{\textit{Mass rate of sucrose in feed} \times \text{X}/100}{\textit{Mass rate of enzyme in the eluent}} \quad (7.6)$$

X (%) =

$$\frac{\textit{Mass rate of sucrose in the feed - Mass rate of sucrose in the extract and raffinate}}{\textit{Mass rate of sucrose in the feed}} \times 100 \quad (7.7)$$

$$\text{PUX (\%)} = \frac{\textit{concentration of fructose in the extract}}{\textit{concentration of (fructose + glucose) in the extract}} \times 100 \quad (7.8)$$

$$\text{PUR (\%)} = \frac{\textit{concentration of glucose in the raffinate}}{\textit{concentration of (fructose + glucose) in the raffinate}} \times 100 \quad (7.9)$$

The flow sheet describing the decision-making process of the algorithm is visualised in Figure 7.1. As an illustrative example, let us consider the case for which the following input parameters shown in Table 7.1 are used.

Table 7.1 Input data used in the SMBR design algorithm

$\gamma_2^{eq}, \gamma_3^{eq}$	0.80,0.41
β	1.1
ΔP / column, μ, C_F	10 bar, 3 cP, 400 g/l
Initial η, final η and $\Delta\eta$	0.2, 1.2, 0.1
Reaction kinetic parameters	As shown in first column of Table 6.2 (Chapter 6)
Adsorption and mass transfer parameters	
Initial guess for L_c	150 cm
Initial value calculated for C_{enz}	7 mg/l
Constraints: $X_{sp}, PUX_{sp}, PUR_{sp}$	99%, 95%, 95%

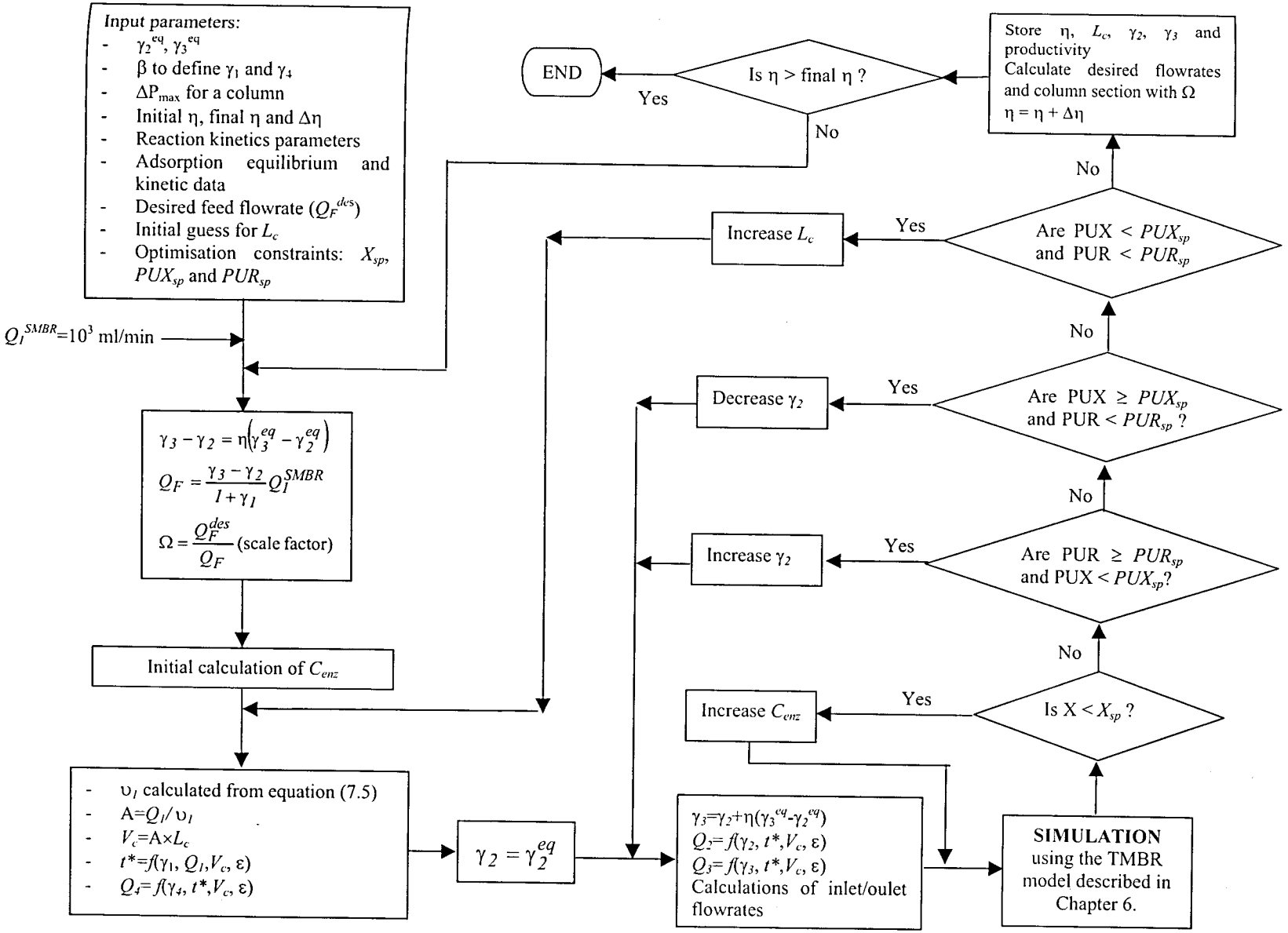

Figure 7.1 Flow sheet of the design algorithm for a SMB.

Starting with η=0.2, the corresponding feed flowrate and scale factor may be calculated as indicated in the flow sheet. If the initial guess $\gamma_2 = \nu K'_{GL}$ is assumed, all the necessary information to run the process simulator is available by now. Table 7.2 illustrates the algorithm steps, obtained performance and the actions taken for η=0.2. When all constraints have been met, the operating, geometric parameters and process performance are stored. Then, η may be increased and the whole methodology described so far is repeated.

With the data stored by the design package, plots of η versus column length and enzyme productivity are constructed. The value of η which maximises productivity is chosen as the adequate operating point. It defines the optimum column length, optimum enzyme concentration and the scale factor Ω. Multiplying the obtained section area and flowrates by Ω, one is able to re-scale all necessary operating conditions for any desired throughput.

Table 7.2 Steps and actions taken by the design algorithm for η=0.2

Step	Input Parameters				Performance (%)			Action
	γ_2	γ_3	L_c (cm)	C_{enz} (mg/l)	X	PUX	PUR	
1	0.41	0.48	150	7	73.2	69.9	85.0	Increase C_{enz}
2	0.41	0.48	150	12	89.2	75.8	87.6	Increase C_{enz}
⋮	⋮	⋮	⋮	⋮	⋮	⋮	⋮	⋮
5	0.41	0.48	150	27	99.4	83.0	95.4	Increase γ_2
6	0.43	0.50	150	27	99.2	86.5	94.6	Increase L_c
7	0.43	0.50	152.5	27	99.4	87.1	95.1	Increase γ_2
8	0.45	0.52	152.5	27	99.3	89.6	94.3	Increase L_c
9	0.45	0.52	155	27	99.4	90.1	94.8	Increase L_c
⋮	⋮	⋮	⋮	⋮	⋮	⋮	⋮	⋮
18	0.50	0.57	167.5	27	99.7	95.3	94.9	Decrease γ_2
19	0.49	0.56	167.5	27	99.7	95.1	95.1	Store data and increment η

7.4 Design and optimization results

The design methodology was applied for a SMBR to invert sucrose and separate glucose from fructose. Equilibrium, mass transfer and reaction parameters are those shown in the first column of Table 6.2. For a feed concentration of 400 g/l, fluid viscosity and density were found to be 3 cP and 1.26 kg/l, respectively (Schiweck and Clarke, 2001). The maximum pressure limit was set at 10 bar/column, 25% of such value being due to the column packing itself and 75% being due to piping and valves. The safety margin β to be used in the calculation of γ_1 and γ_4 was set as 1.1, 1.2 and 1.3 in order to verify the influence of this parameter in the design/optimisation results.

Figure 7.2 shows the plots of η as a function of minimum length L_c, minimum C_{enz} and corresponding productivities that lead to a minimum conversion of 99% and minimum purities of 95%. In this plot, β was set as 1.1. Figure 7.2(a) shows the evolution of enzyme productivity with η. The maximum value of the curve is located at η = 0.5. However, at this value of η, low feed flowrates are treated by the SMBR, which means low product concentration and low adsorbent productivities. One may also verify that, from $0.4<\eta<0.8$, enzyme productivity values are located on a plateau around 3 kg inverted sucrose per g of enzyme. Both column length and adsorbent productivity increase steadily for the η range considered in the algorithm. From η = 0.8 on, the required amount of enzyme (plot b) increases with a greater slope. Therefore, for β=1.1, the best range of operation point for a SMBR seems to lie anywhere between η=0.4 and η=0.8. Figure 7.3 and Figure 7.4 show the same type of plots as in Figure 7.2, with β equal to 1.2 and 1.3, respectively. Similar conclusions as those drawn from Figure 7.2 may be stated. For β equal to 1.2, the ideal operating range is also located at $0.4 < \eta < 0.8$, where the enzyme productivity is about 2 kg/g. For β equal to 1.3, this interval is enlarged to [0.3; 1.0] and maximum enzyme productivities do not go far beyond 1.5 kg/g. For the same η, the minimum column length required to achieve the specified process performance decreases as β increases. This is expected since larger values of β mean better eluent and adsorbent regeneration and hence shorter section lengths are necessary to achieve the same performance. Although the highest enzyme productivities are obtained for β equal to 1.1, SMBR operation at low β values is not recommended because it may not be robust enough. Operating at very high values of β is not advisable as well, since very low enzyme productivities and diluted product concentrations

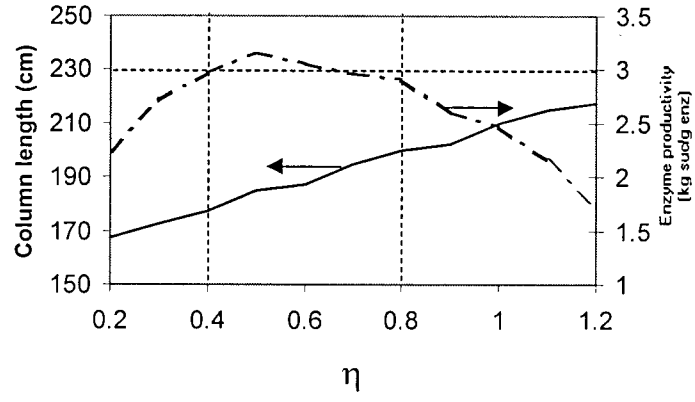

(a)

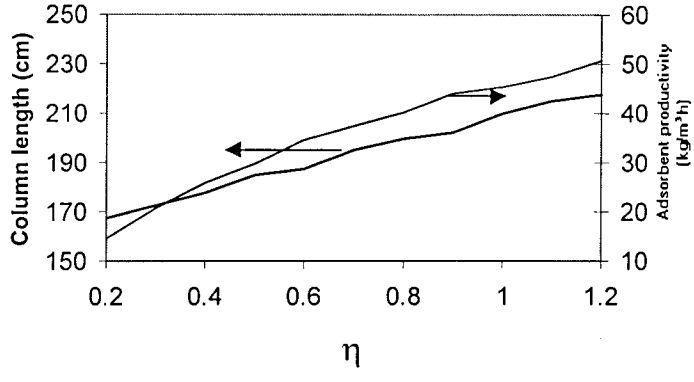

(b)

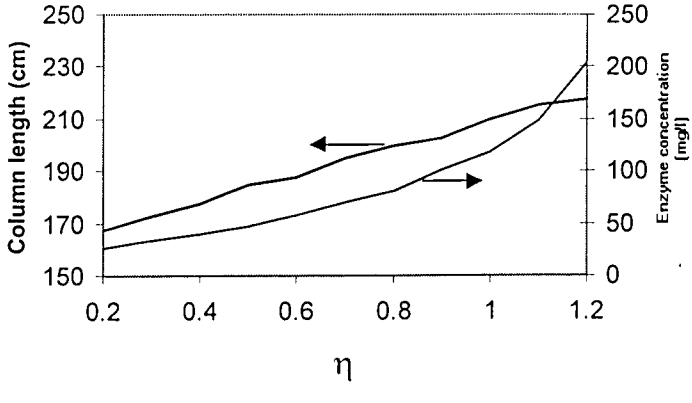

(c)

Figure 7.2 *For β =1.1, plots of dimensionless feed flowrate η against minimum column length L_c and enzyme productivity (a), adsorbent productivity (b) and enzyme concentration (c)*

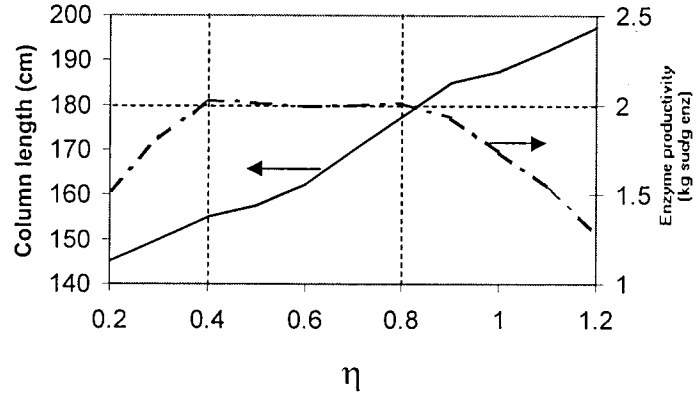

(a)

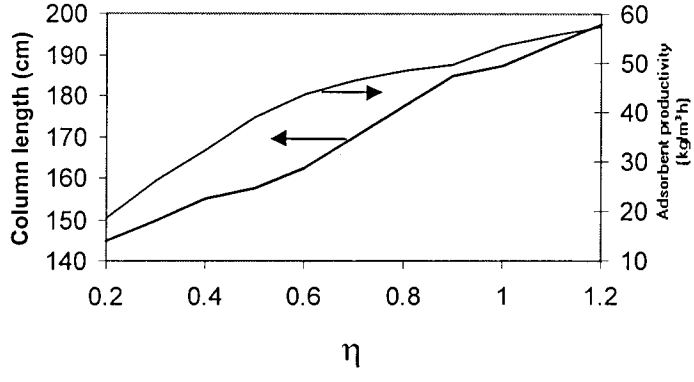

(b)

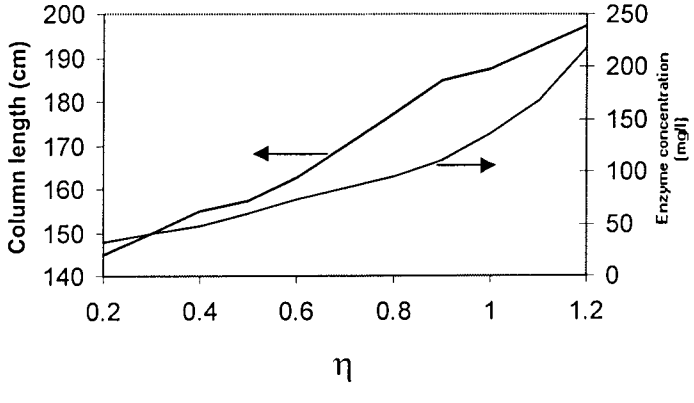

(c)

Figure 7.3 *For β =1.2, plots of dimensionless feed flowrate η against minimum column length L_c and enzyme productivity (a), adsorbent productivity (b) and enzyme concentration (c)*

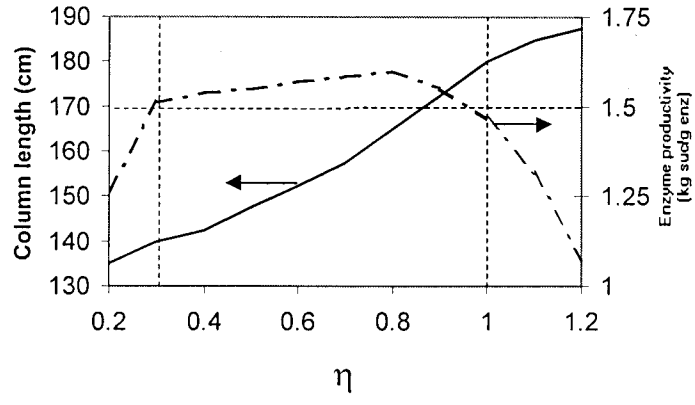

(a)

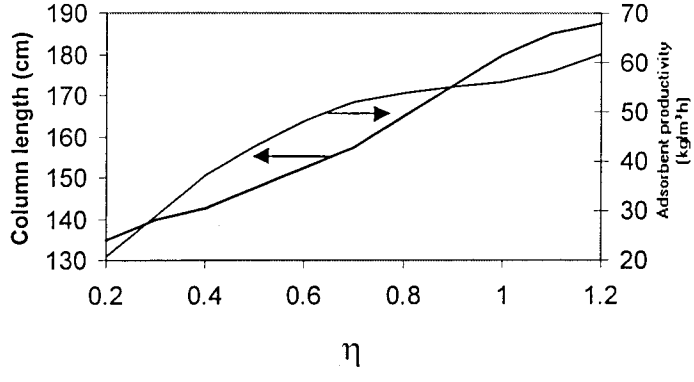

(b)

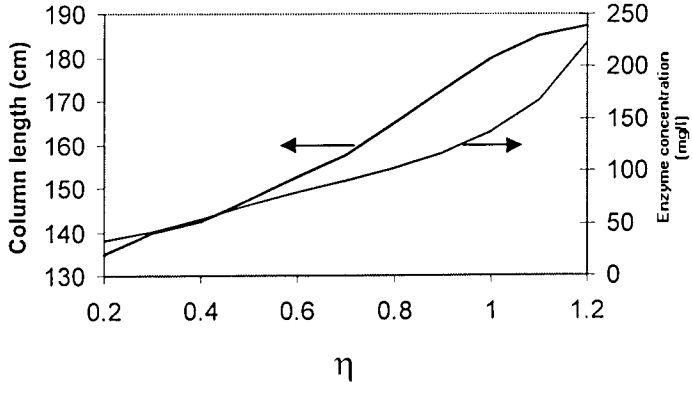

(c)

Figure 7.4 *For β =1.3, plots of dimensionless feed flowrate η against minimum column length L_c and enzyme productivity (a), adsorbent productivity (b) and enzyme concentration (c)*

may be obtained. Comparative plots for the different values of β are shown in Figure 7.5. Solvent consumption does not change much for η>0.7 independently on β. In order to have a robust operation and high adsorbent and enzyme productivity, it would be wise to operate the SMBR at 1.1<β < 1.2 and η > 0.7.

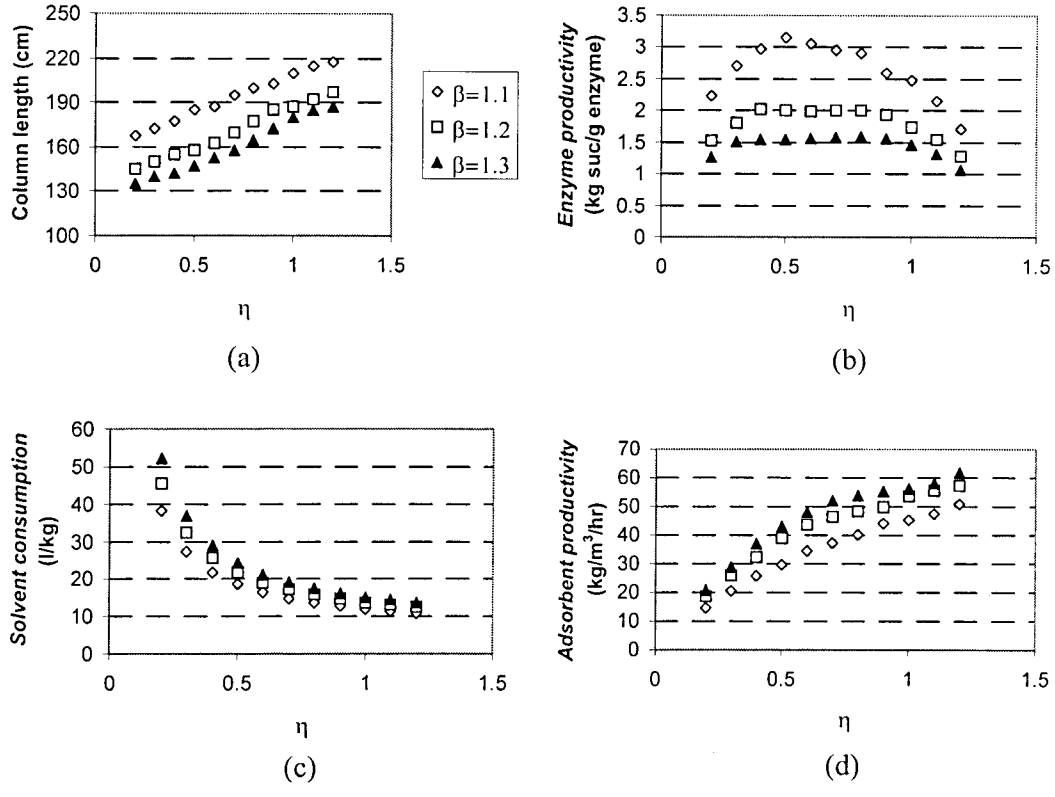

Figure 7.5 *Comparative plots of minimum column lengths (a), enzyme productivity (b), solvent consumption (c) and adsorbent productivity (d) as a function of the dimensionless feed flowrate η for different values of β*

Table 7.3 also summarizes the main results obtained by the design/optimization package. One may note that the optimal column lengths found in Figures 7.2 to 7.4 are quite large as compared to the column diameter. This is due to the limit on maximum pressure drop at 10 bar/column. This limit was reduced to 5 bar/column. The design algorithm results obtained for β=1.2 are shown in Figure 7.6. The plateau of maximum enzyme productivity is enlarged to the η interval [0.4;1.0], although the magnitude of this variable is around 15% less than that obtained for ΔPmax= 10 bar/column. Required column lengths are about 40% smaller than those calculated for a higher pressure limit and cross section area is larger. Product dilution is about the same, though. Energy cost associated with pumping should be

confronted with enzyme and adsorbent cost to make a choice for the most profitable column pressure drop, within the packing mechanical strength limitations.

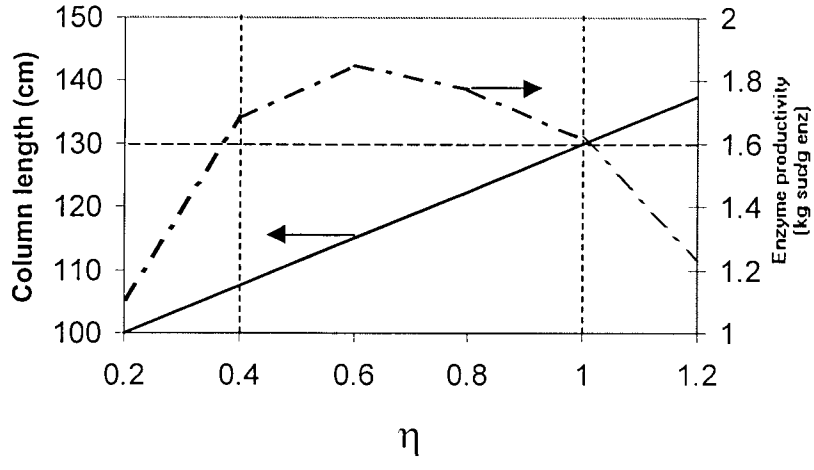

Figure 7.6 Design algorithm results for β =1.2 and with maximum pressure drop of 5 bar per column

Table 7.3 Summary of optimized conditions for a SMBR found by the design package

β	Optimum η range	L_b (cm) D_b (cm)♦	C_{enz} (mg/l)	Fructose in extract (g/l)	Glucose in raffinate (g/l)
1.1	0.4 – 0.8	178-200 6.1-6.5	40-81	67-105	142-237
1.2	0.4 - 0.8	155-178 5.7-6.1	48-95	56-90	129-216
1.2*	0.4 – 1.0	107-130 6.7-7.4	54-137	52-96	116-229
1.3	0.3 – 1.0	140-180 5.4-6.1	42-138	38-92	95-233

♦ Column diameter required for a flowrate in section 1 of 10^3 ml/min
* Design results obtained for a pressure drop limit of 5 bar/column

Figure 7.7 (a) shows the optimal (γ_2,γ_3) pairs obtained for $0.2 < \eta < 1.2$ at the four situations previously analysed. It is interesting to observe that the points lie in a common region and have a common trend which may be roughly described by the straight thick line on the figure. The slope of this line is quite different from the line of optimum operation obtained from an equilibrium model for non-reactive SMB's, both shown in the plot. The "path" falls

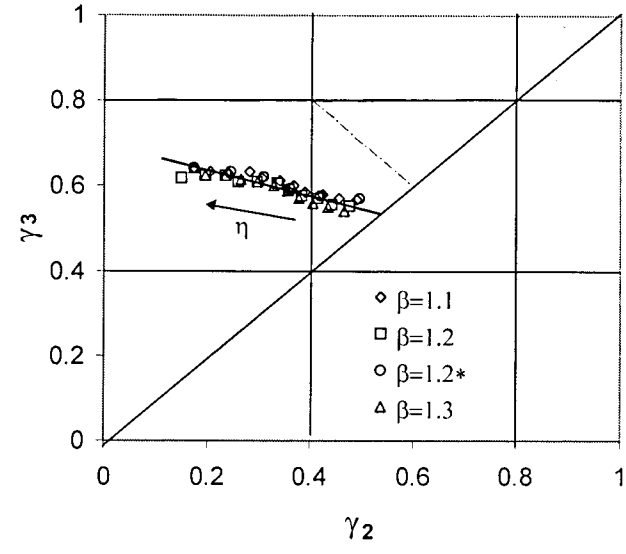

(a)

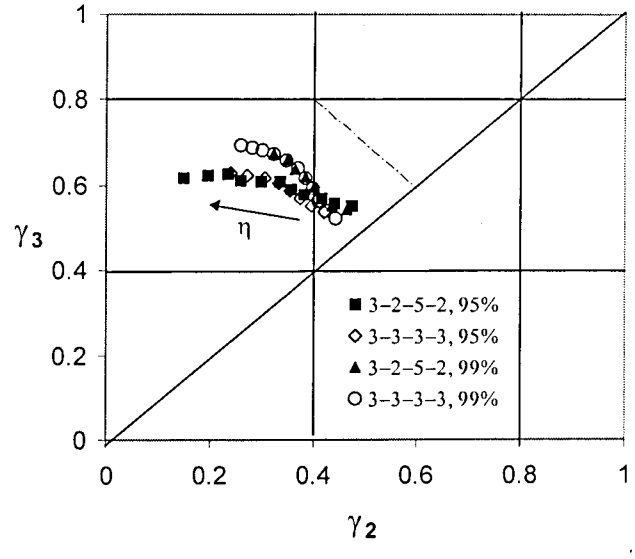

(b)

Figure 7.7 *Optimal operating points in a $\gamma_2 \times \gamma_3$ parameter space for the situations analysed previously (a). The asterisk on the legend stands for the results obtained assuming ΔP= 5 bar/column. Plot (b) illustrates the effects of section subdivision and purity constraints on the design results.*

within the area defined for complete separation only for low flowrates. In such cases, one may say that the amount of substrate entering the SMBR is little enough for reaction to take place in a short portion of section 3 and hence the SMBR behaves as a SMB. As feed flowrate increases, the path leaves the region of complete separation as defined for a non-reactive SMB. The values of γ_3 seem to approach a new limiting value (at about 0.65), which may be due to the fact that flowrates in section 3 need to be lower in order to achieve both high conversions and adsorption of fructose. The values of γ_2 violate the restrictions defined for a non-reactive SMB. This would mean that glucose would not be completely dessorbed in section 2 and hence would contaminate the extract. The correlation between the inclusion of the reaction and the violation of this condition is not straight-forward. It may also be due to the fact that a little contamination (5%) is allowed in our design package. Figure 7.7 (b) shows results of optimum operation points for β=1.2 with different number of columns per section and a different constraint on product purity requirements. Varying the number of columns per section to 3-3-3-3 does not change the path obtained. However, when the purity requirement is 99%, the obtained optimum path deviates from those obtained for 95% purity. Yet, it is quite different form the path for non-reactive SMB's. For the sake of comparison with the non-reactive case, the design algorithm was run for the separation of a fructose-glucose mixture assuming that a completely inverted feed is introduced. If a sucrose solution at a concentration of 400 g/l were completely inverted, a mixture of 210.4 g/l of each sugar (glucose and fructose) would be obtained. For β=1.2, the design results for the SMB and SMBR cases are summarized in Figure 7.8.

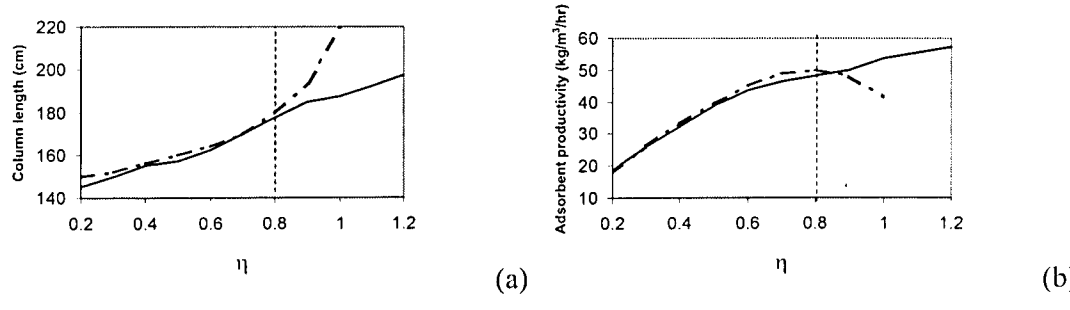

Figure 7.8 *Minimum column length (a) and corresponding adsorbent productivity (b) as a function of required dimensionless throughput η for the case of a SMB (dot-dashed lines) and a SMBR (continuous lines).*

The main differences between the results obtained for a SMB and a SMBR are observed for η>0.8. In the absence of chemical reaction, a maximum feed flowrate (η=1) may be treated, which may be higher if the reaction substrate is fed (SMBR) instead of the reaction products. Figure 7.9 shows the corresponding (γ_2,γ_3) pairs calculated by the algorithm for each η in the SMB and SMBR cases (purity constraint=95%).

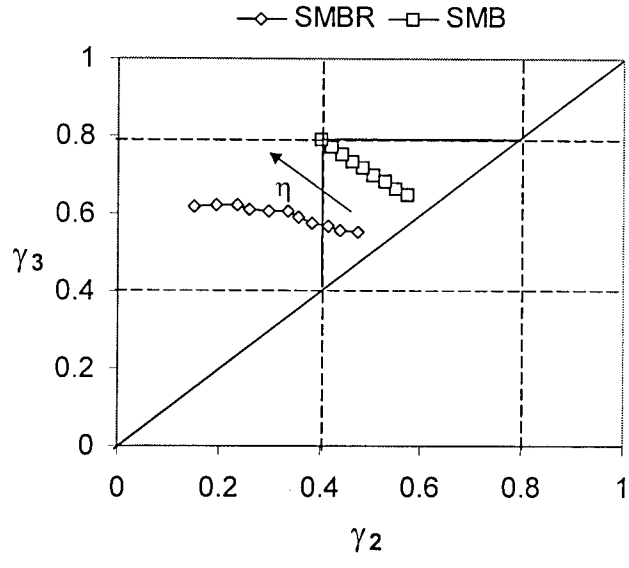

Figure 7.9 Comparison of optimal operating points as calculated from the design algorithm for a SMB and a SMBR case.

The path calculated for the SMB case (separation only) follows the trend stated by the equilibrium theory and all points lie within the equilibrium triangle. This suggests that the violation on γ_2 observed for the SMBR case is not due to the contamination allowed in the purity constraint (95%) but it appears to be a consequence of the inclusion of the reaction kinetics. In practical terms, for the SMBR case, the adsorbent located in section 3 is contacted with a lesser amount of glucose and fructose than for the SMB case under the same feed flowrate. As mentioned previously, there must be a sufficiently long residence time in this section for both reaction and adsorption to take place. This may be achieved by lowering the fluid/solid velocity ratio in the section, which is indeed an observed trend in γ_3. To keep the same η, that is, the same feed flowrate, the velocity ratio in section 2, γ_2, must de decreased by the same magnitude. This also implies in higher extract flowrates and lower raffinate flowrates for the SMBR relative to the corresponding SMB (same γ_1 and γ_4). Therefore, a

more concentrated raffinate and a more diluted extract are achieved in a SMBR. An interesting consequence is that it may be possible to obtain higher glucose concentrations in the raffinate than those in the feed if a completely converted solution were introduced. For instance, at η=0.8 and β=1.1, the glucose concentration in the raffinate for a SMBR is 237 g/l (see Table 7.3). Note that in a SMB adsorber, this figure would never be above 210.4 g/l, which is the feed concentration for a completely inverted sucrose solution (400 g/l).

The design algorithm was also applied to the conditions of the experiments described in the previous Chapter, that is, sucrose concentration of 80 g/l in the feed, η=0.513, β=1.2 (for γ_1) and 1.25 (for γ_4). Pressure drop limitation was set to that measured during the experiments. The results of optimal parameters required to process a feed flowrate of 3.62 ml/min are summarised in Table 7.4. The required column length is 35 cm, 20% longer than the length of the columns used in our experiments. The section area is smaller so that optimum column volume is approximately the same as the actual column volume. The optimal (γ_2,γ_3) pair is very close to the operating point used in the referred experiments.

Table 7.4 Comparison between experimental parameters and those obtained from the design algorithm for the same values of feed flowrate, η and β

Parameter	Value used/obtained in the SMBR experiments	Value calculated from design algorithm
L_c (cm)	29	35
A (cm^2)	5.31	4.08
V_c (cm^3)	154	143
C_{enz} (mg/l)	250[a]/40[b]	45
Enzyme productivity (kg suc/g enz)	0.102[a]/0.636[b]	0.552
$\frac{PRX+PRR}{2}$, kg/m^{3}h	7.43[a]/7.88[b] (5.05[a]/5.36[b] kg/m^3/cycle)	8.36 (5.35 kg/m^3/cycle)
Fructose in extract (g/l)	15.78[a]/15.88[b]	15.07
Glucose in raffinate (g/l)	22.18[a]/22.61[b]	25.49
t* (min)	3.4	3.2
γ_2,γ_3	0.45, 0.65[a] 0.43, 0.63[b]	0.44, 0.64

[a] Value obtained for experiment 1 (see Table 6.3 from Chapter 6)

[b] Value obtained for experiment 2 (see Table 6.3 from Chapter 6)

In other words, if the columns used in our experiment were 35 cm long, the equipment could convert a feed flowrate of $3.62\times(5.31/4.08)$=4.71 ml/min. The amount of enzyme used was 400% overestimated in experiment 1 described in Chapter 6 (see Table 6.3). In SMBR experiment 2, enzyme concentration was very close to the ideal value and one may say that the SMBR equipment was operated in nearly optimised conditions for the throughput of 3.62 ml/min.

7.5 Conclusions

A design and optimisation methodology was proposed in this Chapter for the inversion of sucrose and separation of glucose and fructose in a simulated moving bed reactor. The design algorithm used a detailed process model based on the strategy of a true moving bed reactor (TMBR) as described in Chapter 6. The design algorithm calculates minimum adsorbent inventory (column length and diameter) and enzyme concentrations, for various values of parameters η and β, which lead to a desired process performance in terms of reaction conversion and purity of reaction products. The constraints on process performance were a minimum reaction conversion of 99% and minimum product purities of 95%. Results from the design algorithm (η, β, L_c, C_{enz}) were used and analysed in the optimisation step by defining enzyme productivity as the objective function to be maximised. Plateaux of enzyme productivities were obtained for η interval of [0.4,0.8], at β equal to 1.1 and 1.2, and for the η interval of [0.3,1.0] for β equal to 1.3. For a lower column pressure drop limitations, required column lengths are reduced but optimal velocity ratios remain about the same. The final decision on the optimal SMBR operating and geometric conditions may be made by balancing such criteria as robustness, product dilution, energy and enzyme costs. It was also evidenced that the "path" of the optimal operating points (γ_2,γ_3) is the same independently of the safety margin β, on the imposed pressure drop limitations and on the number of columns per section. The optimal values obtained for (γ_2,γ_3) are lower than those calculated for the non-reactive case. This causes γ_2 values to violate the bounds imposed by the equilibrium theory (applied to non-reactive SMB's) because longer residence times must be achieved for both reaction and adsorption to take place in sections 2 and 3.

7.6 References

H. Schiweck, M. Clarke, "Physical Properties of Aqueous Sugar Solutions (3.2)" in: *Ullmann's Encyclopedia of Industrial Chemistry*. Web version, Wiley-VCH, Weinheim, 2001.

G. Biressi, O. Ludemann-Hombourger, M. Mazzotti, R.-M. Nicoud, M. Morbidelli, "Design and Optimisation of a SMB Unit: Role of Deviations from Equilibrium Theory", *J. Chromatography A* **876**, 3-15 (2000).

C. B. Ching, Z. P. Lu, "Simulated Moving-Bed Reactor: Application in Bioreaction and Separation", *Ind. Eng. Chem. Res.* **36**, 152-159 (1997).

G. Dünnebier, J. Fricke, K.-U. Klatt, "Optimal Design and Operation of Simulated Moving Bed Chromatographic Reactors", *Ind. Eng. Chem. Res.* **39**, 2290-2304 (2000).

C. Migliorini, M. Fillinger, M. Mazzotti, M. Morbidelli, "Analysis of Simulated Moving-Bed Reactors", *Chem. Eng. Sci.* **54**, 2475-2480 (1999).

8. Conclusions and suggestions for future work

This work addressed the issues of modeling, simulation, design, operation and optimization of SMB and SMBR processes applied to sugar systems. Some novel aspects have been focused, which will be highlighted in the following paragraphs together with the most relevant conclusions drawn from each point.

In the modeling of SMB processes, more detailed descriptions of kinetic and equilibrium phenomena within the adsorbent particles have been presented. The bi-linear driving force approximation was used to describe intraparticle mass transfer in the modeling of SMB and SMBR processes. Perfect equivalence with the classical LDF expression has been demonstrated. The use of this more sophisticated formulation may allow studying the effects of particle size and temperature on SMB performance in a more physically meaningful way, especially for non-linear isotherms. Another refinement in the description of mass transfer phenomena in SMB processes was introduced by the inclusion of a finite kinetics of adsorption. This approach may prove useful in the prediction of SMB processes involving protein separation.

A design methodology for SMB plants was introduced under the denomination of the "Separation Volume" analysis. The concept of a separation volume allowed assessing the

effect of sections 1 and 4 in the shape of the area of desired separation in a $\gamma_2 \times \gamma_3$ parameter space. This analysis is especially useful in cases where inefficient columns are used due to mass transfer or axial dispersion limitations. It was the case of glucose-fructose separation in the Licosep 12-26 plant. By tuning γ_1 with the aid of this analysis, it was possible to obtain satisfactory product purities experimentally.

A generalization of the findings from the Separation Volume Analysis was developed in the form of an algorithm to design adequate operating conditions for a given SMB plant. The algorithm searched for the vertices of the separation areas (maximum throughput) at different γ_1 and γ_4 in accordance with the equilibrium theory. An optimization step could be applied, which consisted of finding the minimum γ_1 and maximum γ_4 that allowed treating the highest feed flowrate. To elect optimum switching time, an objective function may be defined. In the present work, this objective function was the ratio between productivity and solvent consumption and a maximum value was searched. With regard to the design of geometric parameters of new SMB plants, a strategy proposed by Biressi *et al* (2000) was improved and applied to the case of fructose-glucose separation. The process model used in the strategy was a detailed TMB-based model instead of the stages-in-equilibrium model originally used by Biressi *et al* (2000). The optimal operating points (γ_2, γ_3) defined by the strategy were in accordance with the predictions from the equilibrium theory. This coherence brought reliability to the design/optimisation strategy.

Fructose and glucose were found in the liquid phase of cashew (Anacardium occidentale, L.) apple juice in appreciable amounts (40-50 g/l), together with a wide variety of organic acids, polyphenols and macromolecules. Separation of these sugars was demonstrated experimentally in a simulated moving bed and steady state behaviour followed very closely to that observed for synthetic mixtures. Due to the limited number of experiments and to the diversity of other compounds present in the juice, a potential change in the characteristics of the resin (capacity, mass transfer resistance, microbial growth) after successive cycles could not be assessed.

The enzymatic inversion of sucrose and separation of fructose and glucose in a simulated moving bed reactor was investigated. From the experimental point of view, adsorption of enzyme invertase on the separation resin was evidenced, which enhanced the reaction rate as compared to that observed in batch reactors. From the standpoint of modeling,

the reaction rate was successfully described by using a pseudo-homogeneous form of the Michaelis Menten equation that included the contribution of the immobilized enzyme. An algorithm to design and optimize a new SMBR plant was presented. The catalyst/enzyme concentration in the eluent was an additional degree of freedom to the problem as compared to that dealt with in the case of non-reactive SMB. The most interesting finding on this topic was the "path" of operating points (γ_2, γ_3) corresponding to increasing throughputs that the plant was required to treat. Unlike the results obtained for a non-reactive SMB, the path violates the equilibrium bound on γ_2 defined by the equilibrium theory in the absence of reaction.

Since every thesis work is limited by either technical or chronological restrictions, many research topics of interest arose from the study described so far. In the following paragraphs, they are suggested as topics for future investigation.

Concerning the modeling of SMB processes, we propose the development and implementation of models including the bi-LDF approximation with non-linear isotherms and/or large-pore particles (convective transport involved). As for the question of non-instantaneous equilibrium of adsorption, an interesting extension of this modeling methodology is the description the particle as a porous solid, rather than the approach of a homogeneous solid used in this work.

The concept of separation volume may be easily extended to non-linear equilibrium systems and the feed concentration may have an interesting effect on the shape of these volumes. Accordingly, the algorithm for design of operating conditions may be applied to the case of non-linear isotherms and feed concentration may be an optimization parameter as well.

Concerning the auspicious results obtained for the separation of fructose and glucose from cashew apple juice, we strongly recommend studies of SMB separations from feed stocks consisting of real mixtures. The effect of other components on the long term life of the stationary phase is another suggested topic for future research

With respect to the operation of a SMBR to invert sucrose by enzymatic action, some suggestions for further experimental investigation are the definition of the ideal conditions of enzyme immobilization and the study of its stability in the immobilized form. As for the

modeling of SMBR processes, we recommend the development of an expression for the reaction rate law that considers the actual heterogeneous reaction. The methodology of design and optimization of SMBR plants may be extended to more complex systems, such as reversible reactions, non-linear adsorption equilibria and large-pore supports. For immobilized/supported catalysts, where the packing is both a reaction and separation agent, this methodology may be adapted so that particle size is an optimization target parameter. As far as economic factors are concerned, we also suggest the inclusion of more a detailed cost function (including labour force, equipment depreciation, packing replacement, etc.) as objective function of the presently proposed design/optimization algorithm.

A. Effects of Adsorption Kinetics on Simulated Moving Bed Performance

A.1 Introduction

The performance of SMB units has been shown to be extremely sensitive to solid/fluid flowrate ratios, column configuration and kinetic/equilibrium parameters. In many cases, it is desirable to have a model as detailed as available computational resources possibly may permit. In the modeling of adsorptive separation processes, local equilibrium at the adsorbent solid surface is a widely accepted and used assumption. However, this is questionable when steric hindrances and affinity effects are present. This seems to be the case of some adsorbents with chiral resolution properties, such as CTA (Pais *et al*, 1998) and it is the general case of protein and macromolecule adsorption. Several stationary phases with chiral recognition properties have been proposed in the literature (Francotte *et al*, 1998; Lehoucq *et al*, 2000; Pais *et al*, 2000). For the great majority of them, the determination of precise multicomponent competitive adsorption isotherms is a crucial aspect. Although the mechanism of chiral recognition is still unclear, the presence of non-chiral and chiral adsorption sites has been frequently reported and accounted for by a modified Langmuir isotherm as expressed in equation (A.1):

$$q_{si}^{*} = K_i C_i + \frac{b_i q_m C_i}{1 + b_A C_A + b_B C_B}, \quad i=A,B \qquad \text{(A.1)}$$

The illustrative example examined in this appendix for such isotherm is that of a microcrystalline cellulose triacetate (CTA) used as a SMB stationary phase for the separation of a chiral epoxide. The use of this adsorbent in its swollen state has been reported in the literature (Blaschke, 1986; Francotte and Junker-Buchheit, 1992; Koller *et al*, 1983; Shibata *et al*, 1986) for various chiral separations. It seems that, unlike common stationary phases, adsorption on microcrystalline CTA is more influenced by steric effects than by the chemical nature of the interaction between the chiral species and the stationary phase substituents (Pais *et al*, 1998). When steric hindrances are present, it is very likely that non-equilibrium adsorption/desorption effects take place. This has been pointed out as the cause of the observed mismatch between predicted and experimental results by some authors (Pais *et al*, 1998; Rodrigues *et al*, 1992; Whitley *et al*, 1993). Whitley et al (Whitley *et al*, 1993) examined the effects of non-equilibrium adsorption/desorption on breakthrough and elution curves in affinity/perfusion chromatographic systems with Langmuir equilibrium isotherms. They concluded that, in analytical and preparative scale chromatography, non-equilibrium at the solid-fluid interface is responsible for such symptoms as symmetric and asymmetric broadening, apparent loss of capacity, loss of coherence and deviations from the interference patterns of local equilibrium systems. Rodrigues et al (1992) also addressed this matter for large pore supports used in chromatographic bioseparations under linear equilibria. They examined the influence of the kinetics of adsorption in the HETP and proposed criteria in order to verify to which extend non-equilibrium effects are important as compared with the other mass transfer/dispersion phenomena.

The contents of this appendix intend to contribute to the effort of a more comprehensive understanding of non-instantaneous local equilibria, applied to the operation of a simulated moving bed. A first order kinetics of adsorption is proposed for linear and non-linear isotherms and the implications of this assumption are examined on SMB modeling and design.

A.2 Theory

A.2.1 Modeling kinetics of adsorption/desorption at the solid-fluid interface

If a homogeneous adsorbent particle is submitted to a concentration C at its surface, the LDF approximation states that the rate of sorbate uptake may be written as:

$$r_{diff} = k_h(q_s - \overline{q}) \tag{A.2}$$

where $\overline{q}$ is the adsorbed phase concentration averaged over the particle volume, k_h is the homogeneous mass transfer rate constant and q_s is the concentration at the particle surface. The hypothesis of instantaneous equilibrium at the solid surface is very often accepted and q_s is related to the fluid phase concentration C by means of the equilibrium isotherm equation.

However, equilibrium is very frequently not attained instantaneously but follows a given kinetics as shown in Figure A-1. For a linear equilibrium isotherm, if kinetics of sorption of first order is assumed, the rate of adsorption can be expressed as:

$$r_{ads} = k_1 C - k_2 q_s = k_2(KC - q_s) \tag{A.3}$$

where k_1 and k_2 represent the adsorption and desorption rate constants, respectively, and K is the adsorption equilibrium constant. If a mixture of species A (more strongly adsorbed component) and B (less adsorbed component) is in contact with the adsorbent, equation (3) is valid for each of the components.

For a Langmuir equilibrium isotherm, the first order kinetic law for the rate of adsorption would be expressed as:

$$r_{adsA} = k_1 C_A(q_m - q_{sA} - q_{sB}) - k_2 q_{sA} = k_2[b_A C_A(q_m - q_{sA} - q_{sB}) - q_{sA}] \tag{A.4}$$

where b is a Langmuir isotherm parameter and q_m is the maximum adsorbent capacity. The subscripts A and B denote the chemical species involved.

For adsorbents with chiral selectivity, a combined linear+Langmuir isotherm has been frequently proposed in the literature (Juza *et al*, 1998; Lehoucq *et al*, 1998). In this case, the rate of adsorption would be the sum of the rates of adsorption for non-chiral and chiral sites denoted by the superscripts ^{NC} and ^{C}, respectively.

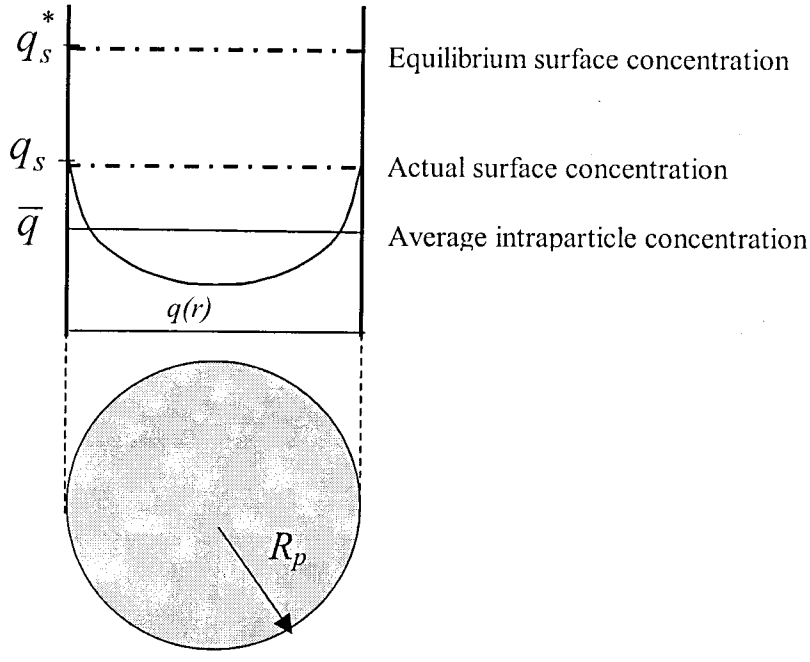

Figure A-1 *Representation of an adsorbent particle with intraparticle mass transport and non-equilibrium adsorption effects on its surface*

$$r_{adsA} = k_2^{NC}(K_A C_A - q_{sA}^{NC}) + k_2^{C}\left[b_A C_A (q_m^C - q_{sA}^C - q_{sB}^C) - q_{sA}^C\right] \qquad \text{(A.5)}$$

Assuming that the non-chiral sites do not exhibit adsorption kinetics, the first term on the right-hand side of equation (A.5) is equal to zero. Consequently, $q_{sA}^C = q_{sA} - K_A C_A$ and $q_{sB}^C = q_{sB} - K_B C_B$. Equation (A.5) may be written as:

$$r_{adsA} = k_2\left[b_A C_A (q_m - q_{sB} + K_B C_B) + (1 + b_A C_A)(K_A C_A - q_{sA})\right] \qquad \text{(A.6)}$$

For modeling purposes of adsorptive processes, the concentration at the adsorbent surface q_{si} (i=A,B) must be related to the other variables of the problem. This may be done by assuming that the rate of adsorption, as given in equations (A.3), (A.4) and (A.6), is equal to the rate of intraparticle mass transfer as given in equation (A.2). By doing so, and solving the remaining equations for q_{si}, one gets the following equations.

For linear equilibrium:

$$q_{si} = \frac{K_i C_i + \Omega \overline{q}_i}{1 + \Omega}, \quad i = \text{A or B} \qquad \text{(A.7)}$$

For Langmuir equilibrium:

$$q_{sA} = \frac{b_A C_A (q_m - q_{sB}) + \Omega \bar{q}_A}{1 + b_A C_A + \Omega} \tag{A.8}$$

$$q_{sB} = \frac{b_B C_B (q_m - q_{sA}) + \Omega \bar{q}_B}{1 + b_B C_B + \Omega} \tag{A.9}$$

For linear+Langmuir isotherm:

$$q_{sA} = \frac{b_A C_A (q_m - q_{sB} + K_B C_B) + (1 + b_A C_A) K_A C_A + \Omega \bar{q}_A}{1 + b_A C_A + \Omega} \tag{A.10}$$

$$q_{sB} = \frac{b_B C_B (q_m - q_{sA} + K_A C_A) + (1 + b_B C_B) K_B C_B + \Omega \bar{q}_B}{1 + b_B C_B + \Omega} \tag{A.11}$$

Ω is the ratio between the mass transfer rate constant k_h and the adsorption/desorption rate constant k_2. From equations (A.7) through (A.11), the extreme cases are easily verified. If $k_2 << k_h$, adsorption kinetics is the limiting rate mechanism; $1/\Omega$ tends to zero and $q_{si} \approx \bar{q}_i$. On the other hand, if $k_h << k_2$, equilibrium at the surface is reached locally; Ω tends to zero and $q_{si} \approx q_{si}^*$, as expressed by the corresponding isotherm. When both sorption and intraparticle mass transfer rates have comparable magnitude, q_s, as given from equation (A.7) through (A.11) may be written as an algebraic equation together with the mass balance equations of the adsorptive process model.

The modeling of a simulated moving bed including effects of adsorption kinetics followed the two strategies already discussed in Chapter 2: 1) an equivalent true moving-bed (TMB) and 2) a dynamic simulated moving bed (SMB). Model equations using both strategies included the description of intraparticle mass transfer by the LDF approximation. Depending on the equilibrium isotherm, any one of equations (A.7) through (A.11) may be added as an algebraic equation to express the concentration of chemical species i at the adsorbent surface, q_{s_i}. The differential mass balances for both approaches are summarized in Table A-1.

Table A-1 Summary of models used in this work to predict SMB performance.

TMB-based model	SMB-based model
- Differential mass balances (steady state) in bulk fluid phase, pore fluid phase and solid phase for species i in a section j :	- Differential mass balances, global and in solid phase for species i in column k :
$\frac{\gamma_j}{Pe_j}\frac{\partial^2 C_{i,j}}{\partial x^2}-\gamma_j\frac{\partial C_{i,j}}{\partial x}-\frac{(1-\varepsilon)}{\varepsilon}\alpha_{i,j}\left(q_{s_{i,j}}-\overline{q}_{i,j}\right)=0$ $\frac{\partial \overline{q}_{i,j}}{\partial x}+\alpha_{i,j}\left[q_{s_{i,j}}-\overline{q}_{i,j}\right]=0$	$\frac{\partial C_{i,k}}{\partial \tau}+\nu_k\frac{\partial \overline{q}_{i,k}}{\partial \tau}=\frac{\psi_k}{Pe_k}\frac{\partial^2 C_{i,k}}{\partial \chi^2}-\psi_k\frac{\partial C_{i,k}}{\partial \chi}$ $\frac{\partial \overline{q}_{i,k}}{\partial \tau}=\alpha_i\left(q_{s_{i,k}}-\overline{q}_{i,k}\right)$
where $x=z/L_j$	where $\chi=\frac{z}{L_c}$ and $\tau=t/t^*$
- Boundary conditions:	- Boundary conditions:
$C_{i,j}^{in}=C_{i,j}(0)-\frac{1}{Pe_j}\frac{\partial C_{i,j}}{\partial x}\qquad \frac{\partial C_{i,j}}{\partial x}(1)=0$	$C_{i,k}^{in}=C_{i,k}(0,\theta)-\frac{1}{Pe_k}\frac{\partial C_{i,k}}{\partial \chi}$
$\overline{q}_{i,j}(1)=\overline{q}_{i,j+1}(0)$	$\frac{\partial C_{i,k}}{\partial \chi}(1,\theta)=0$
- Dimensionless parameters:	- Initial conditions:
$\gamma_j=\frac{U'_{Fj}}{U_S}\qquad Pe_j=U'_{F_j}L/\mathrm{D}_{\mathrm{ax}_j}$	$C_{i,k}(\chi,0)=C_{i,k}^{o}(\chi)\qquad \overline{q}_{i,k}(\chi,0)=\overline{q}_{i,k}^{o}(\chi)$
$\alpha_{i,j}=\frac{k_{h_i}L_j}{U_S}$	- Dimensionless parameters:
	$\psi_k=U_{F_k}t^*/L_c\qquad \alpha_i=k_{h_i}t^*$
- Node balances:	-Node balances:
$C_{i,1}^{in}=\frac{Q'_4}{Q'_4+Q_E}C_{i,4}(1)\qquad C_{i,2}^{in}=C_{i,1}(1)$	$C_{i,k}^{in}=C_{i,k-1}(1,\theta)$, except if column follows feed or eluent port. In such case,
$C_{i,3}^{in}=\frac{Q'_2}{Q'_3}C_{i,2}(1)+\frac{Q_F}{Q'_3}C_{i,F}\qquad C_{i,4}^{in}=C_{i,3}(1)$	$C_{i,k}^{in}=\left[Q_FC_{i,F}+Q_2C_{i,k-1}(1,\theta)\right]/Q_3$ $C_{i,k}^{in}=Q_4C_{i,k-1}(1,\theta)/Q_1$, respectively

A.2.2 Prediction of Separation Regions and Process Performance

It has been said before that one of the keys to a successful SMB separation is the correct design of its operating conditions. For separation of a binary mixture to occur, each of the four sections of the SMB must perform a certain role. If a binary mixture of A (more strongly adsorbed component) and B (more weakly adsorbed component) is fed in a SMB, A

will only move towards the extract port and B to the raffinate port if certain flow constraints are met. These flow constraints may be expressed as the following:

$$\frac{Q'_1 C_{A,1}}{Q_S \bar{q}_{A,1}} > 1 \tag{A.12}$$

$$\frac{Q'_2 C_{B,2}}{Q_S \bar{q}_{B,2}} > 1; \qquad \frac{Q'_2 C_{A,2}}{Q_S \bar{q}_{A,2}} < 1 \tag{A.13}$$

$$\frac{Q'_3 C_{B,3}}{Q_S \bar{q}_{B,3}} > 1; \qquad \frac{Q'_3 C_{A,3}}{Q_S \bar{q}_{A,3}} < 1 \tag{A.14}$$

$$\frac{Q'_4 C_{B,4}}{Q_S \bar{q}_{B,4}} < 1 \tag{A.15}$$

The left hand term in the inequalities above may be re-written as:

$$\Gamma_{i,j} = \gamma_j \nu \frac{C_{i,j}}{\bar{q}_{i,j}} \tag{A.16}$$

From this point on, the term "design" will be used to designate the procedure of determining the finite group of flowrate ratios γ_1, γ_2 , γ_3, and γ_4 that satisfies inequalities (A.12) to (A.15). In the frame of equilibrium theory, design requires only the knowledge of equilibrium data. The graphical representation of equations (A.13) and (A.14) in a parameter space $\gamma_2 \times \gamma_3$ is shown in Tables 3.1, 3.2 and 3.3 (Chapter 3) for different types of equilibrium isotherms.

When kinetic effects are taken into account, the flowrate ratios which enhance separation may only be accessed through numerical simulation of the corresponding steady-state SMB performance. Moreover, performance criteria (e.g. minimum required purities, recoveries, etc.) have to be defined since complete separation (100% extract/raffinate purity) is not achieved. In the following examples, minimum extract and raffinate purity of 99% was chosen as the criteria to define the region of separation in terms of flowrate ratios. The constraint on section 4 together with residence time considerations were used to define arbitrarily the rotation period and recycle flowrate to be considered in the design procedure. Then, for a given value of γ_1, in accordance with equation (A.12), the region of separation in a $\gamma_2 \times \gamma_3$ plane was determined by simulation using the steady-state TMB model.

A.3 Results and Discussion

For the non-linear equilibrium isotherms, the case of SMB separation of a chiral epoxide using a microcrystaline cellulose triacetate was chosen to illustrate non-equilibrium effects. For this stationary phase, Pais et al (1998) have reported the experimental measurement of a modified Langmuir isotherm as expressed in equation (A.1) with K =1.35; q_m=7.32 g/l; b_A=0.163 l/g and b_B=0.087 l/g. The operation of a SMB with 2 columns per section was simulated using the operating conditions as given in Table A-2.

Table A-2 SMB setup for experiment and simulations of chiral epoxide separation

Model parameters	**Operating conditions**	**Columns**
Pe=2000	T=20°C	D_b = 2.6 cm
k_h = 24 min^{-1}	Feed conc. = 5 g/l each	L_b = 9.9 cm
α=160	t*= 3.3 min	Configuration: 2-2-2-2
Ω = 0, 1, 2	Q_{Rec}= 21.38 ml/min Q_X= 8.64 ml/min	Zone length = 19.8 cm
ν=1.5	Q_E= 12.36 ml/min Q_F= 1 ml/min	

Figure A-2 shows simulated and experimental internal profiles for Ω=0 and Ω=2. The evolution of internal profiles of both isomers calculated at the last half period of the 2nd, 4th, 7th and 10th cycles is confronted with that as calculated from the TMB model. As expected, the TMB model fails to predict concentrations around the feed node. This is shown by comparison with the experimental points (triangles for 'A' and squares for 'B). From Figure A-2, the simulated profiles obtained for Ω=0 seem to fit better the experimental points obtained for the most adsorbed component, whereas a better agreement is observed for the least adsorbed component at Ω=2. A crucial performance criterion in SMB enantiomer separation is product purity. Table A-3 compares the purities obtained for both extract and raffinate at different adsorption resistance situations. In general, the SMB model results are less optimistic than those from the TMB model as already evidenced by other authors [7]. Closer results to those obtained experimentally are observed for Ω=2.

From Table A-3, one may also verify that the extract purity is more affected by adsorption effects than the raffinate stream and greater discrepancies between the values as predicted from the TMB and SMB models are obtained for increasing Ω. This may be a problem if extremely product purities are required, which is the case in most separations in

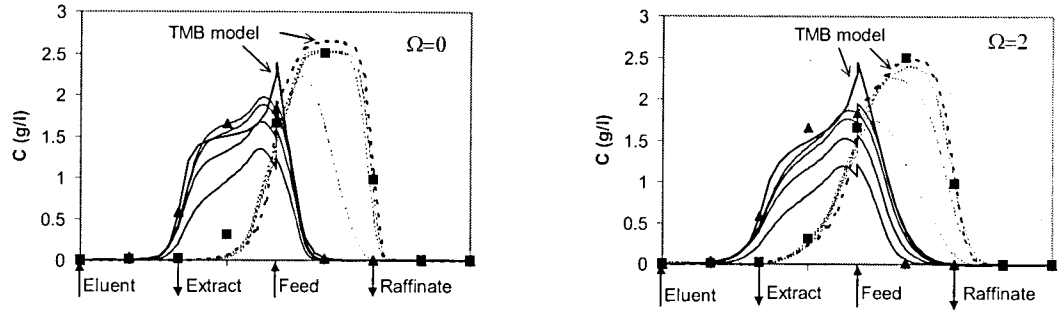

Figure A-2 *Evolution of SMB internal profiles obtained for the configuration as described in Table A-2. Straight lines and triangles stand for enantiomer A, dashed lines and squares stand for B.*

pharmaceutical industry. Figure A-3 shows the evolution of the extract compositions for Ω = 0, 1 and 2. As expected, the composition histories behave in a periodic way for all cases, even when steady state is reached (not shown). The plots also show the average concentration history measured over a period. As Ω increases, there is greater cross contamination and steady state takes longer to be reached. This may be seen by comparing the average concentration after 150 min with the steady state concentrations as predicted from a TMB model.

Table A-3 *Extract and raffinate purities obtained from simulation models and experiment.*

	Ω = 0		Ω = 1		Ω = 2		Experiment
	SMB	TMB	SMB	TMB	SMB	TMB	
PUX (%)	99.9	100	99.4	99.6	97.3	98.6	97.5
PUR (%)	100	100	99.8	100	99.6	99.5	99.6

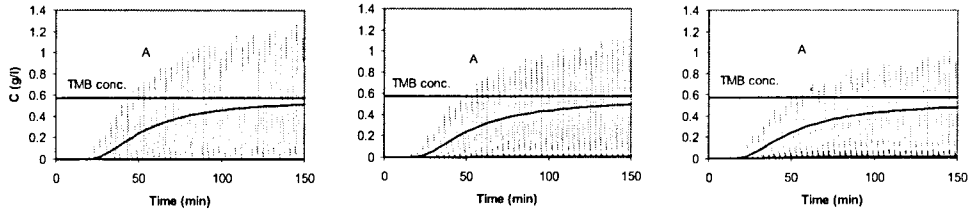

(a) (b) (c)

Figure A-3 *Evolution of extract compositions, average extract composition and stationary TMB composition for Ω = 0 (a), 1 (b) and 2 (c).*

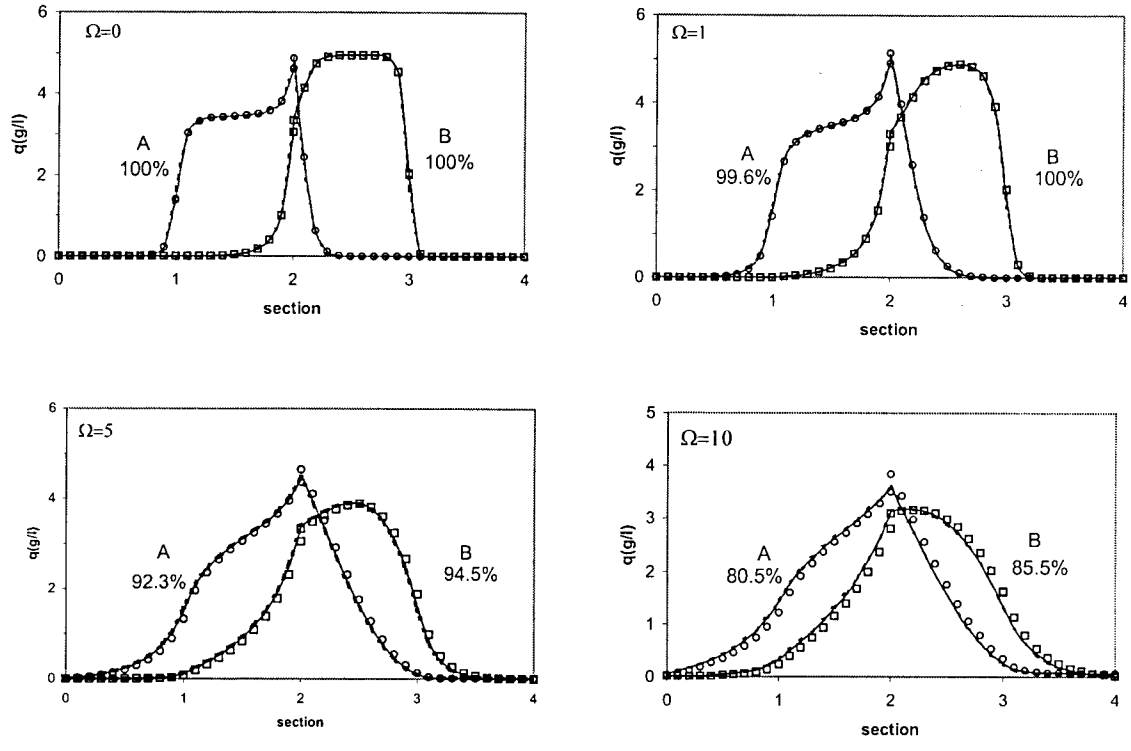

Figure A-4 *Steady-state internal profiles for enantiomer A and B with α=160 and Ω=0, 1, 5 and 10. The dashed curves stand for the mean solid phase concentration, $\overline{q}$; the continuous curves stand for surface concentration, q_s and the points stand for equilibrium surface concentration, q_s^* (circles for A and squares for B). The figures in each graph indicate extract purity (A) and raffinate purity (B)*

Figure A-4 shows the simulated steady-state internal profiles obtained for different values of Ω. In all four examples, the concentration at the surface of the adsorbent particles (continuous curves) is about the same as the mean solid concentration (dashed curves) since the mass transfer rate constant is considerably high (24 min^{-1}). Nevertheless, as the resistance to equilibrium attainment increases (increasing values of Ω), the product purities are greatly affected, even for small values of Ω. Broader profiles are observed with increasing Ω, not only in the solid phase, but also in the fluid phase (not shown) with corresponding product contamination. As Ω increases, the concentration at the surface of the particle should deviate from the concentration that would be in equilibrium with the fluid phase concentration $C_{i,j}$.

To verify the influence of adsorbent particle size, the same case as described in Table A-2 was simulated assuming a particle size twice as large. If the particle diameter is doubled, the intraparticle mass transfer becomes four times as small as the original value. The number

of mass transfer units will go down to 40. The corresponding simulations of SMB performance with the same setup as described in Table A-2 is shown in Figure 6. In all graphs, the difference between the concentration at the particle surface and the mean intraparticle concentration is noticeable. With increasing Ω, the difference between the concentration at the particle surface and the theoretical concentration in equilibrium with the fluid phase also becomes distinct.

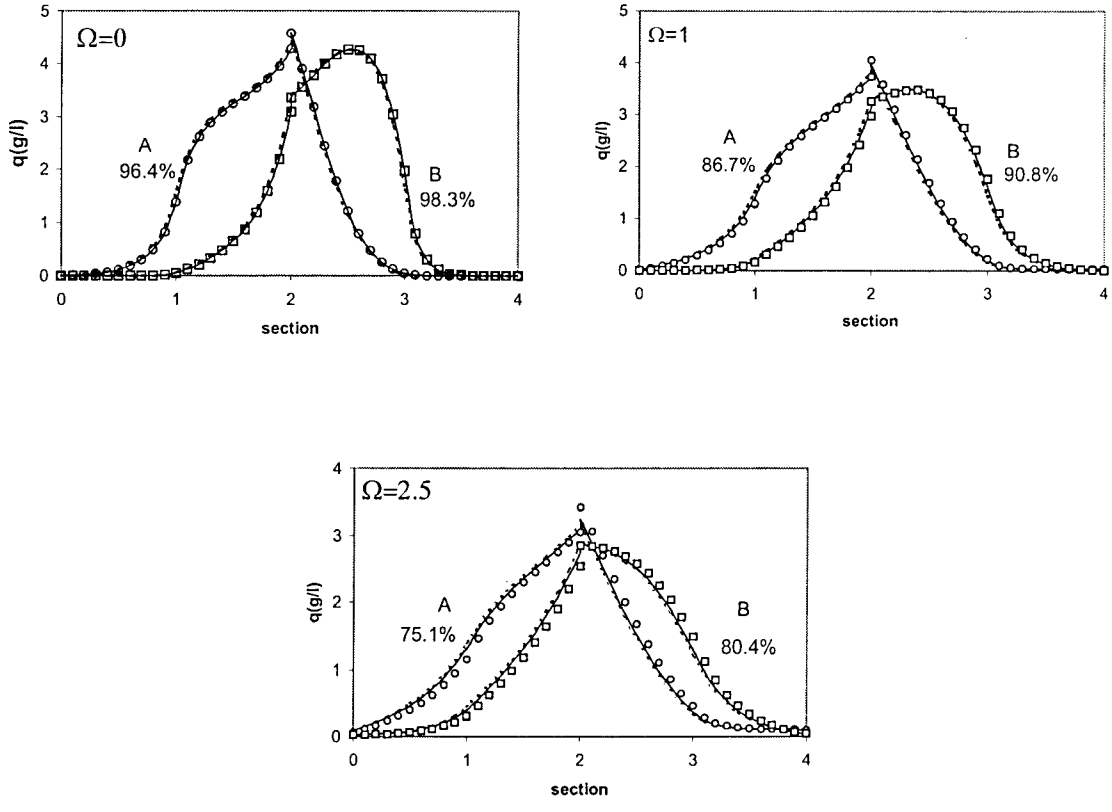

Figure A-5 *Steady-state internal profiles for a SMB unit with α= 40 and Ω=0, 1 and 2.5. Legends are the same as in Figure A-4.*

The design procedure was performed for the case of the extended langmuir isotherm (equation A.1). The column configuration and process parameters used were those found in Table A-2. The rotation period and flowrates in sections 1 and 4 were calculated from retention time considerations and then checked against the constraints given in equations (A.12) to (A.15). These constraints have been determined analitically for modified Langmuir isotherms in the frame of equilibrium theory by Mazzotti et al (1997).

The flowrate in zone 1 is the greatest of all and may be determined by the equipment pressure drop limitations. We chose the value of 34 ml/min. In section 1, the strongly retained component A should be dessorbed so that the solid "leaves" section 1 towards section 4 completely regenerated. Therefore, the rotation period should be larger than the retention time of component A so that there is enough time in a period for it to be washed out of the solid adsorbent. Fluid phase concentrations should be as low as possible so that only the linear portion of the modified Langmuir isotherm may be considered. Hence, the retention time of component A in zone 1 is:

$$t_{RA,1} = \frac{\varepsilon V_b}{Q_1}\left[1 + \nu\left(K_A + b_A q_m\right)\right] \tag{A.17}$$

Using the values illustrated in Table A-2 for column dimensions, phase ratio, equilibrium data and the assigned flowrate of 34 ml/min, the column retention time of component A in zone 1 is 2.98 min. The rotation period was then set to 3.3 min, somewhat higher than the calculated retention time. With these values of rotation period and section 1 flowrate, the flowrate ratio γ_1 is equal to 4.3, which is greater than the minimum value of γ_1 as stated from the equilibrium theory:

$$\gamma_1 > \gamma_1^{\min} = \nu\left(K_A + b_A q_m\right) = 3.81 \tag{A.18}$$

In section 4, the column retention time should be such that the less retained component is adsorbed and carried towards the raffinate port. In this section, the column retention time of component B may be written as:

$$t_{RB,4} = \frac{\varepsilon V_b}{Q_4}\left[1 + \nu\frac{\Delta q^*_{B,F}}{\Delta C_{B,F}}\right] \tag{A.19}$$

where $\Delta q^*_{B,F}/\Delta C_{B,F}$ is the slope of the chord linking points ($C_{B,F}$; $q^*_{B,F}$) to (0,0) with C_A=0. Using the values given in Table A-2, $C_{B,F}$ = 5 g/l and hence $\Delta q^*_{B,F}/\Delta C_{B,F}$ = $K_B+b_B q_m/(1+b_B C_{B,F})$=1.794. Ideally, the column retention time of component B in section 4 should be greater than the rotation period, so that its concentration front does not reach the end of the section and contaminate the eluent moving to section 1. Setting a value of $t_{RB,4}$ = 3.88 min, Q_4 is equal to 20 ml/min as calculated from equation (A.19). With these values, the flowrate ratio γ_4 is 2.36, which is in accordance with the maximum value defined for this constraint (2.72). Although the derivation of the minimum bound on γ_4 is analytical, it

requires some tedious calculations, which is out of the scope of this work and may be found elsewhere (Mazzotti *et al*, 1997).

With these values of Q_1, Q_4 and t^*, the corresponding flowrate ratios in sections 1 and 4 are γ_1=4.3 and γ_4=2.36. By successive simulations, different values of γ_2 and γ_3 in the area defined by the equilibrium theory, with $\gamma_2 < \gamma_3$, were tested for the column configuration as given in Table A-2 in order to find those values which result in both product purities higher than 99%. This was done for different situations of adsorption kinetics and is shown in Figure A-6(a). Note that the number of mass transfer units (α) is high enough so that equilibrium is nearly reached throughout the particle volume. This may be verified by comparing the region of separation as calculated analytically from the equilibrium theory (Mazzotti *et al*, 1997) with that calculated for α=160 and Ω=0. In the other cases shown, the adsorption rate constant is arbitrarily decreased so as to obtain the values of Ω= 1, 1.5 and 2. The major resistance to mass transfer in these cases is due to the non-equilibrium effects at the adsorbent particle interface. When Ω is small enough, the region of separation approaches that obtained in the frame of equilibrium theory. As the resistance to equilibrium attainment is increased, the region of separation disappears at Ω greater than 2. This suggests that care must be taken when designing SMB units to separations which may be subject to non-ideal equilibrium effects, e.g., high affinity solutes and/or steric effects present in stationary phase.

The same optimization procedure was performed again but with γ_1=3.87 and γ_4=2.69. These values are very close to the limiting values as predicted by the equilibrium theory (3.81 and 2.72, respectively). The corresponding regions of separation obtained for Ω= 0, 0.5 and 1 are shown in Figure A-6(b). It is interesting to note that the regions of separation for the same Ω are different from those in plot (a). They tend to disappear at a lower Ω as compared to the previous case. Another interesting aspect to note is that, at Ω=1, the region of separation does not touch the γ_2=γ_3 line, a different behaviour from that observed in plot a. This may be due to the proximity of γ_1 and γ_4 to the constraints given by the equilibrium theory. When mass transfer effects are present, these constraints are dependent on these effects and shift to new limits. This has been shown for SMB optimization of systems with linear equilibrium isotherms (Azevedo and Rodrigues, 1999) and seems to apply to non-linear systems as well. Choosing γ_1 and γ_4 values as defined from the equilibrium theory may be an economic practice (minimum eluent requirement); however, this may lead to inadequate design when mass transfer/non-equilibrium effects are present and lower purities than expected may be

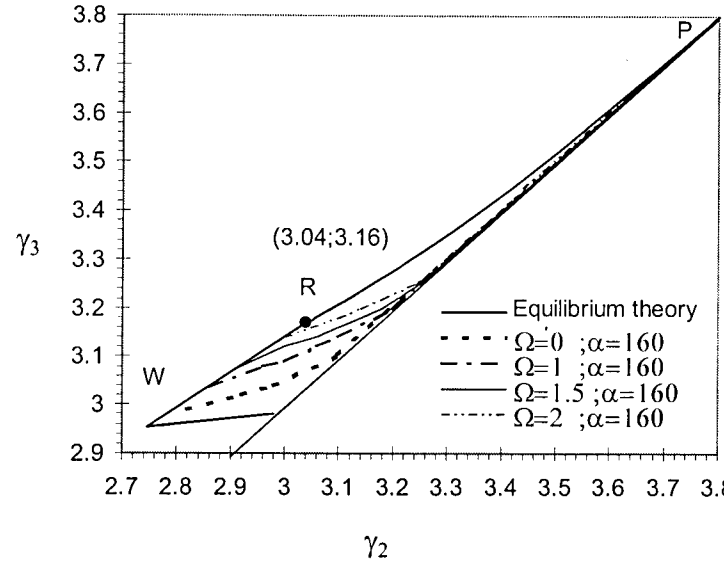

(a)

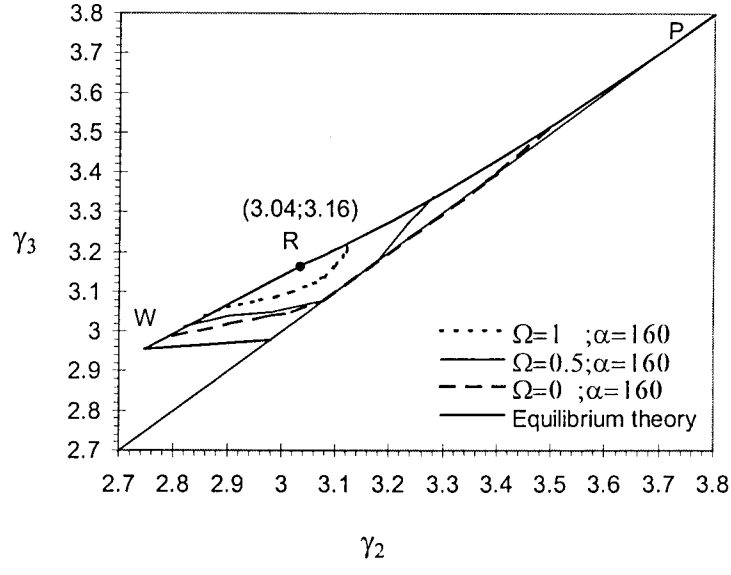

(b)

Figure A-6 Regions of separation in a $\gamma_2 \times \gamma_3$ plane for a SMB subject to non-equilibrium effects under non-linear equilibrium isotherms (linear+Langmuir). In plot (a), $\gamma_1=4.3$ and $\gamma_4=2.14$ and in plot (b), $\gamma_1=3.87$ and $\gamma_4=2.69$.

obtained. Furthermore, the regions seem to converge to point "R", and as indicated in Figure A-6. In the building of the region of separation as stated in the equilibrium theory, the segment WP is composed of a straight line (WR) and a curve (RP), which intersect at the

converging point R. In the vicinity of this point, the highest average purities of both products have been observed for each of the cases simulated.

A.4 Conclusions

The effects of non-equilibrium adsorption kinetics on SMB performance were examined in this work for non-linear (chiral epoxide separation) isotherms. The concentration at the surface of the adsorbent particle was written out as a separate algebraic equation in the model using the assumption of equal rates of adsorption/desorption and intraparticle diffusion. It has been shown that, in spite of not obtaining large differences between the surface concentration and equilibrium solid-phase concentration in steady-state, the presence of non-equilibrium effects affects the performance of a SMB unit considerably. Especially when it comes to the prediction of flowrate ratios that enhance separation (product purities above 99%), the inclusion of non-equilibrium effects is fundamental to a correct design of robust operating conditions. The constraints on γ_1 and γ_4 must also be carefully chosen before performing a search for adequate SMB operating conditions since they are also affected by non-equilibrium effects.

A.5 References

D. C. S. Azevedo, A. E. Rodrigues, "Design of a Simulated Moving Bed in the Presence of Mass-Transfer Resistances", *AIChE J.* **45**, 956-966 (1999).

G. Blaschke, "Chromatographic Resolution of Chiral Drugs on Polyamides and Cellulose Triacetate", *J. Liq. Chromatogr.* **9**, 341-368 (1986).

E. Francotte, A. Junker-Buchheit, "Preparative Chromatographic Separation of Enantiomers", *J. Chromatography A* **576**, 1-45 (1992).

E. Francotte, P. Richert, M. Mazzotti, M. Morbidelli, "Simulated Moving Bed Chromatographic Resolution of a Chiral Antitussive", *J. Chromatography A* **796**, 239-248 (1998).

M. Juza, et al., "Continuous Enantiomer Separation of the Volatile Inhalation Anesthetic Enflurane with a Gas Chromatographic Simulated Moving bed Unit", *J. Chromatography* **813**, 333-347 (1998).

H. Koller, K.-H. Rimbock, Mannschreck, "High Pressure Liquid Chromatography on Triacetylcelulose. Characterization of a Sorbent for the Separation of Enantiomers", *J. Chromatography A* **282**, 89-94 (1983).

S. Lehoucq, A. Vande Wouwer, E. Cavoy, "Chiral Separations using a SMB System: Determination of Competitive Adsorption Equilibrium Isotherms", in *Fundamentals of Adsorption 6* F. Meunier, Ed. (Elsevier, Amsterdam, 1998) pp. 467-472.

S. Lehoucq, D. Verhève, A. V. Wouwer, E. Cavoy, "SMB Enantioseparation: Process Development, Modeling and Operating Conditions", *AIChE J.* **46**, 247-256 (2000).

M. Mazzotti, G. Storti, M. Morbidelli, "Optimal Operation of Simulated Moving Bed Units for Nonlinear Chromatographic Separations", *J. Chromatography A* **769**, 3-24 (1997).

L. S. Pais, J. M. Loureiro, A. E. Rodrigues, "Separation of Enantiomers of a Chiral Epoxide by Simulated Moving Bed Chromatography", *J. Chromatography A* **827**, 215-233 (1998).

L. S. Pais, J. M. Loureiro, A. E. Rodrigues, "Chiral Separation by SMB Chromatography", *Sep. Pur. Technol.* **20**, 67-77 (2000).

A. E. Rodrigues, A. M. D. Ramos, J. M. Loureiro, M. Diaz, Z. P. Lu, "Influence of Adsorption-Desorption Kinetics on the Performance of Chromatographic Processes using Large-Pore Supports", *Chem. Eng. Sci.* **47**, 4405-4413 (1992).

T. Shibata, I. Okamoto, K. Ishii, "Chromatographic Optical Resolution on Polysaccharides and their Derivatives", *J. Liq. Chromatogr.* **9**, 313-340 (1986).

R. D. Whitley, K. E. Van Cott, N.-H. L. Wang, "Analysis of Nonequilibrium Adsorption/Desorption Kinetics and Implications for Analytical and Preparative Chromatography", *Ind. Eng. Chem. Res.* **32**, 149-159 (1993).

B. Breakthrough curves with cashew apple juice

This appendix provides additional information concerning the experiments carried out in fixed bed using filtered cashew apple juice as feed. The main motivation for these experiments was to formulate reasonable hypothesis to explain the observed transient behaviour in SMB separation reported in Chapter 5. Since the steady state performance in the simulated moving bed did not seem to be affected, the possible cause of the observed anomalous behaviour in the initial cycles in experiment 1 is likely to be related to diffusion barriers caused by larger molecules present in the juice such as polyphenols, oligosaccharides or proteins. In order to test this hypothesis, a column packed with resin Dowex Monosphere and a set of breakthrough and regeneration curves were obtained. In the following paragraphs, each experiment is described and the proper conclusions are stated.

B.1 Experiment 1: Breakthrough and regeneration curve using filtered cashew apple juice as feed.

Temperature (°C):	55
Fructose concentration in feed (g/l) :	10
Glucose concentration in the feed (g/l):	10
Volumetric flowrate (ml/min):	5
Column length (cm):	8.5

Column internal diameter (cm): 2.6

The obtained response curve at the exit of the column is shown in Figure B.1(a). At 30 minutes, the feed was switched to distilled and deionized water. The regeneration curve is shown in plot (b). For both plots, the symbols represent concentrations obtained experimentally. The curves were obtained from simulation assuming a synthetic mixture of fructose and glucose with model parameters as determined in Chapter 4.

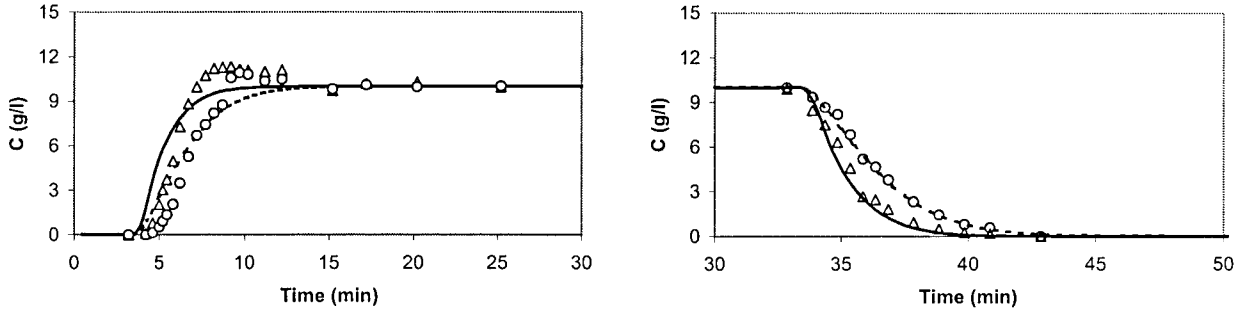

(a) (b)

Figure B.1 Response curves of a column packed with resin Dowex Monosphere: (a)breakthrough curve of sugars fructose and glucose in response to a step in cashew apple juice concentration and (b) regeneration curve in response to a negative step in sugar concentration (eluent only). The symbols are experimental and the curves are simulations assuming synthetic mixtures.

The breakthrough curve shows a small overshoot of both sugar concentrations beyond the feed concentration. This behaviour resembles that observed for experiment 1 in the initial cycles of SMB operation (see Chapter 5). However, the adsorbent capacity seems to remain unchanged, which is evidenced by the experimental regeneration curve. The adsorbed phase concentrations for fructose and glucose, as calculated from the regeneration curve, are 5.47 and 2.95 g/l, respectively. These figures would be 5.10 and 2.80 g/l, respectively, as calculated from the equilibrium isotherm. Therefore, this behaviour might indicate that the diffusion of sugars is hindered by other chemical species being adsorbed, although adsorption equilibria of both sugars (fructose and glucose) on the resin are the same.

B.2 Experiment 2: Breakthrough curve using filtered cashew apple juice as feed at higher concentration.

Temperature (°C):	55
Fructose concentration in feed (g/l) :	27.5
Glucose concentration in the feed (g/l):	27.5
Volumetric flowrate (ml/min):	5

Column length (cm):	8.5
Column internal diameter (cm):	2.6

A new breakthrough curve was obtained for the same column reported in the previous section. This time, cashew apple juice was less diluted so that both fructose and glucose concentrations were 2.5 times as much as in the previous experiment. Figure B.2 shows the obtained experimental curve (symbols) as compared to the simulated curve (continuous). Very good agreement is observed between experiment and the simulated behaviour of a synthetic sugar mixture. The overshoot observed in the previous experiment did not occur.

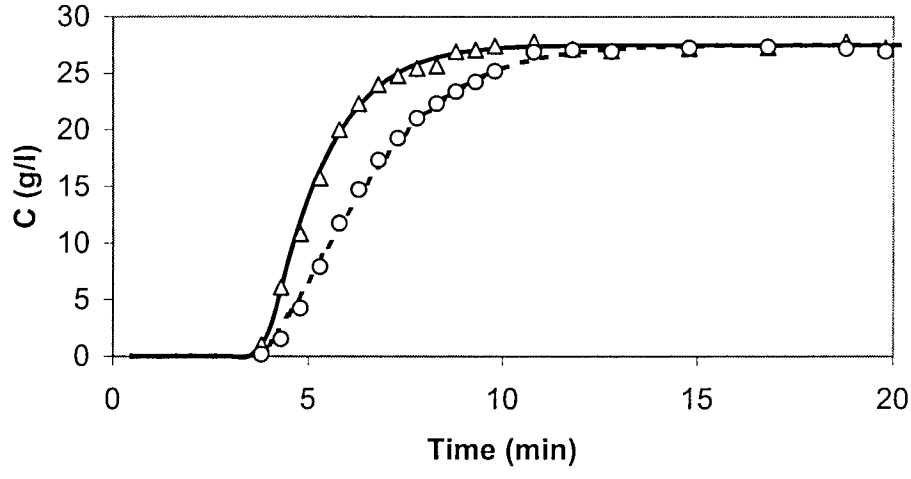

Figure B.2 Breakthrough curve of fructose and glucose in response to a step change in cashew apple juice concentration in the column inlet. The symbols are experimental (triangles for glucose and circles for fructose) and the curves are simulated.

B.3 Experiment 3: Column ion-exchange.

In order to check whether any chemical species had been irreversibly adsorbed on the resin, the same column described in the previous experiments was washed with NaOH. Two liters of a 1N solution were pumped into the column at 4 ml/min so as to completely exchange cations Ca^{++} for Na^{+} and desorb any organic matter that might have been accumulated in the resin. A sample was taken from the collected wash, neutralized with HCl and injected into a HPLC column. The analytical conditions are the same as those used for sugar determination in Chapter 5.

Figure B.3 shows the chromatogram obtained for the NaOH eluate as compared to the chromatogram of cashew apple juice. The peaks at 10 and 17.5 minutes were identified as having been retained in the SMB column. These peaks are presently unidentified but probably correspond to polyphenols or carotenoids. They may have an effect on the observed behaviour both for SMB and fixed bed at low sugar concentrations.

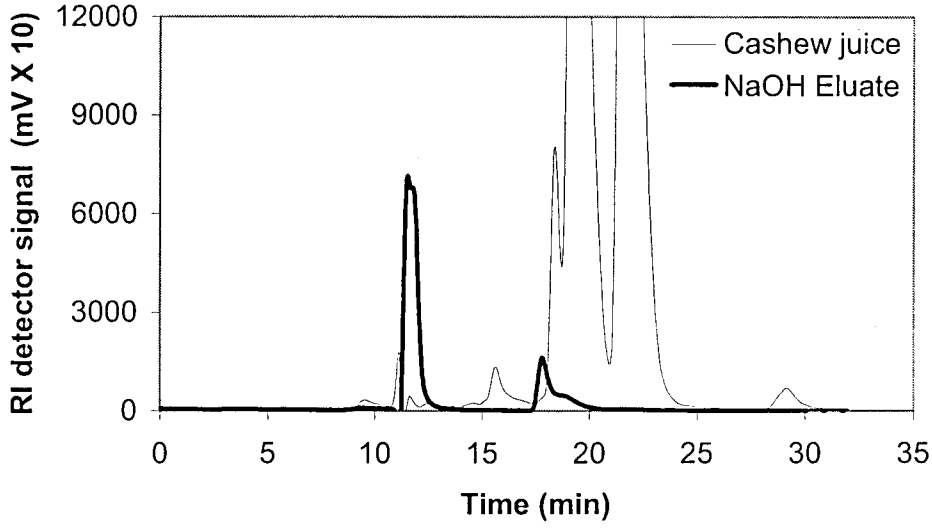

Figure B.3 Chromatograms of cashew apple juice (thin lines) and NaOH eluate (thick lines).

The column was then rinsed with distilled deionized water (1 liter at 5 ml/min). Then to restore the Ca^{++} ionic form, 2 liters of a $CaCl_2$ solution (1N) were pumped into the column at 4 ml/min followed by a rinsing step (1 liter at 5 ml/min).

B.4 Experiment 4: Breakthrough curve in regenerated column.

After being submitted to the regeneration and ion-exchange procedure described in the previous paragraphs, the column was again subjected to a step in cashew apple juice concentration according to the conditions below:

Temperature (°C):	55
Fructose concentration in feed (g/l) :	24
Glucose concentration in the feed (g/l):	24
Volumetric flowrate (ml/min):	5
Column length (cm):	8.5
Column internal diameter (cm):	2.6

Figure B.4 shows the concentration response curve measured at the exit of the column. The experimental points follow fairly well the simulated curves. However, there is some scattering after 7 minutes, which may be misinterpreted as some degree of overshoot. This may indicate that the washing step with NaOH did not completely remove the previously adsorbed components and the resin was not restored to its fresh form. Nevertheless, the capacity, selectivity and mass transfer characteristics remain about the same.

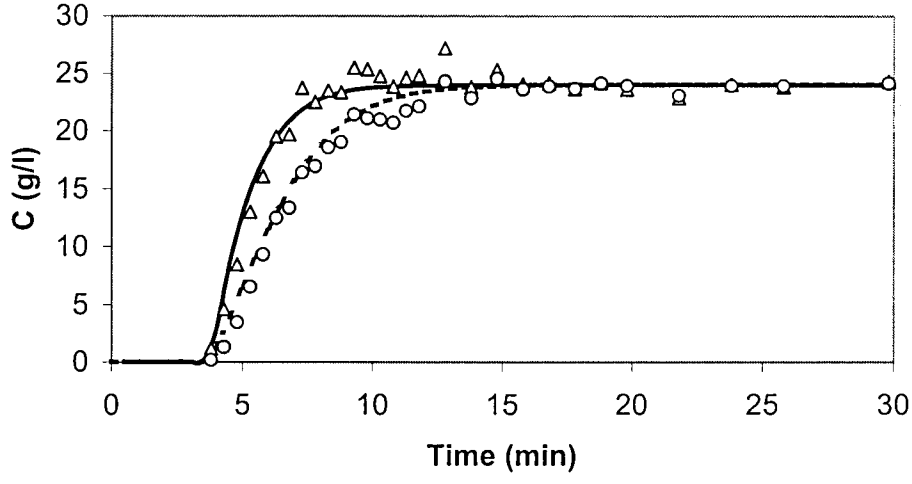

Figure B.4 *Breakthrough curve of fructose and glucose in response to a step change in cashew apple juice concentration in the column inlet. The column has been previously cleaned from organic matter. The symbols are experimental (triangles for glucose and circles for fructose) and the curves are simulated.*

B.5 Conclusions

The experiments described in this appendix together with the SMB experiments for the separation of fructose and glucose from cashew apple juice provide strong evidence to support the following conclusions:

- Some high molecular weight substances (yet to be identified) in the cashew apple juice are irreversibly adsorbed on cation-exchange resin Dowex Monosphere 99/Ca at 55°C;

- When fresh resin is contacted with cashew apple juice for the first time, these substances pose a physical barrier to the diffusion of fructose and glucose, which might lead to the transitory increase in bulk fluid concentration observed both for SMB and fixed bed operation;

- The adsorption of such substances does not significantly alter the resin capacity and selectivity for fructose and glucose operation, at least in the short run.

C. Evidence of immobilization of enzyme invertase onto exchange resin

C.1 Introduction

In the simulations reported in Chapter 6 for the inversion of sucrose in SMBR, the reaction rate parameters used were obtained from experiments performed in a batch reactor (Santos, 1999). By assuming that reaction occurs only in the fluid phase, the experimental data obtained for a SMBR did not follow the predictions from the simulations. This may be verified in Figure C.1 (a). The experimental data revealed that sucrose was actually consumed much faster than expected. However, by increasing the reaction rate seven-fold, the simulated profiles at steady state matched perfectly those obtained experimentally (see Figure C.1(b)). Hence, a contribution to the reaction rate other than that occurring in fluid phase must be added to the overall reaction rate. Our hypothesis was that enzyme invertase adsorbed onto the surface of the separation resin and contributed to the reaction rate proportionally to the amount adsorbed. This appendix describes the experiments performed to verify this assumption. A column packed with cationic resin Dowex Monosphere was subjected to a step changes in the inlet concentration of enzyme invertase. The response at the exit of the column

was recorded by a UV detector. By calculating the stoichiometric times, it was possible to estimate the adsorption isotherm.

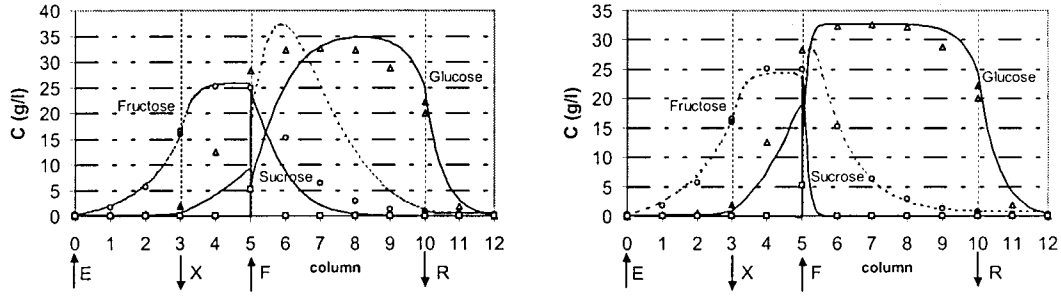

Figure C.1 Experimental concentration profiles obtained at cyclic steady state (see conditions of experiment 1 in Table 6.3) as compared to simulations considering (a) only reaction in the fluid phase and (b) reaction both in the fluid and solid phase due to enzyme adsorbed on the cationic resin.

C.2 Experimental

A column was packed with cationic resin Dowex Monosphere 99/Ca (d_p=320 μm), having the following dimensions: 8.5 cm length and 2.6 cm internal diameter. The column was equilibrated with a pH-4.5 buffered solution (as described in Chapter 6) at the temperature of 55°C. The exit piping of the column was connected to a UV detector (λ=280 nm) and the baseline was checked. A solution of enzyme invertase was prepared at the concentration 30 mg/l using $CaCO_3/C_2H_4O_2$ buffer as solvent. The solution was pumped into the column and the response at the exit was recorded by a UV detector. Figure C.2 shows the obtained curve.

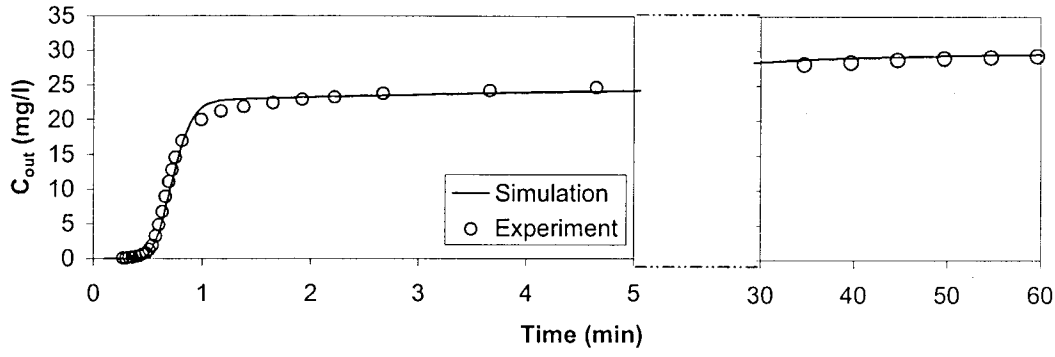

Figure C.2 Breakthrough curve of enzyme invertase (30 mg/l) recorded at the exit of a fixed bed (length = 8.5 cm; i.d.= 2.6 cm) under a flowrate of 25 ml/min.

The curve has a sharp front and a long tail, which reveals a high resistance to mass transfer inside the adsorbent particle. Since the resin is a gel type one with low porosity, it is more likely that most of the enzyme is adsorbed at the surface of the particle. The stoichiometric time was calculated as follows:

$$\int_0^\infty \left[C^o - C(t)\right]dt = C^o t_{st} \tag{C.1}$$

hence

$$t_{st} = \int_0^\infty \left[1 - \frac{C(t)}{C^o}\right]dt \tag{C.2}$$

and

$$q^o = \frac{QC^o t_{st} - \varepsilon C^o V_c}{(1-\varepsilon)V_c} \tag{C.3}$$

where C^o is the enzyme concentration in the feed, Q is the volumetric flowrate, V_c is the column volume and q^o is the concentration of adsorbed enzyme on the resin. The calculated stoichiometric time was 5.1 minutes, which corresponds to a slope $\frac{q^o}{C^o}$ of 3.9.

Successive steps in enzyme concentration of 40 mg/l and 50 mg/l were applied to the column packed with resin. The UV response was recorded and converted into concentration units, which is shown in Figure C.3.

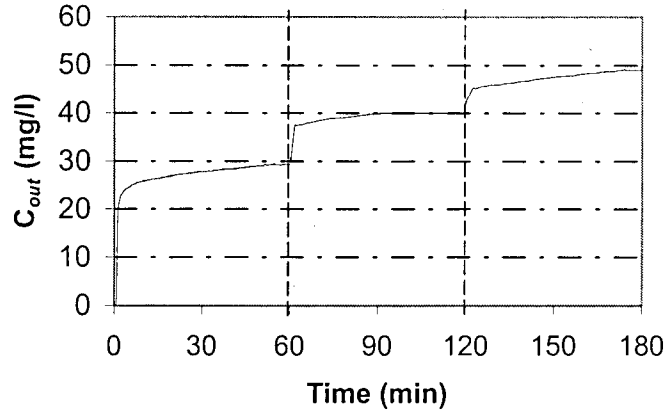

Figure C.3 Enzyme concentration at the exit of the column in response to steps in feed concentration of 30, 40 and 50 mg/l.

The adsorbed concentration at each incremental step was calculated following equations (C.1) to (C.3). The obtained isotherm is shown in Figure C.4. It is nearly linear in the reported concentration range, the adsorption constant being equal to approximately 4. The figure shows the equation obtained from linear regression and the square deviation error.

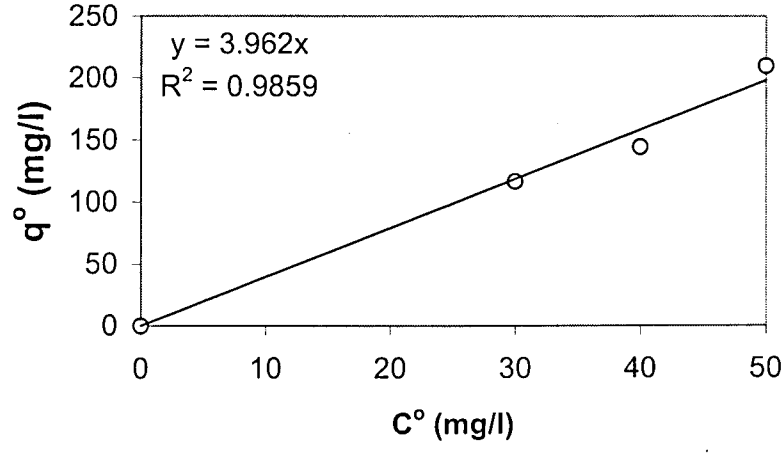

Figure C.4 Equilibrium isotherm of enzyme invertase on cationic resin Dowex Monosphere 99/Ca at 55°C and pH 4.5.

C.3 Reference

M. M. L. Santos, "Produção de Dextrano e Frutose a partir da Sacarose com Leuconostoc mesenteroides NRRL B512 (f)", PhD thesis, University of Porto (1999).